Analysis of the Net Ecosystem Exchange of CO_2 in a 56-year-old Coastal Douglas-fir Stand: Its relation to Temperature, Soil Moisture and Photosynthetically Active Radiation

by

Tiebo Cai

B.Sc., Inner Mongolia Forestry College, 1993

M.Sc., Inner Mongolia Forestry College, 1998

M.Sc., Lakehead University, 2001

A THESIS SUBMITTED IN PARTIAL FULFILLMENT OF

THE REQUIREMENTS FOR THE DEGREE OF

DOCTOR OF PHILOSOPHY

in

THE FACULTY OF GRADUATE STUDIES

(Soil Science)

THE UNIVERSITY OF BRITISH COLUMBIA

Abstract

The primary goal of this thesis was to investigate the relationship of canopy photosynthesis (P) to photosynthetically active radiation (PAR) in a 56-year-old coastal Douglas-fir stand (DF49) located on Vancouver Island. Canopy P was calculated as daytime NEP + daytime R_e, where NEP and R_e are net ecosystem production of CO_2 and ecosystem respiration, respectively. Half-hourly values of NEP were obtained using an EC (eddy covariance) system consisting of a 3-D sonic anemometer-thermometer and a closed-path infrared gas (CO_2/H_2O) analyzer, and daytime R_e was inferred by obtaining the intercept of the relationship between half-hourly values of NEP and PAR. Daytime R_e thus obtained was approximately 71–75% of that calculated by applying the logarithmically-transformed relationship between nighttime NEE (-NEP) and soil temperature (T_s) to daytime half hours. Values of R_{10} (the rate of R_e at T_s = 10 °C), obtained from both annual nighttime and daytime $R_e - T_s$ relationships, increased linearly with increasing soil moisture when averaged over the active growing season (April 1 – Sept 30). However, the effect of soil moisture on R_e shown on the multi-year scale could not be detected on the seasonal or annual scale probably as a result of the confounding effects of other environmental factors on R_e.

The effective PAR (Q_e) contributing to canopy P in this Douglas-fir canopy was well described as $Q_{d0} + kQ_{b0}$, with Q_{d0} and Q_{b0} being sky diffuse and direct PAR, respectively. The parameter k, which accounts for the total scattering of Q_{b0} and the non-scattering effect (e.g., penumbral light spreading) of the solar rays, was found to be approximately 0.22 for this stand. While the Michaelis-Menten equation (the MM model) (i.e., $P = \alpha Q_{t0} A_{\max} / (\alpha Q_{t0} + A_{\max})$, where $Q_{t0} = Q_{d0} + Q_{b0}$) results in significant overestimation of P in sunny conditions and significant underestimation of P in cloudy conditions, its modification into $P = \alpha Q_e A_{\max} / (\alpha Q_e + A_{\max})$ (the Q_e-MM model) eliminated these systematic errors. When k = 1, the Q_e-MM model reduces to the MM model. The Q_e-MM model is a single big-leaf model, but it avoids the type of errors made in earlier generations of single big leaf models of canopy P, i.e., using APAR (the total absorbed PAR by the canopy) to calculate P. The simplicity of the Q_e-MM model makes it convenient to be incorporated into large-scale carbon climate models.

This study also shows that the widely used sun/shade model developed by de Pury and Farquhar (1997) is inadequate, mainly because the sun/shade model fails to account for the incidence angle between the solar beam and individual sunlit leaves. As with the P modeled using the MM model, the modeled P obtained using the sun/shade model has significant systematic errors with respect to Q_{d0}/Q_{t0} (the ratio of Q_{d0} to Q_{t0}). In contrast, using the Q_e-MM model to estimate canopy P for this Douglas-fir stand eliminated these systematic errors with respect to Q_{d0}/Q_{t0}. In addition, the Q_e-MM model developed in this study agrees with the detailed multilayer model of canopy P developed by Norman and Arkebauer (1991) for agricultural crops (i.e., soybean and corn).

Contents

Abstract ... ii

List of Tables ... vi

List of Figures ... viii

List of Symbols and Acronyms ... xiii

Acknowledgements ... xvii

1 Introduction ... 1

2 Methodological uncertainties in estimating nighttime and daytime ecosystem respiration of a 56-year-old Douglas-fir stand from eddy covariance CO_2 fluxes ... 7

2.1 Introduction ... 7

2.2 Methods ... 11

2.2.1 Obtaining $R_e - T_s$ relationships using nighttime NEE measurements ... 14

2.2.2 Obtaining $R_e - T_s$ relationships using daytime NEP measurements ... 16

2.3 Results and discussions ... 18

2.3.1 $R_e - T_s$ relationships obtained using nighttime NEE measurements ... 18

2.3.2 $R_e - T_s$ relationships obtained using daytime NEP measurements ... 23

2.3.3 Comparison of the $R_e - T_s$ relationships obtained using the nighttime and daytime methods ... 31

2.3.4 Estimates of the annual totals of NEP, R_e and P using the nighttime and daytime methods ... 33

2.4 Conclusions ... 41

3 Comparison of different algorithms for partitioning net ecosystem exchange into its component fluxes: ecosystem photosynthesis and respiration ... 43

3.1 Introduction ... 43

3.2 Methods ... 49

3.2.1 Annual fits of the nighttime and daytime $R_e - T_s$ relationships ... 50

3.2.2 Stepwise fits of the annual nighttime and daytime $R_e - T_s$ relationships ... 50

3.3 Results ... 53

3.3.1 Climate and meteorological conditions ... 53

3.3.2 Annual fits of the $R_e - T_s$ relationships ... 57

3.3.3 Stepwise fits of the annual $R_e - T_s$ relationships ... 64

3.4 Discussion ... 72

3.5 Conclusions ... 75

4 A modification of the Michaelis-Menten equation for its application to estimating canopy photosynthesis of a coastal Douglas-fir stand ... 77

4.1 Introduction ... 77

4.2 Methods 84

4.3 The model 85
4.3.1 Model development 85
4.3.2 Model parameterization 98
4.3.3 Model comparisons 99

4.4 Results 100
4.4.1 Variance in P accounted for by adding fractions of Q_{b0} to Q_{d0} 100
4.4.2 Comparisons between the MM, Q_e-LUE, and Q_e-MM models 103
4.4.3 Comparisons between the MM, Q_e-MM and the sun/shade models 107
4.4.4 Comparisons of the performance of the Q_e-MM and m-MM models 110
4.4.5 A case study 120

4.5 Discussion 124

4.6 Conclusions 128

5 Conclusions 130

References 137

Appendix A. The site location, EC system configuration and the PAR measurements for the 56-year-old Douglas-fir stand 153

Appendix B. Comparison of the PAR measurements made using the BF2 and LI-190SB. 156

Appendix C. Inadequacies in the Sun/Shade Model Developed by de Pury and Farquhar (1997) 159

1. Lack of consideration of the angle of incidence of Q_{b0} and the use of area-weighted APAR to calculate P of the big sunlit and shaded leaves, respectively. 159

2. Inadequacies in its scaling algorithm 169

3. Problems in its description of the geometry of light 175

4. Oversimplified representation of canopy structure. 177

Appendix D. Derivation of two key equations in Norman (1980) 180

Appendix E. Comparison of the scaling algorithms used in the complete multilayer, 2-leaf multilayer, 2-leaf single-layer, MM and Q_e-MM models of canopy P 185

List of Tables

Table 2-1. Coefficients obtained for the 5 nighttime methods for DF49 in 2001 (see Figure 2-2 and text for details). Units for A and B are μmol m^{-2} s^{-1} and $°C^{-1}$, respectively. Units for y_0 and RMSE are both μmol m^{-2} s^{-1}. 22

Table 2-2. Coefficients obtained for the MM (Q_{t0}: 0 – 1800 μmol m^{-2} s^{-1}) and LUE (Q_{t0}: 0 – 300 μmol m^{-2} s^{-1}) models with the application of different daytime $u*$ filters for DF49 in 2001 (see Figure 2-3). Units for A and B are μmol m^{-2} s^{-1} and $°C^{-1}$, respectively. The values of A and B were determined using $\ln R_{ed} = \ln A + BT_s$ (see Eq. (5)). 25

Table 2-3. Coefficients of the MM (Q_{t0}: 0 – 1800 μmol m^{-2} s^{-1}) (i.e., Eq. (2)) and LUE (i.e., Eq. (6)) fits for the different months shown in Figure 2-4. Units for α and A_{max} are μmol (CO_2) μmol^{-1} (quanta) and μmol m^{-2} s^{-1}, respectively. 27

Table 2-4. Coefficients obtained for the MM (Q_{t0}: 0 – 1800 μmol m^{-2} s^{-1}, and $u_{*Q_{200}}$) and LUE (Q_{t0}: 0 – 300 μmol m^{-2} s^{-1}, and $u_{*Q_{200}}$) models with different moving window for DF49 in 2001 (see Figure 2-5). Units for A and B are μmol m^{-2} s^{-1} and $°C^{-1}$, respectively. The values of A and B were determined using $\ln R_{ed} = \ln A + BT_s$ (see Eq. (5)). 29

Table 2-5. Annual totals of the R_e and P obtained using different annual nighttime and daytime $R_e - T_s$ relationships (see Figure 2-7 and Figure 2-8 for details). Only the nighttime half-hourly NEE measurements made in conditions where $u* \geq$ 0.3 m s^{-1} were used in the nighttime methods. The daytime half-hourly NEP measurements made in conditions where $u* < 0.3$ m s^{-1} and $Q_{t0} < 200$ μmol m^{-2} s^{-1} were not used in the MM and LUE fits, and only the rest of the daytime data (i.e., not screened by the daytime $u*$ filter) were used in both models to determine R_{ed}. 37

Table 3-1. Climate conditions for the 8 years (1998 – 2005), including canopy air temperature at the 27-m height (T_a), soil temperature at the 5-cm depth (T_s), integrated water content in the 0 – 1-m depth soil layer (θ), total precipitation, mean daily downwelling PAR (Q_{t0}) (45-m height) and mean daily downwelling diffuse PAR (Q_{d0}) (45-m height) for the entire year and for the most active growing season (April 1 – September 30). 54

Table 3-2. The values of A and B for each year obtained from the annual nighttime (Figure 3-3) and daytime (Figure 3-4) relationships. Units for A and B are μmol m^{-2} s^{-1} and $°C^{-1}$, respectively. The values of A and B were obtained using the logarithmic transformation of the corresponding exponential R_e-T_s relationships. The corresponding values of R_{10} and Q_{10} were obtained as: $R_{10} = AQ_{10}$ and $Q_{10} = e^{10B}$. 60

Table 3-3. The coefficients (i.e., c and d) in the linear regressions between annual values of R_{10} and θ and Q_{10} and θ (see Figure 3-5). The nighttime and daytime values of R_{10} and Q_{10} were obtained from the annual nighttime NEE_{u*} - T_s (Figure 3-3) and annual daytime $R_{ed} - T_s$ (Figure 3-4) relationships, respectively. Units of R_{10} and Q_{10} are μmol m^{-2} s^{-1} and $°C^{-1}$, respectively. θ

(m^3 m^{-3}) was calculated by averaging its half-hourly values of each year from April 1 to September 30. 63

Table 3-4. The annual totals of R_e obtained (1) using the annual values of R_{10} and Q_{10} obtained from the annual nighttime and daytime $R_e - T_s$ relationships of each individual year (see Figure 3-3 and Figure 3-4), and (2) using the annual values of R_{10} and Q_{10} modelled for each individual year from the nighttime and daytime $R_{10} - \theta$ and $Q_{10} - \theta$ relationships (see Table 3-3 and Figure 3-5). The nighttime and daytime R_{10} and Q_{10} values were used to calculate the nighttime and daytime half-hourly values of R_e, respectively. The half-hourly values of R_e were then summed to obtain the annual totals. Also shown are the means and standard deviations for the 8-year period. 64

Table 3-5. Annual totals of R_e obtained using the three stepwise methods and the annual relationship method. The nighttime NEE_{us} - T_s and daytime $R_{ed} - T_s$ relationships were used to calculate the nighttime and daytime half-hourly values of R_e, respectively, which were then summed to obtain the annual totals (see Figure 3-6 and Figure 3-7). 68

List of Figures

Figure 1-1. Clouds of ash and steam from the eruption of Mt. Pinatubo on June 12, 1991.... 2
Figure 1-2. The levelling off (arrows) of atmospheric CO_2 concentration after the eruptions of Mt. Agung in 1963 and Mt. Pinatubo in 1991..... 3
Figure 2-1. (a) The relationship between nighttime NEE measurements, representing nighttime ecosystem respiration (R_{en}), and soil temperature (T_s) at the 5-cm depth. (b) The relationship between the logarithmically transformed NEE and T_s. In both plots, the circles are bin averages of 100 half-hourly values, and the vertical bars are ± 1 standard deviation. The assumption of IID $N(0,\sigma^2)$ was met by doing the logarithmic transformation of the half-hourly nighttime NEE. The half-hourly NEE measurements are from 2001 with $u* \geq 0.3$ m s^{-1} (i.e., NEE_{u*}) ($n = 2472$)..... 19
Figure 2-2 .The $R_{en} - T_s$ relationships obtained using 5 different nighttime methods (see text for details).20
Figure 2-3. The $R_{ed} - T_s$ relationships obtained using the MM and LUE models with the application of a daytime $u*$ filter to increasing ranges of Q_{t0}. The total Q_{t0} ranges for the MM model and LUE model are 0 – 1800 μmol m^{-2} s^{-1} and 0 – 300 μmol m^{-2} s^{-1}, respectively. u_{*Q_0}, $u_{*Q_{50}}$, $u_{*Q_{100}}$, $u_{*Q_{200}}$, and $u_{*Q_{300}}$ denotes that the daytime half-hourly NEP measurements made in calm conditions (i.e., $u*$ < 0.3 m s^{-1}) were removed if $Q_{t0} < 0$ μmol m^{-2} s^{-1}, $Q_{t0} < 50$ μmol m^{-2} s^{-1}, Q_{t0} <100 μmol m^{-2} s^{-1}, $Q_{t0} < 200$ μmol m^{-2} s^{-1}, and $Q_{t0} < 300$ μmol m^{-2} s^{-1}, respectively. For example, $u_{*Q_{200}}$, in the case of the MM model, means removing low $u*$ daytime NEP measurements if $Q_{t0} < 200$ μmol m^{-2} s^{-1} and only the high $u*$ NEP measurements associated with $Q_{t0} < 200$ μmol m^{-2} s^{-1} and all the NEP measurements made when $Q_{t0} > 200$ μmol m^{-2} s^{-1} (regardless of their $u*$ values) are used in the MM model fit to determine R_{ed}. In the case of the LUE model, data for Q_{t0} between the upper end of the range and 300 μmol m^{-2} s^{-1} were not $u*$ screened e.g., for $u_{*Q_{100}}$ values for $100 < Q_{t0} < 300$ μmol m^{-2} s^{-1} were not screened. u_{*Q_0} means no daytime $u*$ screening was applied in both the MM and LUE models, because all daytime NEP data are associated with $Q_{t0} > 0$ μmol m^{-2} s^{-1}..... 24
Figure 2-4. Daytime NEP – PAR relationships for different months of 2001. The dots in (a) – (c) are the half-hourly NEP measurements. The circles in (d) are the bin averages of 300 half-hourly NEP measurements and the vertical bars denote ± 1 standard deviation. The thin and thick lines are the respective fits obtained using the MM and LUE models to the half-hourly NEP measurements (not to the bin averages as shown in (d)). The Q_{t0} ranges for the MM model and LUE model are 0 – 1800 μmol m^{-2} s^{-1} and 0 – 300 μmol m^{-2} s^{-1}, respectively..... 26
Figure 2-5. The annual $R_{ed} - T_s$ relationships obtained using the MM and LUE models with moving windows of different sizes for 2001. All the moving windows were increased one day at a time and all the fits were made with the

logarithmic transformation of R_{ed}. The total Q_{10} ranges for the MM model and LUE model are 0 – 1800 μmol m^{-2} s^{-1} and 0 – 300 μmol m^{-2} s^{-1}, respectively. ... 30

Figure 2-6. The $R_e - T_s$ relationships obtained using the LUE model with three Q_{10} ranges: $Q_{10} < 100$ μmol m^{-2} s^{-1} (dotted line), $Q_{10} < 200$ μmol m^{-2} s^{-1} (thin line) and $Q_{10} < 300$ μmol m^{-2} s^{-1} (dashed line). Also shown are the $R_e - T_s$ relationships obtained using the MM model with $Q_{10} < 1800$ μmol m^{-2} s^{-1} (line with solid triangles) and $Q_{10} < 300$ μmol m^{-2} s^{-1} (line with empty triangles) and the $R_e - T_s$ relationship obtained using the nighttime logarithmic fit (the thick line). In all the daytime $R_e - T_s$ relationships, 15-day moving window and daytime $u*$ filter of $u_{*_{Q_{200}}}$ were used. ... 32

Figure 2-7. The annual cumulative NEP for 2001 obtained using different nighttime and daytime derived $R_e - T_s$ relationships. The LUE and MM model use only daytime half-hourly NEP measurements. ... 35

Figure 2-8. Monthly totals of P for 2001 obtained using different nighttime and daytime derived $R_e - T_s$ relationships (see Figure 2-7 for the legend). ... 40

Figure 3-1. Seasonal changes in the 15-day averages of soil temperature (T_s) at the 5-cm depth. ... 55

Figure 3-2. Seasonal changes in the 15-day averages of volumetric soil water content (θ) integrated from the surface to the 1-m depth. The values of field capacity (-1/3 bar) (θ = 0.213 m^3 m^{-3}) and permanent wilting point (-15 bars) (θ = 0.110 m^3 m^{-3}) were taken from Black (1979) for a 26-year-old coastal Douglas fir stand. ... 56

Figure 3-3. The annual nighttime NEE_{u*} - T_s relationships for 1998 – 2005, where NEE_{u*} are the nighttime half-hourly NEE measurements made when $u* > 0.3$ m s^{-1}. Symbols represent the bin averages of the 20 half-hourly NEE_{u*} values in the stratifications of half-hourly values of θ. The annual curve fits were obtained using the original half hourly NEE_{u*} data (not the bin averages). ... 58

Figure 3-4. The annual daytime $R_{ed} - T_s$ relationships for 1998 – 2005 obtained using the LUE model. ... 59

Figure 3-5. Linear regressions of R_{10} and Q_{10} on average θ for the 0-1 m layer (see Table 3-3 for the coefficients). The nighttime and daytime R_{10} and Q_{10} values were obtained using the annual nighttime NEE_{u*} - T_s and annual daytime $R_{ed} - T_s$ (see Figure 3-3 and Figure 3-4) relationships, respectively. The numbers next to the data points indicate the year. ... 62

Figure 3-6. Monthly totals of nighttime R_e (i.e., R_{en}) obtained using the three stepwise fit methods compared with those obtained using the annual nighttime NEE_{u*} - T_s relationships for 1998 – 2005 (see Figure 3-3). All R_e values were calculated half-hourly and then summed to obtain monthly totals. ... 66

Figure 3-7. Monthly totals of daytime R_e (i.e., R_{ed}) obtained using the three stepwise fit methods compared with the annual daytime R_{ed} - T_s relationships for 1998 – 2005 (see Figure 3-4). All R_e values were calculated half-hourly and then summed to give monthly totals. ... 67

Figure 3-8. Seasonal changes in the monthly averages of $f(t)$ for the $A15$-day moving windows (see also Figure 3-6 and Figure 3-7)..... 70
Figure 3-9. Comparison of daytime daily averages of R_e, obtained using the daytime $R_{ed} - T_s$ relationships, with the corresponding nighttime daily averages of R_e obtained using the nighttime NEE_{tt*} - T_s relationships. All the nighttime and daytime half-hourly R_e values were calculated using the $A15$-day stepwise fit method (see Figure 3-6 and Figure 3-7), and then averaged to obtain the corresponding nighttime and daytime daily averages..... 71
Figure 4-1. The dependence of modelled half-hourly light-use efficiency [g CO_2 (MJ IPAR)$^{-1}$] on the fraction of photosynthetically active radiation (PAR) above the canopy that is from direct beam (from Norman and Arkebauer 1991). The canopy light-use efficiency is based on IPAR (intercepted PAR) and the results are for C_3 (o) and C_4 (+) canopies..... 81
Figure 4-2. (a) The sun/shade model aggregates all the sunlit leaves into a big hemispherical sunlit leaf (i.e., assuming the leaf angle distribution of the sunlit leaves is spherical) and uses the mean APAR (absorbed PAR) (i.e., Eq. 8) to compute the photosynthesis for all the sunlit leaves. (b) The direct PAR absorbed by an individual sunlit leaf is given by: $Q_b(\gamma) = (1-\sigma)Q_p \cos\gamma$, where Q_p is the PAR perpendicular to the solar beam (the dotted line) and γ is the incidence angle between the beam and the normal to the leaf surface (the dashed line)..... 86
Figure 4-3. The relationship between f_γ and $\cos\gamma$. γ was stepwise increased from 0° to 90° in steps of 9° ($d\gamma = (9°/180°)\pi = 0.1571$ radians). For each step, $\cos\gamma$ and its corresponding f_γ ($f_\gamma = \sin\gamma d\gamma$, Eq. (10)) were calculated (the circles). Note the f_γ vs. $\cos\gamma$ relationship is independent of solar elevation angle (i.e., β), but the total LAI of the sunlit leaves is not independent of β.... 89
Figure 4-4. (a) The canopy is divided into three conceptual groups: the first group (0-L_1) with all the light-limited sunlit leaves, the second group (L_1 to L_2) with all the light-saturated sunlit leaves, and the third group (L_2 to L) with the shaded leaves. (b) The photosynthetic light response to Q_{ta} (total absorbed PAR) for the shaded leaves is linear with a slope of α. In addition to the absorption of sky diffuse PAR (i.e., $Q_d(1)$) and the scattered direct PAR (i.e., $Q_s(1)$), the light-limited sunlit leaves absorb limited amounts of un-scattered direct PAR (i.e., $Q_{b1}(\gamma)$), and thus its photosynthetic response can still be linear with the slope of α. The photosynthetic response of the light-saturated sunlit leaves can be described using two linear responses: the initial linear response with the slope of α and the second linear response with the slope of $k_0\alpha$..... 91
Figure 4-5. The variance in P accounted for using the Q_e-MM model at three levels of Q_{t0}. Canopy P was related to PAR using $P = \frac{\alpha Q_x A_{max}}{\alpha Q_x + A_{max}}$, where Q_x is defined as $Q_x = Q_{d0} + xQ_{b0}$. x was increased stepwise from 0 to 1, and a corresponding coefficient of determination (i.e., r^2) of the regression was calculated for each x. When $x = 1$, $Q_x = Q_{t0}$, and when $x = 0$, $Q_x = Q_{d0}$..... 102

Figure 4-6. The responses of P to Q_{t0}, Q_{d0}, Q_{b0} and Q_e. The fitted curve in (a) was obtained using $P = \frac{\alpha Q_{t0} A_{\max}}{\alpha Q_{t0} + A_{\max}}$ (i.e., the MM model) with α = 0.050 mol mol^{-1} and A_{max} = 24.79 μmol m^{-2} s^{-1}. The arrow in (b) indicates the sharp increase in P around Q_{d0} of 200 μmol m^{-2} s^{-1}. The fitted curve in (d) was obtained using $P = \frac{\alpha Q_e A_{\max}}{\alpha Q_e + A_{\max}}$ (i.e., the Q_e-MM model) with α = 0.041 mol mol^{-1}, A_{max} = 83.38 μmol m^{-2} s^{-1} and k = 0.22, r^2 = 0.66, RMSE = 4.30 μmol m^{-2} s^{-1}. The dashed line in (d) was obtained using $P = 0.030 Q_e + 1.21$ (i.e., the Q_e-LUE model), with k = 0.23, r^2 = 0.65 and RMSE = 4.38 μmol m^{-2} s^{-1}. Symbols represent bin averages and vertical lines indicate ±1 SD. n = 34785. All fitted curves were obtained using the original half-hourly data, i.e., not obtained using the bin-averaged data..... 104

Figure 4-7. Modeling errors for the MM, Q_e-LUE, and Q_e-MM models. Parameters for these models are given in Figure 4-6. Symbols represent bin averages and vertical lines indicate ±1 SD for the bin averages obtained using the Q_e-MM model. The SD values for the other two models is similar to the corresponding values for the Q_e-MM model (not shown). n = 34785..... 106

Figure 4-8. Modeling errors for the MM and Q_e-MM models with the incorporation of a temperature function for A_{max}, and the corresponding modeling errors using the sun/shade model. Note: the sun/shade model has built-in temperature functions to adjust the values of its V_{cmax} and J_{max}. For the MM model, the modeled P was obtained using, $P = \frac{\alpha Q_{t0} A_{\max} f(T_a)}{\alpha Q_{t0} + A_{\max} f(T_a)}$, where α = 0.065 mol mol^{-1}, A_{max} = 26.48 μmol m^{-2} s^{-1}, and $f(T_a) = e^{-(\frac{T_a - T_0}{\Omega})^2}$ with T_0 = 15.56 °C, and Ω = 13.71. r^2 = 0.59 and RMSE = 4.75 μmol m^{-2} s^{-1}. For the sun/shade model: r^2 = 0.55 and RMSE = 4.80 μmol m^{-2} s^{-1}. For the Q_e-MM model, the modeled P was obtained using $P = \frac{\alpha Q_e A_{\max} f(T_a)}{\alpha Q_e + A_{\max} f(T_a)}$, where α = 0.053 mol mol^{-1}, A_{max} = 67.57 μmol m^{-2} s^{-1}, k = 0.18, and $f(T_a) = e^{-(\frac{T_a - T_0}{\Omega})^2}$ with T_0 = 16.97 °C, and Ω = 11.68. r^2 = 0.73 and RMSE = 3.86 μmol m^{-2} s^{-1}. Symbols represent bin averages and vertical lines indicate ±1 SD. n = 34785..... 109

Figure 4-9. The coefficients of determination (r^2) for regressions using the Q_e-MM and m-MM models obtained by using 15-day moving windows (moving one day at a time) over 5 ½ years of data. The average and standard deviation of the r^2 are 0.6535 and 0.1394 for the Q_e-MM model, and 0.6562 and 0.1384 for the m-MM model, respectively. Symbols represent bin averages and vertical lines indicate ±1 SD for the bin averages obtained using the Q_e-MM model. The values of SD for the m-MM model are virtually identical to those for the Q_e-MM model (not shown)..... 111

Figure 4-10. Distributions of α and A_{max} obtained using the 15-day moving windows for the Q_e-MM model (see also Figure 4-9)..... 113

Figure 4-11. Distributions of k obtained using the 15-day moving windows for the Q_e-MM model (see also Figure 4-9 and Figure 4-10). 114

Figure 4-12. (a) The relationship between k and $\sin\beta$ obtained using the Q_e-MM model (see Figure 4-11). Symbols represent bin averages and vertical lines indicate ±1 SD. (b) the relationship between σ' - $\sin\beta$ calculated for different values of L using $\sigma' = 1 - e^{-K_b L} - (1-\sigma)(1-e^{-K_b L})$, where $K_b = 0.5/\sin\beta$ (see Eq. 21). The value of σ is assumed to be 0.1. 116

Figure 4-13. The temperature response of α_d, α_b, A_{maxd}, and A_{maxb} for the m-MM model obtained using 15-day moving windows for 5 ½ years of data (see Figure 4-9). Filled circles are α_d and A_{maxd}, and open circles are α_b and A_{maxb}. 118

Figure 4-14. Distributions of α_b / α_d and A_{maxb}/A_{maxd} for 5 ½ years of data. The values of α_d, α_b, A_{maxd}, and A_{maxb} were obtained using the 15-day moving windows for the m-MM model (see Figure 4-13). 119

Figure 4-15. Continuous half-hourly values of (a) Q_{t0} (thick line), Q_{d0} (thin line) and Q_{t0mdl} which is the modeled Q_{t0} in a cloudless sky using Eq. B1 in Appendix B (dotted line), (b) T_a (thick line) and D (thin line), and (c) canopy P for 6 days in the 56-year-old Douglas fir stand (DF49), Campbell River, B.C. Squares (□) are modeled P using the Q_e-MM model, and diamonds (◇) are modeled P using the MM model. For the Q_e-MM model, $P = \frac{\alpha Q_e A_{\max}}{\alpha Q_e + A_{\max}}$, where α = 0.048 mol mol^{-1}, A_{max} = 67.86 μmol m^{-2} s^{-1}, k = 0.16, r^2 = 0.56, and RMSE = 4.82 μmol m^{-2} s^{-1}. For the MM-model, $P = \frac{\alpha Q_{t0} A_{\max}}{\alpha Q_{t0} + A_{\max}}$, where α = 0.053, A_{max} = 22.51 μmol m^{-2} s^{-1}, r^2 = 0.28 and RMSE = 6.20 μmol m^{-2} s^{-1}. Note: the measurements of P made in all $u*$ conditions are shown in plot (c), but the measurements of P made in calm conditions ($u* < 0.3$ m s^{-1}) when $Q_{t0} < 200$ μmol m^{-2} s^{-1} were excluded from regressions of the MM and Q_e-MM models. 121

Figure 4-16. Canopy P calculated using the sun/shade model. (a) the Rubisco-limited (A_v) and RuBP-limited (A_j) photosynthetic rates for the big sunlit leaf, P_{sun} = min(A_v, A_j), (b) the corresponding A_v and A_j for the big shaded leaf, P_{shd} = min(A_v, A_j), (c) the modeled P of the entire canopy ($P = P_{sun} + P_{shd}$) using the sun/shade model (circles) and the measured P (lines), r^2 = 0.43, RMSE = 5.54 μmol m^{-2} s^{-1}. Note A_v equals to zero at night in (a) but not in (b) because the fraction of sunlit leaves at night is zero. 123

List of Symbols and Acronyms

$\overline{\cos\gamma_1}$	average of all the $\cos\gamma$ values of the light limited sunlit leaves
σ'	canopy scattering coefficient
α_0	empirical coefficient
K_b'	extinction coefficient for green leaves, $K_b' = K_b\sqrt{1-\sigma}$
f_{Sun}	fraction of sunlit leaves
ϕ	leaf inclination angle to the horizontal, radian or degree
τ	optical air mass
$\cos\gamma_{Threshold}$	cosine of the leaf-sun angle ($\gamma_{Threshold}$) associated with $Q_{bThreshold}$
ℓ	cumulative LAI from canopy top, but mainly used as a variable in integrals
$\overline{\Delta\cos\gamma_{Threshold}}$	difference between the average of all the $\cos\gamma$ values of the light saturated sunlit leaves and $\cos\gamma_{Threshold}$
$\Re$	gas constant, 8.314 J K^{-1} mol^{-1}
σ	variance or leaf scattering (i.e., reflected and transmitted PAR) coefficient depending on the context
α	quantum use efficiency, μmol (CO_2) μmol^{-1} (quanta)
ε	random error (residuals of a fit)
θ	soil volumetric water content, m^3 m^{-3}
β	solar elevation angle, radians
ρ_a	density of dry air
γ	incidence angle between the solar beam and a normal to the leaf surface, radians
f_γ	fraction of sunlit leaf area exposed at incident angle, γ
$f(t)$	time varying variable
α_d, α_b	quantum use efficient modified for diffuse PAR (α_d) and direct PAR (α_b), respectively, μmol (CO_2) μmol^{-1} (quanta)
$\Delta Q_{bThreshold}$	difference between the total un-scattered direct PAR absorbed by the light saturated sunlit leaves and $Q_{bThreshold}$, μmol m^{-2} s^{-1}
ϕ	a curvature parameter
A	a coefficient for R_e (see Eq. (3) of Chapter 2), $A = R_{10}/Q_{10}$, μmol m^{-2} s^{-1}
a	an empirical coefficient used to estimate Q_{t0mdl}
A_c	canopy assimilation rate used in the sun/shade model, μmol m^{-2} s^{-1}
A_j	rate of photosynthesis limited by RuBP regeneration, μmol m^{-2} s^{-1}
A_{jSun}	RuBP-limited rate of photosynthesis for the big sunlit leaf, μmol m^{-2} s^{-1}
A_{max}	a parameter (the asymptote) used in the MM model, μmol m^{-2} s^{-1}
A_{maxd}, A_{maxb}	A_{max} modified for diffuse PAR (A_{maxd}) and direct PAR (A_{maxb}), respectively, μmol m^{-2} s^{-1}
APAR	absorbed total PAR including diffuse and direct PAR, μmol m^{-2} s^{-1}
A_v	rate of photosynthesis limited by Rubisco, μmol m^{-2} s^{-1}

A_{vSun}	Rubisco-limited rate of photosynthesis for the big sunlit leaf, μmol m^{-2} s^{-1}
B	a coefficient for R_e (see Eq. (3) of Chapter 2), $B = (\ln Q_{10})/10$, $°C^{-1}$
D	vapour pressure deficit, kPa
DF49	the Douglas-fir stand planted in 1949
d_{leaf}	the diameter of a leaf, m
d_{sun}	the diameter of the sun, m
$d_{sun\text{-}earth}$	the distance between the sun and the earth, m
d_{umbra}	the length of the umbra, m
E_a	activation energy, J mol^{-1}
E_0	activation energy as defined by Eq (3) of Chapter 3, J mol^{-1}
EBC	energy balance closure which is usually expressed as $(H+LE)/(R_n-G-\Delta S/\Delta t)$, where H and LE are the sensible and latent heat fluxes, respectively. R_n is the net radiation flux, G is soil heat flux and $\Delta S/\Delta t$ is the rate of change of energy storage in the air and biomass between the ground and the height at which H and LE are measured. $R_n-G-\Delta S/\Delta t$ is commonly referred to as the available energy flux.
EC	eddy covariance (technique)
F_c	Half-hourly CO_2 flux, μmol m^{-2} s^{-1}
F_s	a storage term to account for the rate of change in CO_2 in the air column beneath the EC sensors
IID N(0, σ^2)	independently (i.e., random) and identically (i.e., variances are homogeneous) distributed in a normal distribution with zero mean and common variance, σ^2
h_m	the measurement height (i.e., 43 m)
IPAR	incident (intercepted) PAR, μmol m^{-2} s^{-1}
J_{maxi}	the maximum rate of electron transport for i^{th} leaf, μmol m^{-2} s^{-1}
k	the fraction of Q_{d0} added to Q_{b0} to give Q_e, i.e., $Q_e = Q_{d0} + kQ_{b0}$
k_0	a coefficient used to modify α
k_1, k_2	fraction of sunlit leaves that are light limited and light saturated, respectively
K_b	extinction coefficient for direct PAR assuming canopy foliage is black
K_n	vertical extinction coefficient of nitrogen in a canopy
L, L_1, L_2	cumulative LAI from canopy top (0 at the top)
LAI	leaf area index, m^2 (leaf area) m^{-2} (ground area)
L_i	LAI for i^{th} leaf, m^2 m^{-2}
m	empirical coefficient
MM model	Michaelis-Menten model
n	empirical coefficient
NEE	net ecosystem exchange, μmol m^{-2} s^{-1}
NEE_{u*}	nighttime half-hourly NEE measurements made in turbulent conditions (i.e., $u_* > u_{*th}$), μmol m^{-2} s^{-1}
NEP	net ecosystem production, μmol m^{-2} s^{-1}
OLS	ordinary least square algorithm
P	rate of photosynthesis (canopy-level or leaf-level), μmol m^{-2} s^{-1}
PAR	photosynthetically active radiation

P_{sun}	photosynthesis of the big sunlit leaf in the Sun/Shade (2-leaf single layer), μmol m^{-2} s^{-1}
P_i	photosynthesis of i^{th} leaf, μmol m^{-2} s^{-1}
Q_0	the extra-terrestrial PAR quantum flux, 2413 μmol m^{-2} s^{-1}
Q_{10}	temperature sensitivity coefficient describing the relative increase in R_e for a 10 °C increase in T_s, $°C^{-1}$
$Q_b(\gamma)$	un-scattered direct PAR absorbed by a leaf with the sun-leaf angle of γ, μmol m^{-2} s^{-1}
Q_{b0}	incident direct PAR above the canopy, μmol m^{-2} s^{-1}
$Q_{b1}(\gamma)$	un-scattered direct PAR absorbed by the light-limited sunlit leaves, μmol m^{-2} s^{-1}
Q_{ba_sun}	absorbed un-scattered direct PAR by the big sunlit leaf in the sun/shade model, μmol m^{-2} s^{-1}
$Q_{bThreshold}$	maximum un-scattered direct PAR absorbed by a sunlit leaf, in addition to its absorption of $Q_d(\ell) + Q_s(\ell)$, to still maintain the initial linear photosynthetic response with the slope of α, μmol m^{-2} s^{-1}
$Q_d(\ell)$	absorbed sky diffuse PAR at canopy depth, ℓ, μmol m^{-2} s^{-1}
Q_{d0}	incident (sky) diffuse PAR above the canopy, μmol m^{-2} s^{-1}
Q_e	effective amount of PAR contributing to canopy photosynthesis ($Q_e = Q_{d0} + kQ_{b0}$), μmol m^{-2} s^{-1}
Q_p	amount of PAR perpendicular to the solar beam, μmol m^{-2} s^{-1}
$Q_s(\ell)$	absorbed scattered direct PAR at canopy depth, ℓ, μmol m^{-2} s^{-1}
Q_{sat}	the amount of Q_{ta} where the quantum use efficiency of absorbed light begins to decrease, μmol m^{-2} s^{-1}
Q_{t0}	incident total PAR above the canopy, μmol m^{-2} s^{-1}
Q_{t0mdl}	modeled Q_{t0} (total downwelling PAR above the canopy) in a cloudless sky, μmol m^{-2} s^{-1}
Q_{ta}	absorbed total PAR, μmol m^{-2} s^{-1}
Q_{tai}	absorbed total PAR for i^{th} leaf, μmol m^{-2} s^{-1}
Q_{ti}	incident total PAR, μmol m^{-2} s^{-1}
Q_x	$Q_x = Q_{d0} + xQ_{b0}$, used in Figure 4-5 to test the combination of Q_{d0} and Q_{b0}, μmol m^{-2} s^{-1}
r_1, r_2, r_3	empirical coefficients
R_{10}	standardized rate of R_e at T_s = 10 °C, μmol m^{-2} s^{-1}
R_e	ecosystem respiration, μmol m^{-2} s^{-1}
R_{ed}	daytime R_e, μmol m^{-2} s^{-1}
R_{en}	nighttime R_e, μmol m^{-2} s^{-1}
RMSE	root mean square errors, μmol m^{-2} s^{-1} for photosynthesis
Rubisco	ribulose-1,5-biphosphate carboxylase/oxygenase
RuBP	ribulose biphosphate
$r_w(t)$	time (t) varying variable
S_c	CO_2 mixing ratio, mol CO_2 mol^{-1} of dry air
T_a	air temperature, °C
T_s	soil temperature, °C

u_*	friction velocity, m s^{-1}
u_{*Q100}	daytime u_* filter (screening), when Q_{t0} < 100 μmol m^{-2} s^{-1}, daytime half-hourly measurements made in $u_* < u_{*th}$ were not used to estimate R_{ed}. Only the daytime half-hourly measurements made when Q_{t0} > 100 μmol m^{-2} s^{-1} (including all u_* conditions) and when Q_{t0} < 100 μmol m^{-2} s^{-1} with only high u_* conditions were used in the NEP vs. PAR relation ship to calculate R_{ed}. Similar definitions are applied to u_{*Q0}, u_{*Q50}, u_{*Q200} and u_{*Q300}. u_{*Q0} is equivalent to applying no daytime u_* filter, because all daytime data are associated with Q_{t0} > 0 μmol m^{-2} s^{-1}
u_{*th}	u_* threshold value, m s^{-1}
V_c	photosynthetic Rubisco capacity of the entire canopy, μmol m^{-2} s^{-1}
V_{cmax0}	photosynthetic Rubisco capacity at the top of the canopy, μmol m^{-2} s^{-1}
V_{cSh}	photosynthetic Rubisco capacity of the big shaded leaf, μmol m^{-2} s^{-1}
V_{cSun}	photosynthetic Rubisco capacity of the big sunlit leaf, μmol m^{-2} s^{-1}
y_0	empirical coefficient used in Eq. (4) of Chapter 2, μmol m^{-2} s^{-1}
w'	fluctuation in vertical wind speed

Acknowledgements

I am indebted to my supervisor, Professor Andy Black, for his academic guidance and strong support. Andy creates an open-minded research environment, which enabled me to freely explore new ideas that challenge established research models. Andy also sets a personal example for me. He is a gentleman with a humble heart.

I am very grateful for the constructive suggestions from the other members of my supervisory committee: Drs. Rob Guy, Tim Oke and Mike Novak during the course of my PhD research program. Their comments greatly improved the quality of this thesis.

I would like to sincerely thank the wonderful individuals in Andy's biometeorology laboratory: Andrew Sauter, Andrew Balakshin, Armel Castellan, Christopher Schwalm, David Gaumont-Guay, Dominic Lessard, Elyn Humphreys, Gordon Drewitt, Iain Hawthorne, Joe Kidston, Kai Morgenstern, Natascha Kljun, Nick Grant, Paul Jassal, Praveena Krishnan, Rick Ketler, Scott Graham, Shawn O'Neill, Tim Griffis, Zhong Li, Stephanie Thompson and Zoran Nesic. I learned a great deal from these friends and I really appreciate the contibutions they made in the collection of the data essential to my thesis.

I greatly appreciate the postdoctoral position provided by Dr. Lawrence Flanagan at the University of Lethbridge. I would like to acknowledge the encouragement from members of Larry's research group: Chera Emrick, Nicole Geske, Jason Seabrook, Kamran Syed and Bruce Johnson. In particular, I would like to thank Nicole Geske for her kind help with the formatting of my thesis.

I appreciate the financial support through a Natural Sciences and Engineering Research Council of Canada (NSERC) Postgraduate Scholarship and a University Graduate Fellowship (UGF) from the University of British Columbia. Funding for the Vancouver Island research projects was from an NSERC Strategic Grant, NSERC, Canadian Foundation for Climate and Atmospheric Sciences (CFCAS) and BIOCAP Canada grants supporting the Fluxnet-Canada Research Network and an NSERC Discovery Grant to Professor Black.

Special thanks go to my parents and my brother and sisters for their love and constant support. Above all, I would like to thank my wife, Yanli, and my three daughters: Lujia, Joanne and Olivia. They are angels in my life. They have given me a new perspective on life.

1 Introduction

The volcanic eruption of Mt. Pinatubo (in Philippines) on June 12, 1991 (Figure 1-1), the single largest perturbation in climate during the last 100 years, ejected approximately 20 million tons of SO_2 into the troposphere, which greatly enhanced diffuse shortwave radiation (Molineaux and Ineichen 1996) and suddenly interrupted the recent global warming trend by causing a 0.6 °C decrease in mean global surface temperature (Robock 2002). After the eruption, the growth rate of atmospheric CO_2 concentration dramatically slowed down in the early 1990s (Keeling et al. 1995). This slowdown was not purely coincidental, since an apparent levelling off of atmospheric CO_2 concentration was observed following the eruption of Mount Agung (in Indonesia) in February 1963 (Bacastow 1979) (Figure 1-2). A similar pattern in the reduced rise of atmospheric CO_2 concentration was also identified following the eruption of El Chichón (in Mexico) in March 1982 after removing the confounding effect of 1982/83 El Niño event (Keeling et al. 1995).

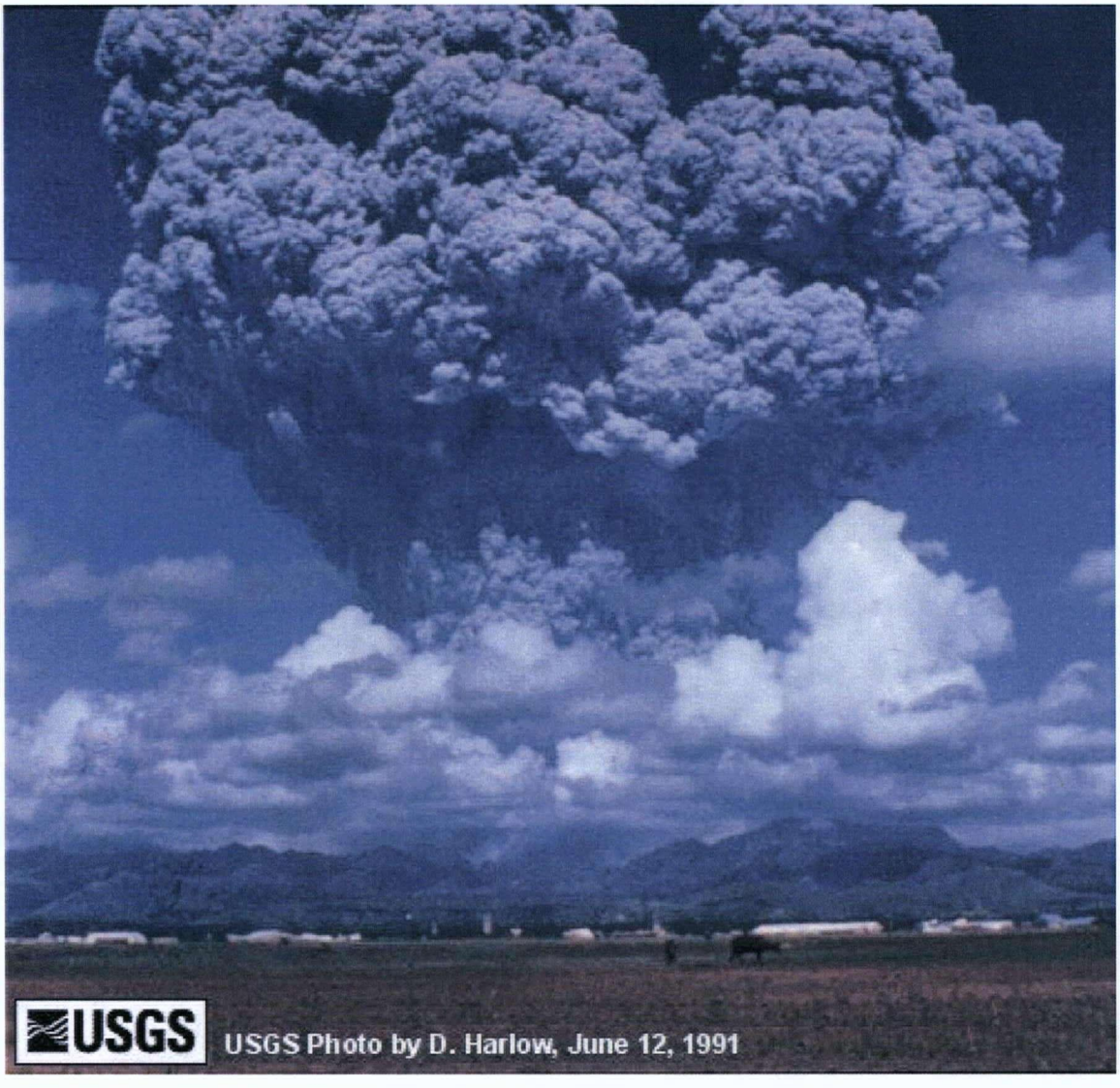

Figure 1-1. Clouds of ash and steam from the eruption of Mt. Pinatubo on June 12, 1991.

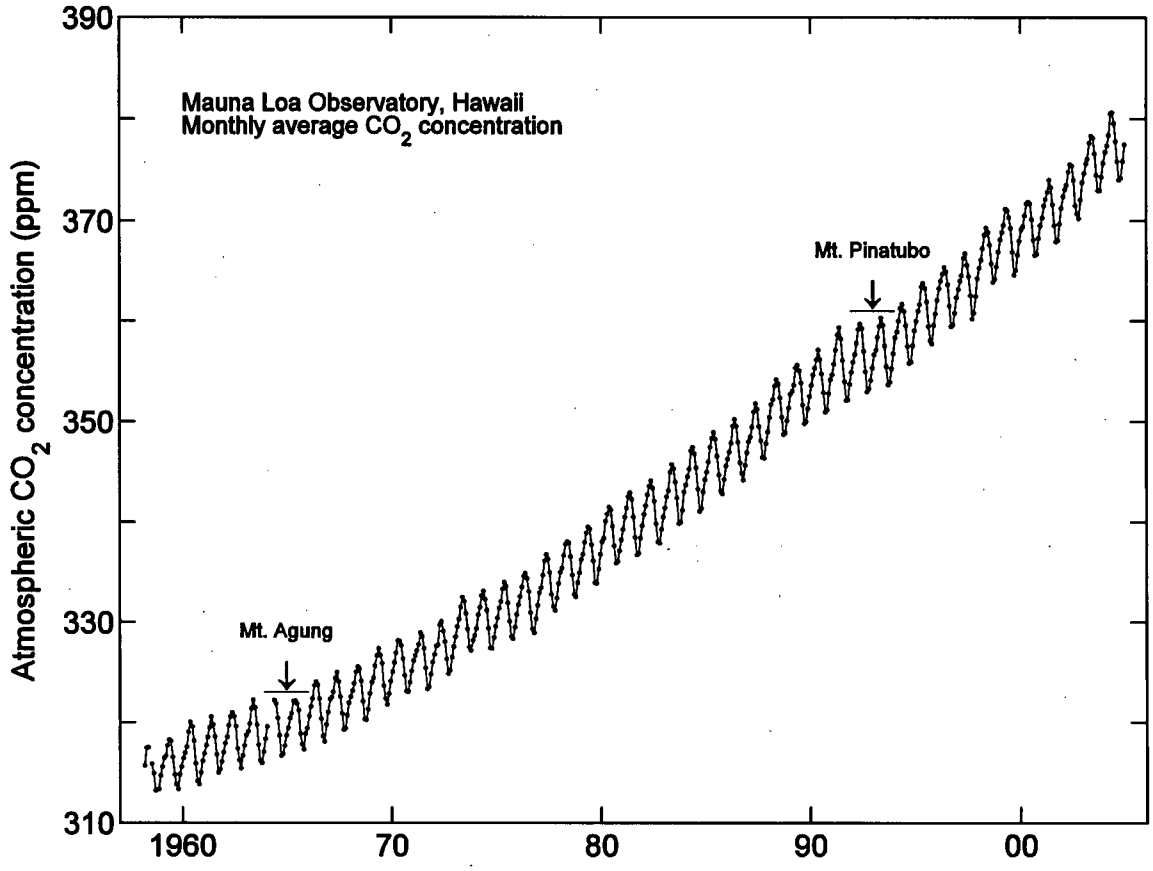

Figure 1-2. The levelling off (arrows) of atmospheric CO_2 concentration after the eruptions of Mt. Agung in 1963 and Mt. Pinatubo in 1991.

One hypothesis for the levelling off of atmospheric CO_2 concentration is that the eruption of Mt. Pinatubo increased the level of sky diffuse PAR (photosynthetically active radiation), which, because plant canopies use diffuse PAR more efficiently than direct PAR in photosynthesis (Roderick et al. 2001), led to a higher rate of canopy photosynthesis (P), removing more CO_2 from the atmosphere (Gu et al. 2003). This hypothesis stems from the long-known observation made by plant eco-physiologists that CO_2 fluxes between a plant canopy and the lower atmosphere is usually higher in cloudy conditions than in clear conditions (e.g., Price and Black 1990, Hollinger et al. 1994). But the explanations for these observations even at canopy-level are very controversial, because other environmental variables (e.g., saturation deficit, foliage temperature) are also quite different between cloudy and clear conditions (Freedman et al. 2001). Also, the "diffuse radiation" hypothesis does not reconcile the narrow tree rings observed following the Pinatubo eruption, which could be due to reduced P (Krakauer and Randerson 2003). Angert et al. (2004) concluded that the enhanced diffuse radiation following the eruption of Mt. Pinatubo was "probably only enough to compensate for the reduction in total radiation".

The net downward CO_2 fluxes above a plant canopy (or net ecosystem productivity, NEP) can be expressed as: $P - R_e$ (ecosystem respiration). The higher downward CO_2 fluxes in cloudy conditions can reflect either higher P (likely due to higher diffuse PAR) or lower R_e (likely as a result of lower temperature). In order to rigorously address the effect of diffuse PAR on canopy P, first we have to reliably estimate P. In this study 8 years (1998 – 2005) of CO_2 flux data from a 56-year-old

coastal Douglas-fir stand on Vancouver Island (DF49) were used to address the uncertainties in estimating canopy P and the role of diffuse and direct PAR in canopy P.

Chapter 2 addressed the methodological uncertainties in estimating nighttime and daytime R_e using one year (2001) of NEP measured using the eddy covariance (EC) method (e.g., Wofsy et al. 1993, Black et al. 1996). Canopy P is generally obtained as daytime NEP + daytime R_e, where daytime R_e has to be estimated. The errors in estimating daytime R_e using both the nighttime and daytime NEP measurements were systematically discussed.

Chapter 3 extended the results of Chapter 2 to provide a reliable flux-partitioning algorithm for estimating P for Chapter 4. This chapter focuses on the effect of soil moisture and phenological (seasonal) change on R_e using 8-years (1998-2005) of NEP data for DF49. The algorithms for partitioning NEP into its component fluxes, P and R_e used in AMERIFLUX (Falge et al. 2002), EUROFLUX (Reichstein et al. 2005), and FLUXNET-CANADA (Barr et al. 2004) were critically reviewed. The interannual variability in the R_{10} and Q_{10} values of R_e was investigated and the main cause for the variability was discussed.

After discussing the uncertainties in estimating P in Chapter 2 and comparing different algorithms for partitioning NEP into P and R_e in Chapter 3, Chapter 4 focused on P and canopy light regime. The history of canopy photosynthesis modelling work was briefly reviewed. The systematic errors of the regular Michaelis-Menten equation ($P = \frac{\alpha Q_{t0} A_{\max}}{\alpha Q_{t0} + A_{\max}}$) for modelling canopy P were examined. A new form of Michaelis-Menten equation (to be referred to as the Q_e-MM model hereafter) was developed for modelling canopy P. In order to evaluate the performance of the Q_e-MM model and to

assess the inadequacies of the existing models, the modelling errors in P using the Q_e-MM model and the Sun/Shade model developed by de Pury and Farquhar (1997) were compared. Additionally, the Q_e-MM model was compared with another modified form of the Michaelis-Menten equation used in Gu et al. (2002 & 2003). This chapter also provides a biophysical explanation for why the quantum use efficiency of direct PAR is lower than that of diffuse PAR.

Chapter 5 summarizes the major results of this study, discusses the relevance of these results in the context of large-scale modelling of gross primary productivity (Ruimy et al. 1999, Still et al. 2004), and identifies areas for extending the findings in the three main chapters for future research.

The thesis also has five appendices. Appendix A briefly shows the site location and the configuration of the EC system. Appendix B reports the calibration of the instrument used to measure diffuse PAR that is essential for the analysis in Chapter 4. Appendix C discusses the shortcomings of the Sun/Shade model developed by de Pury and Farquhar (1997). Appendix D derives the two key equations for the complete multilayer model of P developed by Norman (1980) (i.e., the CUPID model). Appendix C and Appendix D were included, because the algorithms from both models (i.e., the Sun/Shade and the CUPID models) have been widely used in models of canopy P. Appendix E compared the scaling algorithms of five types of canopy P models: the complete multilayer, 2-leaf multilayer, 2-leaf single-layer, MM and Q_e-MM models. Comparison of the models and their validation/invalidation using multiple years of EC-derived measurements of canopy P provided insightful information about the underlying biophysical principles of these models.

2 Methodological Uncertainties in Estimating Nighttime and Daytime Ecosystem Respiration of a 56-year-old Douglas-fir Stand from Eddy Covariance CO_2 fluxes

2.1 Introduction

Net ecosystem CO_2 exchange (NEE) is the difference between CO_2 losses by ecosystem respiration (R_e) and CO_2 gains by canopy photosynthesis (P) and is directly measured using the eddy covariance (EC) technique (e.g., Wofsy et al. 1993, Black et al. 1996). Net ecosystem productivity (NEP) is obtained as NEP = -NEE, which is a good approximation of C sequestration because the leaching losses of dissolved organic and inorganic carbon are usually very small in forest ecosystems. P is obtained as daytime NEP + daytime R_e. Daytime NEP can be directly measured using an EC system, but daytime R_e has to be estimated. The most commonly used method is to infer daytime R_e from nighttime EC measurements of NEE (i.e., nighttime R_e). Nighttime NEE measurements made in calm conditions, as determined by a threshold friction velocity (u_{*th}), are usually rejected (e.g., Barford et al. 2001, Morgenstern et al. 2004, Miller et al. 2004), because much of the respired CO_2 is likely transported horizontally (advection) rather than vertically through the EC flux measurement plane (Baldocchi 2003). Only nighttime NEE measurements made in turbulent conditions (NEE_{u*}) are used to develop an annual relationship with soil temperature at a shallow depth (T_s) so that nighttime R_e values can be calculated to replace the rejected measurements and daytime R_e values can

be estimated using daytime T_s (e.g., Black et al. 2000, Flanagan and Johnson 2005). The annual NEE_{u*} – T_s relationship is often assumed to be exponential as follows:

$$\mathrm{NEE}_{u*} = Ae^{BT_s} + \varepsilon \quad (1)$$

where A and B are two empirical coefficients, and ε is the random error (residual). The values of A and B are commonly determined using a non-linear ordinary least squares (OLS) algorithm (e.g., Lee et al. 1999, Falge et al. 2002, Law et al. 2002, Xu and Baldocchi 2004, Reichstein et al. 2005). However, this is problematic (Morgenstern et al. 2004, Richardson and Hollinger 2005) because OLS algorithms assume (Steel and Torrie 1960) (1) the independent variable (i.e., T_s) is measured without error and (2) the residuals (i.e., ε) are independently and identically distributed in a normal distribution with zero mean and common variance, σ^2. The latter assumption is often abbreviated as IID $\mathrm{N}(0, \sigma^2)$. It is reasonable to assume that the half-hourly measurements of T_s are error-free, but the ε's generally do not have a common variance over the range of T_s as is shown in Figure 2-1a, in which σ^2 markedly increases with T_s.

On the other hand, the validity of extrapolating nighttime R_e –T_s relationship to daytime has also been questioned (e.g., Wohlfahrt et al. 2005a), because light is likely to inhibit foliar mitochondrial respiration during the day, namely the Kok effect (Kok 1948, Sharp et al. 1984, Brooks and Farquhar 1985, Villar et al. 1994, Atkin et al. 2000b, Wang et al. 2001, Shapiro et al. 2004), and the degree of this inhibition at the ecosystem level is largely unknown (Janssens et al. 2001). Concerned about the poor quality of nighttime NEE measurements mainly caused by the lack of nocturnal mixing and the applicability of nighttime R_e to daytime, many workers (e.g., Suyker and Verma 2001, Reichstein et al. 2002a, Griffis et al. 2003, Xu and Baldocchi 2004) have obtained estimates of daytime R_e

using daytime NEP measurements. Daytime NEP can be expressed using the Michaelis-Menten relationship as:

$$\text{NEP} = \frac{\alpha Q_{t0} A_{\max}}{\alpha Q_{t0} + A_{\max}} - R_{ed} + \varepsilon \qquad \text{MM model} \qquad (2)$$

where α is the apparent quantum yield, Q_{t0} is the total incident photosynthetically active radiation (PAR) above the canopy, A_{max} is the canopy-scale maximum photosynthetic capacity, R_{ed} is the estimate of daytime R_e, and ε is the random error (residual). Eq. (2) will be referred to as the MM model. The three parameters (i.e., α, A_{max}, and R_{ed}) are usually determined using a non-linear OLS algorithm (e.g., Suyker and Verma 2001, Reichstein et al. 2002a, Griffis et al. 2003, Xu and Baldocchi 2004). But this methodology is as questionable as it is for Eq. (1). As shown in Figure 2-4d, there are two problems. First, the ε's do not have a common variance over the full range of Q_{t0} (σ^2 increases with Q_{t0}). Second, the ε's are not independently (randomly) distributed because, as will be shown in Chapter 4, Eq. (2) underestimates NEP in cloudy conditions (i.e., the predicted values of NEP using Eq. (2) are less than the bin averages in Figure 2-4d for Q_{t0} approximately between 500 – 1000 μmol m^{-2} s^{-1}) and overestimates NEP in clear conditions (i.e., the predicted values of NEP using Eq. (2) are higher than the bin averages in Figure 2-4d for Q_{t0} greater than 1000 μmol m^{-2} s^{-1}). Therefore, using a non-linear OLS algorithm to obtain parameters for Eq. (2) violates the assumption of IID $N(0, \sigma^2)$. This violation can cause potentially large errors in the estimates of annual R_e, but little attention has been paid to its impact in the literature. As pointed out by Richardson and Hollinger (2005), it is a serious concern that "relatively subtle choices in model construction and assumptions lead to what must be considered significant biases".

An additional concern is that the length of the period for which the NEP – Q_{10} relationship has been developed varies considerably in the literature, e.g., 1 day (Griffis et al. 2003), 3 days (Suyker and Verma 2001), 7 days (Kowalski et al. 2003, Reichstein et al. 2002a, Wohlfahrt et al. 2005a), 15 days (Lee et al. 1999) and 30 days (Falge et al. 2002, Law et al. 2002, Carrara et al. 2004). Lack of a standardized analytical procedure (e.g., the above mentioned different regression periods for the MM model) makes cross-site and cross-biome comparisons of R_e very difficult. Uncertainties in the estimates of daytime R_e also severely limit our understanding of ecosystem respiratory behaviour. For example, the estimates of daytime R_e obtained using the MM model were reported to be lower than that obtained using the nighttime annual NEE_{u*} - T_s relationship, but this could be due to an artefact of curve fitting, and may not necessarily reflect the real effect of light inhibition on ecosystem foliar respiration.

The two objectives of this chapter are to (1) report the methodological uncertainties in the estimates of R_e using both the nighttime and daytime EC-measured NEE, and (2) evaluate the validity of applying the nighttime R_e – T_s relationship to daytime and vice versa. In the second objective, the evidence of possible light inhibition on ecosystem foliar mitochondrial respiration will be examined by comparing the nighttime and daytime R_e – T_s relationships. One year (2001) of flux data for a 56-year-old coastal Douglas-fir stand (DF49) will be used in this study.

2.2 Methods

Study site

The study site is located 10 km southwest of Campbell River on the east coast of Vancouver Island, BC, Canada (49°52'N, 125°20'W) at an elevation of 300 m above sea level. The forest, originally planted with Douglas-fir seedlings in 1949, consists of 80% Douglas-fir (*Pseudotsuga meneziesii* (Mirb.) Franco), 17% western red cedar (*Thuja plicata* Donn ex D. Don) and 3% western hemlock (*Tsuga heterophylla* (Raf.) Sarg.). Its understory is sparse, mainly consisting of salal (*Gaultheria shallon* Pursh.), Oregon grape (*Berberis nervosa* Pursh), vanilla-leaf deer foot (*Achlys triphylla* (Smith) DC), and a thin layer of ferns and mosses. A site survey in 1998 found that the stand density was 1100 stems ha^{-1}, and tree height ranged from 30 m to 35 m, and the average diameter at breast height (DBH) was 29 cm. The soil at this site is a humo-ferric podzol with a gravelly loamy sand texture in the upper 40 cm transitioning to sand with increasing depth. The leaf area index (LAI) was estimated to be 8 ± 1 m^2 m^{-2}. More detailed descriptions of the site can be found in Drewitt et al. (2002), Humphreys et al. (2003), Morgenstern et al. (2004), and Humphreys et al. (2006).

Measurements

Morgenstern et al. (2004) described in detail the climate and eddy flux measurements at the site. Here only a short summary of these measurements is given. The EC sensors were mounted on an open-lattice 50-cm triangular tower at a height of 43 m and consisted of a 3-dimensional sonic anemometer-thermometer (SAT) (model 1012R2,

Gill Instruments, Lymington, UK) and a closed-path infrared gas (CO_2/H_2O) analyzer (model LI-6262, LI-COR, Lincoln, NE, USA). Half-hourly CO_2 fluxes were calculated as $F_C = \overline{\rho_a}\ \overline{w's_C'}$, where $\overline{\rho_a}$ is the mean molar density of dry air, $\overline{w's_C'}$ is the covariance between instantaneous vertical wind speed (w) and CO_2 mixing ratio (s_C) (i.e., mol CO_2 mol^{-1} of dry air). The fluctuations of w and s_C i.e., w' and s_C', were calculated as the difference between the instantaneous values and the arithmetic average for the half hour. The frequency of w and s_C used in the calculations of F_C was 20.83 Hz after digital low-pass filtering and down-sampling of the raw signals. The rate of change in CO_2 storage in the air column beneath the EC sensors was calculated as $F_S = h_m \overline{\rho_a} \Delta\overline{s_C}/\Delta t$ (Hollinger et al. 1994, Morgenstern et al. 2004), where h_m is the measurement height (i.e., 43 m), $\Delta\overline{s_C}$ is the difference between $\overline{s_C}$ (half-hourly average of s_C) of the following and previous half-hours, and Δt = 3600 s. Half-hourly net ecosystem exchange (NEE) of CO_2 was then calculated as $\mathrm{NEE} = F_C + F_S$. Positive values of NEE correspond to CO_2 losses from the ecosystem. Net ecosystem production (NEP) was calculated as $-\mathrm{NEE}$.

In this analysis, energy balance closure (EBC) was not applied to correct half-hourly NEE measurements. When EBC was evaluated on an annual basis for this site, the slopes of the regressions of sensible heat flux + latent heat flux vs. the available energy flux (net radiation - soil heat flux - heat storage terms) were 0.888, 0.879, 0.880, and 0.892 for 1998-2001, respectively (Morgenstern et al. 2004). The EBC correction is still a subject of debate because part of the error may arise from the measurements of net radiation (e.g., it may not be representative of the flux footprint), soil heat flux and the

heat storage terms. In addition, latent heat fluxes can be underestimated because of high frequency loss in the sampling tube as a result of dirt and water vapour adhering to the wall, which can be a worse effect than for CO_2 fluxes. However, if chamber measurements of soil, bole and foliage respiration were scaled up to compare with EC-derived respiration (e.g., Lavigne et al. 1997), it would likely be necessary to account for the lack of EBC (Twine et al. 2000, Barr et al. 2006). Ignoring EBC does not affect the conclusions of this thesis because the corrected NEP, R_e and P would be reduced by the same fraction, i.e., about 11%.

Downwelling total PAR (Q_{t0}) was measured using a quantum PAR sensor (model LI-190SB, LI-COR Inc) mounted at a height of 45 m. Canopy air temperature (T_a) and relative humidity were measured using a relative humidity sensor (model HMP-35C, Vaisala Oyj, Helsinki, Finland) mounted at a height of 27 m. Soil temperature (T_s) was measured using copper-constantan thermocouples buried at different locations and at 5-cm depths. The above climate measurements (e.g., Q_{t0}, T_a, and T_s) were sampled every 5 seconds and averaged over the 30-minute-interval.

Curve fitting algorithm

The measurements made when Q_{t0} = 0 μmol m^{-2} s^{-1} are referred to as nighttime measurements, and those when Q_{t0} > 0 μmol m^{-2} s^{-1} as daytime measurements. Coefficients of the linear and nonlinear regressions were determined using Matlab® Statistics Toolbox®. A robust least squares (RLS) algorithm was used for all the linear regressions of this analysis. In contrast to the commonly used linear OLS algorithm, the RLS algorithm uses an iteratively re-weighted least squares algorithm, with the weights

of each iteration calculated by applying the bisquare function to the residuals from the previous iteration. The RLS algorithm gives lower weight to points that do not fit well and therefore the results are less sensitive to outliers in the data as compared with linear OLS algorithm. Because the RLS algorithm of Matlab® Statistics Toolbox® is not available for non-linear regressions, the Gauss-Newton OLS algorithm was used in all nonlinear regressions of this analysis. Detailed descriptions of the linear RLS and nonlinear OLS algorithms can be found at www.mathworks.com.

2.2.1 Obtaining $R_e - T_s$ relationships using nighttime NEE measurements

The value of u_{*th} for this stand was taken to be 0.3 m s^{-1} following the analysis of Morgenstern et al. (2004), and soil temperature at the 5-cm depth was selected as the temperature best used to predict ecosystem respiration following the analysis of Drewitt et al. (2002). Five methods were used to estimate nighttime ecosystem respiration (R_{en}).

Method 1 assumed an exponential relationship between R_{en} and T_s:

$$R_{en} = Ae^{BT_s} \qquad \text{exponential fit} \qquad (3)$$

Eq. (3) can also be written as $R_{en} = R_{10}Q_{10}^{(T_s-10)/10}$, where R_{10} is the standardized base rate of respiration at T_s = 10 °C, and Q_{10} is the temperature sensitivity coefficient that describes the relative increase in R_{en} for a 10 °C increase in T_s. Eq. (3) and the Q_{10} function are mathematically identical because $Q_{10} = e^{10B}$ and $R_{10} = AQ_{10}$. In Method 1, the empirical coefficients A and B were determined from the annual NEE_{u*} - T_s relationship using half-hourly fluxes and the nonlinear OLS algorithm.

Method 2 assumed a logistic relationship between R_{en} and T_s following Barr et al. (2004):

$$R_{en} = A/(1+e^{(T_s-10)/B}) + y_0 \qquad \text{logistic fit} \qquad (4)$$

where A, B and y_0 are empirical coefficients. Similar to Method 1, the three coefficients A, B and y_0 were determined from the annual NEE_{u*} - T_s relationship using half-hourly fluxes and the nonlinear OLS algorithm.

Method 3 used the logarithmic transformation of Eq. (3):

$$\ln R_{en} = \ln A + BT_s \qquad \text{logarithmic fit} \qquad (5)$$

In Method 3, the coefficients A and B were determined from the annual $\ln(NEE_{u*})$ - T_s relationship using half-hourly fluxes and the linear RLS algorithm. After the coefficients A and B were determined, they were used in the exponential form (i.e., Eq. 3) to calculate the half-hourly R_{en}.

Method 4 used the bin-averaged values of NEE_{u*} for every 100 half-hourly measurements of increased magnitude as was shown in Figure 2-1a. The coefficients A and B were then determined for Eq. (5) by linearly fitting the annual ln(bin-averaged NEE_{u*}) - T_s relationship with the linear RLS algorithm.

Method 5 used nightly averaged values of NEE_{u*} which were obtained by averaging acceptable half-hourly values of NEE_{u*} for each night. The minimum number required for the nightly averaging was 3. The coefficients A and B were determined using Eq. (5) by linearly fitting the annual ln(nightly averaged NEE_{u*}) - T_s relationship with the linear RLS algorithm.

Once the respective coefficients for the five methods were determined, they were used to calculate the half-hourly values of R_e for both calm and turbulent conditions, i.e., the original nighttime half-hourly NEE measurements made in turbulent conditions were not retained, but rather replaced by calculated R_e values in order to obtain an estimate of the annual total R_e. The rationale for replacing the measured NEE_u will be discussed later.

2.2.2 Obtaining $R_e - T_s$ relationships using daytime NEP measurements

In order to reduce the inhomogeneous distribution of σ^2 in the daytime NEP – Q_{t0} relationship (Figure 2-4), the MM model was modified by restricting it to low Q_{t0} conditions and assuming a linear relationship as follows:

$$NEP = \alpha Q_{t0} - R_{ed} + \varepsilon \qquad \text{LUE model} \qquad (6)$$

Eq. (6) will be referred to as the LUE (light use efficiency) model. If unspecified, the Q_{t0} interval for the LUE model is 0 – 300 μmol m^{-2} s^{-1} and the Q_{t0} interval for the MM model is 0 – 1800 μmol m^{-2} s^{-1}. Both models use daytime measurements only. The effect of using a daytime u_* threshold on the estimates of R_{ed} was tested for both the MM and LUE models using 15 days of data and advancing one day at a time (i.e., a 15-day moving window) and by removing the daytime half hourly NEP measurements made when $u_* < u_{*th}$ (u_{*th} = 0.3 m s^{-1}) conditions for increasing levels of Q_{t0}. Five levels of Q_{t0} (i.e., u_{*Q_0}, $u_{*Q_{50}}$, $u_{*Q_{100}}$, $u_{*Q_{200}}$, and $u_{*Q_{300}}$) were used for the daytime u_* screening. Taking the MM model as an example, $u_{*Q_{200}}$ denotes that the daytime half-hourly NEP measurements made when $u_* < 0.3$ m s^{-1} were removed if $Q_{t0} < 200$ μmol m^{-2} s^{-1}, and only the half-

hourly NEP measurements made when $u_* > 0.3$ m s^{-1} and $Q_{t0} < 200$ μmol m^{-2} s^{-1} and all the half-hourly NEP measurements made when $Q_{t0} > 200$ μmol m^{-2} s^{-1} regardless of their u_* values (i.e., all the daytime half-hourly NEE values associated with Q_{t0} of 200 - 1800 μmol m^{-2} s^{-1}) were used in the MM model fit to determine R_{ed}. $u_{*_{Q_0}}$ means that all daytime NEE values were used, i.e., no u_* screening. For the LUE model, $u_{*_{Q_{200}}}$ means that all the NEE measurements associated with $u_* < 0.3$ m s^{-1} when $Q_{t0} < 200$ μmol m^{-2} s^{-1} were removed, only the half-hourly NEE measurements made in $u_* > 0.3$ m s^{-1} when $Q_{t0} < 200$ μmol m^{-2} s^{-1} and all NEE measurements regardless of their u_* values when 200 μmol m^{-2} s^{-1} $< Q_{t0} < 300$ μmol m^{-2} s^{-1} were used. Note the total PAR range for the LUE model is $0 < Q_{t0} < 300$ μmol m^{-2} s^{-1} if not specified otherwise. The effect of the length of the regression periods on the estimates of R_{ed} was investigated by using moving windows of six different sizes (1-, 3-, 7-, 15-, and 30-days) with the daytime u_* filter of $u_{*_{Q_{200}}}$. All the moving windows in this analysis were started on January 1, 2001, and increased 1 day at a time. Therefore, for window sizes of longer than 1 day, the last window extended into 2002 (e.g., until January 29, 2002 for the last 30-day window). Both morning and afternoon data were used to determine the parameters in the MM and LUE models. Three different ranges of Q_{t0} (0 – 100, 0 – 200 and 0 –300 μmol m^{-2} s^{-1}) were tested for the LUE model using the 15-day moving window and daytime u_* filter of $u_{*_{Q_{200}}}$. The minimum number of daytime half-hourly NEP measurements used in the MM and LUE regressions was three. The estimates of R_{ed} for the MM and LUE models were determined using the nonlinear OLS and linear RLS algorithms, respectively. The value of T_s associated with each R_{ed} estimate is the average of the half-hourly values of T_s corresponding to the Q_{t0}

values used in the regression. The annual $R_{ed} - T_s$ relationships obtained using both the MM and LUE models were assumed to be exponential (i.e., $R_{ed} = Ae^{BT_s}$) and their corresponding coefficients A and B were determined using the logarithmic transformation of R_{ed} (i.e., $\ln R_{ed} = \ln A + BT_s$).

2.3 Results and discussions

2.3.1 $R_e - T_s$ relationships obtained using nighttime NEE measurements

As mentioned earlier, the annual nighttime $NEE_{u.}$ - T_s relationship does not have a common variance over the full range of T_s (Figure 2-1a). For example, one standard deviation in the bin averaged value of $NEE_{u.}$ at T_s = 1 °C was less than 2 μmol m^{-2} s^{-1}, but it increased to more than 8 μmol m^{-2} s^{-1} at T_s = 10 °C. In contrast, the values of one standard deviation in the annual $\ln(NEE_{u.}) - T_s$ relationship were very similar over the full range of T_s (Figure 2-1b). The effect of these variance distributions is shown in Figure 2-2. For T_s between 8 and 13 °C, the $R_{en} - T_s$ relationships obtained using the nonlinear OLS algorithm (Methods 1 and 2) gave the highest values of R_{en}, followed in order by the relationships obtained using the bin averaged and nightly averaged $NEE_{u.}$ (Methods 4 and 5), and the relationship obtained using logarithmically transformed half-hourly values of $NEE_{u.}$ (Method 3).

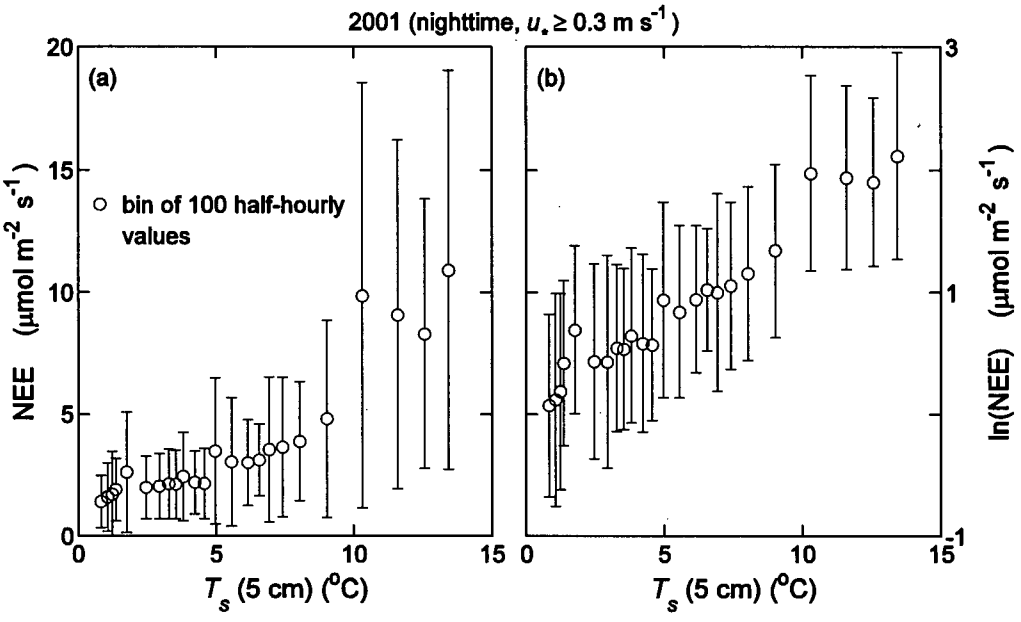

Figure 2-1. (a) The relationship between nighttime NEE measurements, representing nighttime ecosystem respiration (R_{en}), and soil temperature (T_s) at the 5-cm depth. (b) The relationship between the logarithmically transformed NEE and T_s. In both plots, the circles are bin averages of 100 half-hourly values, and the vertical bars are ± 1 standard deviation. The assumption of IID $N(0,\sigma^2)$ was met by doing the logarithmic transformation of the half-hourly nighttime NEE. The half-hourly NEE measurements are from 2001 with $u_* \geq 0.3$ m s^{-1} (i.e., NEE_{u_*}) (n = 2472).

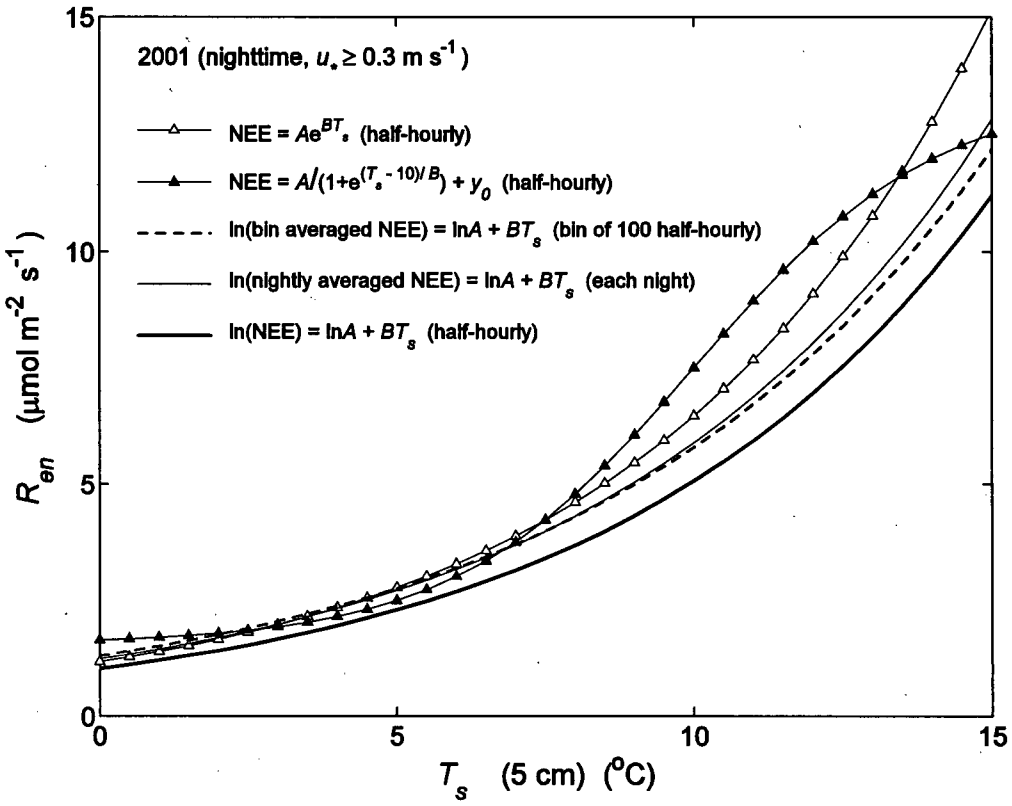

Figure 2-2 .The R_{en} – T_s relationships obtained using five different nighttime methods (see text for details).

The order of these relationships shown in Figure 2-2 coincided with the severity of the violation of IID $N(0,\sigma^2)$ (i.e., in this case, the heterogeneous distribution of σ^2). The variance in the original half-hourly NEE_{u*} (used in Methods 1 and 2) was most heterogeneous (Figure 2-1a), followed by the bin averaged and nightly averaged NEE_{u*} (used in Methods 4 and 5) since the variance was partly reduced by the averaging. The heterogeneity in the logarithmically transformed half-hourly values of NEE_{u*} (used in Method 3) was very small (Figure 2-1b). The heterogeneous distribution of σ^2 steepened the $R_{en} - T_s$ relationship because the large NEE_{u*} values at high T_s had larger residuals than the smaller NEE_{u*} values at low T_s (Figure 2-1a). The reason for this is in the OLS algorithm, the influence of the large NEE_{u*} values being magnified because their large residuals were squared, leading to incorrect higher estimates of R_{en} than otherwise. The R_{en} values obtained using the $R_{en} - T_s$ relationships from the bin and nightly averaged NEE_{u*} (Methods 4 and 5), even with the logarithmic transformation of the averages, were higher than those obtained using the $R_{en} - T_s$ relationship from the original half-hourly NEE_{u*} with the logarithmic transformation (Method 3). This was because the effect of the large NEE_{u*} values had already gone into the averages, and could not be undone using the logarithmic transformation "after the fact". The coefficients (e.g., A and B) obtained using the 5 methods are given in Table 2-1.

Table 2-1. Coefficients obtained for the five nighttime methods for DF49 in 2001 (see Figure 2-2 and text for details). Units for A and B are μmol m^{-2} s^{-1} and $°C^{-1}$, respectively. Units for y_0 and RMSE are both μmol m^{-2} s^{-1}.

Methods	A	B	y_0	R^2	RMSE	n
(1) $NEE = Ae^{BT_s}$ (half-hourly)	1.19	0.17	----	0.40	4.02	2472
(2) $NEE = A/(1+e^{(T_s-10)/B}) + y_0$ (half-hourly)	11.88	-2.02	1.57	0.39	4.09	2472
(3) $\ln(NEE) = \ln A + BT_s$ (half-hourly)	1.04	0.16	----	0.36	4.12	2472
(4) ln(bin averaged NEE) $= \ln A + BT_s$ (bin of 100 half-hourly)	1.31	0.15	----	0.82	0.92	24
(5) ln(nightly averaged NEE) $= \ln A + BT_s$ (each night)	1.25	0.16	----	0.51	3.41	234

They were used to calculate R_e values for all daytime and nighttime half hours, including replacing the original nighttime half-hourly values of NEE_{u*} with model-calculated R_e. On an annual basis, the summation of the half-hourly NEE_{u*} replacements was virtually the same as the summation of the original measured half-hourly NEE_{u*} for the exponential fit (Method 1) ($\sum(NEE_{u*\,mod} - NEE_{u*}) =$ -1.82 g C m^{-2}, where $NEE_{u*\,mod}$ denotes model-calculated NEE_{u*} replacements, n = 2472) and the logistic fit (Method 2) ($\sum(NEE_{u*\,mod} - NEE_{u*})$ = -0.01 g C m^{-2}). In theory, $\sum(NEE_{u*\,mod} - NEE_{u*})$ should be zero because it is the summation of all the residuals in the above two nonlinear OLS fits. The difference, however, became very large, i.e., $\sum(NEE_{u*\,mod} - NEE_{u*})$ = -47.34 g C m^{-2}, for

the logarithmic fit (Method 3) (Figure 2-2). This was because the logarithmic fit was obtained as a least squares fit to the transformed $\ln(\mathrm{NEE}_{u*})$ – T_s relationship (Figure 2-1b), rather than the untransformed NEE_{u*} - T_s relationship (Figure 2-1a).

In our previous analysis (Morgenstern et al. 2004) for this stand and many other studies (e.g., Goulden et al. 1996a, Flanagan and Johnson 2005), the original half-hourly measurements of NEE_{u*} are retained in the dataset, and the model-calculated R_e values were used only to replace nighttime half-hourly NEE measurements made in calm conditions and to estimate daytime ecosystem respiration. However, this practice is questionable. The nighttime half-hourly NEE measurements made even in turbulent conditions should be regarded as discrete (and limited number of) samples of the true ecosystem respiratory signal, and they generally do not follow a normal distribution (i.e., existence of a few extremely large values of NEE_{u*}, for example, approximately 2% of the NEE_{u*} values are greater than 50 μmol m^{-2} s^{-1}) (Figure 2-1a). In view of the IID $N(0,\sigma^2)$ violation, the erratic behaviour inherent in the nighttime half-hourly NEE measurements (samples) made in turbulent conditions should be "logarithmically corrected" to reflect the real behaviour of whole ecosystem respiration (population).

2.3.2 $R_e - T_s$ relationships obtained using daytime NEP measurements

The effect of the daytime $u*$ filter applied to different ranges of Q_{t0} on the $R_{ed} - T_s$ relationships obtained using both the MM and LUE models is shown in Figure 2-3. The pattern of the effect of the daytime $u*$ filter for both the MM and LUE models was similar (compare Figure 2-3a with Figure 2-3b). Note the large difference between the MM and LUE relationships.

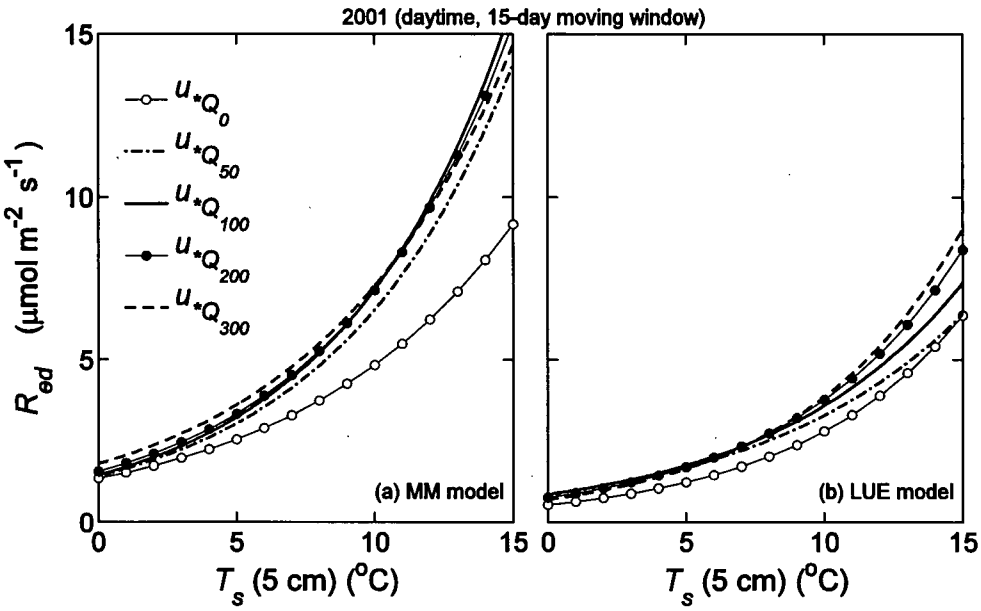

Figure 2-3. The $R_{ed} - T_s$ relationships obtained using the MM and LUE models with the application of a daytime u_* filter to increasing ranges of Q_{t0}. The total Q_{t0} ranges for the MM model and LUE model are 0 – 1800 μmol m^{-2} s^{-1} and 0 – 300 μmol m^{-2} s^{-1}, respectively. u_{*Q_0}, $u_{*Q_{50}}$, $u_{*Q_{100}}$, $u_{*Q_{200}}$, and $u_{*Q_{300}}$ denote that the daytime half-hourly NEP measurements made in calm conditions (i.e., $u_* < 0.3$ m s^{-1}) were removed if $Q_{t0} < 0$ μmol m^{-2} s^{-1}, $Q_{t0} < 50$ μmol m^{-2} s^{-1}, $Q_{t0} < 100$ μmol m^{-2} s^{-1}, $Q_{t0} < 200$ μmol m^{-2} s^{-1}, and $Q_{t0} < 300$ μmol m^{-2} s^{-1}, respectively. For example, $u_{*Q_{200}}$, in the case of the MM model, means removing low u_* daytime NEP measurements if $Q_{t0} < 200$ μmol m^{-2} s^{-1} and only the high u_* NEP measurements associated with $Q_{t0} < 200$ μmol m^{-2} s^{-1} and all the NEP measurements made when $Q_{t0} > 200$ μmol m^{-2} s^{-1} (regardless of their u_* values) are used in the MM model fit to determine R_{ed}. In the case of the LUE model, data for Q_{t0} between the upper end of the range and 300 μmol m^{-2} s^{-1} were not u_* screened e.g., for $u_{*Q_{100}}$ values for $100 < Q_{t0} < 300$ μmol m^{-2} s^{-1} were not screened. u_{*Q_0} means no daytime u_* screening was applied in both the MM and LUE models, because all daytime NEP data are associated with $Q_{t0} > 0$ μmol m^{-2} s^{-1}.

The coefficients for the $R_{ed} - T_s$ relationships in Figure 2-3 are given in Table Table 2-2.

Table 2-2. Coefficients obtained for the MM (Q_{t0}: 0 – 1800 μmol m^{-2} s^{-1}) and LUE (Q_{t0}: 0 – 300 μmol m^{-2} s^{-1}) models with the application of different daytime $u*$ filters for DF49 in 2001 (see Figure 2-3). Units for A and B are μmol m^{-2} s^{-1} and $°C^{-1}$, respectively. The values of A and B were determined using $\ln R_{ed} = \ln A + BT_s$ (see Eq. (5)).

	MM model		LUE model	
	A	*B*	*A*	*B*
u_{*Q_0}	1.34	0.13	0.54	0.16
$u_{*Q_{50}}$	1.41	0.15	0.87	0.13
$u_{*Q_{100}}$	1.45	0.16	0.85	0.14
$u_{*Q_{200}}$	1.55	0.15	0.76	0.16
$u_{*Q_{300}}$	1.79	0.14	0.70	0.17

The R_{ed} values obtained using the annual $R_{ed} - T_s$ relationships were lowest when no daytime $u*$ screening (i.e., u_{*Q_0}) was applied, but the $R_{ed} - T_s$ relationships quickly stabilized when $u_{*Q_{100}}$ was used, presumably because by that time of the day the convective boundary layer (CBL) was well established. To be conservative, the daytime $u*$ filter of $u_{*Q_{200}}$ was applied to all the subsequent analysis.

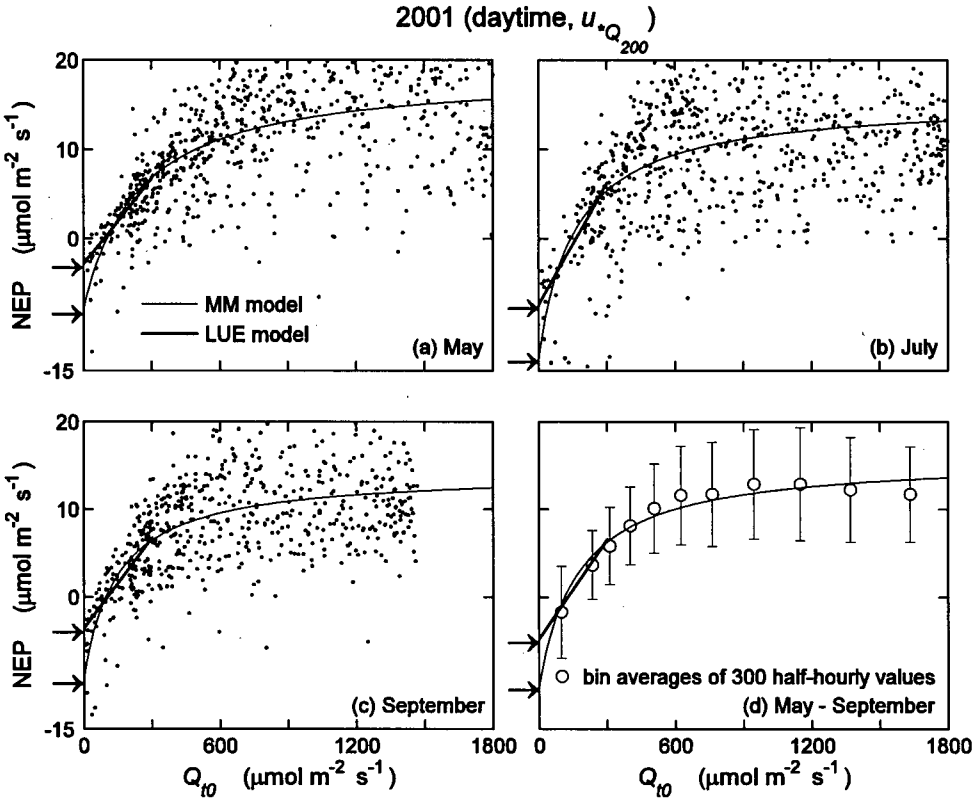

Figure 2-4. Daytime NEP – PAR relationships for different months of 2001. The dots in (a) – (c) are the half-hourly NEP measurements. The circles in (d) are the bin averages of 300 half-hourly NEP measurements and the vertical bars denote ± 1 standard deviation. The thin and thick lines are the respective fits obtained using the MM and LUE models to the half-hourly NEP measurements (not to the bin averages as shown in (d)). The Q_{t0} ranges for the MM model and LUE model are 0 – 1800 μmol m^{-2} s^{-1} and 0 – 300 μmol m^{-2} s^{-1}, respectively.

The reason for the lower values of R_{ed} obtained using the LUE model compared to those using the MM model becomes clear in the analysis of NEP vs Q_{t0} plots shown in Figure 2-4, which shows that the MM model had consistently more negative intercepts than the LUE model. As mentioned in the Introduction of this chapter, the ε's for the MM fit did not meet the IID $N(0,\sigma^2)$ assumption. For non-limiting values of Q_{t0} (e.g., Q_{t0} > 1500 μmol m^{-2} s^{-1}), a higher fraction of the diffuse PAR component led to higher canopy photosynthesis and consequently higher NEP (see Chapter 4 for details, e.g., Figure 4-7a and Figure 4-8a). Therefore, the error bars in Figure 2-4d were not completely random, because positive error bars tended to be associated with cloudy conditions and negative error bars tended to be associated with clear conditions. The coefficients of the MM and LUE fits shown in Figure 2-4 are given in Table 2-3.

Table 2-3. Coefficients of the MM (Q_{t0}: 0 – 1800 μmol m^{-2} s^{-1}) (i.e., Eq. (2)) and LUE (i.e., Eq. (6)) fits for the different months shown in Figure 2-4. Units for α and A_{max} are μmol (CO_2) μmol^{-1} (quanta) and μmol m^{-2} s^{-1}, respectively.

	MM model			LUE model	
	α	A_{max}	R_{ed}	α	R_{ed}
May	0.11	27.06	8.22	0.03	2.93
July	0.18	29.16	13.55	0.05	7.53
September	0.16	23.61	9.40	0.03	3.61
May – September	0.15	26.04	10.11	0.04	4.80

Also as a result of the effect of diffuse PAR, the overall daytime NEP – Q_{t0} relationship was more parabolic than hyperbolic with a peak in NEP at Q_{t0} approximately between 1000 – 1200 μmol m^{-2} s^{-1} where the amount of diffuse PAR was highest.

However, the hyperbolic nature of the MM fit forced it to give the highest estimates of NEP for the highest values of Q_{t0} (e.g., Q_{t0} approximately of 1800 μmol m^{-2} s^{-1}), therefore the MM fit underestimated NEP for Q_{t0} between 500 – 1200 μmol m^{-2} s^{-1}, and overestimated NEP for Q_{t0} > 1200 μmol m^{-2} s^{-1}. Because the frequency of the occurrence of Q_{t0} greater than 1200 μmol m^{-2} s^{-1} was significantly lower than that for Q_{t0} between 500 – 1200 μmol m^{-2} s^{-1}, as indicated by the horizontal distance between the bin averages in Figure 2-4d, the overestimation of NEP for Q_{t0} greater than 1200 μmol m^{-2} s^{-1} did not fully balance the underestimation of NEP for Q_{t0} between 500 – 1200 μmol m^{-2} s^{-1}. The nonlinear OLS algorithm requires the summation of all residuals to be zero, i.e., overestimation + underestimation = 0. Therefore, the OLS algorithm for the MM fit had to overestimate NEP for a large part of Q_{t0} less than 500 μmol m^{-2} s^{-1} in order to compensate for the lack of overestimation at Q_{t0} greater than 1200 μmol m^{-2} s^{-1}, leading to an incorrect higher estimate of R_{ed} (more negative intercept).

The larger the width of the moving windows, the more cloudy and clear conditions are likely to be included into the MM fit, thus increasing the parabolic tendency for the NEP – Q_{t0} relationship and the severity of the violation of IID N(0, σ^2) assumption. Figure 2-5a shows the dramatic effect of the moving window width on the R_{ed} – T_s relationships obtained using the MM model. As it was expected, the wider the moving windows (regression periods), the more serious the violation of the IID N(0, σ^2) assumption, and consequently the more incorrect enhancement for the R_{ed} – T_s curves. For example, at T_s = 15 °C, the R_{ed} value obtained using the 30-day moving window was highest, followed by that obtained using the 15-day moving window, … and that obtained using a 1-day moving window (i.e., on a daily basis) was lowest (Figure 2-5a). In

contrast, the $R_{ed} - T_s$ relationships obtained using the LUE model was almost independent of the window width (Figure 2-5b), indicating its conformity to the IID N(0, σ^2) assumption. The 15-day moving window was chosen for all the subsequent analysis of both the MM and LUE models, because the $R_{ed} - T_s$ relationships tended to stabilize at moving window width of 15-days (Figure 2-5).

Coefficients for the $R_{ed} - T_s$ relationships obtained using the MM and LUE models with different moving windows are given in Table 2-4. As a result of the incorrect enhancement of the $R_{ed} - T_s$ curves obtained using the MM model, the value of A for the MM model was more than twice that for the LUE model. However, the value of B for the LUE model was slightly higher than that for the MM model.

Table 2-4. Coefficients obtained for the MM (Q_{t0}: 0 – 1800 μmol m^{-2} s^{-1}, and $u_{*_{Q_{200}}}$) and LUE (Q_{t0}: 0 – 300 μmol m^{-2} s^{-1}, and $u_{*_{Q_{200}}}$) models with different moving window for DF49 in 2001 (see Figure 2-5). Units for A and B are μmol m^{-2} s^{-1} and $°C^{-1}$, respectively. The values of A and B were determined using $\ln R_{ed} = \ln A + BT_s$ (see Eq. (5)).

	MM model		LUE model	
	A	*B*	*A*	*B*
1-day moving window	1.30	0.14	0.76	0.17
3-day moving window	1.38	0.15	0.60	0.19
7-day moving window	1.51	0.15	0.62	0.18
15-day moving window	1.55	0.15	0.76	0.16
30-day moving window	1.51	0.16	0.75	0.16

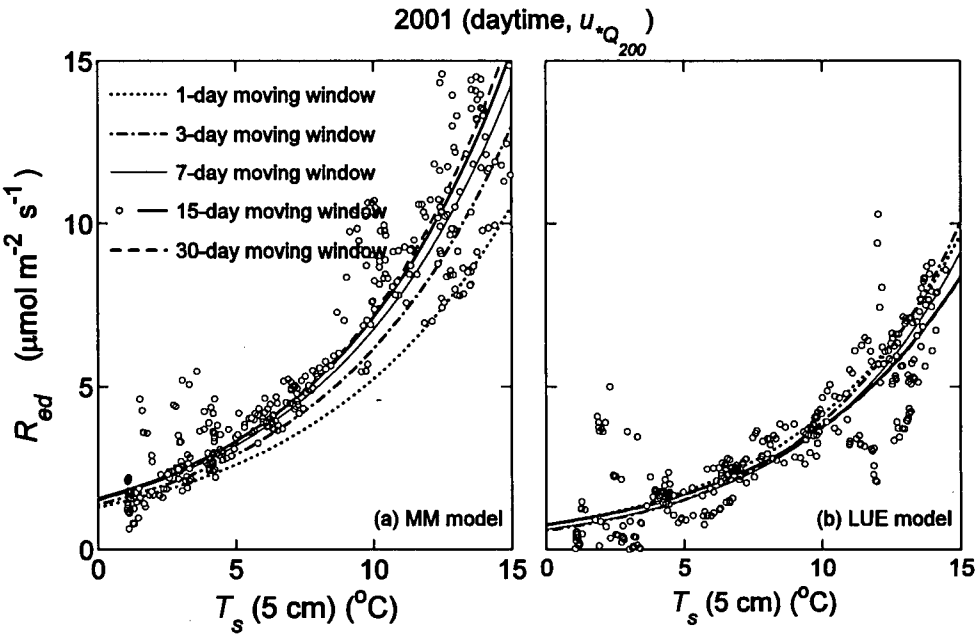

Figure 2-5. The annual $R_{ed} - T_s$ relationships obtained using the MM and LUE models with moving windows of different sizes for 2001. All the moving windows were increased one day at a time and all the fits were made with the logarithmic transformation of R_{ed}. The total Q_{t0} ranges for the MM model and LUE model are 0 – 1800 μmol m^{-2} s^{-1} and 0 – 300 μmol m^{-2} s^{-1}, respectively.

2.3.3 Comparison of the $R_e - T_s$ relationships obtained using the nighttime and daytime methods

Figure 2-6 compares the $R_{ed} - T_s$ relationships obtained using the LUE model for different ranges of Q_{t0} along with the nighttime log transformed R_{en} values. As the range of Q_{t0} increased, the values from the $R_{ed} - T_s$ relationships decreased relative to the $R_{en} - T_s$ relationship, i.e., for a given T_s, the corresponding R_{ed} obtained decreased as the range of Q_{t0} increased. But the decrease in R_e from darkness to Q_{t0} of 0 – 100 μmol m^{-2} s^{-1} was larger than the subsequent decreases in R_e for equal Q_{t0} ranges (e.g., decrease in R_e from Q_{t0} of 0 – 200 μmol m^{-2} s^{-1} to Q_{t0} of 0 – 300 μmol m^{-2} s^{-1}). Wohlfahrt et al. (2005b) surveyed many leaf-level experimental results and showed that the light inhibition on foliar respiration initially falls fast with increasing light and then stabilizes at higher PAR levels. The $R_{ed} - T_s$ relationship obtained with the Q_{t0} range of 0 – 300 μmol m^{-2} s^{-1} possibly best represents the canopy daytime dark respiration, because (1) inclusion of higher values of Q_{t0} risks violating the statistical assumption of IID $N(0, \sigma^2)$ as shown in Figure 2-4, (2) lower levels of Q_{t0} may not have sufficient daytime influence since the majority of the shaded leaves deep in the canopy are still in darkness, and (3) the light inhibition on foliar respiration is saturated at Q_{t0} of 300 μmol m^{-2} s^{-1} at leaf-level for the majority of the plant species reported in the literature (e.g., Brooks and Farquhar 1985, Villar et al. 1994, Atkin et al. 2000b).

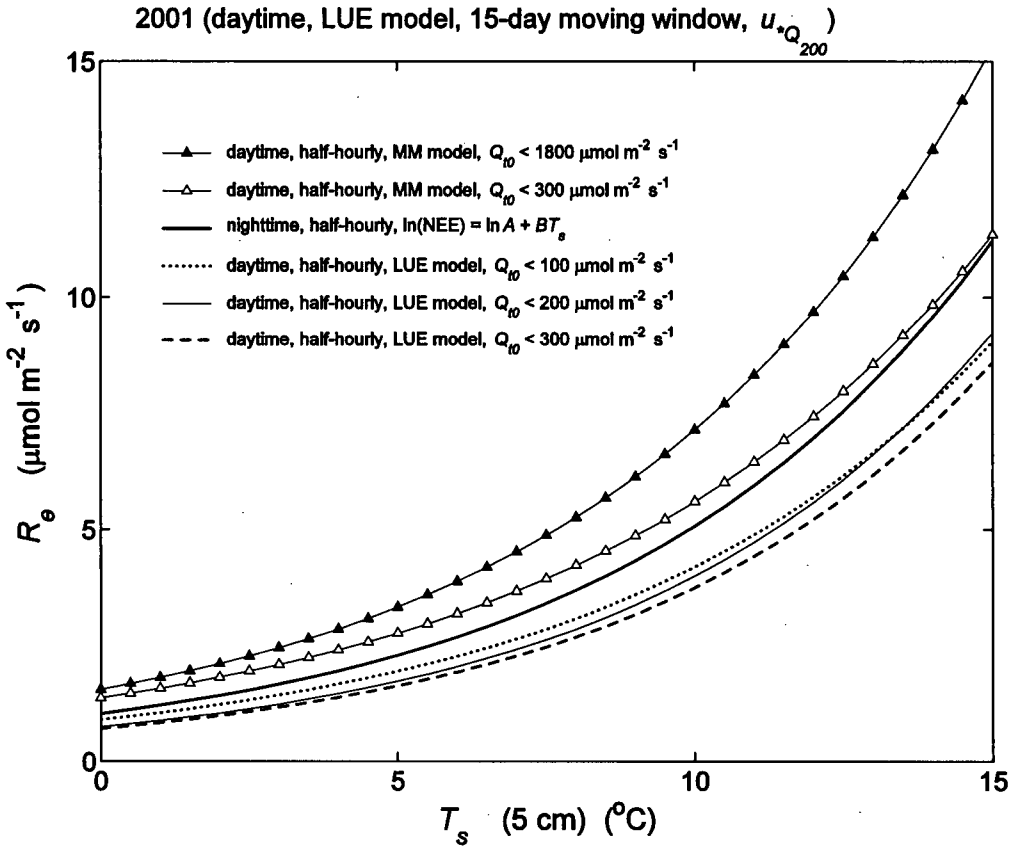

Figure 2-6. The $R_e - T_s$ relationships obtained using the LUE model with three Q_{t0} ranges: Q_{t0} < 100 μmol m^{-2} s^{-1} (dotted line), Q_{t0} < 200 μmol m^{-2} s^{-1} (thin line) and Q_{t0} < 300 μmol m^{-2} s^{-1} (dashed line). Also shown are the $R_e - T_s$ relationships obtained using the MM model with Q_{t0} < 1800 μmol m^{-2} s^{-1} (line with solid triangles) and Q_{t0} < 300 μmol m^{-2} s^{-1} (line with empty triangles) and the $R_e - T_s$ relationship obtained using the nighttime logarithmic fit (the thick line). In all the daytime $R_e - T_s$ relationships, 15-day moving window and daytime $u*$ filter of $u_{*Q_{200}}$ were used.

Also shown in Figure 2-6 are the $R_e - T_s$ relationships obtained using the MM model with Q_{t0} of 0 – 1800 μmol m^{-2} s^{-1} and Q_{t0} of 0 – 300 μmol m^{-2} s^{-1}. As discussed earlier, the violation of IID N(0, σ^2) assumption by the MM model (see also Figure 2-4) likely resulted in the former $R_e - T_s$ relationship being much higher than that obtained using the corresponding LUE model with Q_{t0} of 0 – 300 μmol m^{-2} s^{-1}. The r^2 and RMSE obtained for all the 15-day moving windows using the MM and LUE models (both with Q_{t0} of 0 – 300 μmol m^{-2} s^{-1}) are 0.5434 ± 0.1568, 0.5279 ± 0.1556, and 2.7821 ± 1.3134 μmol m^{-2} s^{-1}, 2.8205 ± 1.3001 μmol m^{-2} s^{-1}, respectively. Therefore, it is difficult to judge the merits of the MM and LUE models purely from a statistical point of view. The $R_e - T_s$ relationship obtained using the MM model with Q_{t0} of 0 –300 μmol m^{-2} s^{-1} is also higher than the nighttime $R_e - T_s$ relationship obtained using the logarithmic transformation of nighttime half-hourly NEE (see Figure 2-1b and Figure 2-2). Thus the $R_e - T_s$ relationship obtained using the MM model even with the relatively narrow Q_{t0} range of 0 – 300 μmol m^{-2} s^{-1} is unlikely to be correct because the foliar biomass is quite large for this Douglas-fir stand (e.g., LAI ≈ 8) and as will be discussed later, the light inhibition on foliar dark respiration is likely to result in the daytime $R_e - T_s$ relationship being lower than the nighttime $R_e - T_s$ relationship.

2.3.4 Estimates of the annual totals of NEP, R_e and P using the nighttime and daytime methods

Figure 2-7 shows the annual cumulative NEP calculated using different $R_e - T_s$ relationships. The annual total NEP obtained using the nighttime exponential fit was 194 g C m^{-2} lower than that obtained using the nighttime logarithmic fit, and was 376 g C m^{-2}

lower than that obtained using the LUE model with Q_{t0} range of 0 – 300 μmol m^{-2} s^{-1}. The annual NEP obtained using the MM model with the 15-day moving window was approximately half of that obtained using the nighttime exponential fit.

In view of the violation of IID N(0, σ^2) assumption, the correct nighttime $R_e - T_s$ relationship in this analysis was assumed to be derived from the nighttime annual half-hourly NEE_u - T_s relationship using the logarithmic fit (Method 3), and the correct daytime $R_e - T_s$ relationship was assumed to be derived from the daytime NEP – Q_{t0} relationship using the LUE model with the 15-day moving window and Q_{t0} of 0 – 300 μmol m^{-2} s^{-1}. Relationships obtained by nighttime methods other than the logarithmic fit and the daytime MM fit violated the IID N(0, σ^2) assumption, and therefore were considered to be incorrect.

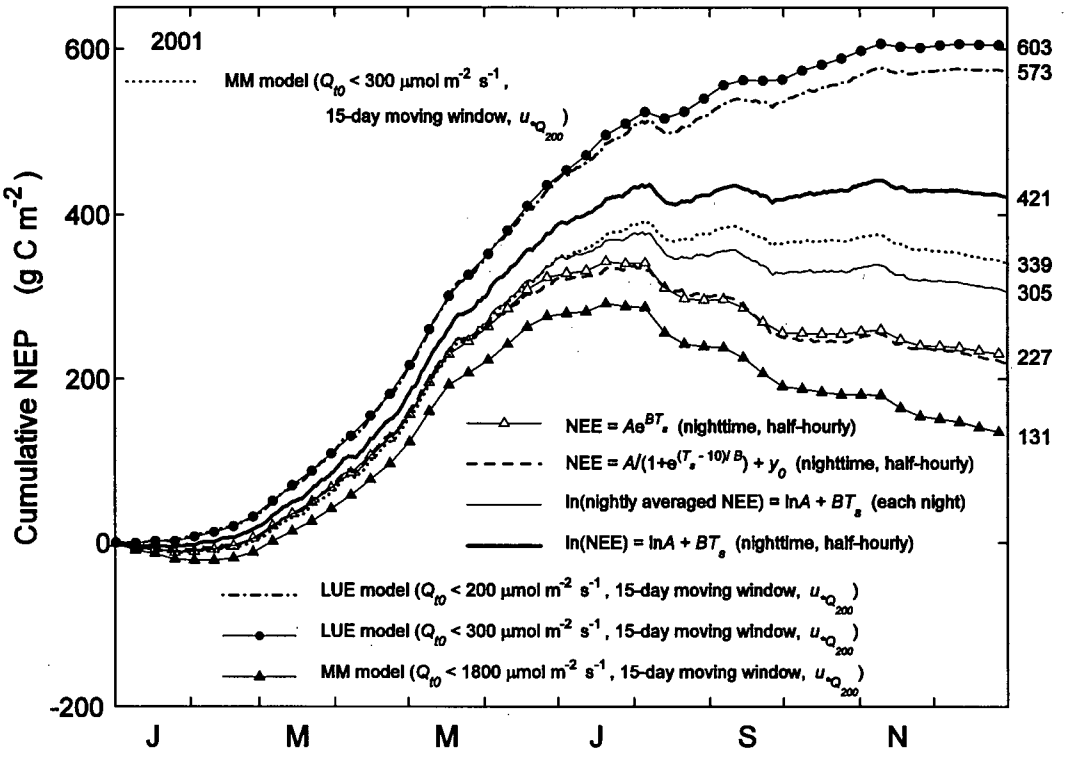

Figure 2-7. The annual cumulative NEP for 2001 obtained using different nighttime and daytime derived $R_e - T_s$ relationships. The LUE and MM model use only daytime half-hourly NEP measurements.

The annual totals of R_e obtained using the exponential and logistic fits were almost identical (Table 2-5), because both used the nonlinear OLS algorithm. The annual total R_e obtained using the nighttime logarithmic fit was 464 g C m^{-2} lower than that obtained using the nighttime exponential fit, but was 415 g C m^{-2} higher than that obtained using the LUE model with Q_{t0} of 0 – 300 μmol m^{-2} s^{-1}. The annual total R_e obtained using the MM model with the 15-day moving window was 1070 g C m^{-2} higher than that obtained using the LUE model with Q_{t0} of 0 – 300 μmol m^{-2} s^{-1}, and was even 191 g C m^{-2} higher than that obtained using the nighttime exponential fit.

Table 2-5. Annual totals of the R_e and P obtained using different annual nighttime and daytime $R_e - T_s$ relationships (see Figure 2-7 and Figure 2-8 for details). Only the nighttime half-hourly NEE measurements made in conditions where $u_* \geq 0.3$ m s^{-1} were used in the nighttime methods. The daytime half-hourly NEP measurements made in conditions where $u_* < 0.3$ m s^{-1} and $Q_{t0} < 200$ μmol m^{-2} s^{-1} were not used in the MM and LUE fits, and only the rest of the daytime data (i.e., not screened by the daytime u_* filter) were used in both models to determine R_{ed}.

g C m^{-2} yr^{-1}	R_e			P
Nighttime and daytime $R_e - T_s$ relationships	Nighttime	Daytime	Total	
NEE = Ae^{BT_s} (nighttime, half-hourly)	900	1186	2086	2313
NEE = $A/(1+e^{(T_s-10)/B}) + y_0$ (nighttime, half-hourly)	909	1172	2081	2299
ln(nightly averaged NEE) = $\ln A + BT_s$ (each night)	822	1061	1883	2188
ln(NEE) = $\ln A + BT_s$ (nighttime, half-hourly)	706	916	1622	2043
LUE model (Q_{t0}: 0 – 200 μmol m^{-2} s^{-1}, 15-day moving window, $u_{*_{Q_{200}}}$)	555	729	1284	1856
LUE model (Q_{t0}: 0 – 300 μmol m^{-2} s^{-1}, 15-day moving window, $u_{*_{Q_{200}}}$)	525	682	1207	1809
MM model (Q_{t0}: 0 – 1800 μmol m^{-2} s^{-1}, 15-day moving window, $u_{*_{Q_{200}}}$)	997	1280	2277	2407
MM model (Q_{t0}: 0 – 300 μmol m^{-2} s^{-1}, 15-day moving window, $u_{*_{Q_{200}}}$)	788	993	1781	2120
Best estimates in this analysis	706	682	1388	1809

In this analysis, the correct annual total of nighttime and daytime R_e was assumed to be derived from the nighttime logarithmic fit and daytime LUE fit, respectively. Therefore, the annual total of R_e for 2001 was 706 (nighttime) + 682 (daytime) = 1388 g C m^{-2}.

The annual R_e obtained using the LUE fit was approximately 75% of that obtained using the nighttime logarithmic fit, indicating a 25% reduction in R_e possibly as a result of the light inhibition on foliar respiration. Our soil (Jassal et al. 2005) and leaf chamber (unpublished) measurements indicated that the total foliar respiration of this closed canopy (LAI ≈ 8) was approximately 50% of the total R_e, and thus the 25% reduction in R_e suggested a 50% reduction for leaf-level foliar respiration in light relative to that in darkness. Interestingly, Gilbert Ethier at the University of Victoria (personal communication) found that leaf-level foliar respiration for the Douglas-fir shoots in the light was 50% of that in the darkness when the foliar respiration in the light was obtained using the Laisk method (see Brooks and Farquhar 1985). The 50% reduction of leaf-level respiration in light was in the middle of the published reduction range, i.e., 20 – 100% (e.g., Atkin et al. 1997, Brooks and Farquhar 1985, Villar et al. 1994, Shapiro et al. 2004). The best estimate of R_e in this analysis (i.e., 1388 g C m^{-2}) was approximately 14% less than that obtained using the nighttime logarithmic fit (i.e., 1622 g C m^{-2}) (no reduction for nighttime annual R_e). The 14% reduction in annual total R_e agreed very well with what has been used in other studies, such as 15% reduction hypothesized for European forests (Janssens et al. 2001), and 8 – 13% reduction modeled for a mountain meadow (Wohlfahrt et al. 2005b).

Figure 2-8 shows the seasonal variation of P obtained using the nighttime and daytime $R_e - T_s$ relationships shown in Figure 2-7. The discrepancy in the monthly totals of P obtained using the different $R_e - T_s$ relationships became larger with increasing T_s. The annual total of daytime NEP was directly measured using the EC system (i.e., 1127 g C m^{-2} for 2001), so the difference in P for the different $R_e - T_s$ relationships followed that for the R_e (Table 2-1). The significantly different curves in Figure 2-8 demonstrates the challenges in validating the process-based models such as C-CLASS (Arain et al. 2002) using EC derived canopy photosynthesis.

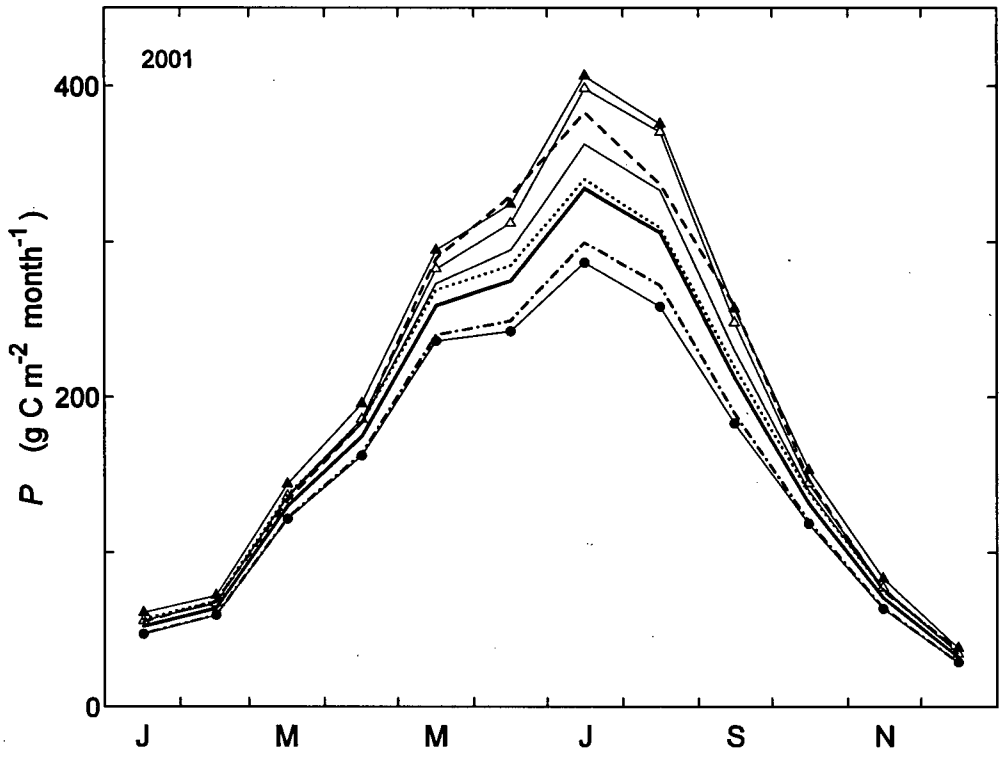

Figure 2-8. Monthly totals of P for 2001 obtained using different nighttime and daytime derived $R_e - T_s$ relationships (see Figure 2-7 for the legend).

2.4 Conclusions

(1) Using a nonlinear OLS algorithm to fit nighttime NEE_{u*} - T_s relationship violates the statistical IID $N(0,\sigma^2)$ assumption, because the variability in half-hourly NEE_{u*} markedly increases with T_s. The $R_e - T_s$ relationships obtained using the nonlinear OLS algorithm are strongly influenced by the severity of the violation of IID N(0, σ^2) and therefore are likely unreliable and incorrect. In comparison with other approaches (e.g., exponential fit, bin and nightly averaging), the logarithmic transformation of the half-hourly NEE_{u*} (i.e., $\ln(NEE_{u*}) = \ln A + BT_s$) best meets the IID N(0, σ^2) requirements. The annual R_e obtained for 2001 using the logarithmic fit was 464 g C m^{-2} lower than that obtained using the exponential fit.

(2) When calculating the annual total nighttime respiration, half-hourly NEE measurements at night made in turbulent conditions (i.e., NEE_{u*}) should be replaced by the estimates of R_e calculated using the logarithmic fit, because the half-hourly measurements of NEE_{u*} are discrete (and limited) samples of ecosystem respiration and generally do not follow a normal distribution. The statistical distribution of the NEE_{u*} measurements (samples) should be "logarithmically corrected" to meet the IID N(0, σ^2) requirement and to better represent the whole ecosystem respiration (population). Replacement of the original measured NEE_{u*} (n = 2472) with R_e obtained using the logarithmic fit led to a significant increase in the annual NEP (e.g., by 47 g C m^{-2} for 2001).

(3) The estimates of daytime R_e obtained by using the Michaelis-Menten equation to fit daytime NEP – Q_{t0} relationship (for the almost full range of PAR values, i.e., 0-1800 μmol m^{-2} s^{-1}) are likely overestimated, because (1) the estimates are strongly influenced by the moving window widths used as a result of the serious violation of IID N(0, σ^2) assumption in using the Michaelis-Menten fit and (2) they are significantly larger than log transformed nighttime values. Even restricting the Q_{t0} range to 0-300 μmol m^{-2} s^{-1} resulted in R_e values greater than predicted using the nighttime log transformed relationship.

(4) Using the LUE model to fit daytime NEP – Q_{t0} relationship meets the IID N(0, σ^2) assumption, and the obtained daytime R_e – T_s relationships are virtually independent of the widths of the moving windows. However, the main uncertainty in using the LUE model is the selection of the Q_{t0} ranges. In this analysis, the Q_{t0} of 0 – 300 μmol m^{-2} s^{-1} was assumed to be the Q_{t0} range from which the intercepts of the LUE regressions were most representative of daytime R_e.

(5) The annual daytime R_e obtained using the LUE model (i.e., the LUE model with 15-day moving window and Q_{t0} of 0 – 300 μmol m^{-2} s^{-1}) was approximately 25% lower than that obtained by applying the nighttime annual NEE_{u*} - T_s relationship (with the logarithmic transformation) to daytime. The 25% reduction was likely caused by light inhibition of ecosystem foliar respiration.

3 Comparison of Different Algorithms for Partitioning Net Ecosystem Exchange into Its Component Fluxes: Ecosystem Photosynthesis and Respiration

3.1 Introduction

In order to understand the effect of environmental and biotic variables on ecosystem assimilatory and respiratory processes, it is necessary to partition the half-hourly values of NEE (NEE = R_e – P) into its component fluxes: R_e (ecosystem respiration) and P (canopy or ecosystem photosynthesis). As discussed in Chapter 2, the simplest and most commonly used algorithm is to develop an annual relationship between NEE_{u*} and T_s, and then use it to calculate both nighttime and daytime half-hourly values of R_e (e.g., Goulden et al. 1996b, Morgenstern et al. 2004). NEE_{u*} denotes nighttime half-hourly NEE measurements made in turbulent conditions (i.e., $u* > u*_{th}$, a threshold value of $u*$) and T_s is the soil temperature at a shallow depth. One implicit assumption in using the annual NEE_{u*} - T_s relationship to estimate half-hourly R_e is that R_e is only a function of T_s. This underlying assumption is rarely met in any natural ecosystems. Plant stands, especially the grasslands (e.g., Flanagan and Johnson 2005) and deciduous forests (e.g., Barr et al. 2004), are usually very dynamic, with other plant and environmental factors affecting R_e. Lee et al. (1999) observed significant hysteresis in the annual $R_e - T_s$ relationship for a temperate deciduous forest, which probably was caused by the seasonality of soil temperature wave penetration and litter input. There is increasing evidence that the temperature sensitivity of respiration is strongly influenced by soil

moisture (Reichstein et al. 2002b, Xu and Baldocchi 2004, Flanagan and Johnson 2005). R_e has also been positively related to P (e.g., Janssens et al. 2001, Hogberg et al. 2001, Bowling et al. 2002, Scott-Denton et al. 2005, Tang et al. 2005). In addition, there are reports of seasonal acclimation of R_e to soil temperature (Atkin et al. 2000a, Luo et al. 2001, Kirschbaum 2004). The complex interactions between the factors controlling R_e have hindered the development of mechanistic models for predicting ecosystem respiration (Flanagan and Johnson 2005). For example, the rapid and transient response of R_e to rainfall, especially after a relatively dry period, (Irvine and Law 2002, Lee et al. 2004, Xu and Baldocchi 2004, Jassal et al. 2005) cause the conventional models of soil respiration (e.g., Bunnell et al. 1977) to fail. Furthermore, it has proved to be extremely difficult even to formulate quantitative relationships between R_e and its controlling factors, such as the interaction between R_e and P.

In order to account for the effect of other factors on R_e but without developing the quantitative relationships, Falge et al. (2002) used a 30-day moving window technique to stepwise estimate half-hourly values of R_e for different EC sites of FLUXNET (http://www.fluxnet.ornl.gov/fluxnet/index.cfm). The annual NEE_{u*} - T_s relationship was assumed to follow the Arrhenius equation as follows:

$$R_e = R_{10}(t)e^{\frac{E_a}{\Re}(\frac{1}{283.16} - \frac{1}{T_s+273.16})} \qquad (1)$$

where $R_{10}(t)$ is the time (t) varying R_e at T_s = 10 °C, E_a is the activation energy (J mol^{-1}) and $\Re$ is the gas constant (8.134 J K^{-1} mol^{-1}). The value of E_a was first obtained using the annual NEE_{u*} - T_s relationship (i.e., $NEE_{u*} = R_{10}e^{\frac{E_a}{\Re}(\frac{1}{283.16} - \frac{1}{T_s+273.16})}$), and then held constant for the regressions of NEE_{u*} vs. T_s in the 30-day moving windows from which

values of $R_{10}(t)$ were obtained. After the value of $R_{10}(t)$ was determined for each moving window in high $u*$ ($u* \geq u*_{th}$) conditions, it was used along with the obtained annual E_a value to calculate R_e in low $u*$ conditions ($u* < u*_{th}$) at night, and to calculate daytime half-hourly values of R_e in all $u*$ conditions. The regressions of NEE_{u*} vs. T_s in the 30-day moving windows were made semi-dependent on the annual NEE_{u*} - T_s relationship by using the annual E_a value because of concern about the large noise inherent in the short-term nighttime NEE_{u*} - T_s relationship (Baldocchi 2003). The assumptions are that the R_e values for a short period of time (e.g., 1 month) can be obtained by fine-tuning the annual NEE_{u*} - T_s relationship and the effects of other factors are relatively constant during that short period.

A similar concept has been used by Barr et al. (2004) and adopted as the standard procedure for estimating R_e for the Fluxnet Canada Research Network (FCRN) (http://www.fluxnet-canada.ca). Barr et al. (2004) assumed a logistic NEE_{u*} - T_s relationship:

$$R_e = \frac{r_w(t) r_1}{1 + e^{r_2(r_3 - T_s)}} \qquad (2)$$

where r_1, r_2, and r_3 are empirical coefficients, and $r_w(t)$ is a time varying variable. The values of the empirical coefficients (r_1, r_2, and r_3) were obtained from the annual nighttime NEE_{u*} - T_s relationship (i.e., $NEE_{u*} = \frac{r_1}{1 + e^{r_2(r_3 - T_s)}}$) and were held constant for regressions of NEE_{u*} vs. T_s in the subsequent moving windows. The value of $r_w(t)$ obtained from each moving window together with the annual values of r_1, r_2 and r_3 obtained from the annual NEE_{u*} - T_s relationship were then used to calculate the

nighttime half-hourly values of R_e in low $u*$ conditions and to calculate daytime half-hourly values of R_e in all $u*$ conditions.

Very recently the algorithm used in Falge et al. (2002) was questioned because the annual value of E_a obtained from the annual NEE_{u*} - T_s relationship may not represent the value of E_a (i.e., the temperature sensitivity) for the short-term R_e – T_s relationship (Reichstein et al. 2005). The value of E_a during the active growing season was hypothesized to be significantly higher than that during the passive growing season. Reichstein et al. (2005) replaced Eq. (1) with a similar equation developed by Lloyd and Taylor (1994) as follows:

$$R_e = R_{10}(t)e^{E_0(\frac{1}{56.02} - \frac{1}{T_s+46.02})} \quad (3)$$

where $R_{10}(t)$ is the time varying R_e at T_s = 10 °C, and E_0 plays a similar role (i.e., determine the temperature sensitivity) as E_a in Eq. (1). In contrast to the procedure used in Falge et al. (2002), they calculated E_0 in two steps: (1) a 15-day moving window technique was used to obtain values of $R_{10}(t)$ and E_0 for consecutive 15 days, and (2) all the E_0 values obtained in step (1) were averaged. The obtained averaged value of E_0 was assumed to better represent the short-term temperature sensitivity of R_e than the annual E_0 value obtained directly from the single fit of the annual nighttime NEE_{u*} - T_s relationship, and therefore it was held constant over the entire year to calculate half-hourly values of R_e by determining a new set of $R_{10}(t)$ values in another round of moving window regressions.

The common features of the above three algorithms are (1) they use OLS (ordinary nonlinear least squares) algorithms to obtain parameters from the annual

nighttime NEE_{u*} - T_s relationship, (2) they use the parameters obtained from the annual nighttime NEE_{u*} - T_s relationship to calculate half-hourly values of R_e during the daytime, and (3) they obtain the half-hourly values of R_e at finer time scales (e.g., 30-day moving window) by adjusting the values of either $R_{10}(t)$ in Eqs. (1) and (3) or $r_w(t)$ in Eq. (2) while holding other parameters (e.g., E_a in Eq. (1)) constant. As discussed in Chapter 2, using OLS algorithms to obtain parameters (e.g., E_a in Eq.(1)) from the annual nighttime NEE_{u*} - T_s relationship and applying them to daytime hours may cause significant errors in the estimates of daytime half-hourly R_e. More importantly, the underlying assumptions in the above three flux partitioning procedures have not been thoroughly tested. For example, obtaining one E_a value from the annual nighttime NEE_{u*} - T_s relationship and holding it constant for regressions of NEE_{u*} vs. T_s in the 30-day moving windows may not be necessary, because the influence of EC measurement noise inherent in the nighttime NEE_{u*} - T_s relationship can be considerably reduced if the logarithmic transformation as described in Chapter 2 were applied. Also, adjusting the values of $R_{10}(t)$ in Eq. (1) to predict half-hourly values of R_e in each 30-day moving window is empirical in nature, because Eq. (1) could also be modified by obtaining an annual R_{10} value from the annual NEE_{u*} - T_s relationship and holding it constant for the moving windows but with the use of a time varying E_a ($E_a(t)$) (i.e., $R_e = R_{10} e^{\frac{E_a(t)}{\Re}(\frac{1}{283.16} - \frac{1}{T_s+273.16})}$). Furthermore, it is difficult to independently verify any of these flux-partitioning procedures since only the nighttime NEE_{u*} - T_s relationship is used. Reichstein et al. (2005) assume that their modified procedure is "more correct" than

the one originally used in Falge et al. (2002), and than using the single fit of the nighttime annual NEE_{u*} - T_s relationship. There are still considerable gaps in our understanding of how the R_{10} and Q_{10} (the relative temperature sensitivity of R_e to be discussed later), especially for ecosystems with a deep rooting depth (e.g., tall forests) would respond to changes in the soil moisture regime, and to phenological (seasonal) changes in the physiological activities of the entire ecosystem (e.g., rise and fall of fine root growth).

The objectives of this chapter are (1) to investigate the variability in the annual R_{10} and Q_{10} values of R_e and its main causes, and (2) to compare several flux-partitioning algorithms for estimating nighttime and daytime R_e. The obtained half-hourly values of daytime R_e obtained in this chapter will be used to estimate canopy photosynthesis in Chapter 4. Objective (1) provides the rationale for objective (2), e.g., if there are significant relationships of annual R_{10} and Q_{10} values to soil moisture, then using a single fit of the annual nighttime NEE_{u*} - T_s relationship to estimate half-hourly values of R_e is not valid. In this study, the nighttime NEE_{u*} - T_s relationship was used to estimate nighttime half-hourly values of R_e, and the daytime $R_{ed} - T_s$ relationship obtained from the LUE model described in Chapter 2 was used to estimate daytime half-hourly values of R_e. The main hypothesis in this study is that there should exist a consistency between the nighttime NEE_{u*} - T_s relationship and daytime $R_{ed} - T_s$ relationship. For example, if the effect of soil moisture is evident in the nighttime NEE_{u*} - T_s relationship, it is expected that its effect (although not necessarily exactly the same) is also evident in the daytime R_{ed} – T_s relationship. If the nighttime annual NEE_{u*} - T_s relationship overestimates/underestimates nighttime R_e in certain periods of the year, then it is

expected that the daytime annual $R_{ed} - T_s$ relationship also overestimates/underestimates daytime R_e in the corresponding periods.

Eight years (1998 – 2005) of EC-measured NEE data for the 56-year-old Douglas-fir stand (DF49) described in Chapter 2 are used in this study. In comparison with previous studies (e.g., Reichstein et al. 2005), this study has two advantages: (1) the long record of NEE data (i.e., 8 years) provides a rare opportunity to investigate the interannual variability in R_e and its main causes, and (2) two $R_e - T_s$ relationships (i.e., nighttime and daytime, respectively) are used, and the expected consistency between the nighttime and daytime $R_e - T_s$ relationships would increase confidence in the flux-partitioning algorithms used. This chapter builds on the results from Chapter 2, and provides a flux-partitioning algorithm for estimating P for Chapter 4.

3.2 Methods

The study site, EC CO_2 flux and auxiliary meteorological measurements were described in detail in Chapter 2. Half-hourly flux measurements made when Q_{t0} (incident total PAR) = 0 μmol m^{-2} s^{-1} and $Q_{t0} > 0$ μmol m^{-2} s^{-1} are considered to be nighttime and daytime values, respectively. In this study, the estimates of nighttime half-hourly R_e were obtained using the nighttime NEE_{u*} - T_s relationship, and the estimates of daytime half-hourly R_e were obtained using the daytime $R_{ed} - T_s$ relationship that was constructed from regressions using the LUE model. The value of $u*_{th}$ for this stand was taken to be 0.3 m s^{-1} following the analysis of Morgenstern et al. (2004). The LUE model is $NEP = \alpha Q_{t0} - R_{ed}$ for $Q_{t0} \leq 300$ μmol m^{-2} s^{-1} with a daytime $u*$ filter of $u*_{Q_{200}}$ (see Figure 2-5b of Chapter 2 for the daytime annual $R_{ed} - T_s$ relationship obtained for 2001).

3.2.1 Annual fits of the nighttime and daytime $R_e - T_s$ relationships

The method of estimating half-hourly R_e using annual fits (i.e., not done stepwise) of equations describing nighttime and daytime annual (for each year separately) $R_e - T_s$ relationships to measurements was described in Chapter 2. Here only a brief summary is given. An exponential relationship was assumed between R_e and T_s as follows:

$$R_e = Ae^{BT_s} \qquad \text{annual fit method} \qquad (4)$$

where R_e denotes nighttime or daytime ecosystem respiration, and A and B are two empirical coefficients. B is the relative temperature sensitivity of R_e as it is equal to $\frac{dR_e / R_e}{dT_s}$. T_s was taken as the soil temperature at the 5-cm depth following the analysis of Drewitt et al. (2002). Eq. (4) will be referred to as the annual fit method hereafter. The parameters A and B were determined using a linear regression after the logarithmic transformation of Eq. (4), i.e.,

$$\ln R_e = \ln A + BT_s \qquad (5)$$

Eq. (4) can also be written in the Q_{10} form as $R_e = R_{10}Q_{10}^{(T_s-10)/10}$, where Q_{10} and R_{10} are related to A and B as $Q_{10} = e^{10B}$, and $R_{10} = AQ_{10}$. After the coefficients A and B were determined using Eq. (5), they were used in Eq. (4) to calculate half-hourly values of R_e. Nighttime half-hourly measurements of NEE_{tt} were not retained but rather replaced by the model-calculated R_e values as explained in Chapter 2.

3.2.2 Stepwise fits of the annual nighttime and daytime $R_e - T_s$ relationships

Modifications of Eq. (4) were used to stepwise fit the annual nighttime (Figure 3-3) and daytime $R_e - T_s$ (Figure 3-4) relationships. Moving windows with a window size of 15 days were used in this study and were advanced 1 day at a time. Therefore, for any given half hour, there were 15 estimates of R_e obtained respectively from 15 different windows. The arithmetic average of the fifteen R_e estimates was assumed to be the best estimate of R_e obtained for that given half hour. Three stepwise fit methods were used in this analysis.

Method 1 assumed that the $R_e - T_s$ relationship in each moving window could be approximated by modifying Eq. (4) as:

$$R_e = f(t)Ae^{BT_s} \qquad A15\text{-day method} \qquad (6)$$

where A and B are the empirical coefficients obtained from the annual (Jan 1 – Dec 31) nighttime or daytime $R_e - T_s$ relationships (as determined using Eq. (5)), and were kept constant for regressions of the 15-day moving windows. Eq. (6) will be referred to as the A15-day method, where "A" indicates that the parameter "A" in Eq. (4) from the annual nighttime and daytime $R_e - T_s$ relationships was modified (in the sense that it's multiplied by $f(t)$ or A is replaced by $f(t)A$). The time-varying variable $f(t)$ for each window was obtained as follows: taking the logarithmic transformation of Eq. (6) and averaging both sides of the transformed equation gives:

$$\overline{\ln f(t)} = \overline{\ln R_e - (\ln A + BT_s)} \qquad (7)$$

The value of $f(t)$ for each moving window is fixed (i.e., a single value of $f(t)$ is obtained for each window), but the value of $f(t)$ is different for different moving windows, so $\overline{\ln f(t)} = \ln f(t)$. Therefore,

$$f(t) = e^{\overline{\ln R_e - (\ln A + BT_s)}} \quad (8)$$

In contrast with the previous practice (Falge et al. 2002, Barr et al. 2004, Reichstein et al. 2005), the value of $f(t)$ was not directly obtained as $R_e/(Ae^{BT_s})$ using an OLS algorithm, because of the potential violation of the statistical IID N$(0,\sigma^2)$ assumption in the $R_e - T_s$ relationships as discussed in Chapter 2. The modifier $f(t)$ in Eq. (6) does not change the relative temperature sensitivity of R_e since B is not "modified".

Method 2 assumed that the $R_e - T_s$ relationship in each moving window could be approximated by modifying Eq. (4) as:

$$R_e = Ae^{f(t)BT_s} \qquad B15\text{-day method} \quad (9)$$

where, similar to Method 1, A and B are the empirical coefficients obtained from the annual nighttime or daytime $R_e - T_s$ relationships and were kept constant for regressions in each moving window. Eq. (9) will be referred to as the $B15$-day method, where "B" indicates that the parameter "B" in Eq. (4) from the annual nighttime and daytime $R_e - T_s$ relationships was modified by being multiplied by $f(t)$. The time varying variable $f(t)$ in a given moving window was determined by logarithmic transformation of Eq. (9) and averaging both sides of the transformed equation:

$$f(t) = \overline{(\ln R_e - \ln A)/BT_s} \quad (10)$$

The relative temperature sensitivity of Eq. (9) is given as: $\frac{dR_e/R_e}{dT_s} = f(t)B$.

Method 3 assumed that the $R_e - T_s$ relationship in each moving window was exponential (i.e., $R_e = Ae^{BT_s}$). The coefficients A and B were obtained in the same way as it was for the annual nighttime and daytime $R_e - T_s$ relationships (i.e., $\ln R_e = \ln A + BT_s$).

In Method 3, both A and B in the $R_e - T_s$ relationships were determined for each window rather than just A or B as in A15- and B15-day methods, respectively. Method 3 will be referred to as AB15-day method.

3.3 Results

3.3.1 Climate and meteorological conditions

Figure 3-1 and Figure 3-2 show the seasonal variation of T_s (soil temperature at the 5-cm depth) and θ (volumetric soil water content averaged for the 0 – 1 m depth) for the 8 years (1998 – 2005). The mean annual T_s for the 8 years was 7.45 ± 0.62 °C, with 2004 being the warmest year (8.57 °C) and 1999 being the coolest (6.59 °C) (Table 1). The 1998/1999 El Niño/La Niña cycle led to a prolonged snow accumulation on the forest floor in the February and March of 1999, so T_s was almost constant during these two months. The sharp decrease of T_s in early March of 2002 was associated with a week of below freezing air temperature (data not shown). The mean annual total precipitation for the 8 years was 1296 ± 266 mm, with less than 25% (305 ± 100 mm) falling in the most active growing season between April and September inclusively (Table 1). Therefore, θ was highest during the winter months, and in general decreased progressively until the middle of September when the rainy winter season generally restarted. The largest variation in θ also occurred in September (Figure 3-2) as a result of the large variability in the month's rainfall. The mean value of the rainfall received in September for 1999 – 2003 and 2005 was 34 ± 5 mm, but values for 1998 and 2004 were 6 mm and 103 mm, respectively.

Table 3-1. Climate conditions for the 8 years (1998 – 2005), including canopy air temperature at the 27-m height (T_a), soil temperature at the 5-cm depth (T_s), integrated water content in the 0 – 1-m depth soil layer (θ), total precipitation, mean daily downwelling PAR (Q_{t0}) (45-m height) and mean daily downwelling diffuse PAR (Q_{d0}) (45-m height) for the entire year and for the most active growing season (April 1 – September 30).

	1998	1999	2000	2001	2002	2003	2004	2005	Mean ± SD
Jan 1 – Dec 31									
Mean T_a (°C)	9.10	7.66	8.21	8.09	8.47	8.48	8.77	8.33	8.39 ± 0.44
Mean T_s (°C)	8.12	6.59	7.42	7.33	7.74	8.07	8.57	8.14	7.45 ± 0.62
Mean θ (m^3 m^{-3})	0.186	0.223	0.212	0.212	0.201	0.217	0.223	0.228	0.212 ± 0.013
Total precipitation (mm)	1749	1613	952	1116	1113	1271	1234	1324	1296 ± 266
Q_{t0} (mol m^{-2} d^{-1})	22.94	22.21	22.40	21.33	22.96	21.78	21.51	19.98	21.89 ± 0.98
Q_{d0} (mol m^{-2} d^{-1})	N/A	N/A	N/A	10.32	9.69	10.01	9.67	9.87	9.91 ± 0.27
April 1 – Sept 30									
Mean T_a (°C)	14.10	11.75	12.63	12.19	12.83	13.07	13.75	12.75	12.88 ± 0.77
Mean T_s (°C)	12.15	10.07	11.17	10.76	11.36	11.54	12.40	11.65	11.39 ± 0.74
Mean θ (m^3 m^{-3})	0.166	0.209	0.195	0.191	0.178	0.190	0.199	0.212	0.193 ± 0.015
Total precipitation (mm)	216	290	278	259	211	310	358	521	305 ± 100
Q_{t0} (mol m^{-2} d^{-1})	37.24	34.25	34.75	32.23	36.39	34.19	34.58	30.51	34.27 ± 2.14
Q_{d0} (mol m^{-2} d^{-1})	N/A	N/A	N/A	14.74	13.63	14.34	13.90	14.15	14.15 ± 0.42

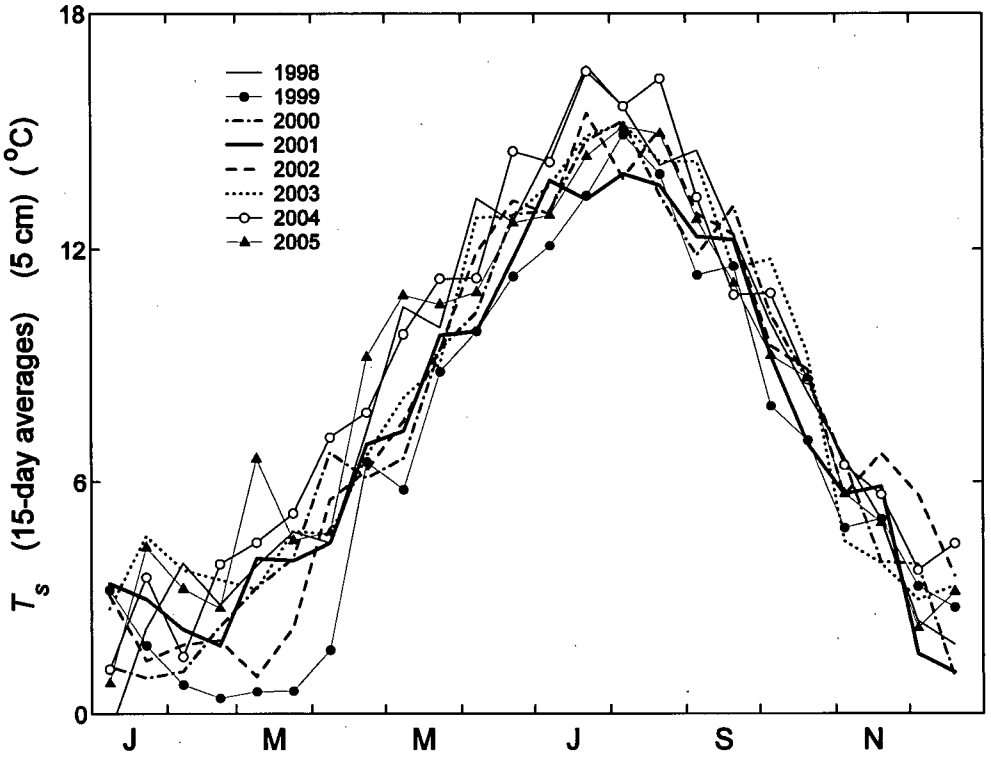

Figure 3-1. Seasonal changes in the 15-day averages of soil temperature (T_s) at the 5-cm depth.

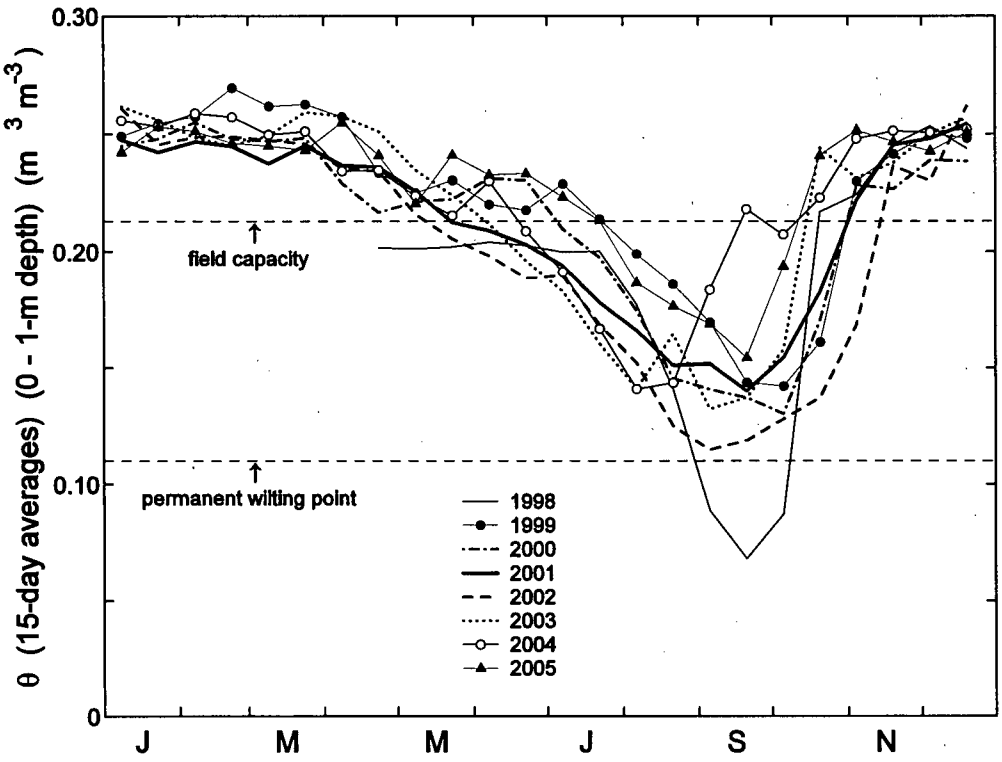

Figure 3-2. Seasonal changes in the 15-day averages of volumetric soil water content (θ) integrated from the surface to the 1-m depth. The values of field capacity (-1/3 bar) (θ = 0.213 m^3 m^{-3}) and permanent wilting point (-15 bars) (θ = 0.110 m^3 m^{-3}) were taken from Black (1979) for a 26-year-old coastal Douglas fir stand.

3.3.2 Annual fits of the $R_e - T_s$ relationships

Figure 3-3 and Figure 3-4 show the annual nighttime NEE_u - T_s and annual daytime R_{ed} – T_s relationships respectively for the 8 years (1998 – 2005). In each relationship, θ was stratified into three levels: ≥ 0.2 m^3 m^{-3}, 0.15 – 0.2 m^3 m^{-3} and < 0.15 m^3 m^{-3} in an attempt to detect the possible effect of θ on R_e. Figure 3-3a and Figure 3-4a show that, when θ < 0.15 m^3 m^{-3} (e.g., in September of 1998), the nighttime and daytime values of R_e fell below the annual fitted curves likely as a result of the limitation of θ on R_e. However, caution must be exercised when interpreting the effect of θ from this crude stratification, because of possible correlations between θ and other environmental and biotic variables. For example, θ > 0.2 m^3 m^{-3} mainly occurs in winter and early spring, and θ < 0.15 mainly occurs in August and September. In early spring (e.g., April) the overall physiological activities of the stand (e.g., growth of fine roots, new shoots and soil microorganisms) presumably are more active than those in August and September, so that lower R_e values in those latter two months can not be totally attributed to the effect of lower θ.

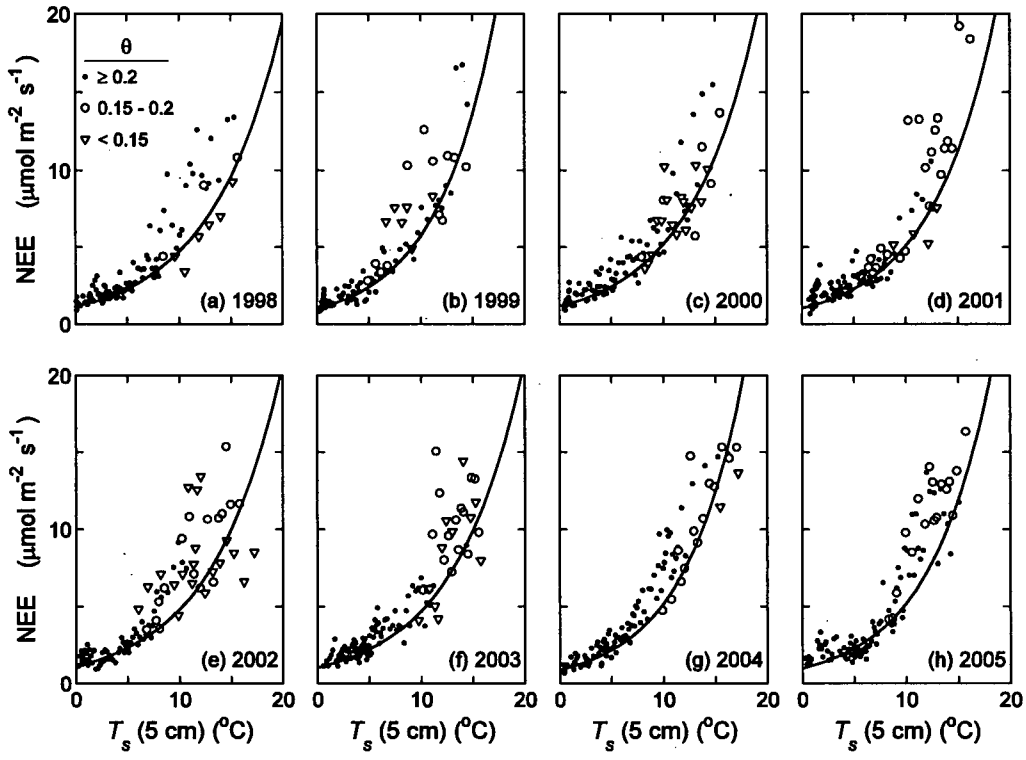

Figure 3-3. The annual nighttime NEE_{u*} - T_S relationships for 1998 – 2005, where NEE_{u*} are the nighttime half-hourly NEE measurements made when $u* > 0.3$ m s^{-1}. Symbols represent the bin averages of the 20 half-hourly NEE_{u*} values in the stratifications of half-hourly values of θ (volumetric soil moisture, 0 –1-m depth). The annual curve fits were obtained using the original half hourly NEE_{u*} data (not the bin averages).

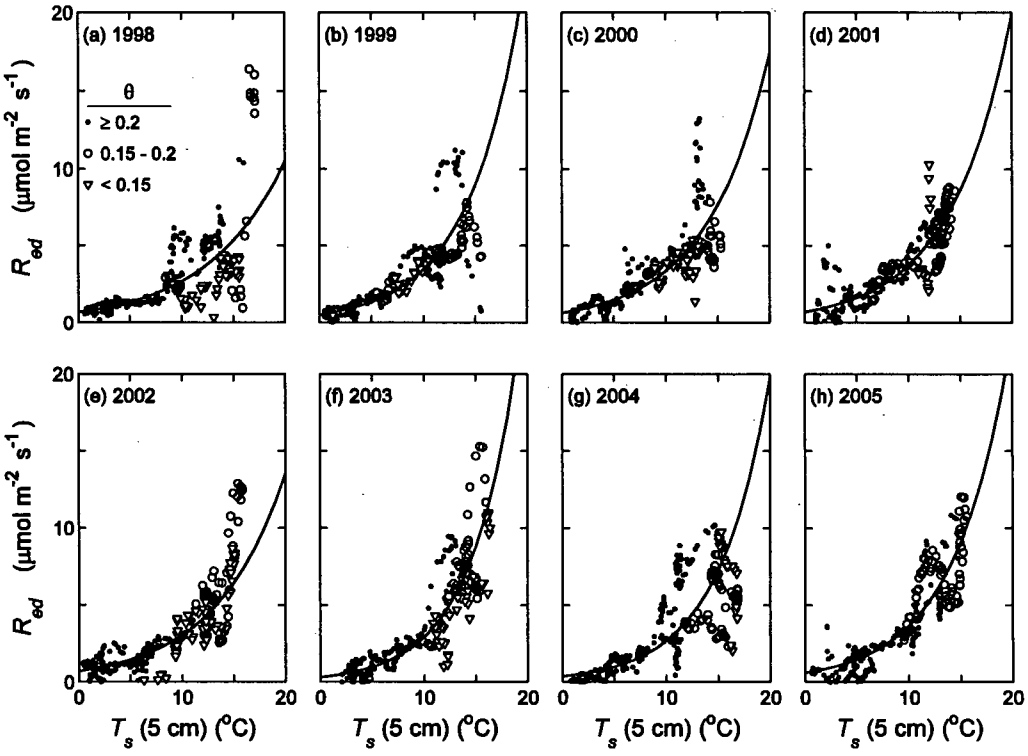

Figure 3-4. The annual daytime $R_{ed} - T_s$ relationships for 1998 – 2005 obtained using the LUE model. θ is the volumetric soil moisture spatially integrated over 0 – 1-m depth.

The potential significant seasonal and phenological effects (e.g., seasonal variation in the quantity and quality of both roots and soil microorganisms (Lavigne et al. 2004)) possibly masked the effect of θ on R_e in other years (Figure 3-3b-h and Figure 3-4b-h). This echoes the view of other researchers (e.g., Lee et al. 1999, Morgenstern et al. 2004, Reichstein et al. 2005) that it is extremely difficult to directly relate EC CO_2 flux measurements made over short periods of time to other variables due to the large variability inherent in EC CO_2 flux measurements and the complex interactions between θ and other variables (e.g., phenology). Soil chamber CO_2 efflux measurements conducted at a mixed conifer forest site in Colorado showed that both T_s and θ are important drivers of soil respiration rate, but they confound each other and function as primary controls at different timescales: T_s is a primary control seasonally, and θ is a primary control inter-annually (Scott-Denton et al. 2003). The values of A and B for each year obtained using the annual nighttime (Figure 3-3) and daytime (Figure 3-4) relationships are given in Table 3-2.

Table 3-2. The values of A and B for each year obtained from the annual nighttime (Figure 3-3) and daytime (Figure 3-4) relationships. Units for A and B are μmol m^{-2} s^{-1} and $°C^{-1}$, respectively. The values of A and B were obtained using the logarithmic transformation of the corresponding exponential R_e-T_s relationships. The corresponding values of R_{10} and Q_{10} were obtained as: $R_{10} = AQ_{10}$ and $Q_{10} = e^{10B}$.

	Annual nighttime relationship				Annual daytime relationship			
Year	A	B	R_{10}	Q_{10}	A	B	R_{10}	Q_{10}
1998	1.13	0.14	4.70	4.14	0.69	0.13	2.67	3.84
1999	1.02	0.17	5.73	5.64	0.53	0.19	3.49	6.60
2000	1.16	0.15	5.17	4.44	0.65	0.16	3.37	5.16
2001	1.04	0.16	5.07	4.89	0.76	0.16	3.76	4.95
2002	1.12	0.15	4.81	4.31	0.69	0.15	3.06	4.44
2003	1.05	0.15	4.70	4.48	0.33	0.22	2.92	8.87
2004	0.90	0.18	5.20	5.77	0.37	0.20	2.69	7.34
2005	0.99	0.17	5.19	5.26	0.60	0.18	3.67	6.14

In order to minimize the influence of EC CO_2 flux measurement noise and the confounding effect of other variables, the annual values of R_{10} and Q_{10} obtained from the annual nighttime NEE_{u*} - T_s and annual daytime $R_{ed} - T_s$ relationships of each individual year were compared in Figure 3-5. The advantage of using the annual $R_e - T_s$ relationships are (1) the range in T_s is wide enough, so R_{10} and Q_{10} values can be reliably estimated (Rayment and Jarvis 2000, Lavigne et al. 2004), and (2) the effects of seasonal and phenological changes are minimized in the interannual comparison, because every year the stand goes through a similar seasonal and phenological cycle (e.g., active and passive growing phases). As will be discussed later, using the annual R_{10} and Q_{10} values, obtained from the single fits of the annual nighttime NEE_{u*} - T_s and daytime $R_{ed} - T_s$ relationships of each individual year, to estimate half-hourly values of R_e within a particular year is problematic. However, the annual R_{10} and Q_{10} values most likely reflect the annually integrated composite response of R_e to T_s, and therefore comparison of the annual R_{10} and Q_{10} values between different years can still provide valuable insights on the overall behavior of ecosystem respiration.

Figure 3-5 shows that the values of R_{10} and Q_{10} obtained for the annual nighttime NEE_{u*} - T_s relationships increased linearly with θ, and this was also observed with the daytime annual $R_{ed} - T_s$ relationships. The $R_{10} - \theta$ and $Q_{10} - \theta$ relationships were all significant ($p < 0.05$) and their coefficients are given in Table 3-3.

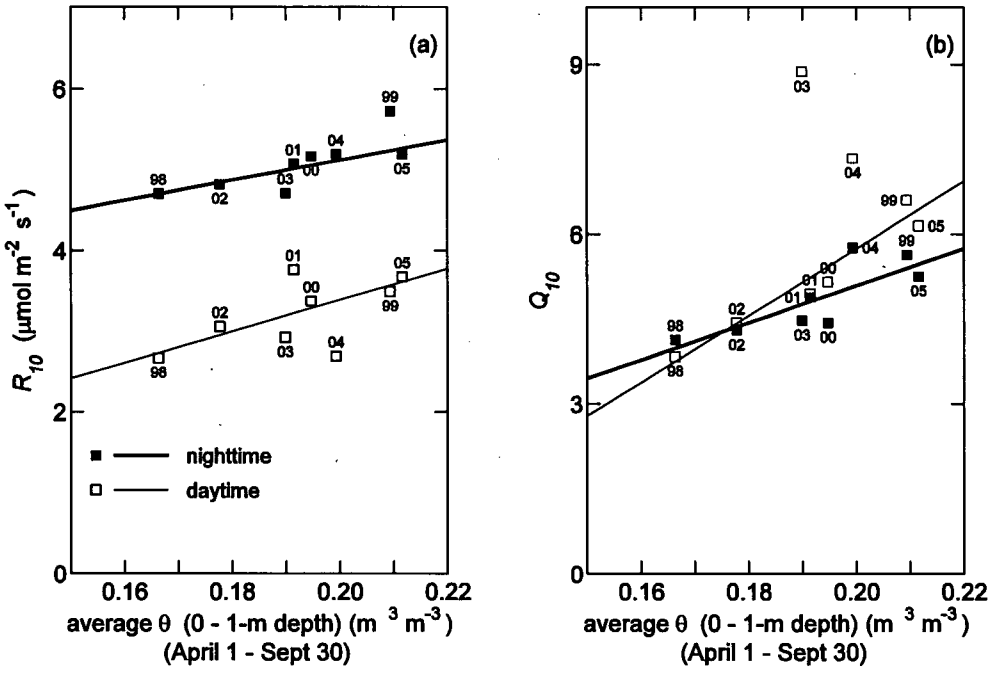

Figure 3-5. Linear regressions of R_{10} and Q_{10} on average θ for the 0-1 m layer (see Table 3-3 for the coefficients). The nighttime and daytime R_{10} and Q_{10} values were obtained using the annual nighttime $NEE_{n.}$ - T_s and annual daytime $R_{ed} - T_s$ (see Figure 3-3 and Figure 3-4) relationships, respectively. The numbers next to the data points indicate the year.

Table 3-3. The coefficients (i.e., *c* and *d*) in the linear regressions between annual values of R_{10} and θ and Q_{10} and θ (see Figure 3-5). The nighttime and daytime values of R_{10} and Q_{10} were obtained from the annual nighttime NEE_{u*} - T_s (Figure 3-3) and annual daytime $R_{ed} - T_s$ (Figure 3-4) relationships, respectively. Units of R_{10} and Q_{10} are μmol m^{-2} s^{-1} and $°C^{-1}$, respectively. θ (m^3 m^{-3}) was calculated by averaging its half-hourly values of each year from April 1 to September 30.

	Nighttime			Daytime		
	c	*d*	r^2	*c*	*d*	r^2
$R_{10} = c\theta + d$	12.68	2.58	0.56	19.52	-0.51	0.34
$Q_{10} = c\theta + d$	32.85	-1.47	0.66	60.45	-6.23	0.15

The R_{10} values obtained from the annual daytime $R_{ed} - T_s$ relationships were lower than the corresponding R_{10} values obtained from the annual nighttime NEE_{u*} - T_s relationships. As discussed in Chapter 2, the lower R_{10} values during the daytime were most likely the result of light inhibition of foliar mitochondrial respiration. However, the Q_{10} values obtained from the annual daytime $R_{ed} - T_s$ relationships were generally higher than the corresponding Q_{10} values obtained from the annual nighttime annual NEE_{u*} - T_s relationships.

Table 3-4 shows the annual values of R_e for the 8 years obtained using the R_{10} and Q_{10} values modeled using the linear $R_{10} - \theta$ and $Q_{10} - \theta$ relationships from Table 3-3. The modeled nighttime R_{10} and Q_{10} values were used to calculate nighttime half-hourly values of R_e, and the modeled daytime R_{10} and Q_{10} values were used to calculate daytime

half-hourly values of R_e. The nighttime and daytime half-hourly R_e values were then summed to obtain an annual value of R_e. In general, the relative error of the predicted annual values of R_e is small (i.e., –0.87 ± 3.58% (Mean ± SD)).

Table 3-4. The annual totals of R_e obtained (1) using the annual values of R_{10} and Q_{10} obtained from the annual nighttime and daytime $R_e - T_s$ relationships of each individual year (see Figure 3-3 and Figure 3-4), and (2) using the annual values of R_{10} and Q_{10} modelled for each individual year from the nighttime and daytime $R_{10} - \theta$ and $Q_{10} - \theta$ relationships (see Table 3-3 and Figure 3-5). The nighttime and daytime R_{10} and Q_{10} values were used to calculate the nighttime and daytime half-hourly values of R_e, respectively. The half-hourly values of R_e were then summed to obtain the annual totals. Also shown are the means and standard deviations for the 8-year period.

R_e (g C m^{-2} yr^{-1})	1998	1999	2000	2001	2002	2003	2004	2005	Mean ± SD
Using R_{10} and Q_{10} obtained from individual years	1339	1337	1410	1388	1345	1486	1648	1595	1443 ± 121
Using R_{10} and Q_{10} modelled for individual years	1351	1289	1385	1287	1331	1485	1731	1608	1433 ± 162
Relative modelling error (%)*	0.90	-3.59	-1.77	-7.21	-1.04	-0.07	5.04	0.82	-0.87 ± 3.58

* Relative modelling error (%) was calculated as 100×(row 2 – row 1)/row 1.

3.3.3 Stepwise fits of the annual $R_e - T_s$ relationships

The statistically significant linear $R_{10} - \theta$ and $Q_{10} - \theta$ relationships shown in Figure 3-5 strongly suggest that the effect of θ on R_e must also exist within a year. The

failure to detect the effect of θ within a given year in Figure 3-3 and Figure 3-4 may be due to the confounding effect of other factors (e.g., seasonality). The effects of θ and other factors undermine the validity of using the annual nighttime and daytime R_e - T_s relationships to estimate half-hourly values of R_e, because R_e is not solely dependent on T_s. The nighttime and daytime monthly values of R_e calculated using the three stepwise fit methods (i.e., A15-day, B15-day and AB15-day methods) are compared with those calculated using the annual relationships in Figure 3-6 and Figure 3-7, respectively. The estimates of R_e were calculated half-hourly and then summed to obtain monthly values. In general, all three stepwise fits methods gave similar results. In contrast, using the values of A and B obtained from the annual nighttime and daytime R_e – T_s relationships to calculate half-hourly values of R_e resulted in significant systematic errors (in comparison with the stepwise methods): underestimating R_e in the active growing season (April – July) and overestimating R_e in the passive growing season (August – March). The patterns of underestimation and overestimation of half-hourly R_e values using the nighttime and daytime methods were generally similar (e.g., compare Figure 3-6 and Figure 3-7), although the extent of under- and overestimations varied considerably among years.

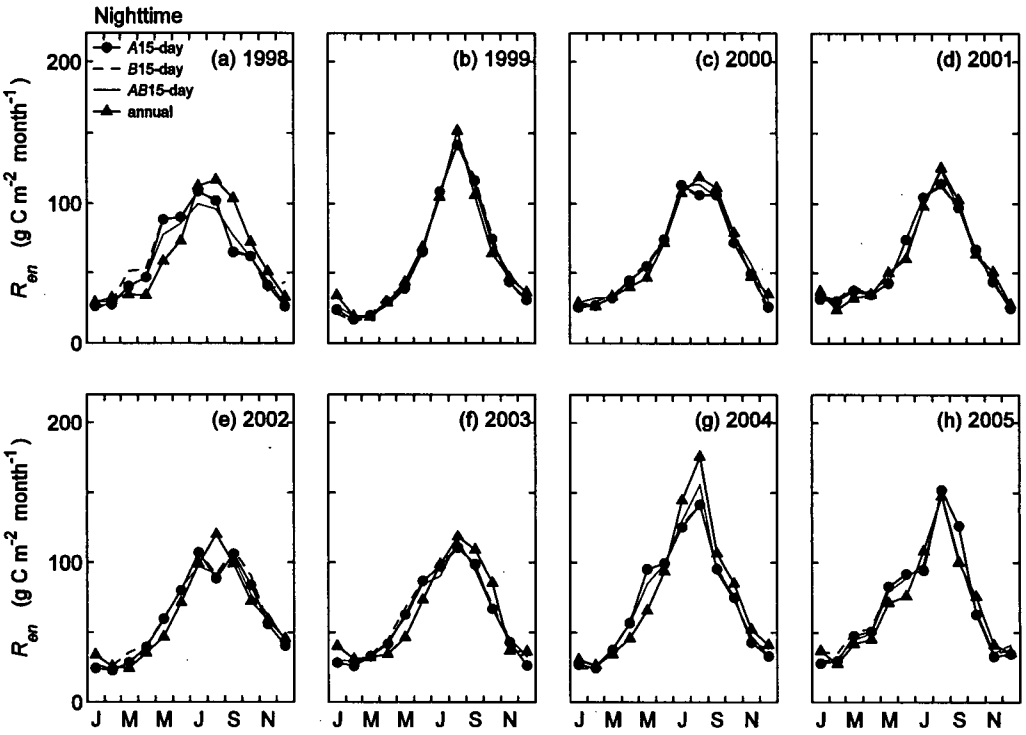

Figure 3-6. Monthly totals of nighttime R_e (i.e., R_{en}) obtained using the three stepwise fit methods compared with those obtained using the annual nighttime NEE_{u*} - T_s relationships for 1998 – 2005 (see Figure 3-3). All R_e values were calculated half-hourly and then summed to obtain monthly totals.

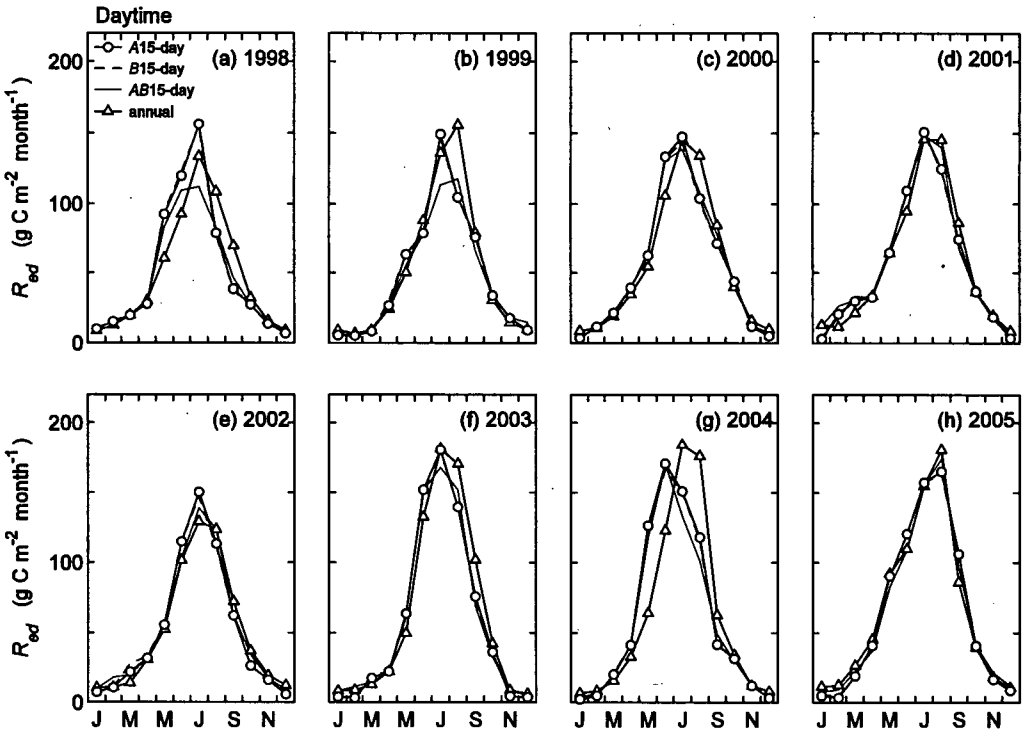

Figure 3-7. Monthly totals of daytime R_e (i.e., R_{ed}) obtained using the three stepwise fit methods compared with the annual daytime R_{ed} - T_s relationships for 1998 – 2005 (see Figure 3-4). All R_e values were calculated half-hourly and then summed to give monthly totals.

The annual totals of R_e obtained using the stepwise fits and annual relationships are given in Table 3-5.

Table 3-5. Annual totals of R_e obtained using the three stepwise methods and the annual relationship method. The nighttime NEE_{night} - T_s and daytime $R_{ed} - T_s$ relationships were used to calculate the nighttime and daytime half-hourly values of R_e, respectively, which were then summed to obtain the annual totals (see Figure 3-6 and Figure 3-7).

R_e (g C m^{-2} yr^{-1})	1998	1999	2000	2001	2002	2003	2004	2005	Mean ± SD
*A*15-day moving window	1350	1316	1402	1383	1367	1455	1595	1622	1436 ± 114
*B*15-day moving window	1390	1329	1401	1388	1400	1468	1605	1650	1454 ± 114
*AB*15-day moving window	1271	1291	1434	1407	1367	1458	1570	1586	1423 ± 116
Annual relationship	1339	1337	1410	1388	1345	1486	1648	1595	1443 ± 121

The average R_e for the 8 years estimated using the *A*15-day method (i.e., 1436 g C m^{-2} yr^{-1}) was almost identical to that estimated using the annual relationship (i.e., 1443 g C m^{-2} yr^{-1}). The average values of R_e obtained using the *B*15-day and *AB*15-day methods were 1454 and 1423 g C m^{-2} yr^{-1}, respectively. The *B*15-day and *AB*15-day methods occasionally gave unrealistic monthly estimates of R_e. For example, the *B*15-day method gave unrealistically high monthly estimates of nighttime R_e in March and December of 1998 (Figure 3-6a), and the *AB*15-day method gave an unrealistically high monthly estimate of daytime R_e in December of 1999 (Figure 3-7b). These unrealistically high estimates using these two methods were probably caused by the modification of

parameter B (e.g., $f(t)B$ in Eq. (9)). Since the $A15$-day method performed best, it was decided to use it to calculate the half-hourly values of daytime and nighttime R_e in Chapter 4.

The seasonal change in the monthly average values of $f(t)$ obtained for the $A15$-day method (Eq. (6)) is shown in Figure 3-8. In general, most of the monthly $f(t)$ values fell between 0.5 and 1.5. The monthly $f(t)$ values were generally greater than 1 for the active growing season (April to July) and less than 1 for the passive growing season (August – March). The seasonal trend of $f(t)$ does not correspond well with the seasonal trend in θ (compare Figure 3-2 and Figure 3-8). For example, θ was highest in January (Figure 3-2), but the monthly values of $f(t)$ in January obtained using both nighttime (Figure 3-8a) and daytime (Figure 3-8b) methods were significantly less than 1. Therefore, $f(t)$ probably reflects more of the effect of biological activities than that of θ on R_e in January.

The daytime daily average values of R_e obtained during the 8 years using the $A15$-day method are compared with the corresponding nighttime daily averages in Figure 3-9. The daily averages (as opposed to daily totals) were used in order to remove the effect of day length. The relationship between the daytime and nighttime daily averages was strong (r^2 = 0.85). On average, R_e during the daytime was about 30% less than at night. This reduction is likely largely due to the effect of light inhibition on canopy foliar respiration (see also Figure 3-5a and Figure 2-6).

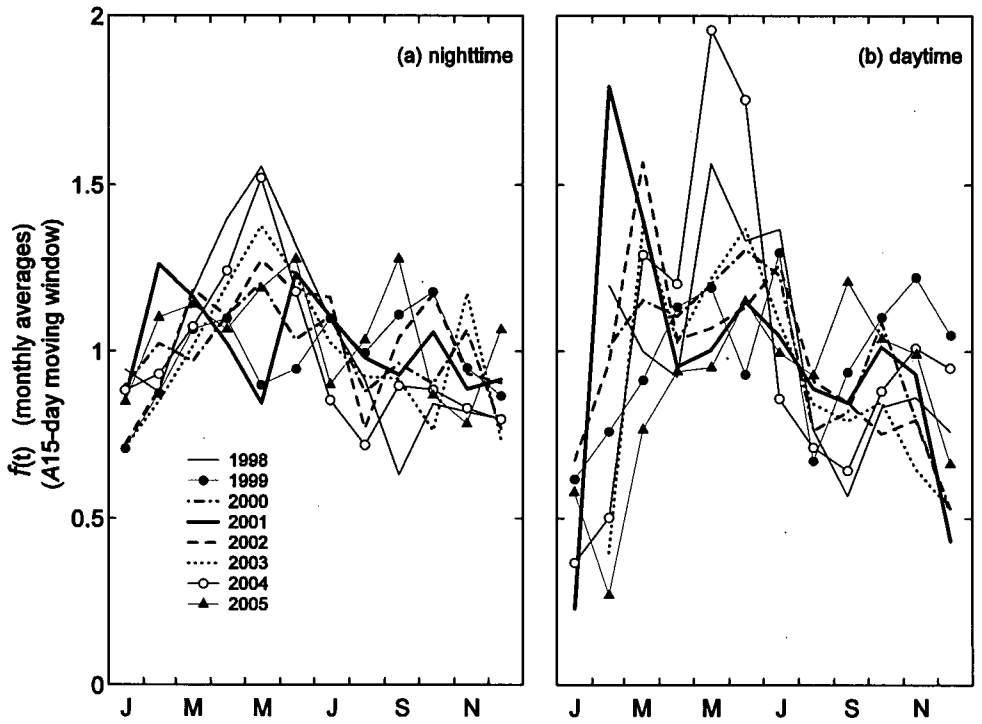

Figure 3-8. Seasonal changes in the monthly averages of $f(t)$ for the A15-day moving windows (see also Figure 3-6 and Figure 3-7).

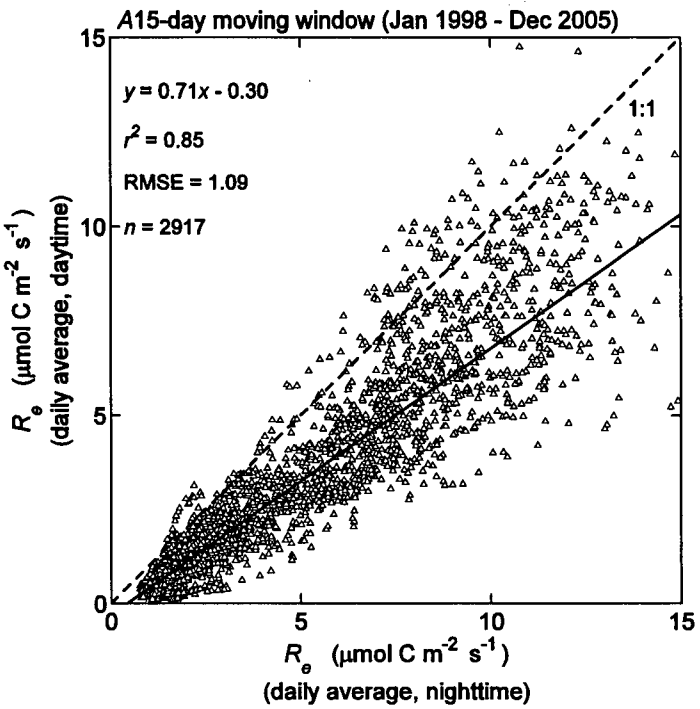

Figure 3-9. Comparison of daytime daily averages of R_e, obtained using the daytime R_{ed} – T_s relationships, with the corresponding nighttime daily averages of R_e obtained using the nighttime NEE_{u*} - T_s relationships. All the nighttime and daytime half-hourly R_e values were calculated using the *A*15-day stepwise fit method (see Figure 3-6 and Figure 3-7), and then averaged to obtain the corresponding nighttime and daytime daily averages.

3.4 Discussion

Ecosystem respiration is the sum of autotrophic (e.g., roots and foliar respiration) and heterotrophic (e.g., fungi and bacteria) respiration. The positive linear $R_{10} - \theta$ and $Q_{10} - \theta$ relationships shown in Figure 3-5 likely reflect the control by θ on the ecosystem respiration. Similar responses have also been reported by Reichstein et al. (2002b) for R_e in two Mediterranean evergreen Holm Oak forests, and by Xu and Baldocchi (2004) and Flanagan and Johnson (2005) for R_e in a Mediterranean grassland in California and a mixed grassland in southern Alberta, respectively. Recent chamber measurements of soil respiration, such as those for a 60-year-old mixed hardwood stand (Savage and Davidson 2001), an 8-year-old ponderosa pine stand (Xu and Qi 2001), a 40-year-old balsam fir stand (Lavigne et al. 2004), and a mixed grass prairie (Chimner and Welker 2005), indicate that θ is an important controlling factor for soil respiration in a wide range of ecosystems with different rooting depths. The effect of θ on R_e has significant implications for future climate change scenarios (e.g., warmer and drier climate) (Cox et al. 2000). It is a concern that R_e may increase more than gross primary production in response to global warming, leading to less carbon sequestration by vegetation. The effect of θ on R_e suggests that the potentially high R_e in warmer years will be damped by low θ and the potentially low R_e in cooler years will be enhanced by high θ, because warmer years tend to be drier and cooler years tend to be wetter. For example, Ciais et al. (2005) reported that R_e for different European ecosystems significantly decreased rather than increased with temperature during the Europe-wide heat wave in 2003 as a result of its associated severe drought. Using a recent satellite normalized difference vegetation index (NDVI) data set and climate data, Angert et al.

(2005) concluded that drier summers cancel out the CO_2 uptake enhancement induced by warmer springs in both mid and high latitudes, even though temperature is considered to be a major limiting factor for canopy photosynthesis in high-latitude ecosystems.

The Q_{10} values (see Figure 3-5b) obtained for this stand varied approximately from 4 to 6 for the nighttime annual fit relationship method and from 4 to 9 for the daytime annual relationship method, respectively. They are well beyond the Q_{10} range expected for the respiratory response to temperature (1.5 – 3.0) (Tjoelker et al. 2001). In a previous analysis of CO_2 flux data for the first 4 years (1998 – 2001) of EC measurements in this stand (Morgenstern et al. 2004), the high Q_{10} values were attributed to the use of soil temperature at one depth (i.e., 5-cm) to represent the temperature of an entire ecosystem. An additional cause of the high Q_{10} values may be the strong phenological change in R_e due to changes in respiring biomass. Q_{10} values can be significantly overestimated if the seasonal variation in respiring biomass is not taken into account (Lavigne et al. 2004). For example, Epron et al. (2001) calculated a Q_{10} = 3.9 for root respiration when the change in root biomass was not taken into account, but obtained a Q_{10} = 2.2 after accounting for the increase in fine root biomass. The effect of phenology (e.g., seasonal growth of fine roots) on R_e (see Figure 3-8) has also been observed for other ecosystems, such as for a sphagnum moss (Goulden et al. 1998), and a mixed boreal spruce and pine forest (Morén and Lindroth 2000). The phenological change in respiring organisms/tissue is likely to be coupled with the seasonal change in photosynthesis and the pattern of photosynthate allocation. Janssens et al. (2001) showed that canopy photosynthesis was more important than temperature in explaining variation in R_e when the R_e of several European forests were compared. In the large-scale girdling experiments

of a 45-55-year-old Scots pine stand, where the stem bark was stripped to the depth of the current xylem at breast height to terminate the supply of photosynthate to roots, Hogberg et al. (2001) found that soil respiration was decreased by 40% in 5 days and 56% in 14 days. Results from these experiments showed that the supply of current photosynthate may be a key driver for soil respiration and the models of soil respiration should incorporate the effect of canopy photosynthesis and the seasonal allocation pattern of photosynthate to roots. Scott-Denton et al. (2005) conducted a similar girdling experiment in a sub-alpine forest dominated by lodgepole pine trees and showed that soil respiration rates in plots with girdled trees were reduced by 31-44% at the mid-summer respiratory maximum in comparison with control plots with non-girdled trees. Recent carbon isotope studies have also shown that a large fraction of R_e comes from the metabolism of recently fixed carbohydrates (e.g., Bowling et al. 2002, McDowell et al. 2004). For example, Bowling et al. (2002) reported that the measured carbon isotopic composition of R_e for six coniferous stands along a precipitation gradient in western Oregon could be successfully predicted using models for photosynthetic carbon isotope discrimination. Consistent with findings of Hogberg et al. (2001), Flanagan and Johnson (2005) found that the above ground biomass was a good proxy for accounting for the variation in R_e of a mixed temperate grassland in southern Alberta.

The three stepwise fit methods (i.e., *A*15-day, *B*15-day, and *AB*15-day methods) for estimating half-hourly R_e agreed reasonably well (Figure 3-6 and Figure 3-7), because the 15-day moving window technique can be thought of as a smoothing interpolation approach (see also Eqs. 8 and 10), so it does not matter whether A, B or both A and B are modified. The window size of 15 days is a tradeoff between two competing requirements.

The first requirement is that it must be short enough to avoid significant changes in phenology and other environmental variables (e.g., θ). The second requirement is that it must be long enough to provide sufficient data points for the regression analysis. Window sizes of 7, 30, 60 and 90 days were also tested for the $A15$-day method (i.e., Eq. (6)) (data not shown). The results showed that (1) the monthly integrated values of R_e obtained using the 7-day moving windows were very similar to those obtained using the 15-day moving windows, and (2) the monthly integrated values of R_e obtained using window sizes longer than 15 days (i.e., 30, 60 and 90 days) gradually began to show the same underestimation and overestimation pattern observed with the annual relationship (see Figure 3-6 and Figure 3-7). The choice of the window size of 15 days was also supported by the spectral analysis of the half-hourly air temperature measurements at the site, which indicated that the time required for a significant change in the weather for the Campbell River area is 10 – 15 days (data not shown).

3.5 Conclusions

(1) The annual values of R_{10} and Q_{10} for the 8 years (1998 – 2005) obtained from the annual nighttime NEE_{nt} – T_s relationships linearly increased with average θ in the 0 to 1-m-depth soil layer. This was confirmed by the linear $R_{10} - \theta$ and $Q_{10} - \theta$ relationships obtained from the corresponding annual daytime R_{ed} – T_s relationships, suggesting a significant effect of θ on R_e.

(2) The effect of θ on R_e shown at the interannual scale (see Conclusion 1) was not detected at seasonal and annual timescales probably due to the confounding

effects of other factors (e.g., phenology) which co-vary with the seasonal change in θ.

(3) In comparison with the stepwise fits of the annual nighttime and daytime $R_e - T_s$ relationships, the annual nighttime and annual daytime $R_e - T_s$ relationships generally gave lower values of R_e for the active growing season (April – July) before any water limiting effects occurred in Aug and Sept, and larger values for the passive growing season (August – March). However, the systematic seasonal errors of using the annual $R_e - T_s$ relationships had little effect on the annual totals of R_e, because the underestimation and overestimation usually were similar in magnitude. The systematic errors probably were caused by the interacting effect of θ and other factors (e.g., phenology), which support Conclusions 1 and 2.

4 A Modification of the Michaelis-Menten Equation for Its Application to Estimating Canopy Photosynthesis of a Coastal Douglas-fir Stand

4.1 Introduction

The impact of the geometry of light (e.g., Kimball and Hand 1922, Moon and Spencer 1942, Liu and Jordan 1960, Robinson 1966, Steven 1977, McArthur and Hay 1981) on photosynthesis has been realized for a long time. Early studies largely focused on shoot-level chamber CO_2 gas exchange measurements (e.g., Kramer and Decker 1944, Zelawski et al. 1973, Young and Smith 1983, Smolander et al. 1987) and theoretical canopy radiation and photosynthesis modelling work (e.g., de Wit 1965, Cowan 1968, Grace 1971, Horn 1971, Allen et al. 1974, Sinclair et al. 1976, Goudriaan 1977, Norman 1982, Weiss and Norman 1985, Spitters et al. 1986, Goudriaan 1988). Theoretical modelling of canopy photosynthesis remains very active (Wang and Jarvis 1990, Goudriaan and van Laar 1994, de Pury and Farquhar 1997, Wang and Leuning 1998, Choudhury 2000, Roderick et al. 2001, Cohan et al. 2002).

Understanding the effect of diffuse radiation on canopy photosynthesis based on field observations has been more controversial and mainly restricted to the fact that CO_2 fluxes above a plant canopy on cloudy days are usually higher than on sunny days (e.g., Price and Black 1990, Hollinger et al. 1994, Hollinger et al. 1998). To some extent, this observational understanding is oversimplified and speculative (Gu et al. 1999) because other environmental variables are also different between sunny and cloudy days

(Baldocchi 1997, Lindroth et al. 1998, Freedman et al. 2000, Law et al. 2002). The first manipulative experiment attempting to overcome this observational dilemma was reported by Healey et al. (1998), who found increased biomass accumulation and radiation use efficiency for two grass canopies shaded using layers of solarweave shadecloth. Gu et al. (2002) studied the quantum use efficiencies of diffuse and direct photosynthetically active radiation (PAR) for CO_2 fluxes above canopies of five different C_3 species. This was one of the earliest studies using eddy covariance (EC) flux measurements to investigate the effect of diffuse PAR on canopy photosynthesis.

Recently, the rapid change in the global radiation environment (Stanhill and Cohen 2001) and the widespread use of the EC technique (e.g., Baldocchi 2003) rekindled interest in the impact of diffuse radiation on canopy photosynthesis and especially its effect on the terrestrial carbon cycle. One example involves the explanations suggested for the levelling off of atmospheric CO_2 concentration following eruption of Mt. Pinatubo in 1992. Although the cooler temperature following the eruption was successfully used to account for the levelling off (McCormick et al. 1995, Jones and Cox 2001, Lucht et al. 2002, Robock 2002, Soden et al. 2002), Roderick et al. (2001) and Gu et al. (2003) argued that the enhanced sky diffuse radiation (Molineaux and Ineichen 1996) following the eruption could be the main reason. However, this "diffuse radiation hypothesis" was seriously challenged by the following observations: (1) the levelling off of atmospheric CO_2 concentration started before the eruption (Keeling et al. 1995), (2) tree ring studies appeared not to support it (Briffa et al. 1998, Krakauer and Randerson 2003), (3) the annual cumulative carbon sequestration in 1992 at Harvard Forest (which was used to test the "diffuse radiation hypothesis") was reported to be lowest within the

1992-2000 period (Barford et al. 2001), (4) El Chichón enhanced sky diffuse radiation (Wendler 1984, Garrison 1995) as did Mt. Pinatubo, but no obvious levelling off of atmospheric CO_2 concentration was observed (Jones and Cox 2001). Angert et al. (2004) concluded that the enhanced diffuse radiation following the eruption of Mt. Pinatubo was "probably only enough to compensate for the reduction in total radiation".

In the early models of canopy photosynthesis (e.g., de Wit 1965, Norman 1980), the plant canopy was usually divided into N layers and in each layer the foliage was divided into sunlit and shaded leaves. Additionally, the sunlit leaves were divided into M leaf-sun angle classes to account for the incidence angles of direct PAR. Photosynthesis of the sunlit leaves from the M leaf-sun angle classes of each layer was totalled to be the photosynthetic contribution of all sunlit leaves of that layer. Canopy P was then calculated as the sum of photosynthesis of the sunlit and shaded leaves of each layer. This type of canopy P model will be referred to as complete multilayer models hereafter. Subsequent development of canopy P models mainly involves simplification of the complete multilayer models. One important aspect of the simplification has been reducing the M leaf-sun angle classes for the sunlit leaves to a single average leaf-sun angle class and using the average leaf-sun angle to calculate the absorbed un-scattered direct PAR for all the sunlit leaves (e.g., Sinclair et al. 1976, Spitters 1986, Leuning et al. 1995, de Pury and Farquhar 1997). The average leaf-sun angle for the sunlit leaves with a spherical leaf inclination angle distribution is approximately 60° (see Appendix D). As shown in Appendix E, using the single average leaf-sun angle to represent the incidence angles of direct PAR for all the sunlit leaves (e.g., as in 2-leaf models, including 2-leaf multilayer and 2-leaf single-layer models) leads to systematic errors in the estimates of

canopy P with respect to the fraction of sky diffuse PAR. In other words, 2-leaf models cannot reliably predict canopy P for a mixture of sunny and cloudy days (see Figure E-1a, E-1b and E-1c).

The lack of simple and reliable analytical methods contributes significantly to the uncertainty regarding the role of diffuse radiation in canopy photosynthesis. It remains a challenge to incorporate the effect of diffuse radiation on canopy photosynthesis into existing canopy photosynthesis models. Roderick et al. (2001) incorporated the work of Norman and Arkebauer (1991) (Figure 4-1), Anderson et al. (2000), and Choudhury (2000 & 2001) into the well-known light-use efficiency model (Monteith 1972) to accommodate the effect of diffuse radiation:

$$\overline{P} = \overline{\alpha}\ \overline{f}\ \overline{Q_{t0}} \qquad \text{(LUE model)} \qquad (1)$$

where $\overline{P}$ is monthly average canopy photosynthesis, $\overline{Q_{t0}}$ is monthly average incident total PAR, $\overline{f}$ is the monthly average fraction of $\overline{Q_{t0}}$ absorbed by the canopy, and $\overline{\alpha}$ is monthly average photosynthetic quantum use efficiency for $\overline{Q_{t0}}$. Roderick et al. (2001) assumed $\overline{\alpha}$ to be a linear function of $\overline{Q_{d0}}/\overline{Q_{t0}}$, where $\overline{Q_{d0}}$ is monthly average incident diffuse PAR, as follows: $\overline{\alpha} = 0.024\overline{Q_{d0}}/\overline{Q_{t0}} + 0.012$. This modification follows closely the modification of α used for a prairie ecosystem in Anderson et al. (2000), i.e., $\overline{\alpha} = 0.024\overline{Q_{d0}}/\overline{Q_{t0}} + 0.018$. The LUE model is widely used for estimating regional and global carbon fluxes at monthly and annual time scales.

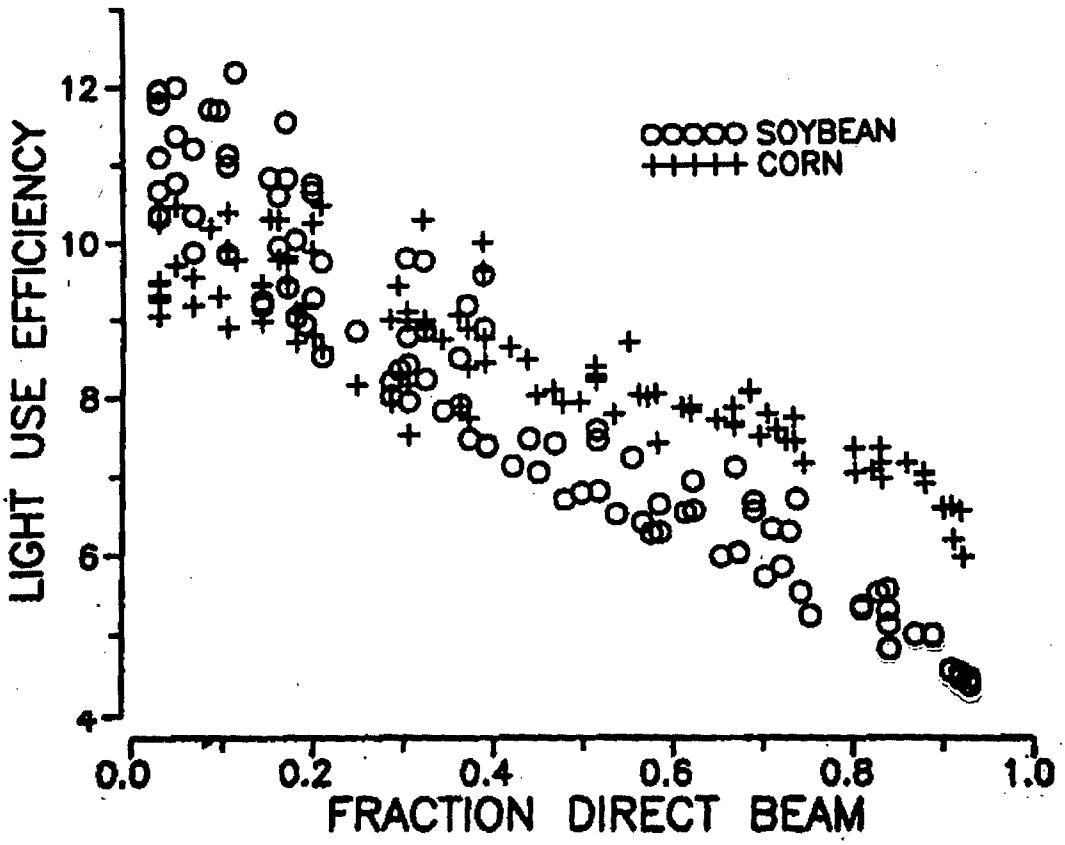

Figure 4-1. The dependence of modelled half-hourly light-use efficiency [g CO_2 (MJ IPAR)$^{-1}$] on the fraction of photosynthetically active radiation (PAR) above the canopy that is from direct beam (from Norman and Arkebauer 1991). The canopy light-use efficiency is based on IPAR (intercepted PAR) and the results are for C_3 (o) and C_4 (+) canopies.

At half-hourly time scale, the hyperbolic Michaelis-Menten model is more commonly used (e.g., Wofsy et al. 1993, Morgenstern et al. 2004, Xu and Baldocchi 2004, Goulden et al. 2004):

$$P = \frac{\alpha Q_{t0} A_{\max}}{\alpha Q_{t0} + A_{\max}} \qquad \text{(MM model)} \qquad (2)$$

where Q_{t0} is the half-hourly average incident total PAR on the canopy, α is the half-hourly average quantum use efficiency, and $A_{\max}$ is the half-hourly average maximum assimilation rate of the canopy. In order to incorporate the effect of diffuse PAR into the MM model, Gu et al. (2002 & 2003) extended the work of Norman and Arkebauer (1991) and Roderick et al. (2001) by modifying both α and $A_{\max}$ to be linear functions of Q_{d0}/Q_{t0}, where Q_{d0} is half-hourly incident diffuse PAR above the canopy:

$$\alpha = \alpha_d \frac{Q_{d0}}{Q_{t0}} + \alpha_b \frac{Q_{b0}}{Q_{t0}} \qquad (3)$$

$$A_{\max} = A_{\max d} \frac{Q_{d0}}{Q_{t0}} + A_{\max b} \frac{Q_{b0}}{Q_{t0}} \qquad (4)$$

where Q_{b0} is the incident direct PAR above the canopy, α_d and α_b are α for Q_{d0} and Q_{b0}, respectively, and $A_{\max d}$ and $A_{\max b}$ are $A_{\max}$ for Q_{d0} and Q_{b0}, respectively. Substituting Eqs. (3) and (4) into Eq. (2) gives a modified form of the MM model:

$$P = \frac{(\alpha_d Q_{d0} + \alpha_b Q_{b0})(A_{\max d} Q_{d0} + A_{\max b} Q_{b0})}{(\alpha_d Q_{d0} + \alpha_b Q_{b0}) Q_{t0} + (A_{\max d} Q_{d0} + A_{\max b} Q_{b0})} \qquad \text{(m-MM model)} \qquad (5)$$

Although the m-MM model was considered a significant step in understanding the effect of diffuse PAR on canopy photosynthesis, it has several drawbacks: (1) it does not completely separate the roles of direct and diffuse PAR in canopy photosynthesis because

of its retention of Q_{t0} in the denominator of Eq. (5) (note the multicolinearity between Q_{t0}, Q_{b0} and Q_{d0} as a result of these three quantities being related to each other as: Q_{t0} = Q_{b0} + Q_{d0}), (2) α is tightly tied to sky conditions (ideally α should reflect actual canopy-level photosynthetic processes), (3) it does not have an explicit parameter relating to the effect of canopy structure, and (4) it is a complicated non-linear model which makes it difficult to be incorporated into global carbon – climate models (Cox et al. 2000).

Additionally, in order to gain insights into the role of diffuse PAR, we have to examine the other side of the issue: the role of direct PAR. With the attention given to the role of diffuse PAR in canopy photosynthesis (Farquhar and Roderick 2003), the role of direct PAR has largely been ignored and relatively poorly understood. Gu et al. (2002 & 2003) concluded that α_d was significantly greater than α_b, but did not address the role of direct PAR explicitly.

The objectives of this study are to (1) introduce an alternatively modified MM model (hereafter referred to as the Q_e-MM model) with a focus on the photosynthetically effective radiation (i.e., Q_e) within a canopy, and (2) to provide a biophysical explanation of why α_b is less than α_d, and (3) provide a simple algorithm to fill gaps in half-hourly canopy P data for the 56-year-old coastal Douglas-fir stand described earlier (i.e., DF49). This study effectively extends the concept of the MM model to half-hourly canopy CO_2 fluxes by greatly reducing the errors associated with earlier versions of single big-leaf models of canopy P (e.g., Sellers et al. 1996). A potential contribution of this work is to produce algorithms that will increase the accuracy of large-scale carbon – climate models. The explicit separation of diffuse and direct PAR in the Q_e-MM model should

also help better understand the perturbations to the terrestrial carbon cycle caused by changes of aerosol levels.

4.2 Methods

The study site, EC CO_2 flux and auxiliary meteorological measurements were described in detail in Chapter 2. Downwelling total PAR (Q_{t0}) and diffuse PAR (Q_{d0}) were measured respectively using a quantum PAR sensor (model LI-190SB, LI-COR Inc) and a diffuse PAR sensor (Wood et al. 2003) (model BF2, Delta-T Devices, UK) mounted at a height of 45 m. The BF2 was installed in May 2000. The BF2 diffuse PAR sensor measures both Q_{t0} and Q_{d0}. Q_{t0} measured using the BF2 was compared with Q_{t0} measured using the LI-190SB, and the agreement was very satisfactory (Q_{t0} (BF2) = 1.02Q_{t0} (LI-190SB) + 8.77, r^2 = 0.98, RMSE = 61.87 μmol m^{-2} s^{-1}, n = 47644) (Figure B-1). In order to check the accuracy of the measurements of Q_{d0}, the half-hourly Q_{t0} measurements from the LI-190SB made in overcast conditions were compared with the corresponding half-hourly Q_{d0} measurements from the BF2. The overcast conditions were determined independently using a simple model of atmospheric attenuation of radiation (see Appendix B for details). For the overcast conditions, Q_{t0} (BF2) = 0.96Q_{t0} (LI-190SB) + 18.42 (r^2 = 0.98, RMSE = 24.61 μmol m^{-2} s^{-1}, n = 16444) and Q_{d0} (BF2) = 0.87Q_{t0} (LI-190SB) + 22.72 μmol m^{-2} s^{-1} (r^2 = 0.96, RMSE = 31.23 μmol m^{-2} s^{-1}, n = 16444) (Figure B-2). This agreement is satisfactory and falls in the technical accuracy specification (±15%) of BF2. Approximately 10% of total PAR was classified as direct radiation by BF2 in the overcast conditions defined in this study (see Appendix B). This is reasonable, because by definition diffuse radiation is isotropic, but the realistic sky brightness of overcast conditions is not isotropic (uniform) (i.e., Uniform vs. Standard

Overcast Sky) (Moon and Spencer 1942). Downwelling direct PAR (Q_{b0}) was calculated as the difference between Q_{t0} and Q_{d0}.

4.3 The model

4.3.1 Model development

Let us define the sunlit leaves of a plant canopy as the leaves that are in the gaps, receiving both direct and diffuse PAR, and the shaded leaves as the leaves that are in shade, receiving diffuse PAR only. Two-leaf models (e.g., the sun/shade model developed by de Pury and Farquhar 1997) aggregate all the sunlit leaves of a canopy (Figure 4-2a), regardless of their orientations to the solar beam, into a big sunlit leaf (group), and calculate the absorbed un-scattered direct PAR for the big sunlit leaf as:

$$Q_{ba\_sun} = (1-\sigma)Q_{b0}K_b \qquad (6)$$

where Q_{ba_sun} is the un-scattered direct PAR absorbed by the big sunlit leaf, σ is the leaf scattering (i.e., reflected and transmitted PAR) coefficient, Q_{b0} is the direct PAR incident on the canopy, and K_b is the extinction coefficient for direct PAR assuming that canopy foliage is "black" (i.e., total absorption of the incident PAR) and randomly distributed. The value of K_b can be obtained as:

$$K_b = 0.5/\sin\beta \qquad (7)$$

where β is the solar elevation angle. The factor 0.5 is the ratio of the projected area of the big hemispherical sunlit leaf (group) to its surface area (i.e., $\pi R^2/(2\pi R^2)$) when the sun is at zenith, and the factor $1/\sin\beta$ is used to adjust the projected area when the sun is at other angles (Figure 4-2a).

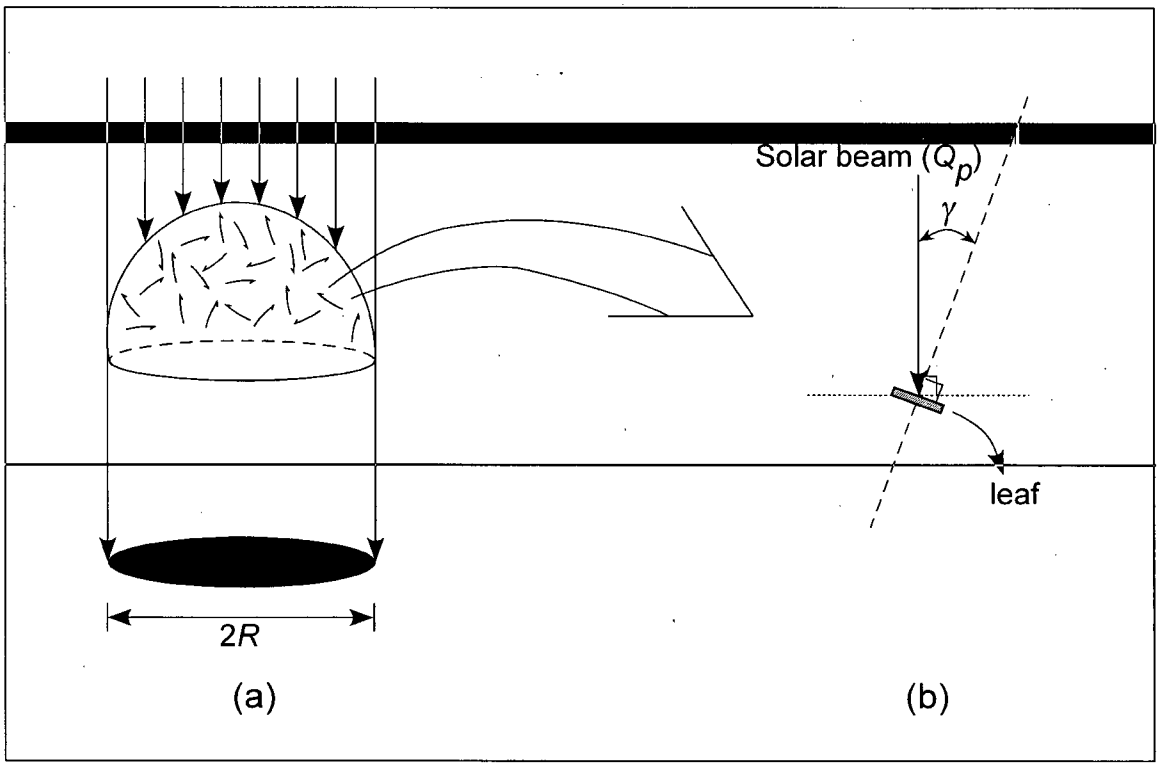

Figure 4-2. (a) The sun/shade model aggregates all the sunlit leaves into a big hemispherical sunlit leaf (i.e., assuming the leaf angle distribution of the sunlit leaves is spherical) and uses the mean APAR (absorbed PAR) (i.e., Eq. 8) to compute the photosynthesis for all the sunlit leaves. (b) The direct PAR absorbed by an individual sunlit leaf is given by: $Q_b(\gamma) = (1-\sigma)Q_p \cos\gamma$, where Q_p is the PAR perpendicular to the solar beam (the dotted line) and γ is the incidence angle between the beam and the normal to the leaf surface (the dashed line).

Substituting Eq. (7) into Eq. (6) gives:

$$Q_{ba\_sun} = (1-\sigma)Q_p / 2 \qquad (8)$$

where Q_p is the PAR perpendicular to the solar beam (Figure 4-2b), and is given as: $Q_p = Q_{b0} / \sin\beta$.

Therefore, the APAR (absorbed PAR) calculated by the sun/shade model for the big sunlit leaf is simply an estimate of the averaged beam flux density in the direction of the solar beam. It cannot be used to calculate the PAR absorbed by individual sunlit leaves (Figure 4-2b). As pointed out by Norman (1979) "In a canopy with foliage spherically distributed, there is a continuous range of flux densities from the full beam flux density (perpendicular to the incident beam) to zero (parallel to the incident beam) because of the range of leaf angles". Using the APAR calculated with Eq. (8) to compute the photosynthesis of the sunlit leaves makes the same type of errors as using the APAR to compute the total canopy P in single big leaf models. The solar beam is unidirectional, so the angle at which it strikes the leaf surface must be accounted for. The un-scattered direct PAR absorbed by an individual sunlit leaf can be calculated using:

$$Q_b(\gamma) = (1-\sigma)Q_p \cos\gamma \qquad (9)$$

where γ is the angle between the solar beam and a normal to the leaf surface, i.e., the angle of incidence (Figure 4-2b). For a spherical leaf angle distribution, the mean leaf-sun angle, $\bar{\gamma}$, is 57.3° (usually approximately as 60°) (see Appendix D). Therefore, $Q_b(\bar{\gamma}) = (1-\sigma)Q_p \cos\bar{\gamma} = (1-\sigma)Q_p \cos 60° = (1-\sigma)Q_p / 2$, which is essentially the same as the absorbed un-scattered direct PAR calculated using Eq. (8) for the big sunlit leaf (group).

Let us assume the leaf angle distribution of the sunlit leaves is spherical, so the "distribution of leaf inclination angles to the horizontal is the same as the distribution of leaf-sun angles" (Norman 1980). The fraction of sunlit leaf area (f_γ) exposed at incidence angle γ is given by (see derivation in Appendix D):

$$f_\gamma = \sin\gamma d\gamma \qquad (10)$$

Figure 4-3 shows that approximately 15% of the sunlit leaves don't absorb direct PAR at all (i.e., when $\cos\gamma = 0$ or $\gamma = 90^\circ$ in Eq. (9)). Approximately 45% of the sunlit leaves absorb less than 30% of Q_p (i.e., $\cos\gamma < 0.3$). If we take Q_p = 2000 μmol m^{-2} s^{-1} and σ = 0.1 as an example, $Q_b(\gamma) < 540$ μmol m^{-2} s^{-1} (calculated using Eq. (9)) when $\cos\gamma < 0.3$. This means that even when the sunlit leaves could potentially receive the maximum direct PAR (i.e., Q_p = 2000 μmol m^{-2} s^{-1}), there is still 45% of the sunlit leaves that are likely to be light limited (i.e., the leaves absorbed less than 540 μmol m^{-2} s^{-1} of direct PAR). If we take Q_p = 1000 μmol m^{-2} s^{-1} and still assume that when leaves absorb less than 540 μmol m^{-2} s^{-1} un-scattered direct PAR, they are light-limited, we can calculate the cosine of the leaf-sun angles (i.e., $\cos\gamma$) for these light limited leaves as $\cos\gamma < 540/((1-\sigma)Q_p) = 0.6$. Figure 4-3 shows that approximately 72% of $\cos\gamma$ values are less than 0.6, i.e., 72% of the sunlit leaves are light-limited in this case.

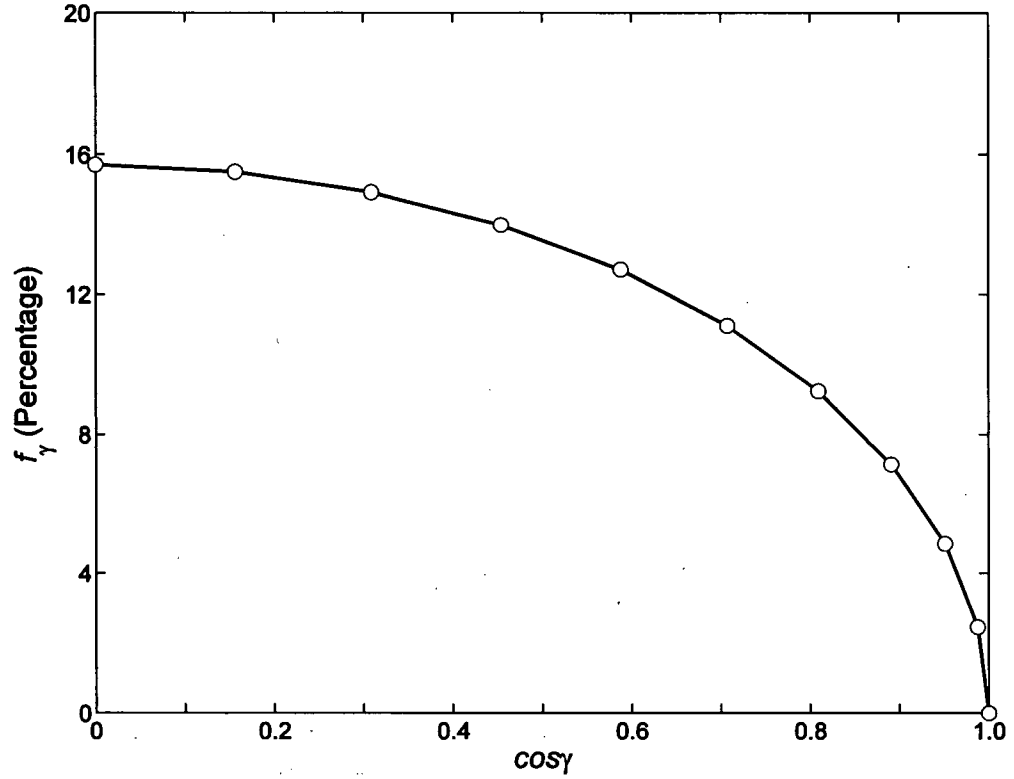

Figure 4-3. The relationship between f_γ and $\cos\gamma$. γ was stepwise increased from 0° to 90° in steps of 9° ($d\gamma = (9°/180°)\pi = 0.1571$ radians). For each step, $\cos\gamma$ and its corresponding f_γ ($f_\gamma = \sin\gamma d\gamma$, Eq. (10)) were calculated (the circles). Note the f_γ vs. $\cos\gamma$ relationship is independent of solar elevation angle (i.e., β), but the total LAI of the sunlit leaves is not independent of β.

Figure 4-3 supports the statements made by de Pury and Farquhar (1997) (on their page 544) "(sunlit) leaves nearly perpendicular to the sun-beam direction have the highest absorbed irradiance (1830 – 2040 μmol m^{-2} s^{-1}), and are only a small proportion of the sunlit leaves, while (sunlit) leaves parallel to the beam direction absorb only diffuse radiation (220 – 430 μmol m^{-2} s^{-1}) and are a high proportion of the sunlit leaves". Figure 4-3 suggests that the photosynthesis of the sunlit leaves has to be further partitioned into a light-limited subgroup (e.g., for the parallel sunlit leaves absorbing 220 μmol m^{-2} s^{-1} PAR) and a light-saturated subgroup (e.g., for the perpendicular sunlit leaves absorbing 1830 μmol m^{-2} s^{-1} PAR).

Let us divide the entire canopy into three conceptual groups: the first group with all the light-limited sunlit leaves, the second group with all the light-saturated sunlit leaves, and the third group with all the shaded leaves. All the shaded leaves are assumed to be light-limited (Figure 4-4a). Therefore, the entire canopy P can be written as:

$$P = P_{sun\_LightLimited} + P_{sun\_LightSaturated} + P_{shd} \qquad (11)$$

where $P_{sun\_LightLimited}$ and $P_{sun\_LightSaturated}$ are the respective photosynthetic rates of the light-limited and light-saturated leaves in the sunlit group. P_{shd} is the photosynthetic rate of the shaded leaves.

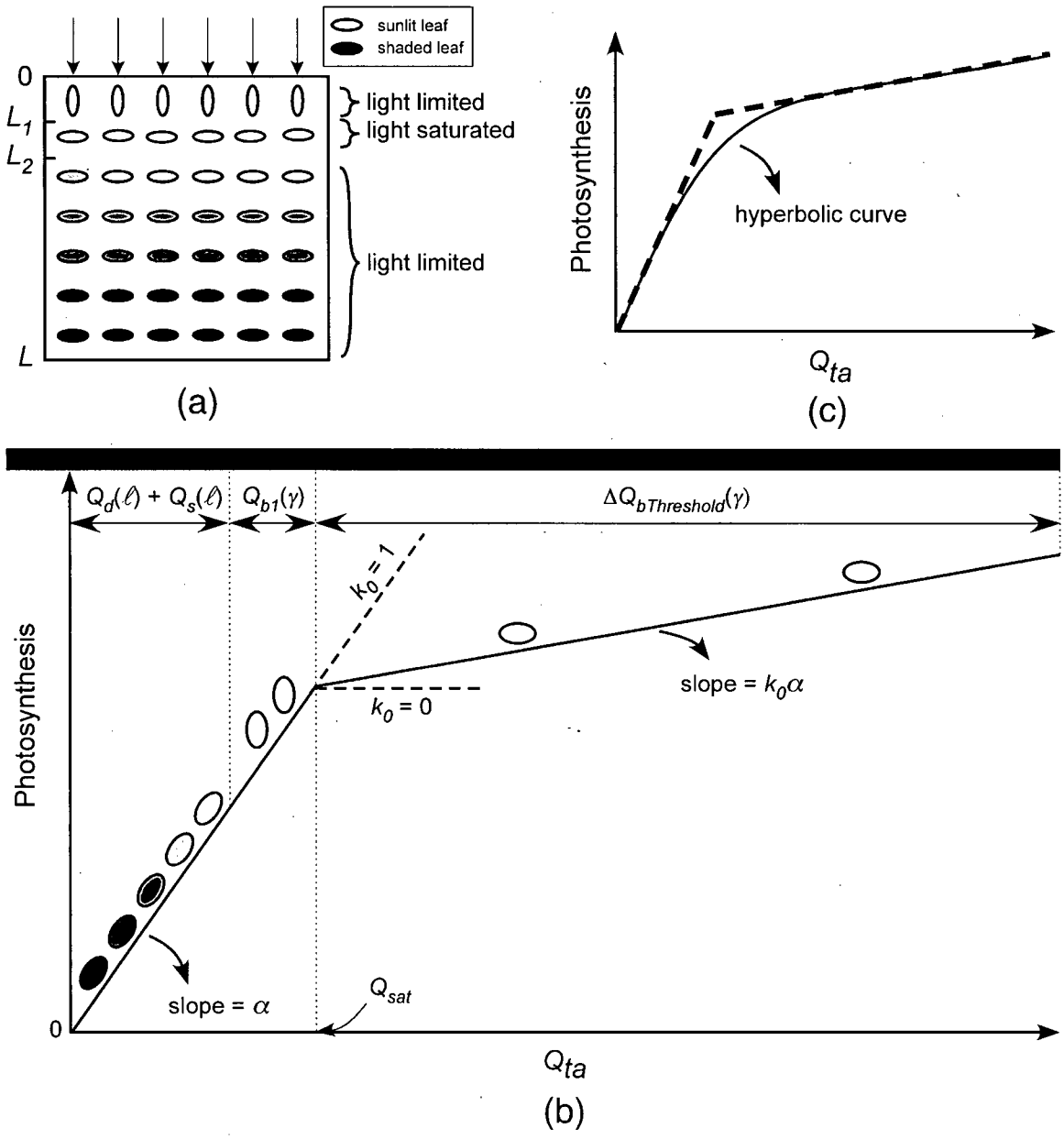

Figure 4-4. (a) The canopy is divided into three conceptual groups: the first group (0-L_1) with all the light-limited sunlit leaves, the second group (L_1 to L_2) with all the light-saturated sunlit leaves, and the third group (L_2 to L) with the shaded leaves. L_1, L_2 and L are cumulative LAI. (b) The photosynthetic light response to Q_{ta} (total absorbed PAR) for the shaded leaves is linear with a slope of α. In addition to the absorption of sky diffuse PAR (i.e., $Q_d(\ell)$) and the scattered direct PAR (i.e., $Q_s(\ell)$), the light-limited sunlit leaves

absorb limited amounts of un-scattered direct PAR (i.e., $Q_{b1}(\gamma)$), and thus its photosynthetic response can still be linear with the slope of α. The photosynthetic response of the light-saturated sunlit leaves can be described using two linear responses: the initial linear response with the slope of α and the second linear response with the slope of $k_0\alpha$.

The total photosynthesis of all the light limited sunlit leaves is given by:

$$P_{sun\_LightLimited} = \int_0^{L_1} \alpha[Q_d(\ell)+Q_s(\ell)+Q_{b1}(\gamma)]d\ell \qquad (12)$$

where $Q_d(\ell)$ and $Q_s(\ell)$ are the absorbed sky diffuse PAR and the scattered direct PAR at canopy depth, ℓ (cumulative LAI), respectively. $Q_{b1}(\gamma)$ is the additional (limited) amount of un-scattered direct PAR absorbed by the light-limited sunlit leaves. The photosynthetic response of these light-limited sunlit leaves to Q_{ta} (total absorbed PAR) is linear with a slope of α (Figure 4-4b), because the Q_{ta} values for these sunlit leaves are not exceeding Q_{sat}, where Q_{sat} is the saturating level of Q_{ta} above which the quantum use efficiency of absorbed PAR is significantly reduced.

The total photosynthesis of the light saturated sunlit leaves is given by:

$$P_{sun\_LightSaturated} = \int_{L_1}^{L_2} \alpha[Q_d(\ell)+Q_s(\ell)+Q_{bThreshold}]d\ell + \int_{L_1}^{L_2} k_0\alpha\Delta Q_{bThreshold}(\gamma)d\ell \qquad (13)$$

where $Q_{bThreshold}$ is the maximum amount of un-scattered direct PAR (i.e., $Q_{bThreshold}$ is the maximum of all the $Q_{b1}(\gamma)$ values) absorbed by a sunlit leaf, in addition to its absorption of $Q_d(\ell)+Q_s(\ell)$, to still maintain the initial linear photosynthetic response with the slope of α. The total amount of PAR absorbed by the light saturated sunlit leaves is

$Q_d(\ell)+Q_s(\ell)+Q_{bThreshold}+\Delta Q_{bThreshold}(\gamma) = Q_{sat}+\Delta Q_{bThreshold}(\gamma)$. The second integration of Eq. (13) (Figure 4-4b) reflects the photosynthetic contribution of the absorption of the un-scattered direct PAR in excess of $Q_{bThreshold}$ (i.e., $\Delta Q_{bThreshold}(\gamma)$), where $\Delta Q_{bThreshold}(\gamma)$ is the difference between the total un-scattered direct PAR absorbed by the light saturated sunlit leaves and $Q_{bThreshold}$. The quantum use efficiency for $\Delta Q_{bThreshold}(\gamma)$ is only $k_0\alpha$, because some of the absorbed $\Delta Q_{bThreshold}(\gamma)$ is dissipated as heat and used in photochemical processes other than photosynthesis (e.g., xanthophyll cycle). Let us use an example to illustrate the key points in Figure 4-4b. As with the previous example, let us take Q_p = 2000 μmol m^{-2} s^{-1}, σ = 0.1 and also assume $Q_d(\ell)+Q_s(\ell)\approx 160$ μmol m^{-2} s^{-1} throughout the canopy layers from 0 to L_2 (Figure 4-4a). If the photosynthesis of an individual sunlit leaf is assumed to be saturated at Q_{ta} (total absorbed PAR) of 700 μmol m^{-2} s^{-1} (i.e, Q_{sat} = 700 μmol m^{-2} s^{-1}), then $Q_{bThreshold}$ can be calculated as: $Q_{bThreshold}$ = 700 – 160 = 540 μmol m^{-2} s^{-1}. Values of $Q_{b1}(\gamma)$ are any values that are less than $Q_{bThreshold}$ (i.e., 540 μmol m^{-2} s^{-1} in this case). The leaf-sun angles (i.e., γ) for the light limited sunlit leaves can be calculated as γ > 73° using Eq. (9) (i.e., $\cos\gamma < Q_{bThreshold}/((1-\sigma)Q_p) = 0.3 \Rightarrow \gamma > \arccos(0.3) = 73°$). The light saturated sunlit leaves are the sunlit leaves that receive more than 540 μmol m^{-2} s^{-1} un-scattered direct PAR. $\Delta Q_{bThreshold}(\gamma) = (1-\sigma)Q_p\cos(\gamma) - Q_{bThreshold}$, where $\cos\gamma > 0.3$. The leaf-sun angles for the light saturated sunlit leaves are γ < 73°.

The photosynthesis of the shaded leaves is given by:

$$P_{shd} = \int_{L_2}^{L} \alpha[Q_d(\ell)+Q_s(\ell)]d\ell \qquad (14)$$

Substituting Eqs. (12), (13) and (14) into Eq. (11) gives the photosynthesis of the entire canopy:

$$P = \int_0^L \alpha[Q_d(\ell)+Q_s(\ell)]d\ell + \int_0^{L_1} \alpha Q_{b1}(\gamma)d\ell + \int_{L_1}^{L_2} \alpha Q_{bThreshold}d\ell + \int_{L_1}^{L_2} k_0\alpha\Delta Q_{bThreshold}(\gamma)d\ell \quad (15)$$

The absorbed sky diffuse PAR at ℓ is given by (Goudriaan and van Laar 1994):

$$Q_d(\ell) = Q_{d0}K_d e^{-K_d\ell} \quad (16)$$

where K_d is the extinction coefficient for Q_{d0} and is usually approximated as 0.7. Eq. (16) is obtained as $-d(Q_{d0}e^{-K_d\ell})/d\ell$, where the minus sign indicates that Q_{d0} is decreasing throughout the canopy.

The scattering of the solar beam (Goudriaan and van Laar 1994) can be approximated by:

$$Q_s(\ell) = Q_{b0}(K_b^{'}e^{-K_b^{'}\ell} - (1-\sigma)K_b e^{-K_b\ell}) \quad (17)$$

where Q_{b0} is the incident direct PAR (on a horizontal plane) above the canopy, $K_b^{'}$ is the extinction coefficient of the solar beam for green leaves. $K_b^{'} = K_b\sqrt{1-\sigma}$.

The last three integrations of Eq. (15) are all related to the absorption of the un-scattered direct PAR. As shown in Eq. (9) and Norman (1980) (his Table 4), the absorption of the un-scattered direct PAR is dependent on the leaf orientation (i.e., γ) rather than canopy depth (i.e., ℓ). Note the fraction of sunlit leaf area is not independent of ℓ.

Because $Q_{b1}(\gamma)$ and $\Delta Q_{bThreshold}(\gamma)$ are independent of *l*, so we can write the last three integrations of Eq. (15), with the use of Eq. (9), as:

$$\int_0^{L_1} \alpha Q_{b1}(\gamma)d\ell = \alpha(1-\sigma)Q_p\overline{\cos\gamma_l}L_l \quad (18a)$$

$$\int_{L_1}^{L_2} \alpha Q_{bThreshold} d\ell = \alpha(1-\sigma) Q_p \cos\gamma_{Threshold} (L_2 - L_1) \quad (18b)$$

$$\int_{L_1}^{L_2} k_0 \alpha \Delta Q_{bThreshold}(\gamma) d\ell = k_0 \alpha (1-\sigma) Q_p \overline{\Delta \cos\gamma_{Threshold}} (L_2 - L_1) \quad (18c)$$

where $\overline{\cos\gamma_1}$ is the average of all the $\cos\gamma$ values of the light limited sunlit leaves. $\cos\gamma_{Threshold}$ is the cosine of the leaf-sun angle ($\gamma_{Threshold}$) associated with $Q_{bThreshold}$. $\overline{\Delta\cos\gamma_{Threshold}}$ is the difference between the average of all the $\cos\gamma$ values of the light saturated sunlit leaves and $\cos\gamma_{Threshold}$ (see the definition of $\Delta Q_{bThreshold}(\gamma)$).

The total sunlit LAI (L_2) (Figure 4-4a) in a canopy is given by (Norman 1980):

$$L_2 = \int_0^L e^{-K_b \ell} d\ell = (1 - e^{-K_b L}) / K_b \quad (19)$$

Let us write:

$$L_1 = k_1 L_2 \quad (20a)$$

$$L_2 - L_1 = (1 - k_1) L_2 \quad (20b)$$

where k_1 is the fraction of the sunlit leaves that are light limited, and 1 - k_1 is the fraction of the sunlit leaves that are light saturated.

Substituting Eqs. (16), (17), (18) and (20) into Eq. (15) gives:

$$P = \alpha Q_{d0}(1 - e^{-K_d L}) + \alpha\sigma' Q_{b0} + \alpha(1-\sigma) Q_p k_2 L_2 \quad (21)$$

where $\sigma' = 1 - e^{-K_b' L} - (1-\sigma)(1 - e^{-K_b L})$. $\sigma' \approx \sigma$ if L is very large (e.g., L > 8). $k_2 = k_1 \overline{\cos\gamma_1} + (1-k_1)\cos\gamma_{Threshold} + k_0(1-k_1)\overline{\Delta\cos\gamma_{Threshold}}$.

The L for this stand is approximately 7 – 8, so the exponential terms in Eqs. (19) and (21) (including the exponential terms in σ') are quite small. Ignoring these exponential terms and substituting Eq. (19) (i.e., using $L_2 \approx 2\sin\beta$) into Eq. (21) gives:

$$P = \alpha(Q_{d0} + \sigma Q_{b0} + 2k_2(1-\sigma)Q_p \sin\beta)$$

$$= \alpha(Q_{d0} + \sigma Q_{b0} + 2k_2(1-\sigma)Q_{b0})$$

$$= \alpha Q_e \qquad \text{Qe-LUE} \qquad (22)$$

Note $\sin\beta$ disappears from Eq. 22 since $Q_{b0} = Q_p \sin\beta$. $Q_e = Q_{d0} + kQ_{b0}$ with $k = \sigma + 2k_2(1-\sigma)$. The first component (i.e., σ) of k accounts for the photosynthetic contribution of scattered direct PAR, and the second component (i.e., $2k_2(1-\sigma)$) accounts for the photosynthetic contribution from the un-scattered direct PAR.

In the above derivation, we considered that leaves within the canopy are either light-limited or light-saturated. In reality, leaves saturate over a narrow range of PAR as opposed to having an absolute fixed saturating point of PAR (Figure 4-4c). In order to smooth the transition from the P of the light-limited layer to that of the light-saturated layer, let us re-write Eq. (22) in its hyperbolic form:

$$P = \frac{\alpha(Q_{d0} + kQ_{b0})A_{\max}}{\alpha(Q_{d0} + kQ_{b0}) + A_{\max}}$$

$$= \frac{\alpha Q_e A_{\max}}{\alpha Q_e + A_{\max}} \qquad \text{Qe-MM model} \qquad (23)$$

where A_{max} (the asymptote) denotes the maximum rate of canopy photosynthetic assimilation. Eq. (23) will be referred to as the Q_e-MM model. The magnitude of A_{max} is mainly determined by temperature (see Figure 4-7c and Figure 4-8c) and the Rubisco (nitrogen) content of the leaves (e.g., Evans and Vogelmann 2003). When k = 1, the Q_e-MM model becomes the regular MM model. If the LAI of a canopy is not as large as this 56-year-old Douglas-fir stand, α obtained in this case for the Q_e-MM model would be the apparent quantum yield based on incident PAR as opposed to absorbed PAR.

In the above derivation, the solar beam was assumed to be parallel rays, ignoring the finite angular radius of the solar disk (e.g., Horn 1971). The angular radius of the solar disk, which is 0.5°, results in a strong penumbral light spreading effect (see Appendix C), especially in coniferous stands (Miller and Norman 1971, Oker-Blom 1985, Stenberg 1998, Palmroth et al. 1999). In a sense, the existence of penumbrae in a plant canopy undermines the rationality of the pure black-and-white separation of canopy foliage into sunlit and shaded groups (Ross 1991), since the majority of the foliage can be in penumbrae (e.g., Oker-Blom 1985, Palmroth et al. 1999). Therefore, k in the Q_e-MM model likely includes the penumbral light spreading effect of the solar rays. The role of penumbral light spreading on canopy P is rarely accounted for in "mechanistic" bottom-up models (e.g., the sun/shade model), because it is not existent at the leaf level and thus cannot be simply scaled up to the canopy level. In this analysis, the penumbral effect of solar rays is hypothesized to be proportional to Q_{b0} (i.e., part of kQ_{b0} in Eq. (23)), which is consistent with the findings in recent studies (e.g., Stenberg 1998).

Alternatively, the Q_e-MM model can be derived from the MM model. Substituting Eq. (3) into Eq. (2) gives:

$$P = \frac{(\alpha_d Q_{d0} + \alpha_b Q_{b0}) A_{\max}}{(\alpha_d Q_{d0} + \alpha_b Q_{b0}) + A_{\max}} \tag{24}$$

Rewriting Eq. (24) by factoring out α_d gives the form of the Q_e-MM model:

$$P = \frac{\alpha_d (Q_{d0} + \frac{\alpha_b}{\alpha_d} Q_{b0}) A_{\max}}{\alpha_d (Q_{d0} + \frac{\alpha_b}{\alpha_d} Q_{b0}) + A_{\max}} \tag{25}$$

where α_d and $Q_{d0}+\frac{\alpha_b}{\alpha_d}Q_{b0}$ correspond to the α and Q_e in the Q_e-MM model, respectively. $\frac{\alpha_b}{\alpha_d}$ corresponds to k in the Q_e-MM model. Comparison of Eqs. 23 and 25 reveals that the modification of A_{max} (i.e., $A_{\max}=A_{\max d}\frac{Q_{d0}}{Q_{t0}}+A_{\max b}\frac{Q_{b0}}{Q_{t0}}$ in Eq. 4) is unnecessary, because α and A_{max} are not completely independent (they appear as a product of $\alpha Q_{t0}A_{\max}$ in the numerator of the MM model, i.e., Eq. 2). As will be shown later (e.g., Figure 4-9), the modification of α to incorporate the effect of diffuse PAR makes the modification of A_{max} unnecessary. Derivation of the Q_e-MM model using the results from Norman and Arkebauer (1991) (i.e., Figure 4-1) is given in Appendix C (i.e., Eq. (3) in this appendix).

4.3.2 Model parameterization

In this analysis, only the measured half-hourly values of NEE (NEP) were used, i.e., gap filled values were excluded. The u_* (friction velocity) threshold was chosen as u_{*th} = 0.3 m s^{-1} following Morgenstern et al. (2004). In addition, the half-hourly NEE (NEP) measurements made in calm conditions (i.e., $u_* < u_{*th}$) both at night and during the daytime periods when Q_{t0} < 200 μmol m^{-2} s^{-1} were also excluded. It was found that the lack of nocturnal mixing extended to daytime conditions when light was very low (generally Q_{t0} < 100 μmol m^{-2} s^{-1}). To be conservative, the u_* filter was applied to daytime NEP measurements made in conditions when Q_{t0} < 200 μmol m^{-2} s^{-1} (see Chapter 2 for details). Canopy P was calculated as the sum of daytime NEP and daytime

ecosystem respiration (R_{ed}). The latter was obtained using the *A*15-day method described in Chapter 3. The data used in this analysis were from May 2000 to December 2005. The parameters (e.g., α, A_{max}, and k) in the MM, Q_e-MM and m-MM models were determined using the nonlinear Gauss-Newton algorithm provided by the Matlab® Statistics Toolbox®.

4.3.3 Model comparisons

In order to evaluate the performance of the Q_e-MM model and to assess the inadequacies of the existing models of canopy *P*, the Q_e-MM model was compared with the MM model (Figure 4-7, Figure 4-8 and Figure 4-15), with the sun/shade model (Figure 4-8 and Figure 4-16) and with the m-MM model (Figure 4-9). Performance of the models was evaluated based on three criteria: (1) whether the model has systematic errors with respect to the change in sky diffuse PAR (e.g., Figure 4-8a), (2) whether the model has systematic errors with respect to the change in the calculated sunlit/shade fractions (which basically is a function of solar elevation angle) (e.g., Figure 4-8b), and (3) whether the model correctly responds to a change in air temperature (e.g., Figure 4-8c).

The sun/shade model used in this study was directly taken from de Pury and Farquhar (1997). The numerical example given by de Pury and Farquhar (1997) in their Table 6 was reproduced before the sun/shade model was applied to the EC data, indicating the sun/shade model was coded correctly for this analysis. The three inputs to the sun/shade model for the DF49 stand were V_{cmax25} (leaf-level maximum catalytic capacity of Rubisco at 25 °C) = 44 μmol m^{-2} s^{-1} (see Warren et al. 2003, Ethier and

Livingston 2004 for the A/C_i curves for this stand), K_n (nitrogen extinction coefficient through the canopy) = 0.28, and L (total LAI) = 8. The value of K_n was determined using an optimization procedure in which K_n values were increased from 0 to 0.7 in steps of 0.02. The sun/shade model was applied to the EC measurements (from May 2000 to December 2005) and the value of r^2 for the regression of measured P against modeled P was computed for each value of K_n. The K_n value corresponding to the maximum r^2 between the measured and modelled P (i.e., K_n = 0.28) was chosen as the best estimate of K_n for this 56-year-old stand. The value of K_n is very similar to the K_n found for a wheat crop by de Pury and Farquhar (1997) (i.e., K_n = 0.713/2.4 = 0.2971, their Table 5).

4.4 Results

4.4.1 Variance in *P* accounted for by adding fractions of Q_{b0} to Q_{d0}

A new variable was defined as: $Q_x = Q_{d0} + xQ_{b0}$, where x is a fraction of Q_{b0} added to Q_{d0}. When x = 0, $Q_x = Q_{d0}$, and when x = 1, $Q_x = Q_{t0}$. x was increased stepwise from 0 to 1 in steps of 0.01, and for each x, P was regressed against the corresponding Q_x using $P = \frac{\alpha Q_x A_{\max}}{\alpha Q_x + A_{\max}}$ to obtain a coefficient of determination (r^2) for each regression. Figure 4-5 shows that when $Q_{t0} \leq 300$ μmol m^{-2} s^{-1}, r^2 is insensitive to x. The insensitivity of r^2 to x when $Q_{t0} \leq 300$ μmol m^{-2} s^{-1} is expected, because canopy P tends to be light limited and Q_{d0} is the predominant component of Q_{t0}, therefore, adding the fraction x of Q_{b0} to Q_{d0} does not account for significantly more variance in canopy P. In theory, when $Q_{t0} \leq 300$ μmol m^{-2} s^{-1}, there is no need to distinguish between diffuse

and direct PAR, so the maximum correlation between P and Q_x should occur when $x = 1$ (i.e., $Q_x = Q_{t0}$). The x value corresponding to the maximum correlation between P and Q_x is k, i.e., $k = \max(x)$. As Q_{t0} increases above 300 μmol m^{-2} s^{-1}, r^2 shows considerable variation with respect to x, and the general patterns are (1) Q_{d0} accounts for more variance in P than Q_{t0} (e.g., when Q_{t0} > 900 μmol m^{-2} s^{-1}, Q_{d0} accounts for approximately 29% of the variance in P, while Q_{t0} accounts for almost no variance), and (2) r^2 initially increases with x to a maximum and then significantly decreases with further increases in x. The values of x associated with the maximum r^2 (i.e., k) are $x = 0.25$ and $x = 0.22$ for Q_{t0} between 300 – 900 μmol m^{-2} s^{-1} and Q_{t0} greater than 900 μmol m^{-2} s^{-1}, respectively.

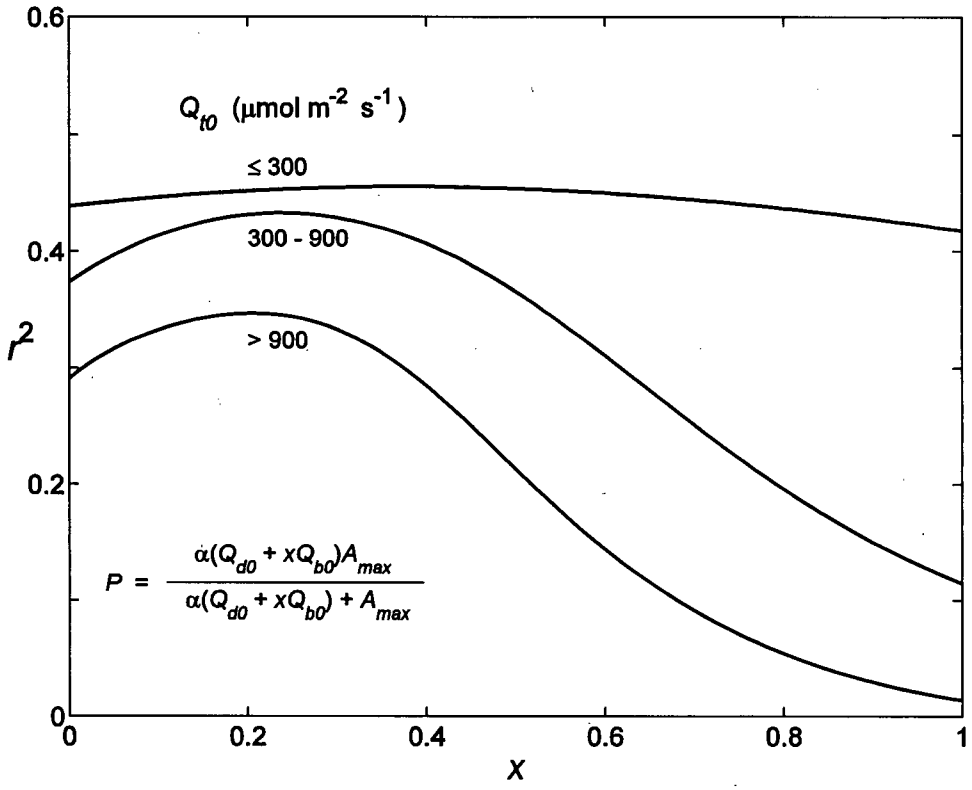

Figure 4-5. The variance in P accounted for using the Q_e-MM model at three levels of Q_{t0}. Canopy P was related to PAR using $P = \frac{\alpha Q_x A_{max}}{\alpha Q_x + A_{max}}$, where Q_x is defined as $Q_x = Q_{d0} + xQ_{b0}$. x was increased stepwise from 0 to 1, and a corresponding coefficient of determination (i.e., r^2) of the regression was calculated for each x. When $x = 1$, $Q_x = Q_{t0}$, and when $x = 0$, $Q_x = Q_{d0}$.

4.4.2 Comparisons between the MM, Q_e-LUE, and Q_e-MM models

Figure 4-6 shows the responses of canopy P to Q_{t0}, Q_{d0}, Q_{b0} and Q_e. As expected, the response of P to Q_{t0} appears to be hyperbolic, and a hyperbolic fit using the MM model accounts for 50% of the variance in P (Figure 4-6a). The response of P to Q_{d0} is curvilinear except for the sharp increase in P around Q_{d0} of 200 μmol m^{-2} s^{-1} (Figure 4-6b). Canopy P appears to have a very weak response to Q_{b0} (Figure 4-6c). The response of P to Q_e is well described using the Q_e-MM model (r^2 = 0.66) (Figure 4-6d). The responses of P to Q_{t0} and Q_e are both hyperbolic, but the response of P to Q_e is more linear than the former as indicated by its larger value of A_{max}. The A_{max} obtained using Q_e-MM model is 83.38 μmol m^{-2} s^{-1} while that for the MM model is 24.79 μmol m^{-2} s^{-1}. In fact, a linear relationship between P and Q_e using the Q_e-LUE model accounts for 65% of the variance in P (Figure 4-6d). The linear fit using the Q_e-LUE model has an intercept of 1.21 μmol m^{-2} s^{-1}, which is possibly a consequence of lack of accounting for the transition from light-limited photosynthesis to light-saturated photosynthesis (Figure 4-4c). But the Q_e-LUE model would be useful in estimating daily and monthly canopy P (data not shown), and preferable to the regular LUE model (i.e., Eq. (1)). The values of k obtained using the Q_e-MM and Q_e-LUE models are k = 0.22 and k = 0.23, respectively.

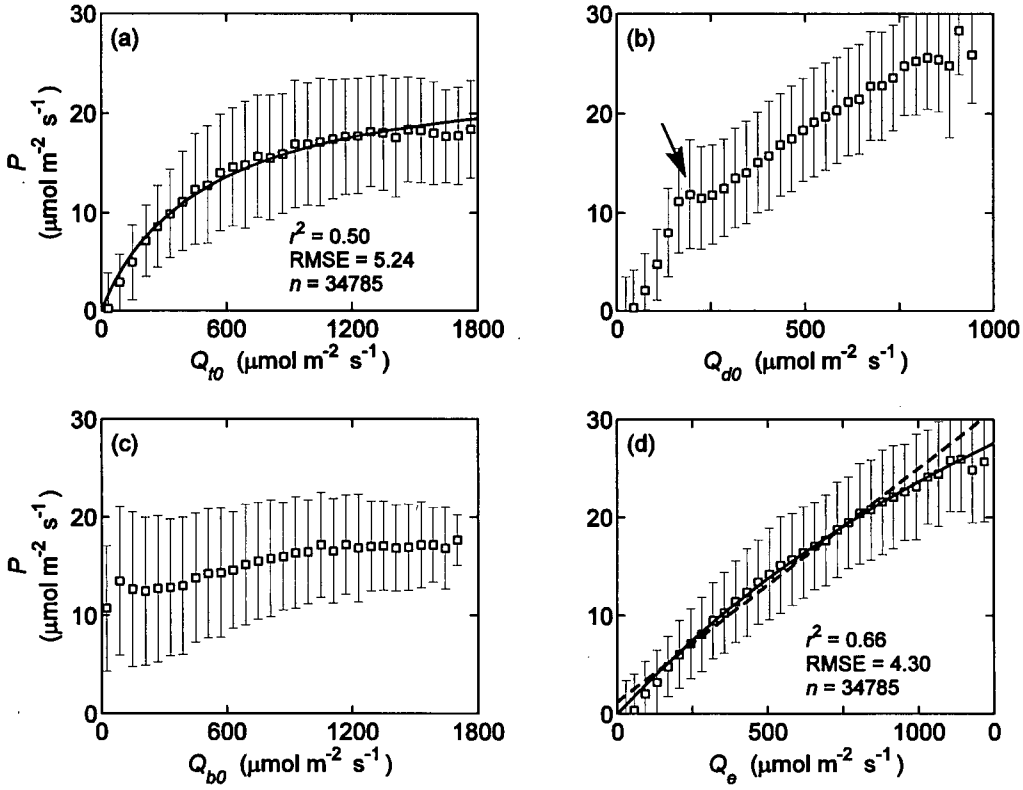

Figure 4-6. The responses of P to Q_{t0}, Q_{d0}, Q_{b0} and Q_e. The fitted curve in (a) was obtained using $P = \frac{\alpha Q_{t0} A_{\max}}{\alpha Q_{t0} + A_{\max}}$ (i.e., the MM model) with α = 0.050 mol mol^{-1} and A_{max} = 24.79 μmol m^{-2} s^{-1}. The arrow in (b) indicates the sharp increase in P around Q_{d0} of 200 μmol m^{-2} s^{-1}. The fitted curve in (d) was obtained using $P = \frac{\alpha Q_e A_{\max}}{\alpha Q_e + A_{\max}}$ (i.e., the Q_e-MM model) with α = 0.041 mol mol^{-1}, A_{max} = 83.38 μmol m^{-2} s^{-1} and k = 0.22, r^2 = 0.66, RMSE = 4.30 μmol m^{-2} s^{-1}. The dashed line in (d) was obtained using $P = 0.030 Q_e + 1.21$ (i.e., the Q_e-LUE model), with k = 0.23, r^2 = 0.65 and RMSE = 4.38 μmol m^{-2} s^{-1}. Symbols represent bin averages and vertical lines indicate ±1 SD. n = 34785. All fitted curves were obtained using the original half-hourly data, i.e., not obtained using the bin-averaged data.

The errors of the MM, Q_e-LUE and Q_e-MM models are shown in Figure 4-7 as modelled P minus measured P. The MM model overestimates P in low Q_{d0} conditions, and progressively underestimates P as Q_{d0} increases. The Q_e-LUE model overestimates P when $Q_{d0} < 100$ μmol m^{-2} s^{-1}, slightly underestimates P for Q_{d0} between 100 and 600 μmol m^{-2} s^{-1}, and then progressively overestimates P for $Q_{d0} > 600$ μmol m^{-2} s^{-1}. In contrast, the Q_e-MM model has the smallest modelling error with respect to Q_{d0}. (Figure 4-7a). The systematic errors of the three models with respect to $\sin\beta$, where β is the solar elevation angle, are shown in Figure 4-7b. All three models overestimate P when $\sin\beta < 0.5$ and underestimate P when $\sin\beta > 0.5$, but the magnitude of the errors for the MM model are more than three times larger than those for the Q_e-LUE and Q_e-MM models. When solar elevation angle is low, e.g., $\sin\beta < 0.2$, the correlation between Q_{d0} and $\sin\beta$ is very strong, so the modeling errors with respect to Q_{d0} and $\sin\beta$ may come from the same source. Figure 4-7c shows that the three models have very similar systematic errors with respect to canopy T_a . They all significantly overestimate P when $T_a < 10$ °C or $T_a > 20$ °C, and underestimate P between 10 °C $< T_a <$ 20 °C, suggesting an independent effect of T_a on P, which cannot be accounted for by light.

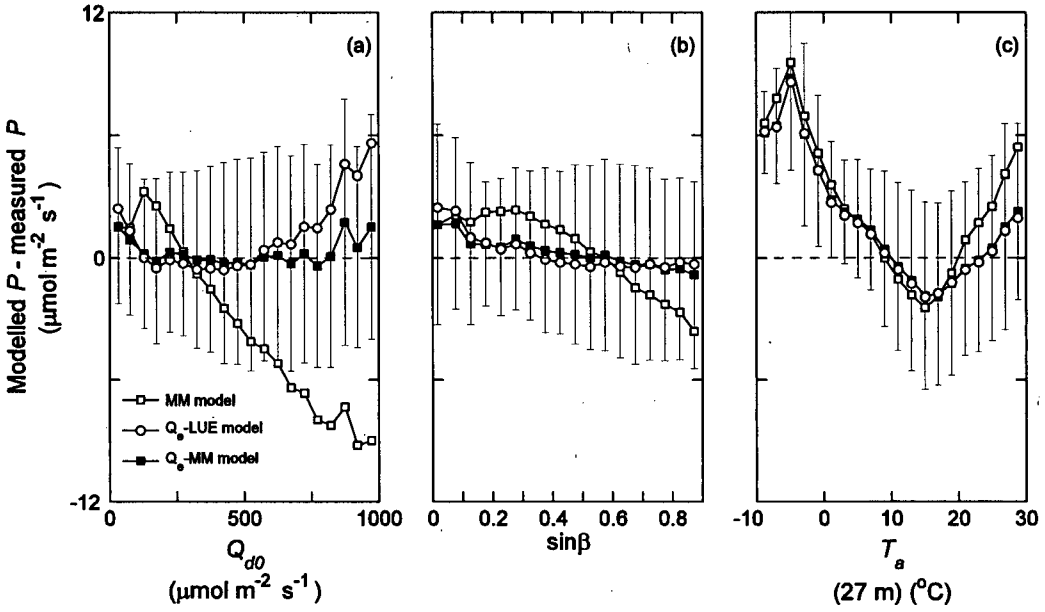

Figure 4-7. Modeling errors for the MM, Q_e-LUE, and Q_e-MM models. Parameters for these models are given in Figure 4-6. Symbols represent bin averages and vertical lines indicate ±1 SD for the bin averages obtained using the Q_e-MM model. The SD values for the other two models is similar to the corresponding values for the Q_e-MM model (not shown). n = 34785.

4.4.3 Comparisons between the MM, Q_e-MM and the sun/shade models

In order to account for the effect of T_a on P shown in Figure 4-7c, A_{max} in the Q_e-MM and MM models was related to T_a using a Gaussian function following June et al. (2004), i.e., $f(T_a) = e^{-(\frac{T_a - T_0}{\Omega})^2}$ where T_a is half-hourly average canopy air temperature (27 m), and T_0 and Ω are empirical coefficients. Thus the Q_e-MM model becomes $P = \frac{\alpha Q_e A_{\max} f(T_a)}{\alpha Q_e + A_{\max} f(T_a)}$. The $f(T_a)$ function, which is symmetric, with T_0 = 16.97, and Ω = 11.68 corrects most of the systematic errors in the Q_e-MM model associated with T_a (Figure 4-8c) except for T_a < 0 °C. With the incorporation of the $f(T_a)$ function, the Q_e-MM model accounted for 73% of the variance in P.

The modeling errors of the sun/shade model are larger even than those of the MM model with a $f(T_a)$ function included. With the incorporation of $f(T_a)$ into the MM model (i.e., $P = \frac{\alpha Q_{10} A_{\max} f(T_a)}{\alpha Q_{10} + A_{\max} f(T_a)}$), it accounts for 59% of the variance in P while the sun/shade model, which includes temperature dependence of V_{cmax} and J_{max}, only accounts for 55%. What is more unacceptable is that the sun/shade model does little to reduce the systematic errors of the MM model with respect to Q_{d0} (Figure 4-8a). Comparing the modelling errors of the MM and Q_e-MM models with respect to Q_{d0} in Figure 4-7a and those in Figure 4-8a shows that introducing the temperature function, $f(T_a)$, has little effect on the errors with respect to Q_{d0}. Therefore, the systematic errors with respect to Q_{d0} shown in Figure 4-8a for the sun/shade model cannot be caused by its built-in temperature functions for V_{cmax} and J_{max}. These functions were fine tuned numerous times in this analysis but these fine-tunings failed to correct the systematic

errors of the sun/shade model with respect to Q_{d0} shown in Figure 4-8a. As discussed in the Q_e-MM model development and also in Appendix C, these systematic errors of the sun/shade model shown in Figure 4-8a reflect the inadequacies in the light regime physics in the sun/shade model and the inadequacies of its algorithm for scaling P_{sun} and P_{shd} from leaf-level to canopy level. Also, Figure 4-8c shows that the sun/shade model has large systematic errors with respect to T_a, indicating the failure of applying the V_{cmax} and J_{max} temperature functions of spinach or tobacco (as the sun/shade model requires) to a Douglas-fir stand.

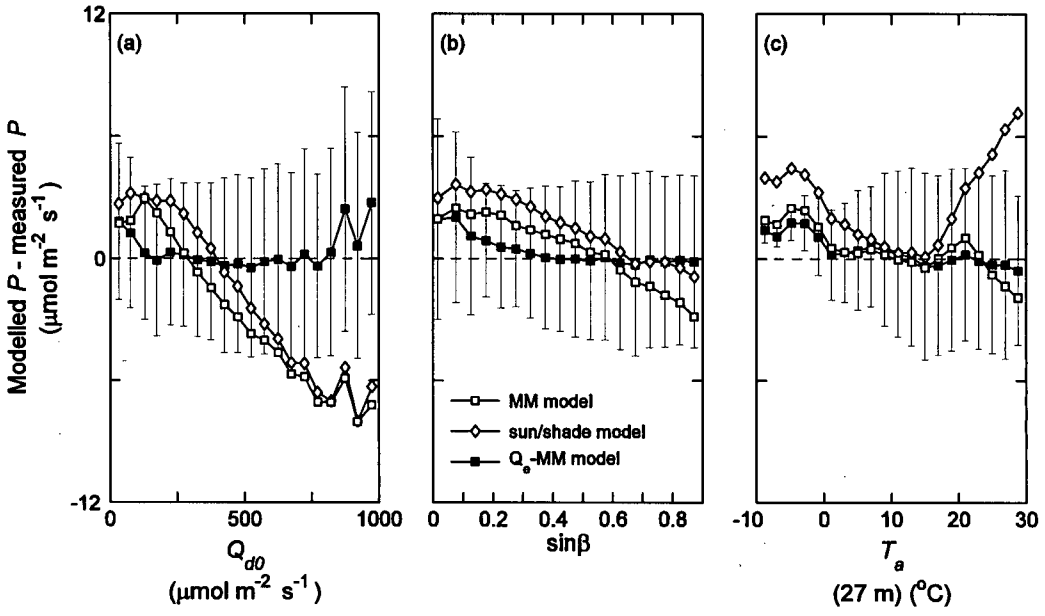

Figure 4-8. Modeling errors for the MM and Q_e-MM models with the incorporation of a temperature function for A_{max}, and the corresponding modeling errors using the sun/shade model. Note: the sun/shade model has built-in temperature functions to adjust the values of its V_{cmax} and J_{max}. For the MM model, the modeled P was obtained using $P = \frac{\alpha Q_{t0} A_{\max} f(T_a)}{\alpha Q_{t0} + A_{\max} f(T_a)}$, where α = 0.065 mol mol^{-1}, A_{max} = 26.48 μmol m^{-2} s^{-1}, and $f(T_a) = e^{-(\frac{T_a - T_0}{\Omega})^2}$ with T_0 = 15.56 °C, and Ω = 13.71. r^2 = 0.59 and RMSE = 4.75 μmol m^{-2} s^{-1}. For the sun/shade model: r^2 = 0.55 and RMSE = 4.80 μmol m^{-2} s^{-1}. For the Q_e-MM model, the modeled P was obtained using $P = \frac{\alpha Q_e A_{\max} f(T_a)}{\alpha Q_e + A_{\max} f(T_a)}$, where α = 0.053 mol mol^{-1}, A_{max} = 67.57 μmol m^{-2} s^{-1}, k = 0.18, and $f(T_a) = e^{-(\frac{T_a - T_0}{\Omega})^2}$ with T_0 = 16.97 °C, and Ω = 11.68. r^2 = 0.73 and RMSE = 3.86 μmol m^{-2} s^{-1}. Symbols represent bin averages and vertical lines indicate ±1 SD. n = 34785.

4.4.4 Comparisons of the performance of the Q_e-MM and m-MM models

In order to compare the performance of the Q_e-MM and m-MM models, a moving window technique was used in the analysis following that of Gu et al. (2002). The windows were 15 days wide and moved 1 day at a time. For each window, half-hourly values of P calculated using the Q_e-MM and m-MM models (with no $f(T_a)$ included) were regressed against measured values of P. To determine performance of the models as a function of T_a, values of the r^2 for the two models were averaged for 1 °C T_a bin widths for the 5 and half years of data. Figure 4-9 shows that the r^2 associated with both the Q_e-MM and m-MM models changed considerably with T_a, indicating a significant temperature effect on P (see also Figure 4-7c), especially when T_a < 5 °C. The average values of r^2 for the Q_e-MM and m-MM models were 0.6535 and 0.6562, respectively. The Q_e-MM model accounted for as much variance in P as the m-MM model, indicating the modification of A_{max} in Eq. (4) is unnecessary.

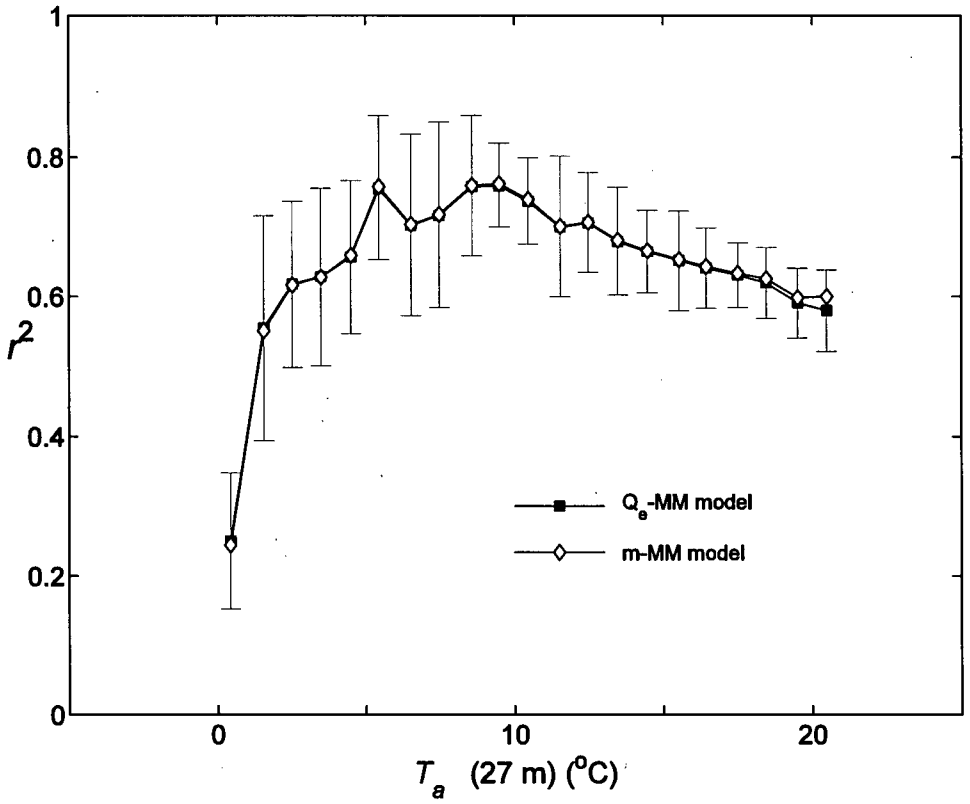

Figure 4-9. The coefficients of determination (r^2) for regressions using the Q_e-MM and m-MM models obtained by using 15-day moving windows (moving one day at a time) over 5 ½ years of data. The average and standard deviation of the r^2 are 0.6535 and 0.1394 for the Q_e-MM model, and 0.6562 and 0.1384 for the m-MM model, respectively. Symbols represent bin averages and vertical lines indicate ±1 SD for the bin averages obtained using the Q_e-MM model. The values of SD for the m-MM model are virtually identical to those for the Q_e-MM model (not shown).

Figure 4-10 and Figure 4-11 show the distribution of α (Figure 4-10a), A_{max} (Figure 4-10b) and k (Figure 4-11) obtained using the Q_e-MM model. Approximately 50% of the α values fell between 0.03 and 0.05. The distribution of A_{max} was wider than that of α with roughly 27% of the A_{max} values being greater than 100 μmol m^{-2} s^{-1}. When A_{max} is very large, the Q_e-MM model becomes the Q_e-LUE model, i.e., $\lim_{A_{\max}\to\infty} \frac{\alpha Q_e A_{\max}}{\alpha Q_e + A_{\max}} = \alpha Q_e$. The very large A_{max} values mainly occurred in overcast conditions, where the photosynthetic response to Q_e was almost linear. Note: A_{max} > 100 μmol m^{-2} s^{-1} does not imply that the canopy maximum photosynthetic assimilation can exceed 100 μmol m^{-2} s^{-1} of CO_2. It only means that the photosynthetic response to Q_e is almost linear and the A_{max} needs to be very large to reduce the Q_e-MM model to the Q_e-LUE model. In order to derive a valid A_{max} reflecting the integrated measure of canopy P, the Q_e range must be wide enough (e.g., using several years of data rather than 15 days of data). More than 80% of the k values were between 0.1 and 0.3. Less than 3% of k values were between 0.5 and 0.9 (Figure 4-11). The extremely low occurrence of the k values falling between k = 0.5 and k = 1.0 indicates Q_{t0} was a very poor predictor of P (see also the $P - Q_x$ relationship for Q_{t0} > 900 μmol m^{-2} s^{-1} in Figure 4-5). The average (n = 1995) of all k values was 0.22 ± 0.10 (average ± std). Large k values (e.g., k > 0.5) mainly occurred in overcast conditions when adding fractions of Q_{b0} didn't contribute significantly to explaining the variance in P as was shown in the x values in Figure 4-5 when $Q_{t0} \leq 300$ μmol m^{-2} s^{-1}.

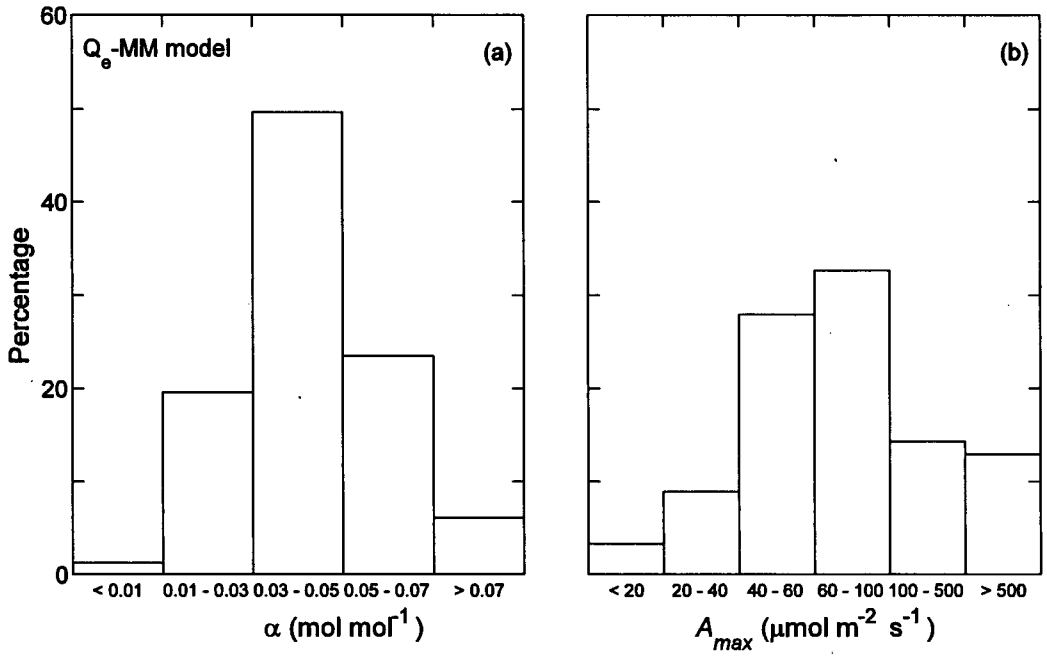

Figure 4-10. Distributions of α and A_{max} obtained using the 15-day moving windows for the Q_e-MM model (see also Figure 4-9).

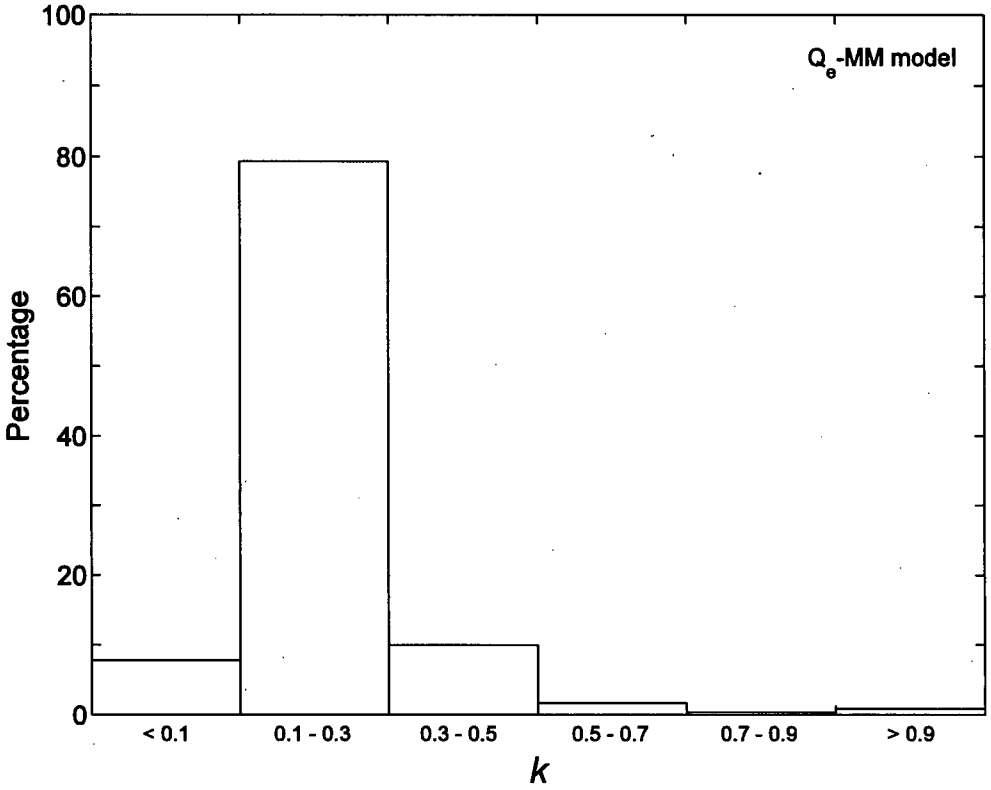

Figure 4-11. Distributions of k obtained using the 15-day moving windows for the Q_e-MM model (see also Figure 4-9 and Figure 4-10).

The relationship between k and $\sin\beta$ obtained using the Q_e-MM model is shown in Figure 4-12a together with the predicted relationship between σ' calculated using $\sigma' = 1 - e^{-K_b' L} - (1-\sigma)(1-e^{-K_b L})$ (see Eq. (21)) and $\sin\beta$ for different values of L (Figure 4-12b). The relationship between k and $\sin\beta$ is similar in shape to the relationship between σ' and $\sin\beta$ for L = 8. Both have a weak dependence on $\sin\beta$, however, the values of k are almost twice those of σ'.

Figure 4-12b shows that for a given $\sin\beta$, σ' is smaller for an open canopy (i.e., low LAI) than for a closed canopy (i.e., high LAI). Results of our analysis of P data for a nearby 16-year-old Douglas-fir stand ($L \approx 4$) and a clear-cut with planted 4-year-old Douglas-fir seedlings ($L \approx 2$) (see Humphreys 2004 for description of the two sites) indicate values of k of 0.16 and 0.12, respectively. The k values for the three Douglas-fir sites also follow the trend predicted by the relationship of σ' to $\sin\beta$ and L. As mentioned earlier when discussing the Q_e-MM model, k also includes the penumbral effect of the solar rays. It is difficult to find an exact relationship between the penumbral component of k and $\sin\beta$ for canopies of different LAI. From Eqs. 30 and 31 in Denholm (1981b), it is reasonable to assume that the penumbral component of k also decreases with $\sin\beta$ similar in pattern to the relationship between σ' and $\sin\beta$. Therefore, the very weak decrease of k with respect to $\sin\beta$ in Figure 4-12a is reasonable. Fully accounting for the scattering of Q_{b0} (e.g., secondary scattering) and the penumbral light spreading effect of solar rays (e.g., multi-fold penumbra) in a canopy is difficult.

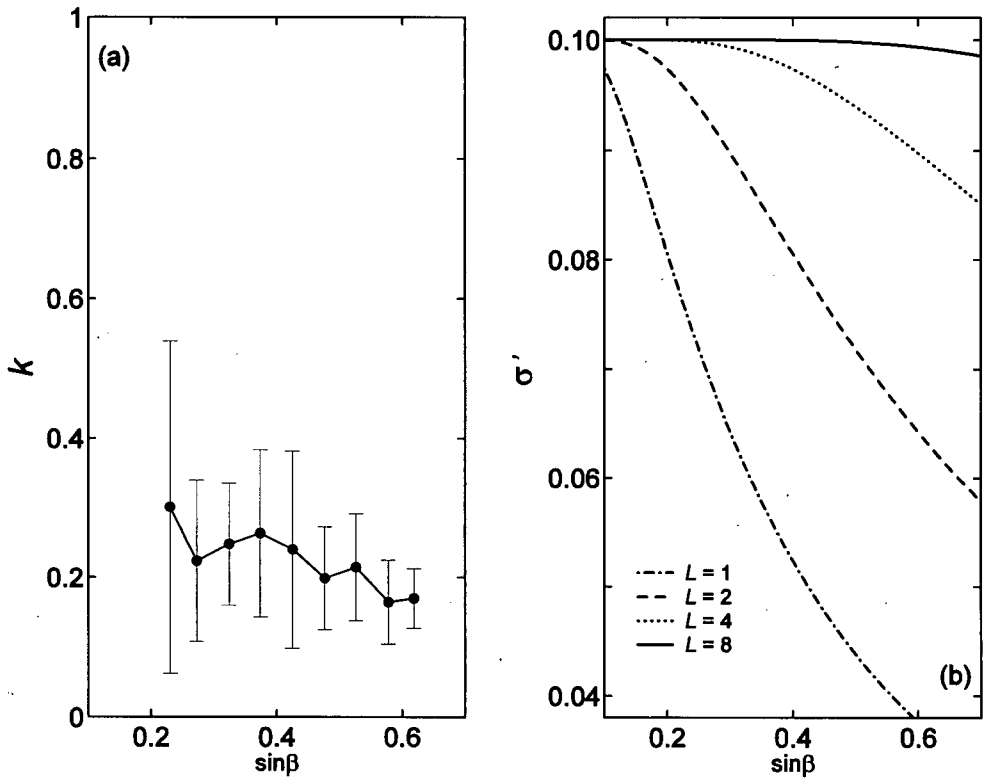

Figure 4-12. (a) The relationship between k and $\sin\beta$ obtained using the Q_e-MM model (see Figure 4-11). Symbols represent bin averages and vertical lines indicate ±1 SD. (b) the relationship between σ' and $\sin\beta$ calculated for different values of L using $\sigma' = 1 - e^{-K_b' L} - (1-\sigma)(1-e^{-K_b L})$, where $K_b = 0.5/\sin\beta$ (see Eq. 21). The value of σ is assumed to be 0.1.

Since k appears to have a weak dependence on $\sin\beta$ for this 56-year-old Douglas-fir stand, using a fixed value of k (i.e., k = 0.22) as a bulk parameter in the Q_e-MM model to calculate canopy P appears to be reasonable (see Figure 4-6d and Figure 4-8). The introduction of the parameter k into the MM model is useful because it provides a simple way of quantifying the effective canopy radiation regime. Furthermore, it can be easily estimated.

The parameters obtained using the m-MM model are shown in relation to air temperature in Figure 4-13. On average, α_b is significantly lower than α_d (Figure 4-13a), but the distinction between $A_{\max b}$ and $A_{\max d}$ is much less clear-cut (Figure 4-13b). Both α_b and α_d slightly increase with T_a. These results agree with the findings in Gu et al. (2002). The distribution of α_b / α_d is shown in Figure 4-14a, which is similar in pattern (i.e., the most observed values are between 0.1 and 0.3) to the distribution of k obtained using the Q_e-MM model (Figure 4-11). In comparison with the distribution of α_b / α_d, the distribution of $A_{\max b} / A_{\max d}$ tends to shift towards higher values, for example, approximately 34% of $A_{\max b} / A_{\max d}$ values are greater than 0.7.

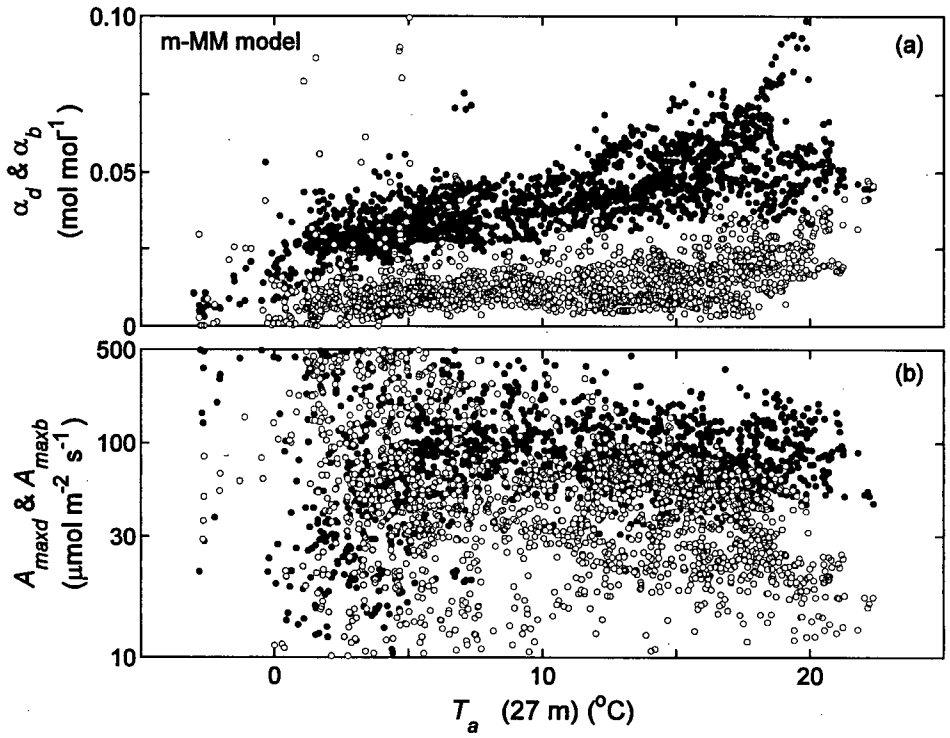

Figure 4-13. The temperature response of α_d, α_b, A_{maxd}, and A_{maxb} for the m-MM model obtained using 15-day moving windows for 5 ½ years of data (see Figure 4-9). Filled circles are α_d and A_{maxd}, and open circles are α_b and A_{maxb}.

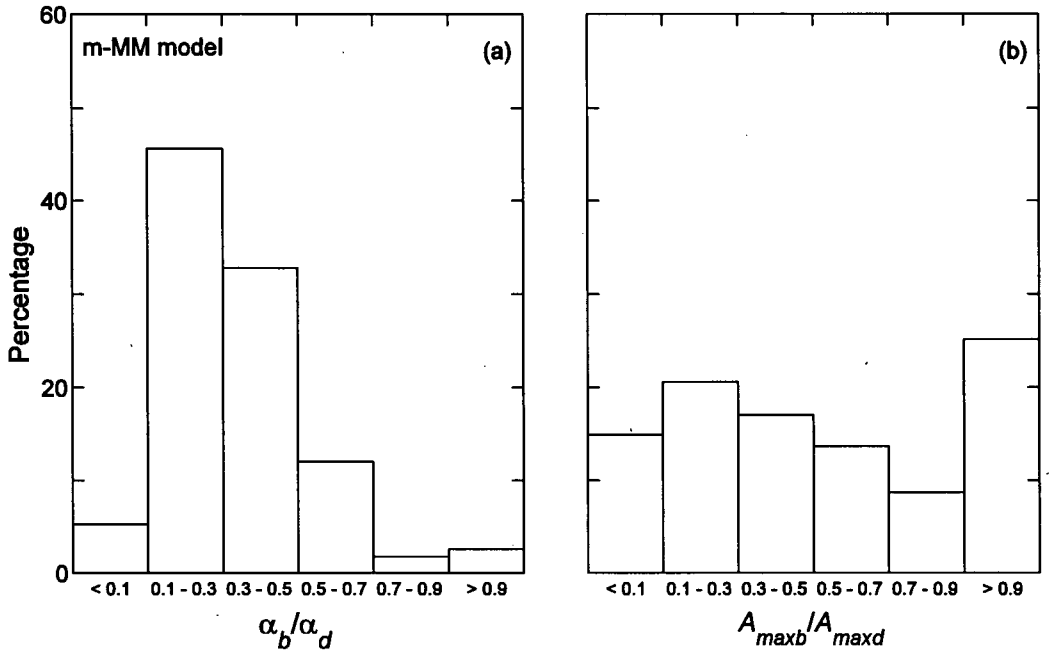

Figure 4-14. Distributions of α_b / α_d and A_{maxb}/A_{maxd} for 5 ½ years of data. The values of α_d, α_b, A_{maxd}, and A_{maxb} were obtained using the 15-day moving windows for the m-MM model (see Figure 4-13).

4.4.5 A case study

The Q_e-MM and MM models were used to estimate P for a period of six days with alternating cloudy and sunny conditions. In cloudy conditions, Q_{d0} reached 600 μmol m^{-2} s^{-1} (e.g., July 29), but in sunny conditions Q_{d0} was steady and between 200 – 300 μmol m^{-2} s^{-1} (e.g., August 3) (Figure 4-15a). The fluctuations in Q_{t0} in cloudy conditions indicated the passage of clouds (e.g., July 29). T_a and D, which are highly correlated, tended to be lower in cloudy (e.g., July 29) than in sunny conditions (e.g., July 30) (Figure 4-15b). Canopy P was significantly lower in sunny (e.g., August 1) than in cloudy conditions (e.g., July 31 and August 2) (Figure 4-15c) even with comparable T_a and D (Figure 4-15b).

The Q_e-MM model described P reasonably well (r^2 = 0.56) (Figure 4-15c), but the MM model significantly underestimated P in cloudy conditions (e.g., July 29, 31 and August 2) and significantly overestimated P in sunny conditions (e.g., August 1 and 3) (Figure 4-15c), and as a result, the MM model accounted for only 28% of the variance in P. The r^2 obtained using the m-MM model was the same as that for Q_e-MM model, and the values of P calculated using the two models were almost identical (data not shown).

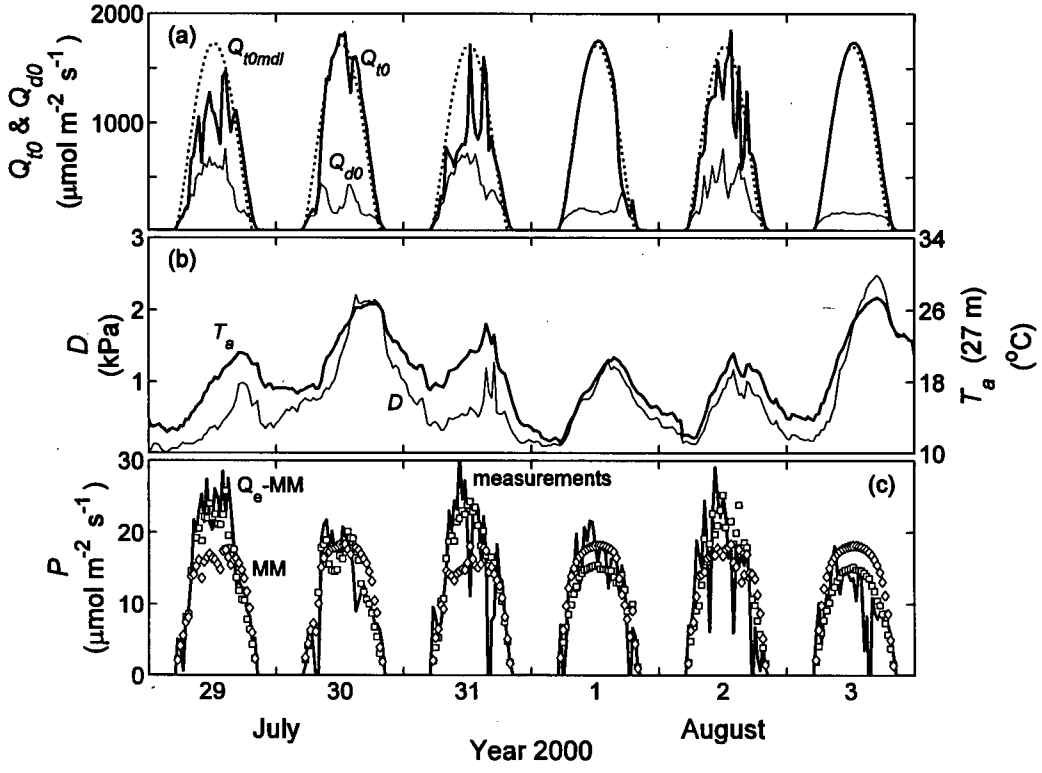

Figure 4-15. Continuous half-hourly values of (a) Q_{t0} (thick line), Q_{d0} (thin line) and Q_{t0mdl} which is the modeled Q_{t0} in a cloudless sky using Eq. B1 in Appendix B (dotted line), (b) T_a (thick line) and D (thin line), and (c) canopy P for 6 days in the 56-year-old Douglas fir stand (DF49), Campbell River, B.C. Squares (□) are modeled P using the Q_e-MM model, and diamonds (◇) are modeled P using the MM model. For the Q_e-MM model, $P = \frac{\alpha Q_e A_{\max}}{\alpha Q_e + A_{\max}}$, where α = 0.048 mol mol^{-1}, A_{max} = 67.86 μmol m^{-2} s^{-1}, k = 0.16, r^2 = 0.56, and RMSE = 4.82 μmol m^{-2} s^{-1}. For the MM-model, $P = \frac{\alpha Q_{t0} A_{\max}}{\alpha Q_{t0} + A_{\max}}$, where α = 0.053, A_{max} = 22.51 μmol m^{-2} s^{-1}, r^2 = 0.28 and RMSE = 6.20 μmol m^{-2} s^{-1}. Note: the measurements of P made in all u_* conditions are shown in plot (c), but the measurements of P made in calm conditions (u_* < 0.3 m s^{-1}) when Q_{t0} < 200 μmol m^{-2} s^{-1} were excluded from regressions of the MM and Q_e-MM models.

The modeled canopy P for the sunlit and shade leaves using the sun/shade model for the same six days is shown in Figure 4-16. It is clear that P_{sun} is always limited by its photosynthetic capacity (i.e., A_v) (Figure 4-16a), which agrees with the findings of de Pury and Farquhar (1997) (their Figure 11). The value of A_v is driven by V_{cmax25} (which is a function of T_a), K_n (which is assumed to be constant in this study) and K_b (which is a function of solar elevation angle), and that is why the diurnal change of A_v for the sunlit leaf is smooth (see Eq. 22 in de Pury and Farquhar 1997). As is discussed in detail in Appendix C, that P of the sunlit leaves is always Rubisco-limited (i.e., decoupled from the amount of PAR the sunlit leaves actually absorbed) is questionable, because a high proportion of the sunlit leaves are oriented approximately parallel to the solar beam and are light limited (i.e., not Rubisco-limited). On the other hand, P_{shd} tends to be RuBP-limited (i.e., $A_j < A_v$). However when Q_{d0} is high, for example, during the noon hours on the three cloudy days (July 29, 31 and August 2), P_{shd} also becomes Rubisco-limited (i.e., $A_v < A_j$) and during these noon hours the P of the entire canopy becomes Rubisco-limited, i.e., has nothing to do with the PAR incident on the canopy. The modeled values of P during these noon hours are questionable and are a direct result of the flaws in the scaling algorithm of the sun/shade model (see Appendix C for details). The bottom shaded leaves should always be light-limited for this dense canopy, i.e., cannot be Rubisco-limited as predicted by the sun/shade model. The sun/shade model accounted for approximately 43% of the variance in canopy P (Figure 4-16c), which is less satisfactory than the performance of the Q_e-MM model.

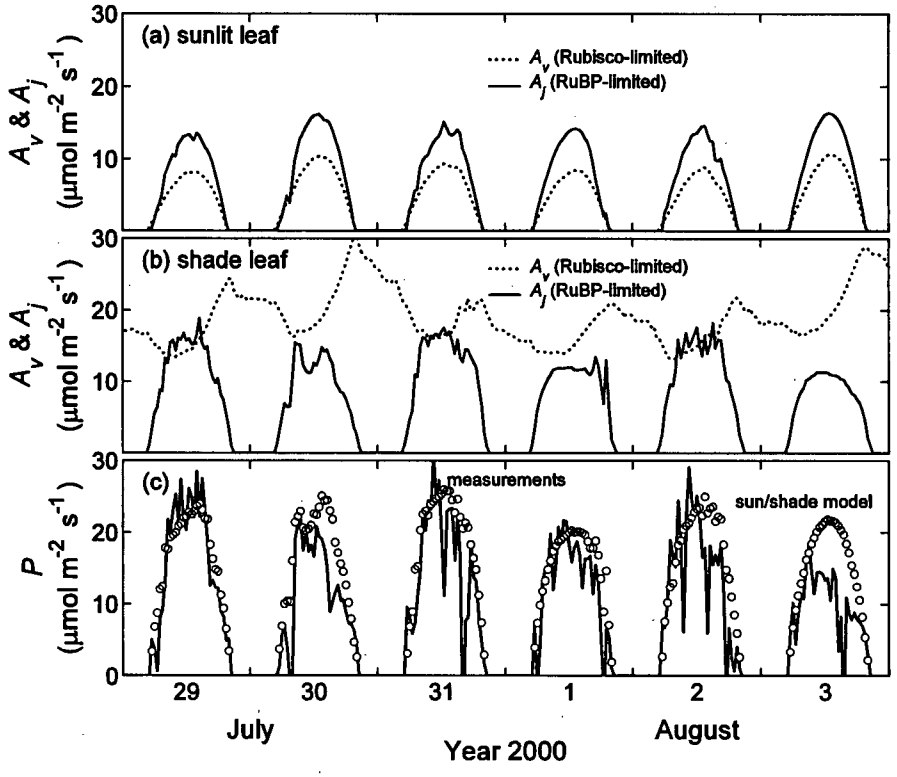

Figure 4-16. Canopy P calculated using the sun/shade model. (a) the Rubisco-limited (A_v) and RuBP-limited (A_j) photosynthetic rates for the big sunlit leaf, $P_{sun} = \min(A_v, A_j)$, (b) the corresponding A_v and A_j for the big shaded leaf, $P_{shd} = \min(A_v, A_j)$, (c) the modeled P of the entire canopy ($P = P_{sun} + P_{shd}$) using the sun/shade model (circles) and the measured P (lines), $r^2 = 0.43$, RMSE = 5.54 μmol m^{-2} s^{-1}. Note A_v equals to zero at night in (a) but not in (b) because the fraction of sunlit leaves at night is zero.

4.5 Discussion

The models presented in this study are closely related. If $A_{\max d} = A_{\max b}$, then the m-MM model (Eq. (5)) becomes the Q_e-MM model (Eqs. (23) and (25)). If A_{max} in the Q_e-MM model is infinitely large, the Q_e-MM model reduces to the Q_e-LUE model (Eq. (22)). If k = 1 in the Q_e-MM model, it becomes the MM model (Eq. (2)). The m-MM model has two more variables (i.e., Q_{t0} and A_{maxb}) than the Q_e-MM model, but does not account for significantly more variance in P than the latter (Figure 4-9). Therefore, the modification of A_{max} to be a function of Q_{d0}/Q_{t0} appears to be unnecessary (Eq. (4)). Even from a computational perspective, the modification of A_{max} (i.e., $A_{\max} = A_{\max d}\frac{Q_{d0}}{Q_{t0}} + A_{\max b}\frac{Q_{b0}}{Q_{t0}}$) for the MM model is unnecessary because α and A_{max} appear as a product in the numerator of the MM model. Also, the modification of A_{max} is not supported by the modelling in Norman and Arkebauer (1991) because their model, Cupid, used an MM model with fixed values of α and A_{max} (see Eq. (11) in Norman 1980) to estimate P of the sunlit leaves in different leaf-sun angle classes and P of the shaded leaves at different canopy depths. The Cupid model doesn't assign an A_{maxb} for direct PAR and an A_{maxd} for diffuse PAR, respectively.

The average value of k for this Douglas-fir forest is approximately 0.22 (Figure 4-6d and Figure 4-11). k reflects the magnitude of the scattering as well as non-scattering effects (e.g., the penumbral effect) of the solar beam. The scattering of the solar beam in a plant canopy (e.g., Forseth and Norman 1993, Goudriaan and van Laar 1994, Campbell and Norman 1998) depends on many factors, such as foliar optical properties (Gausman and Allen 1973), leaf angular distribution (Campbell and Norman 1989), and the

structure of the canopy (Miller 1967, Idso and de Wit 1970, Lemeur 1973, Lang et al. 1985, Campbell 1986, Chen et al. 1997, Ross and Ross 1998). Scattered PAR has been reported to be as high as sky diffuse PAR within a deciduous canopy (Hutchison and Matt 1976) and to be significant beneath a coniferous canopy (Black et al. 1991). Penumbrae caused by the solar rays homogenize the light distribution and significantly reduce the completely shaded area (i.e., umbra) (e.g., Denholm 1981a, Stenberg 1998). Jarvis and Leverenz (1983) found that the photosynthetic light response was significantly more linear at canopy level than at leaf level for Sitka spruce possibly as a result of the scattering and penumbral component of the solar beam which leads to "a fairly uniform light distribution with the majority of leaf surfaces at intermediate quantum flux densities". The penumbrae in a Scots pine canopy simulated using a Monte Carlo technique were found to occur more frequently than full sun (i.e., gaps) and full shade (i.e., umbrae) (Oker-Blom 1985). Palmroth et al. (1999) investigated the distribution of direct sunlight on a plane shaded by a Scots pine shoot situated at varying distances using a multipoint PAR measurement system, and found that the distribution changed from clearly bimodal (full sun – full shade) to the one concentrated around the mean (penumbral irradiance) as the shoot was moved further away from the multipoint PAR measurement system. The heterogeneity and complexity of canopy structure makes it difficult to both reasonably measure (e.g., Black et al. 1991, Palmroth et al. 1999) and model (Oker-Blom 1985, Stenberg 1998) the full extent of the scattering and non-scattering effects of the solar beam in a plant canopy. The Q_e-MM model may provide a new approach to study the radiation regime in a canopy (i.e., the estimation of the magnitude of k). The advantage of this approach is that half-hourly EC CO_2 flux

measurements are made over a large flux footprint, so it effectively gives an integrated measure of the canopy radiation regime.

Gu et al. (2002) found that the light use efficiency for direct beam (i.e., α_b) was significantly lower than that for diffuse PAR (i.e., α_d) for canopies of five different C_3 species. This study supports that conclusion because the application of the Q_e-MM model indicates that α_b is only a fraction k of α_d (i.e., $\alpha_b = k\alpha_d$) (see Eq. (25)). In this study, k is hypothesized to be the effective fraction of Q_{b0} contributing to canopy photosynthesis. Gu et al. (2002) found that the five different C_3 stands had different ratios of α_b to α_d, likely reflecting differences in canopy structure and leaf photosynthetic and optical characteristics. The m-MM model focuses on the light use efficiency (i.e., $\alpha = \alpha_d \frac{Q_{d0}}{Q_{t0}} + \alpha_b \frac{Q_{b0}}{Q_{t0}}$) while the Q_e-MM model focuses on light (i.e., $Q_e = Q_{d0} + kQ_{b0}$), since it is light that drives canopy photosynthesis. The advantage of focusing on light is that we can add a fraction of Q_{b0} to Q_{d0} (i.e., $Q_x = Q_{d0} + xQ_{b0}$ in Figure 4-5) to investigate to the maximum correlation between PPFD and canopy P. We cannot do this in the case of α, i.e., by adding a fraction of α_b to α_d, since the two quantities are not additive.

The Q_e-MM model suggests that the separation of canopy foliage into sunlit and shaded groups is not important (i.e., $\sin\beta$ is not finally required in Eq. (22)), because Q_e can be reasonably assumed to be isotropic and consequently the whole canopy can be treated as a single big leaf. The Q_e-MM model is a single big-leaf model, but it avoids the type of errors made in the earlier single big-leaf models of canopy P (Amthor 1994, Lloyd et al. 1995, Sellers et al. 1996) and therefore makes it particularly suitable for regional and global scale carbon balance modelling.

In this study, the temperature effect on P was determined using an empirical Gaussian function (i.e., $f(T_a) = e^{-(\frac{T_a - T_0}{\Omega})^2}$) (see Figure 4-8), and no effort was made to separate the effect of air temperature (Morgenstern et al. 2004) from that of D on P (e.g., Anthoni et al. 2002, Goulden et al. 2004). The Q_e-MM model developed in this study is a simple top-down model of canopy P. All its parameters can be easily inferred from EC measurements (e.g., Figure 4-6d and Figure 4-8), and they provide a useful integrated measure of canopy photosynthetic behavior. The bottom-up models (e.g., de Pury and Farquhar 1997), built from detailed mechanistic representations of leaf-level processes and scaled up to the canopy level, are much more complex. As pointed out by Jarvis (1993), bottom-up models are often more susceptible to errors in inputs (because the selection of parameter values is difficult *a priori*) and scaling assumptions than their top-down counterparts which are constrained to the 'realm of observations'. Consequently, bottom-up models do not necessarily guarantee better accuracy (Anderson et al. 2000) (see also the comparison of the performance of the Q_e-MM model with that of the sun/shade model in Figure 4-8). For example, in most bottom-up models, the leaf angle distribution is assumed to be random and clumping is not considered (i.e., leaves are treated as randomly distributed elements analogous to the randomly distributed molecules in a solution, so Beer's law of light attenuation can be applied to a canopy). In reality, however, the needles are regularly arranged on a shoot and the clumping factor for a coniferous stand can be as low as 0.4 (Campbell and Norman 1998). There are large uncertainties regarding how to incorporate the clumping factor into existing bottom-up models. Another example is that the effect of penumbra cannot be simply scaled up from the leaf-level to the canopy-level because it does not exist at the leaf-level. When the

bottom-up models become very complicated, it is difficult to do sensitivity tests for the model parameters.

Volcanic eruptions (Hoecker et al. 1985, Olmo et al. 1999, Dutton and Bodhaine 2001), forest fires (Wotawa and Trainer 2000, Page et al. 2002), biomass burning (Dennis et al. 2002, Pan et al. 2004), urban air pollution (Wesely and Lipschutz 1976, Aguado 1990, Nichol 1997, Lamanna and Goldstein 1999, Kobayashi et al. 2004), and dust storms (Husar et al. 2001) all modify the sky diffuse radiation regime in different ways, and therefore exert significant impacts on the regional and global terrestrial carbon cycle (Niyogi et al. 2004). The increased aerosol loading from natural and anthropogenic sources can lead to both global dimming (Stanhill and Cohen 2001) and global warming (Timmermann et al. 1999). How the two processes interact to affect the global terrestrial carbon cycle requires further investigation (Farquhar and Roderick 2003). The Q_e-MM model presented in this study could be used as a simple diagnostic tool for studies of the impact of diffuse radiation on gross primary production of terrestrial ecosystems.

4.6 Conclusions

(1) A canopy can be treated as a single big leaf to estimate its photosynthesis with the replacement of Q_{t0} in the Michaelis-Menten (MM) model (i.e., $P = \frac{\alpha Q_{t0} A_{\max}}{\alpha Q_{t0} + A_{\max}}$) with $Q_e = Q_{d0} + kQ_{b0}$ (i.e., $P = \frac{\alpha Q_e A_{\max}}{\alpha Q_e + A_{\max}}$, referred to as the Q_e-MM model). k is the fraction of Q_{b0} added to Q_{d0}, and was approximately 0.22 for this Douglas-fir stand. It is hypothesized that the value of k reflects the magnitude of scattering and non-scattering (e.g., the penumbral light-spreading) effects of the solar rays.

(2) The quantum yield for direct PAR (α_b) is only fraction k of that for diffuse PAR (α_d) because the effective flux of direct PAR for canopy P is approximately kQ_{b0}.

(3) The MM model significantly overestimates canopy P in sunny conditions, and significantly underestimates canopy P in cloudy conditions. The Q_e-MM model has no systematic errors with respect to Q_{d0}, and with the incorporation of the effect of temperature on P, accounted for 73% of the variance in P (derived half-hourly EC measurements for DF49 from May 2000 to December 2005).

(4) The modification of A_{max} (i.e., $A_{\max} = A_{\max d}\frac{Q_{d0}}{Q_{t0}} + A_{\max b}\frac{Q_{b0}}{Q_{t0}}$) in the m-MM model (i.e., Eq. (4) by Gu et al. 2002) appears to be unnecessary. The Q_e-MM model is demonstrated to be almost identical to the m-MM model in terms of estimating canopy P for this coastal Douglas-fir stand, but it significantly reduces the complexity of modelling canopy P.

(5) The EC-derived half-hourly values of canopy P for the DF49 do not support the sun/shade model developed by de Pury and Farquhar (1997) (see Figure 4-8a) because the sun/shade model fails to address the heterogeneity of the light environment within the big sunlit leaf (group) (see Appendix C for details).

5 Conclusions

This study has examined the effect of soil temperature (Chapter 2), phenology and soil moisture on ecosystem respiration (Chapter 3), and the role of direct and diffuse PAR in canopy photosynthesis (Chapter 4) of a 56-year-old coastal Douglas-fir stand (DF49) on Vancouver Island. This chapter summarizes and discusses the major findings of the study.

(1) Respiration at night (R_{en}) is best estimated using the relationship between the logarithm of half-hourly measurements of NEE and temperature rather than the exponential relationship because the former best meets the IID $N(0,\sigma^2)$ requirements.

(2) The estimates of R_{ed} obtained by fitting the Michaelis-Menten equation (i.e., $NEP = \frac{\alpha Q_{t0} A_{max}}{\alpha Q_{t0} + A_{max}} - R_{ed}$) to half-hourly EC measurements of NEP during the daytime (i.e., full range of PAR) were found to be strongly influenced by the length of the regression periods used (e.g., 3-day vs. 30-day moving windows). They were considered to be unreliable. Reasons for this are (a) the variability of the daytime half-hourly EC measurements of NEP significantly increases with increasing Q_{t0}, and (b) the residuals from the MM fit are not entirely random because negative residuals tend to associate with cloudy conditions and positive residuals with clear conditions. Thus, using the Michaelis-Menten equation to obtain a daytime NEP – Q_{t0} relationship severely violates the statistical IID $N(0,\sigma^2)$ assumption. This is similar to the problem of using an OLS algorithm (i.e., the exponential relationship) for the nighttime NEE_{tt} - T_s relationship to

determine R_{en} (nighttime R_e). These estimates of R_{ed} are also considered unreliable because they are significantly greater than estimates obtained using the logarithmically transformed relationship between nighttime NEE and soil temperature to daytime half hours. Light inhibition of foliar respiration is expected to cause daytime R_e to be less than nighttime R_e at the same temperature. Even restricting the PAR range to 0-300 μmol m^{-2} s^{-1} resulted in R_{ed} estimates greater than those estimated from the nighttime relationship so it was concluded that regardless of PAR range use of the MM relationship overestimated daytime R_e.

(3) In contrast to the use of the MM model, using the LUE model (i.e., $NEP = \alpha Q_{t0} - R_{ed}$) applied to PAR < 300 μmol m^{-2} s^{-1} to obtain a daytime NEP – Q_{t0} relationship provided plausible estimates of daytime R_{ed}. This is because the estimates were virtually independent of the moving window widths used and the violation of the statistical IID $N(0,\sigma^2)$ assumption was eliminated. The relationship provided half-hourly values of R_{ed} that were less (28% less at 5 °C, 26% less at 10 °C and 23% less at 15 °C) than those calculated using the nighttime logarithmic relationship.

(4) The annual totals of daytime R_e obtained using the LUE model were approximately 25% less than that obtained by applying the nighttime $NEE_{u.}$ - T_s relationship to determine daytime R_e. This was observed for all the 8 years (1998 – 2005) studied. The reduction is most likely caused by the light inhibition on ecosystem foliar respiration, which is supported by an independent leaf-level study at the same site.

(5) The values of R_{10} and Q_{10} for the 8 years (1998 – 2005) obtained from the eight annual nighttime NEE_{u*} - T_s relationships linearly increased with increasing θ (soil volumetric moisture content averaged from the surface to the to 1-m depth). However, the effect of θ on R_e evident on the interannual scale could not be detected on the seasonal or annual scale, probably as a result of the confounding effects of other environmental and biotic factors (e.g., the phenology and dependence of R_e on P) on R_e.

(6) Using annual nighttime and daytime R_e – T_s relationships to estimate nighttime and daytime half-hourly R_e values, respectively underestimated R_e for the active growing season (April – July), and overestimated R_e for the passive growing season (August – March). However, the systematic errors of using annual relationships had little effect on the estimation of annual totals of R_e, because the underestimation and overestimation were similar in magnitude. The three stepwise fit methods developed to overcome the errors associated with using annual relationships agreed reasonably well. However, they do not provide any mechanistic understanding of R_e, and they should be viewed more as methods of interpolating R_e from nighttime turbulent conditions to nighttime calm conditions, and from daytime daily averages of R_e (obtained using the LUE model) to daytime half-hourly R_e estimates.

(7) Canopy P can be described by replacing the Q_{t0} in the MM model (i.e., $P = \frac{\alpha Q_{t0} A_{\max}}{\alpha Q_{t0} + A_{\max}}$) with $Q_e = Q_{d0} + kQ_{b0}$ (i.e., $P = \frac{\alpha Q_e A_{\max}}{\alpha Q_e + A_{\max}}$, referred to as the Q_e-MM model). k, which is the fraction of Q_{b0} added to Q_{d0} to obtain an estimate of effective canopy radiation (Q_e), was found to be approximately 0.22 for this

Douglas-fir stand. The value of k reflects the magnitude of scattering and non-scattering effects of the solar beam. The Q_e-MM model developed in this study is consistent with the findings of Norman and Arkebauer (1991).

(8) The MM model significantly overestimates canopy P in sunny conditions, and significantly underestimates it in cloudy conditions. In contrast, the Q_e-MM model has no systematic errors with respect to Q_{d0}, and with the incorporation of an empirical function for the effect of air temperature on P, it accounted for 73% of the variance in P over a 8-year period for this 56-year-old Douglas-fir stand.

(9) This study showed that the sun/shade model developed by de Pury and Farquhar (1997) performed as poorly as the regular MM model. Like the MM model, the sun/shade model also has systematic modeling errors with respect to Q_{d0}, mainly because it does not take into account the effect of the leaf inclination angle distribution and uses LAI-weighted APAR (absorbed PAR) to calculate the P of the sunlit leaves.

The evidence for the light inhibition on ecosystem foliar respiration (Chapter 2) in other stands should be examined. My hypothesis is that as LAI decreases, the nighttime $NEE_{u.}$ - T_s relationship will converge with the daytime R_{ed} – T_s relationship obtained using the LUE model, because as LAI decreases, the proportion of R_e due to foliar respiration decreases and the effect of light inhibition of foliar respiration decreases accordingly. Humphreys (2004) already showed that in a recently clearcut-harvested Douglas-fir stand (i.e., a very low LAI stand), soil respiration fluxes obtained using a portable soil chamber were similar to values of R_e calculated using nighttime NEE

measurements, but for this 56-year-old Douglas-fir stand, R_e was significantly greater than soil respiration. Therefore, it is highly likely that ecosystem foliar respiration in this 56-year-old Douglas-fir stand is large. Without accurately accounting for the effect of light inhibition on ecosystem foliar respiration, calculations of the regional and global carbon balances (e.g., Ciais et al. 2005) will likely be in large error. The exact mechanism for light inhibition on foliar respiration is still debatable (Pinelli and Loreto 2003), but it is generally accepted that foliar dark respiration is reduced in light relative to that in darkness (Sharp et al. 1984, Brooks and Farquhar 1985, Villar et al. 1994, Shapiro et al. 2004). Additional leaf-level measurements are needed to address in-depth questions, such as the seasonal change in the effect of light inhibition and how it is affected by other environmental variables (e.g., leaf temperature, light intensity and soil moisture).

The effect of θ on R_e discussed in Chapter 3 also merits further investigation and the same analysis used here (i.e., both nighttime and daytime NEP were used to estimate R_e) can be easily extended to other ecosystems. It is a little surprising that the sensitivity of the annually obtained Q_{10} to θ in this deep-rooting coastal Douglas-fir ecosystem is almost as high as that in a mixed grassland with shallow-rooting depth (Flanagan and Johnson 2005). The values of R_{10} and Q_{10} obtained from the annual nighttime and daytime $R_e - T_s$ relationships are integrated measures of R_e over the entire year, so they provide little detailed information about the linkage between P and R_e and the partitioning between the heterotrophic and autotrophic ecosystem respiration. Continued modeling efforts using soil respiration (Jassal et al. 2005) and ^{13}C isotope (Ponton et al. 2006) measurements in this stand will provide valuable insights on the coupling between

P and R_e and the partitioning of R_e between the heterotrophic and autotrophic components.

The Q_e-MM model presented in Chapter 4 has considerable potential to be incorporated into large-scale carbon climate models (e.g., Ruimy et al. 1999, Still et al. 2004). This analysis only focused on modifying the MM model, but the concept of Q_e (i.e., the photosynthetically effective PAR in the canopy) can be applied to other forms of equations that are also frequently used to describe the leaf-level photosynthetic response to light in the literature. For example, the photosynthetic response to light at leaf-level can be described by a general quadratic equation as:

$$\phi P^2 - (\alpha Q_{t0} + A_{\max})P + \alpha Q_{t0} A_{\max} = 0 \qquad (1)$$

where α, Q_{t0} and A_{max} are the apparent quantum use efficiency, incident total PAR and maximum assimilation rate, respectively. ϕ is a curvature parameter (Ögren 1993). Eq. (1) can easily be modified for its application at canopy level by replacing Q_{t0} in Eq. (1) with Q_e:

$$\phi P^2 - (\alpha Q_e + A_{\max})P + \alpha Q_e A_{\max} = 0 \qquad (2)$$

where ϕ, P, α, and A_{max} have the same meanings as in Eq. (1) except for at canopy scale. It is desirable to extend the methodology of Chapter 4 to other stands, so the characteristics of k can be systematically investigated before the Q_e-MM model can be reliably applied at large scales.

It is well-accepted that the evapotranspiration of a canopy can be approximated using the big leaf model described by the Penman-Monteith equation (e.g., Jarvis and McNaughton 1986) with a "canopy conductance" representing the entire canopy and the water transport in the soil-plant-atmosphere continuum can also be reasonably described

by resistors and capacitors representing the hydraulic resistance and water storage of soil and plant tissues (e.g., Jones 1992). However, it is generally accepted that estimation of canopy *P* requires, at minimum, a 2-leaf model (e.g., the sun/shade model in de Pury and Farquhar 1997). An important contribution of this analysis is the development of the Q_e-MM model, which provides an option of retaining the single big leaf concept to estimate canopy *P*. The Q_e-MM model is particularly easy to couple with the Penman-Monteith equation, the soil-plant-atmosphere liquid water transfer equations, and the biochemical equations of leaf photosynthesis (e.g., Farquhar et al. 1980).

References

Aguado, E., 1990. Effect of advected pollutants on solar radiation attenuation: Mojave Desert, California. Atmospheric Environment, 248: 153-157.

Allen, L.H., Stewart, D.W. and Lemon, E.R., 1974. Photosynthesis in plant canopies: effect of light response curves and radiation source geometry. Photosynthetica, 8: 184-207.

Amthor, J.S., 1994. Scaling CO_2 - photosynthesis relationships from the leaf to canopy. Photosynthesis Research, 39: 321-350.

Anderson, M.C., Norman, J.M., Meyers, T.P. and Diak, G.R., 2000. An analytical model for estimating canopy transpiration and carbon assimilation fluxes based on canopy light use efficiency. Agricultural and Forest Meteorology, 10: 265-289.

Angert, A., Biraud, S., Bonfils, C., Buermann, W. and Fung, I., 2004. CO_2 seasonality indicates origins of post-Pinatubo sink. Geophysical Research Letters, 31: doi:10.1029/2004GL019760.

Angert, A., Biraud, S., Bonfils, C., Henning, C.C., Buermann, W., Pinzon, J., Tucker, C.J. and Fung*, I., 2005. Drier summers cancel out the CO_2 uptake enhancement induced by warmer springs. Proceedings of the National Academy of Sciences, 102: 10823-10827.

Anthoni, P.M., Unsworth, M.H., Law, B.E., Irvine, J., Baldocchi, D.D., Van Tuyl, S. and Moore, D., 2002. Seasonal differences in carbon and water vapor exchange in young and old-growth ponderosa pine ecosystems. Agricultural and Forest Meteorology, 111: 203-222.

Arain, M.A., Black, T.A., Barr, A.G., Jarvis, P.G., Massheder, J.M., Verseghy, D.L. and Nesic, Z., 2002. Effects of seasonal and interannual climate variability on net ecosystem productivity of boreal deciduous and conifer forests. Canadian Journal of Forest Research, 32: 878-891.

Atkin, O.K., Edwards, E.J. and Loveys, B.R., 2000a. Response of root respiration to changes in temperature and its relevance to global warming. New Phytologist, 147: 141-154.

Atkin, O.K., Evans, J.R., Ball, M.C., Lambers, H. and Pons, T.L., 2000b. Leaf respiration of snow gum in the light and dark: Interactions between temperature and irradiance. Plant Physiology, 122: 915-923.

Atkin, O.K., Westbeek, M.H.M., Cambridge, M.L., Lambers, H. and Pons, T.L., 1997. Leaf respiration in light and darkness. Plant Physiology, 113: 961-965.

Bacastow, R., 1979. Dip in the atmospheric CO_2 level during the mid-1960's. Journal of Geophysical Research, 84: 3108-3114.

Baldocchi, D., 1997. Measuring and modeling carbon dioxide and water vapour exchange over a temperate broad-leaved forest during the 1995 summer drought. Plant, Cell and Environment, 20: 1108-1122.

Baldocchi, D.D., 2003. Assessing the eddy covariance technique for evaluating carbon dioxide exchange rates of ecosystems: past, present and future. Global Change Biology, 9: 479-492.

Barford, C.C., Wofsy, S.C., Goulden, M.L., Munger, J.W., Pyle, E.H., Urbanski, S.P., Hutyra, L., Saleska, S.R., Fitzjarrala, D. and Moore, K., 2001. Factors controlling long- and short-term sequestration of atmospheric CO_2 in a mid-latitude forest. Science, 294: 1688-1691.

Barr, A.G., Black, T.A., Hogg, E.H., Kljun, N., Morgenstern, K. and Nesic, Z., 2004. Inter-annual variability in the leaf area index of a boreal aspen-hazelnut forest in relation to net ecosystem production. Agricultural and Forest Meteorology, 126(237-255).

Barr, A.G., Morgenstern, K., Black, T.A., McCaughey, J.H. and Nesic, Z., 2006. Surface energy balance closure by the eddy-covariance method above three boreal forest stands and implications for the measurement of the CO_2 Flux. Agricultural and Forest Meteorology, In press.

Björkman, O., Boardman, N.K., Anderson, J.M., Thorne, S.W., Goodchild, D.J. and Pyliotis, N.A., 1972. Effect of light intensity during growth of *Atriplex patula* on the capacity of photosynthetic reactions, chloroplast components and structure. Carnegie Institution Year Book, 71: 115-135.

Black, T.A., 1979. Evapotranspiration from Douglas fir stands exposed to soil water deficit. Water Resources Research, 15(1): 164-170.

Black, T.A., Chen, J.-M., Lee, X. and Sagar, R.M., 1991. Characteristics of shortwave and longwave irradiances under a Douglas-fir stand. Canadian Journal of Forest Research, 21: 1020-1028.

Black, T.A., Chen, W.J., Barr, A.G., Arain, M.A., Chen, Z., Nesic, Z., Hogg, E.H., Neumann, H.H. and Yang, P.C., 2000. Increased carbon sequestration by a boreal deciduous forest in years with a warm spring. Geophysical Research Letters, 27(9): 1271-1274.

Black, T.A., den Hartog, G., Neumann, H.H., Blanken, P.D., Yang, P.C., Russell, C., Nexic, Z., Lee, X., Chen, S.G., Staebler, R. and Novak, M.D., 1996. Annual cycles of water vapour and carbon dioxide fluxes in and above a boreal aspen forest. Global Change Biology, 2: 219-229.

Bowling, D.R., McDowell, N.G., Bond, B.J., Law, B.E. and Ehleringer, J.R., 2002. ^{13}C content of ecosystem respiration is linked to precipitation and vapor pressure deficit. Oecologia, 131(1): 113-124.

Briffa, K.R., Jones, P.D., Schweingruber, F.H. and Osborn, T.J., 1998. Influence of volcanic eruptions on Northern Hemisphere summer temperature over the past 600 years. Nature, 393: 450-455.

Brooks, A. and Farquhar, G.D., 1985. Effect of temperature on the CO_2/O_2 specificity of ribulose-1,5-bisphosphate carboxylase/oxygenase and the rate of respiration in the light. Planta, 165: 397-406.

Bunnell, F.L., Tait, D.E.N., Flanagan, P.W. and van Cleve, K., 1977. Microbial respiration and substrate weight loss. I. A general model of the influence of abiotic variables. Soil Biol. Biochem., 9: 33-40.

Campbell, G.S., 1986. Extinction coefficients for radiation in plant canopies calculated using an ellipsoidal inclination angle distribution. Agricultural and Forest Meteorology, 36: 317-321.

Campbell, G.S. and Norman, J.M., 1989. The description and measurement of plant canopy structure. In: G. Russell, B. Marshall and P.G. Jarvis (Editors), Plant canopies: their growth, form and function. Cambridge University Press, Cambridge, pp. 178.

Campbell, G.S. and Norman, J.M., 1998. An introduction to environmental biophysics. Springer-Verlag, New York, 286 pp.

Carrara, A., Janssens, I.A., Yuste, J.C. and Ceulemans, R., 2004. Seasonal changes in photosynthesis, respiration and NEE of a mixed temperate forest. Agricultural and Forest Meteorology, 126: 15-31.

Chen, J.M., Rich, P.M., Gower, S.T., Norman, J.M. and Plummer, S., 1997. Leaf area index of boreal forests: Theory, techniques, and measurements. Journal of Geophysical Research, 102(D24): 29429-29443.

Chimner, R.A. and Welker, J.M., 2005. Ecosystem respiration responses to experimental manipulations of winter and summer precipitation in a Mixedgrass Prairie, WY, USA. Biogeochemistry, 73(1): 257-270.

Choudhury, B.J., 2000. A sensitivity analysis of the radiation use efficiency for gross photosynthesis and net carbon accumulation by wheat. Agricultural and Forest Meteorology, 101: 217-234.

Choudhury, B.J., 2001. Modeling radiation- and carbon-use efficiencies of maize, sorghum, and rice. Agricultural and Forest Meteorology, 106: 317-330.

Ciais, P., Reichstein, M., Viovy, N., Granier, A., Oge´e, J., Allard6, V., Aubinet, M., Buchmann, N., Bernhofer, C., Carrara, A., Chevallier, F., Noblet, N.D., Friend, A.D., Friedlingstein, P., Gru¨nwald, T., Heinesch, B., Keronen, P., Knohl, A., Krinner, G., Loustau, D., Manca, G., Matteucci, G., Miglietta, F., Ourcival, J.M., Papale, D., Pilegaard, K., Rambal, S., Seufert, G., Soussana, J.F., Sanz, M.J., Schulze, E.D., Vesala, T. and Valentini, R., 2005. Europe-wide reduction in primary productivity caused by the heat and drought in 2003. Nature, 437: 529-533.

Cohan, D.S., Xu, J., Greenwald, R., Bergin, M.H. and Chameides, W.L., 2002. Impact of atmospheric aerosol light scattering and absorption on terrestrial net primary productivity. Global Biogeochemical Cycles, 16: doi:10.1029/2001GB001441.

Cowan, I.R., 1968. The interception and absorption of radiation in plant stands. Journal of Applied Ecology, 5(2): 367-379.

Cox, P.M., Betts, R.A., Jones, C.D., Spall, S.A. and Totterdell, I.J., 2000. Acceleration of global warming due to carbon-cycle feedbacks in a coupled climate model. Nature, 408: 184-187.

de Pury, D.G.G. and Farquhar, G.D., 1997. Simple scaling of photosynthesis from leaves to canopies without the errors of big-leaf models. Plant, Cell and Environment, 20: 537-557.

de Wit, C.T., 1965. Photosynthesis of leaf canopies. Cent. for Agric. Publ. and Doc., Wageningen, 57 pp.

Denholm, J.V., 1981a. The influence of penumbra on canopy photosynthesis I. Theoretical considerations. Agricultural Meteorology, 25: 145-166.

Denholm, J.V., 1981b. The influence of penumbra on canopy photosynthesis II. Canopy of horizontal circular leaves. Agricultural Meteorology, 25: 167-194.

Dennis, A., Fraser, M., Anderson, S. and Allen, D., 2002. Air pollutant emissions associated with forest, grassland, and agricultural burning in Texas. Atmospheric Environment, 36: 3779-3792.

Drewitt, G.B., Black, T.A., Nesic, Z., Humphreys, E.R., Jork, E.M., Swanson, R., Ethier, G.J., Griffis, T. and Morgenstern, K., 2002. Measuring forest floor CO_2 fluxes in a Douglas-fir forest. Agricultural and Forest Meteorology, 110(4): 299-317.

Dutton, E.G. and Bodhaine, B.A., 2001. Solar irradiance anomalies caused by clear-sky transmission variations above Mauna Loa: 1958-99. Journal of Climate, 14: 3255-3262.

Epron, D., Le Dantec, V., Dufrene, E. and Granier, A., 2001. Seasonal dynamics of soil carbon dioxide efflux and simulated rhizosphere respiration in a beech forest. Tree Physiology, 21: 145-152.

Ethier, G.J. and Livingston, N.J., 2004. On the need to incorporate sensitivity to CO_2 transfer conductance into the Farquhar-von Caemmerer-Berry leaf photosynthesis model. Plant Cell and Environment, 27(2): 137-153.

Evans, J.R. and Vogelmann, T.C., 2003. Profiles of ^{14}C fixation through spinach leaves in relation to light absorption and photosynthetic capacity. Plant, Cell and Environment, 26: 547-560.

Falge, E., Baldocchi, D., Tenhunen, J., Aubinet, M., Bakwin, P., Berbigier, P., Bernhofer, C., Burba, G., Clement, R., Davis, K.J., Elbers, J.A., Goldstein, A.H. and Grelle, A., 2002. Seasonality of ecosystem respiration and gross primary production as derived from FLUXNET measurements. Agricultural and Forest Meteorology, 113: 53-74.

Farquhar, G.D. and Roderick, M.L., 2003. Pinatubo, diffuse light, and the carbon cycle. Science, 299: 1997-1998.

Farquhar, G.D., von Caemmerer, S. and Berry, J.A., 1980. A biochemical model of photosynthetic CO_2 assimilation in leaves of C_3 species. Planta, 149: 78-90.

Flanagan, L.B. and Johnson, B.G., 2005. Interacting effects of temperature, soil moisture and plant biomass production on ecosystem respiration in a northern temperate grassland. Agricultural and Forest Meteorology, 130: 237–253.

Forseth, I.N. and Norman, J.M., 1993. Modelling of solar irradiance, leaf energy budget and canopy photosynthesis. In: D.O. Hall, J.M.O. Scurlock, H.R. Bolhar-Nordenkampf, R.C. Leegood and S.P. Long (Editors), Photosynthesis and Production in a Changing Environment: a Field and Laboratory Manual, pp. 207-219.

Freedman, J.M., Fitzjarrald, D.R., Moore, K.E. and Sakai, R.K., 2000. Boundary layer clouds and vegetation - atmosphere feedbacks. Journal of Climate, 14: 180-197.

Freedman, J.M., Fitzjarrald, D.R., Moore, K.E. and Sakai, R.K., 2001. Boundary layer clouds and vegetation - atmosphere feedbacks. Journal of Climate, 14: 180-197.

Garrison, J., 1995. An evaluation of the effect of volcanic eruptions on the solar radiation at six Canadian stations. Solar Energy, 55: 513-525.

Gausman, H.W. and Allen, W.A., 1973. Optical parameters of leaves of 30 plant species. Plant Physiology, 52: 57-62.

Goudriaan, J., 1977. Crop micrometeorology and a simulation study. Cent. for Agric. Publ. and Doc., Wageningen, 249 pp.

Goudriaan, J., 1988. The bare bones of leaf-angle distribution in radiation models for canopy photosynthesis and energy exchange. Agricultural and Forest Meteorology, 43: 155-169.

Goudriaan, J. and van Laar, H.H., 1994. Modelling potential crop growth processes - textbook with exercises. Kluwer Academic Publishers, Amsterdam, 238 pp.

Goulden, M.L., Miller, S.D., Rocha, H.R.d., Menton, M.C., Freitas, H.C.d., Figueira, A.M.E.S. and Sousa, C.A.D.d., 2004. Diel and seasonal patterns of tropical forest CO_2 exchnage. Ecological Applications, 14: S42-S54.

Goulden, M.L., Munger, J.W., Fan, S.-M., Daube, B.C. and Wofsy, S.C., 1996a. Measurements of carbon sequestration by long-term eddy covariance: methods and a critical evaluation of accuracy. Global Change Biology, 2: 169-182.

Goulden, M.L., Munger, W., Fan, S.M. and Daube, B.C., 1996b. Measurements of carbon sequestration by long-term eddy covariance: Methods and a critical evaluation of accuracy. Global Change Biology, 2: 169-182.

Goulden, M.L., Wofsy, S.C., Harden, J.W., Trumbore, S.E., Crill, P.M., Gower, S.T., Fries, T., Daube, B.C., Fan, S.-M., Sutton, D.J., Bazzaz, A. and Munger, J.W., 1998. Sensitivity of boreal forest carbon balance to soil thaw. Science, 279: 214-217.

Grace, J., 1971. The directional distribution of light in natural and controlled environment conditions. Journal of Applied Ecology, 8(1): 155-164.

Griffis, T.J., Black, T.A., Morgenstern, K., Barr, A.G., Nesic, Z., Drewitt, G.B., Gaumont-Guay, D. and McCaughey, J.H., 2003. Ecophysiological controls of the carbon balance of three southern boreal forests. Agricultural and Forest Meteorology, 117: 53-71.

Gu, L., Baldocchi, D., Verma, S.B., Black, T.A., Vesala, T., Falge, E.M. and Dowty, P.R., 2002. Advantages of diffuse radiation for terrestrial ecosystem productivity. Journal of Geophysical Research, 107: 10.1029/2001JD001242.

Gu, L., Baldocchi, D.D., Wofsy, S.C., Munger, J.W., Michalsky, J.J., Urbanski, S.P. and Boden, T.A., 2003. Response of a deciduous forest to the Mount Pinatubo eruption: enhanced photosynthesis. Science, 299: 2035-2038.

Gu, L., Fuentes, J.D. and Shugart, H.H., 1999. Responses of net ecosystem exchanges of carbon dioxide to changes in cloudiness: Results from two North America deciduous forests. Journal of Geophysical Research, 104: 31421-31434.

Healey, K.D., Rickert, K.G., Hammer, G.L. and Bange, M.P., 1998. Radiation use efficiency increases when the diffuse component of incident radiation is enhanced under the shade. Australian Journal of Agricultural Research, 49: 665-672.

Hoecker, W.H., Flowers, E.C. and Cotton, G.F., 1985. Variation of direct beam solar radiation in the United States due to the El Chichon debris cloud. Bulletin American Meteorology Society, 66: 14-19.

Hogberg, P., Nordgren, A., Buchmann, N., Taylor, A.F.S., Ekblad, A., Hogberg, M., Nyberg, G., Ottosson-Lofvenius, M. and Read, D.J., 2001. Large-scale forest girdling shows that current photosynthesis drives soil respiration. Nature, 411: 789-792.

Hollinger, D.Y., Kelliher, F.M., Byers, J.N., Hunt, J.E., McSeveny, T.M. and Weir, P.L., 1994. Carbon dioxide exchange between an undisturbed old-growth temperate forest and the atmosphere. Ecology, 75(1): 134-150.

Hollinger, D.Y., Kelliher, F.M., Schulze, E.-D., Bauer, G., Arneth, A., Byers, J.N., Hunt, J.E., McSeveny, T.M., Kobak, K.I., Milukova, I., Sogatchev, A., Tatarinov, F., Varlargin, A., Ziegler, W. and Vygodskaya, N.N., 1998. Forest-atmosphere carbon dioxide exchange in eastern Siberia. Agricultural and Forest Meteorology, 90: 291-306.

Horn, H.S., 1971. The adaptive geometry of trees. Princeton University Press, New Jersey, 144 pp.

Humphreys, E.R., 2004. Net ecosystem production of three coastal Douglas-fir stands at different stages of development after harvesting. Ph.D. Thesis, University of British Columbia, Vancouver, 155 pp.

Humphreys, E.R., Black, T.A., Ethier, G.J., Drewitt, G.B., Spittlehouse, D.L., Jork, E.-M., Nesic, Z. and Livingston, N.J., 2003. Annual and seasonal variability of sensible and latent heat fluxes above a coastal Douglas-fir forest, British Columbia, Canada. Agricultural and Forest Meteorology, 115: 109-125.

Humphreys, E.R., Black, T.A., Morgenstern, K., Cai, T., Drewitt, G.B., Nesic, Z. and Trofymow, J.A., 2006. Carbon dioxide fluxes in coastal Douglas-fir stands at different stages of development after clearcut harvesting. Agricultural and Forest Meteorology: In press.

Husar, R.B., Tratt, D.M., Schichtel, B.A., Falke, S.R., Li, F., Jaffe, D., Gasso, S., Gill, T., Laulainen, N.S., Lu, F., Reheis, M.C., Chun, Y., Westphal, D., Holben, B.N., Gueymard, C., McKendry, I., Kuring, N., Feldman, G.C., McClain, C., Frouin, R.J., Merrill, J., Dubois, D., Vignola, F., Murayama, T., Nickovic, S., Wilson, W.E., Sassen, K., Sugimoto, N. and Malm, W.C., 2001. Asian dust events of April 1998. Journal of Geophysical Research, 106(D16): 18317-18330.

Hutchison, B.A. and Matt, D.R., 1976. Beam enrichment of diffuse radiation in a deciduous forest. Agricultural Meteorology, 17: 93-110.

Idso, S.B. and de Wit, C.T., 1970. Light relations in plant canopies. Applied Optics, 9(1): 177-184.

Irvine, J. and Law, B.E., 2002. Contrasting soil respiration in young and old growth ponderosa pine. Global Change Biology, 8: 1183-1194.

Janssens, I.A., Lankreijer, H., Matteucci, G., Kowalski, A.S., Buchmann, N., Epron, D., Pilegaard, K., Kutsch, W., Longdoz, B., Grünwald, T., Montagnani, L., Dore, S., Rebmann, C., Moors, E.J., Grelle, A., Rannik, Ü., Morgenstern, K., Clement, R., Guðmundsson, J., Minerbi, S., Berbigier, P., Ibrom, A., Moncrieff, J., Aubinet, M., Bernhofer, C., Jensen, N.O., Vesala, T., Granier, A., Schulze, E.-D., Lindroth, A., Dolman, A.J., Jarvis, P.G., Ceulemans, R. and Valentini, R., 2001. Productivity and disturbance overshadow temperature in determining soil and ecosystem respiration across European forests. Global Change Biology, 7: 269-278.

Jarvis, P.G., 1993. Prospects for bottom-up models. In: J.R. Ehleringer and C.B. Field (Editors), Scaling Physiological Processes Leaf to Globe. Academic Press, San Diego, pp. 115-126.

Jarvis, P.G. and Leverenz, J.W., 1983. Productivity of temperate, deciduous and evergreen forests. In: O.L. Lange, P.S. Nobel, C.B. Osmond and H. Zeigler (Editors), Encyclopedia of Plant Physiology. Springer, Berlin, pp. 233-280.

Jarvis, P.G. and McNaughton, K.G., 1986. Stomatal control of transpiration: scaling up from leaf to region. Advances in Ecological Research, 15: 1-49.

Jassal, R., Black, A., Novak, M., Morgenstern, K., Nesic, Z. and Gaumont-Guay, D., 2005. Relationship between soil CO2 concentrations and forest-floor CO2 effluxes. Agricultural and Forest Meteorology, 130(3-4): 176-192.

Jones, C.D. and Cox, P.M., 2001. Modeling the volcanic signal in the atmospheric CO_2 record. Global Biogeochemical Cycles, 15(2): 453-465.

Jones, H.G., 1992. Plants and Microclimate: A Quantitative Approach to Environmental Plant Physiology. Cambridge University Press, 413 pp.

June, T., Evans, J.R. and Farquhar, G.D., 2004. A simple new equation for the reversible temperature dependence of photosynthetic electron transport: a study on soybean leaf. Functional Plant Biology, 31(3): 275-283.

Keeling, C.D., Whorf, T.P., Wahlen, M. and van der Pflicht, J., 1995. Interannual extremes in the rate of rise of atmospheric carbon dioxide since 1980. Nature, 375: 666-670.

Kimball, H.H. and Hand, I.F., 1922. Daylight illumination on horizontal, vertical, and sloping surfaces. Monthly Weather Review, 50(12): 615-628.

Kirschbaum, M.U.F., 2004. Soil respiration under prolonged soil warming: are rate reductions caused by acclimation or substrate loss? Global Change Biology, 10: 1-8.

Kobayashi, H., Matsunaga, T., Hoyano, A., Aoki, M., Komori, D. and Boonyawat, S., 2004. Satellite estimation of photosynthetically active radiation in Southeast Asia:

Impacts of smoke and cloud cover. Journal of Geophysical Research, 109: D04102, doi:10.1029/2003JD003807.

Kok, B., 1948. A critical consideration of the quantum yield of *Chlorella* photosynthesis. Enzymology, 13: 1-56.

Kowalski, S., Sartore, M., Burlett, R., Berbigier, P. and Loustau, D., 2003. The annual carbon budget of a French pine forest (*Pinus pinaster*) following harvest. Global Change Biology, 9: 1051-1065.

Krakauer, N.Y. and Randerson, J.T., 2003. Do volcanic eruptions enhance or diminish net primary production? Evidence from tree rings. Global Biogeochemical Cycles, 17(4): 1118, doi:10.1029/2003GB002076.

Kramer, P.J. and Decker, J.P., 1944. Relation between light intensity and rate of photosynthesis of loblolly pine and certain hardwoods. Plant Physiology, 19: 350-358.

Lamanna, M.S. and Goldstein, A.H., 1999. In situ measurements of C_2-C_{10} volatile organic compounds above a Sierra Nevada ponderosa pine plantation. Journal of Geophysical Research, 104: 21247-21262.

Lang, A.R.G., Xiang, Y. and Norman, J.M., 1985. Crop structure and the penetration of direct sunlight. Agricultural and Forest Meteorology, 35: 83-101.

Lavigne, M., Ryan, M. and Anderson, D., 1997. Comparing nocturnal eddy covariance measurements to estimates of ecosystem respiration made by scaling chamber measurements. Journal of Geophysical Research, 102: 28977-28986.

Lavigne, M.B., Foster, R.J. and Goodine, G., 2004. Seasonal and annual changes in soil respiration in relation to soil temperature, water potential and trenching. Tree Physiology, 24: 415–424.

Law, B.E., Falge, E., Gu, L., Baldocchi, D.D., Bakwin, P., Berbigier, P., Davis, K., Dolman, A.J., Falk, M., Fuentes, J.D., Goldstein, A., Granier, A., Grelle, A., Hollinger, D., Janssens, I.A., Jarvis, P., Jensen, N.O., Katul, G., Mahli, Y., Matteucci, G., Meyers, T., Monson, R., Munger, W., Oechel, W., Olson, R., Pilegaard, K., Paw, K.T., Thorgeirsson, H., Valentini, R., Verma, S., Vesala, T., Wilson, K. and Wofsy, S., 2002. Environmental controls over carbon dioxide and water vapor exchange of terrestrial vegetation. Agricultural and Forest Meteorology, 113(1-4): 97-120.

Lee, X., Fuentes, J.D., Staebler, R.M. and Neumann, H.H., 1999. Long-term observation of the atmospheric exchange of CO2 with a temperature deciduous forest in southern Ontario, Canada. Journal of Geophysical Research, 104(13): 15975-15984.

Lee, X., Wu, H.-J., Sigler, J., Oishi, C. and Siccama, T., 2004. Rapid and transient response of soil respiration to rain. Global Change Biology, 10(6): 1017-1026.

Lemeur, R., 1973. A method for simulating the direct solar radiation regime in sunflower, Jerusalem artichoke, corn and soybean canopies using actual stand structure data. Agricultural Meteorology, 12: 229-247.

Lindroth, A., Grelle, A. and Moren, A.-S., 1998. Long-term measurements of boreal forest carbon balance reveal large temperature sensitivity. Global Change Biology, 4: 443-450.

Liu, B.Y.H. and Jordan, R.C., 1960. The interrelationship and characteristic distribution of direct, diffuse, and total solar radiation. Solar Energy, 4(3): 1-19.

Lloyd, J., Grace, J., Miranda, A.C., Meir, P., Wong, S.C., Miranda, H.S., Wright, I.R., Gash, J.H.C. and McIntyre, J., 1995. A simple calibrated model of Amazon rainforest productivity based on leaf biochemical properties. Plant, Cell and Environment, 18: 1129-1145.

Lloyd, J. and Taylor, J.A., 1994. On temperature dependence of soil respiration. Functional Ecology, 8: 315-323.

Lucht, W., Prentice, I.C., Myneni, R.B., Sitch, S., Friedlingstein, P., Cramer, W., Bousquet, P., Buermann, W. and Smith, B., 2002. Climatic control of the high-latitude vegetation greening trend and Pinatubo effect. Science, 296: 1687-1689.

Luo, Y., Wan, S., Hui, D. and Wallace, L.L., 2001. Acclimatization of soil respiration to warming in a tall grass prairie. Nature, 413: 622-625.

McArthur, L.J.B. and Hay, J.E., 1981. A technique for mapping the distribution of diffuse solar radiation over the sky hemisphere. Journal of Applied Meteorology, 20: 421-429.

McCormick, M.P., Thomason, L.W. and Trepte, C.R., 1995. Atmospheric effects of the Mt. Pinatubo eruption. Nature, 373: 399-404.

McDowell, N.G., Bowling, D.R., Schauer, A., Irvine, J., Bond, B.J., Law, B.E. and Ehleringer, J.R., 2004. Associations between carbon isotope ratios of ecosystem respiration, water availability and canopy conductance. Global Change Biology, 10(10): 1767-1784.

Miller, E.E. and Norman, J.M., 1971. A sunfleck theory for plant canopies. 1. Lengths of sunlit segments along a transect. Agron. J., 63: 735-738.

Miller, J.B., 1967. A formula for average foliage density. Australian Journal of Botany, 15: 141-144.

Miller, S.D., Goulden, M.L., Menten, M.C., Rocha, H.R.d., Freitas, H.C.d., Figueira, A.M.E.S. and Sousa, C.A.D.d., 2004. Biometric and micrometeorological measurements of tropical forest carbon balance. Ecological Applications, 14(4): S114-S126.

Molineaux, B. and Ineichen, P., 1996. Impact of Pinatubo aerosols on the seasonal trends of global, direct and diffuse irradiance in two northern mid-latitude sites. Solar Energy, 58: 91-101.

Monteith, J., 1972. Solar radiation and productivity in tropical ecosystems. Journal of Applied Ecology, 9: 747-766.

Moon, P. and Spencer, D.E., 1942. Illumination from a non-uniform sky. Trans. Illum Eng. Soc., 37: 707-726.

Morén, A.-S. and Lindroth, A., 2000. CO_2 exchange at the floor of a boreal forest. Agricultural and Forest Meteorology, 101(1-14).

Morgenstern, K., Black, T.A., Humphreys, E.R., Griffis, T.J., Drewitt, G.B., Cai, T., Nesic, Z., Spittlehouse, D.L. and Livingston, N.J., 2004. Sensitivity and uncertainty of the carbon balance of a Pacific Northwest Douglas-fir forest during an El Niño/La Niña cycle. Agricultural and Forest Meteorology, 123: 201-219.

Nichol, J., 1997. Bioclimatic impacts of the 1994 smoke haze event in southeast Asia. Atmospheric Environment, 31(8): 1209-1219.

Niyogi, D., Chang, H.-I., Saxena, V.K., Holt, T., Alapaty, K., Booker, F., Chen, F., Davis, K.J., Holben, B., Matsui, T., Meyers, T., Oechel, W.C., Sr., R.A.P., Wells, R., Wilson, K. and Xue, Y., 2004. Direct observations of the effects of aerosol loading on net ecosystem CO_2 exchanges over different landscapes. Geophysical Research Letters, 31: doi:10.1029/2004GL020915.

Norman, J., 1982. Simulation of microclimates. In: J.L. Hatfield and I.J. Thomason (Editors), Biometeorology in Integrated Pest Management. Academic Press, New York, pp. 65-99.

Norman, J.M., 1979. Modeling the complete crop canopy. In: B.J. Barfield and J.F. Gerber (Editors), Modification of the aerial environment of plants. American Society of Agricultural Engineers, St. Joseph, pp. 249-277.

Norman, J.M., 1980. Interfacing leaf and canopy light interception models. In: J.D. Hesketh and J.W. Jones (Editors), Predicting Photosynthesis for Ecosystem Models. CRC Press, Boca Raton, pp. 49-67.

Norman, J.M. and Arkebauer, T.J., 1991. Predicting canopy light-use efficiency from leaf characteristics. In: J. Hanks and J. Ritchie (Editors), Modeling Plant and Soil Systems. Agronomy Monograph. ASA-CSSA-SSSA, pp. 125-143.

Ögren, E., 1993. Convexity of the photosynthetic light response curve in relation to intensity and direction of light during growth. Plant Physiology, 101: 1013-1019.

Oker-Blom, P., 1985. Photosynthesis of a Scots pine shoot: simulation of the irradiance distribution and photosynthesis of a shoot in different radiation fields. Agricultural and Forest Meteorology, 34: 31-40.

Oker-Blom, P., 1986. Photosynthesis of a Scots pine shoot: simulation of the irradiance distribution and photosynthesis of a shoot in different radiation fields. Agricultural and Forest Meteorology, 34: 31-40.

Olmo, F.J., Tovar, J., Alados-Arboledas, L., Okulov, O. and Ohvril, H.O., 1999. A comparison of ground level solar radiative effects of recent volcanic eruptions. Atmospheric Environment, 33: 4589-4596.

Page, S.E., Siegert, F., Rieley, J.O., Boehm, H.-D.V., Jaya, A. and Limin, S., 2002. The amount of carbon released from peat and forest fires in Indonesia during 1997. Nature, 420: 61-65.

Palmroth, S., Palva, L., Stenberg, P. and Kotisaari, A., 1999. Fine scale measurement and simulation of penumbral radiation formed by a pine shoot. Agricultural and Forest Meteorology, 95: 15-25.

Pan, Z., Segal, M., Arritt, R.W. and Takle, E.S., 2004. On the potential change in solar radiation over the US due to increases of atmospheric greenhouse gases. Renewable Energy, 29: 1923-1928.

Pinelli, P. and Loreto, F., 2003. $^{12}CO_2$ emission from different metabolic pathways measured in illuminated and darkened C_3 and C_4 leaves at low, atmospheric and elevated CO_2 concentration. Journal of Experimental Botany, 54: 1761–1769.

Ponton, S., Flanagan, L.B., Alstad, K.P., Johnson, B.G., Morgenstern, K.A.I., Kljun, N., Black, T.A. and Barr, A.G., 2006. Comparison of ecosystem water-use efficiency among Douglas-fir forest, aspen forest and grassland using eddy covariance and carbon isotope techniques. Global Change Biology, 12(2): 294-310.

Price, D.T. and Black, T.A., 1990. Effects of short-term variation in weather on diurnal canopy CO_2 flux and evapotranspiration of a juvenile Douglas-fir stand. Agricultural and Forest Meteorology, 50: 139-158.

Rayment, M.B. and Jarvis, P.G., 2000. Temporal and spatial variation of soil CO_2 efflux in a Canadian boreal forest. Soil Biology and Biochemistry, 32: 35-45.

Reichstein, M., Falge, E., Baldocchi, D., Papale, D., Aubinet, M., Berbigier, P., Bernhofer, C., Buchmann, N., Gilmanov, T., Granier, A., Grunwald, T., Havrankova, K., Ilvesniemi, H., Janous, D., Knohl, A., Laurila, T., Lohila, A., Loustau, D., Matteucci, G., Meyers, T., Miglietta, F., Ourcival, J.-M., Pumpanen, J., Rambal, S., Rotenberg, E., Sanz, M., Tenhunen, J., Seufert, G., Vaccari, F.,

Vesala, T., Yakir, D. and Valentini, R., 2005. On the separation of net ecosystem exchange into assimilation and ecosystem respiration: review and improved algorithm. Global Change Biology, 11(9): 1424-1439.

Reichstein, M., J.D., T., Roupsard, O., Ourcival, J.-M., Rambal, S., Miglietta, F., Peressottis, A., Pecchiari, M., Tirone, G. and Valentini, R., 2002a. Severe drought effects on ecosystem CO_2 and H_2O fluxes at three Mediterranean evergreen sites: revision of current hypothesis? Global Change Biology, 8: 999-1017.

Reichstein, M., Tenhunen, J.D., Roupsard, O., Ourcival, J.M., Rambal, S., Dore, S. and Valentini, R., 2002b. Ecosystem respiration in two Mediterranean evergreen Holm Oak forests: drought effects and decomposition dynamics. Functional Ecology, 16(1): 27-39.

Richardson, A.D. and Hollinger, D.Y., 2005. Statistical modeling of ecosystem respiration using eddy covariance data: Maximum likelihood parameter estimation,and Monte Carlo simulation of model and parameter uncertainty, applied to three simple models. Agricultural and Forest Meteorology, 131: 191-208.

Robinson, N., 1966. Solar Radiation. Elsevier Pub. Co., New York, 347 pp.

Robock, A., 2002. The climatic aftermath. Science, 295: 1242-1244.

Roderick, M.L., Farquhar, G.D., Berry, S.L. and Noble, I.R., 2001. On the direct effect of clouds and atmospheric particles on the productivity and structure of vegetation. Oecologia, 129: 21-30.

Ross, J., 1991. Introduction. In: J. Ross (Editor), Photon-Vegetation Interactions-Applications in Optical Remote Sensing and Plant Ecology. Springer-Verlag, pp. 1-7.

Ross, J. and Ross, V., 1998. Statistical description of the architecture of a fast growing willow coppice. Agricultural and Forest Meteorology, 91: 23-37.

Ruimy, A., Kergoat, L., Bondeau, A., Bondeau, A., Churkina, G., Cramer, W., Colinet, G., Collatz, J., Dedieu, G., Emanuel, W., Esser, G., Field, C., Francois, L. and Friend, A., 1999. Comparing global models of terrestrial net primary productivity (NPP): analysis of differences in light absorption and light-use efficiency. Global Change Biolology, 5(s1): 56-64.

Savage, K.E. and Davidson, E.A., 2001. Interannual variation of soil respiration in two New England forests. Global Biogeochemical Cycles, 15(2): 337-350.

Scott-Denton, L.E., Rosenstiel, T.N. and Monson, R.K., 2005. Differential controls by climate and substrate over the heterotrophic and rhizospheric components of soil respiration. Global Change Biology, 11: 1-12.

Scott-Denton, L.E., Sparks, K.L. and Monson, R.K., 2003. Spatial and temporal controls of soil respiration rate in a high-elevation, subalpine forest. Soil Biology & Biochemistry, 35: 525-534.

Sellers, P.J., Randall, D.A., Collatz, G.J., Berry, J.A., Field, C.B., Dazlich, D.A., Zhang, C., Collelo, G.D. and Bounoua, L., 1996. A revised land surface parameterization (SiB2) for GCMs. Part I: Model formulation. Journal of Climate, 9/4: 676-705.

Shapiro, J.B., Griffin, K.L., Lewis, J.D. and Tissue, D.T., 2004. Response of Xanthium strumarium leaf respiration in the light to elevated CO2 concentration, nitrogen availability and temperature. New Phytologist, 162(2): 377-386.

Sharp, R.E., Matthews, M.A. and Boyer, J.S., 1984. Kok effect and the quantum yield of photosynthesis: light partially inhibits dark respiration. Plant Physiology, 75: 95-101.

Sinclair, T.R., Murphy, C.E. and Knoerr, K.R., 1976. Development and evaluation of simplified models for simulating canopy photosynthesis and transpiration. Journal of Applied Ecology, 13: 813-829.

Smolander, H., Oker-Blom, P., Ross, J., Kellomaki, S. and Lahti, T., 1987. Photosynthesis of a Scots pine shoot: test of a shoot photosynthesis model in a direct radiation field. Agricultural and Forest Meteorology, 39: 67-80.

Soden, B.J., Wetherald, R.T., Stenchikov, G.L. and Robock, A., 2002. Global cooling after the eruption of Mount Pinatubo: a test of climate feedback by water vapor. Science, 296: 727730.

Spitters, C.J.T., Toussaint, H.A.J.M. and Goudriaan, J., 1986. Separating the diffuse and direct component of global radiation and its implications for modeling canopy photosynthesis. Part I. components of incoming radiation. Agricultural and Forest Meteorology, 38: 217-229.

Stanhill, G. and Cohen, S., 2001. Global dimming: a review of the evidence for a widespread and significant reduction in global radiation with discussion of its probable causes and possible agricultural consequences. Agricultural and Forest Meteorology, 107: 255-278.

Steel, R.G.D. and Torrie, J.H., 1960. Principles and Procedures of Statistics. McGraw-Hill, New York, 481 pp.

Stenberg, P., 1998. Implications of shoot structure on the rate of photosynthesis at different levels in a coniferous canopy using a model incorporating grouping and penumbra. Functional Ecology, 12: 82-91.

Steven, M.D., 1977. Standard distributions of clear sky radiance. Quarterly Journal of the Royal Meteorological Society, 106: 57-61.

Still, C.J., Randerson, J.T. and Fung, I.Y., 2004. Large-scale plant light-use efficiency inferred from the seasonal cycle of atmospheric CO_2. Global Change Biolology, 10(8): 1240-1252.

Suyker, A.E. and Verma, S.B., 2001. Year-round observations of the net ecosystem exchange of carbon dioxide in a native tallgrass prairie. Global Change Biology, 7(3): 279-289.

Tang, J., Baldocchi, D.D. and Xu, L., 2005. Tree photosynthesis modulates soil respiration on a diurnal time scale. Global Change Biology, 11: 1298-1304.

Timmermann, A., Oberhuber, J., Bacher, A., Esch, M., Latif, M. and Roeckner, E., 1999. Increased El Niño frequency in a climate model forced by future greenhouse warming. Nature, 398: 694-697.

Tjoelker, M.G., Oleksyn, J. and Reich, P.B., 2001. Modelling respiration of vegetation: evidence for a general temperature-dependence Q_{10}. Global Change Biology, 7: 223-230.

Twine, T.E., Kustas, W.P., Norman, J.M., Cook, D.R., Houser, P.R., Meyers, T.P., Prueger, J.H., Starks, P.J. and Wesely, M.L., 2000. Correcting eddy-covariance flux underestimates over a grassland. Agricultural and Forest Meteorology, 103: 279-300.

Villar, R., Held, A.A. and Merino, J., 1994. Dark leaf respiration in light and darkness of an evergreen and a deciduous plant species. Plant Physiology, 107: 421-427.

Wang, X., Lewis, J., Tissue, D., Seemann, J. and Griffin, K., 2001. Effects of elevated atmospheric CO2 concentration on leaf dark respiration of *Xanthium strumarium* in light and in darkness. Proceedings of the National Academy of Sciences, USA, 98: 2479-2484.

Wang, Y.-P. and Leuning, R., 1998. A two-leaf model for canopy conductance, photosynthesis and partitioning of available energy I: Model description and comparison with a multi-layered model. Agricultural and Forest Meteorology, 91: 89-111.

Wang, Y.P., 2000. A refinement to the two-leaf model for calculating canopy photosynthesis. Agricultural and Forest Meteorology, 101: 143-150.

Wang, Y.P. and Jarvis, P.G., 1990. Effect of incident beam and diffuse radiation on PAR absorption, photosynthesis, and transpiration of sitka spruce - A simulation study. Silva Carelica, 15: 167-180.

Warren, C.R., Ethier, G.J., Livingston, N.J., Grant, N.J., Turpin, D.H., Harrison, D.L. and Black, T.A., 2003. Transfer conductance in second growth Douglas-fir (*Pseudotsuga menziesii* (Mirb.) Franco) canopies. Plant, Cell and Environment, 26: 1215-1227.

Weiss, A. and Norman, J.M., 1985. Partitioning solar radiation into direct and diffuse, visible and near-infrared components. Agricultural and Forest Meteorology, 34: 205-213.

Wendler, G., 1984. Effects of the El Chichon volcanic cloud on solar radiation received at Fairbanks, Alaska. Bulletin American Meteorological Society, 65(3): 216-218.

Wesely, M.L. and Lipschutz, R.C., 1976. A method for estimating hourly averages of diffuse and direct solar radiation under a layer of scattered clouds. Solar Energy, 18: 467-473.

Wofsy, S.C., Goulden, M.L., Munger, J.W., Fan, S.M., Bakwin, P.S., Daube, B.C., Bassow, S.L. and Bazzaz, F.A., 1993. Net exchange of CO_2 in a mid-latitude forest. Science, 260: 1314-1317.

Wohlfahrt, G., Anfang, C., Bahn, M., Haslwanter, A., Newesely, C., Schmitt, M., Dro¨sler, M., Pfadenhauer, J.r. and Cernusc, A., 2005a. Quantifying nighttime ecosystem respiration of a meadow using eddy covariance, chambers and modelling. Agricultural and Forest Meteorology, 128: 141–162.

Wohlfahrt, G., Bahn, M., Haslwanter, A., Newesely, C. and Cernusca, A., 2005b. Estimation of daytime ecosystem respiration to determine gross primary production of a mountain meadow. Agricultural and Forest Meteorology, 130: 13-25.

Wood, J., Muneer, T. and Kubie, J., 2003. Evaluation of a new photodiode sensor for measuring global and diffuse irradiance, and sunshine duration. Journal of Solar Energy Engineering, 125: 43-48.

Wotawa, G. and Trainer, M., 2000. The influence of Canadian forest fires on pollutant concentrations in the United States. Science, 288: 324-328.

Xu, L. and Baldocchi, D.D., 2004. Seasonal variation in carbon dioxide exchange over a Mediterranean annual grassland in California. Agricultural and Forest Meteorology, 123(1-2): 79-96.

Xu, M. and Qi, Y., 2001. Spatial and seasonal variations of Q_{10} determined by soil respiration measurements at a Sierra Nevadan forest. Global Biogeochemical Cycles.

Young, D.R. and Smith, W.K., 1983. Effect of cloudcover on photosynthesis and transpiration in the subalpine understory species *Arnica Latifolia*. Ecology, 64(4): 681-687.

Zelawski, W., Szaniawski, R., Dybczynski, W. and Piechurowski, A., 1973. Photosynthetic capacity of conifers in diffuse light of high illuminance. Photosynthetica, 7(4): 351-357.

Appendix A. The Site Location, EC System Configuration and the PAR Measurements for the 56-year-old Douglas-fir Stand

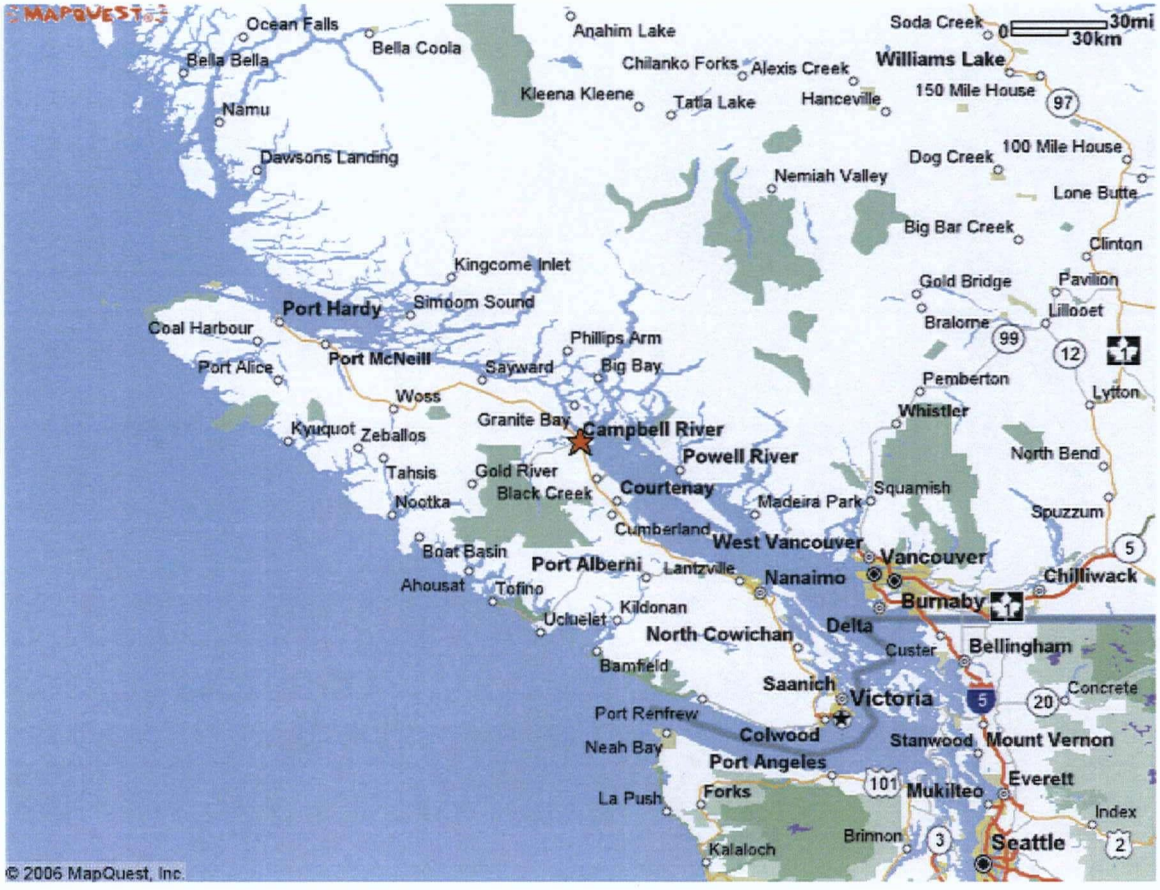

Figure A-1. Location of the 56-year-old Douglas-fir stand (DF49) on the east coast of Vancouver Island. The red star indicates the town of Campbell River. Map was obtained from http://www.mapquest.com/maps/.

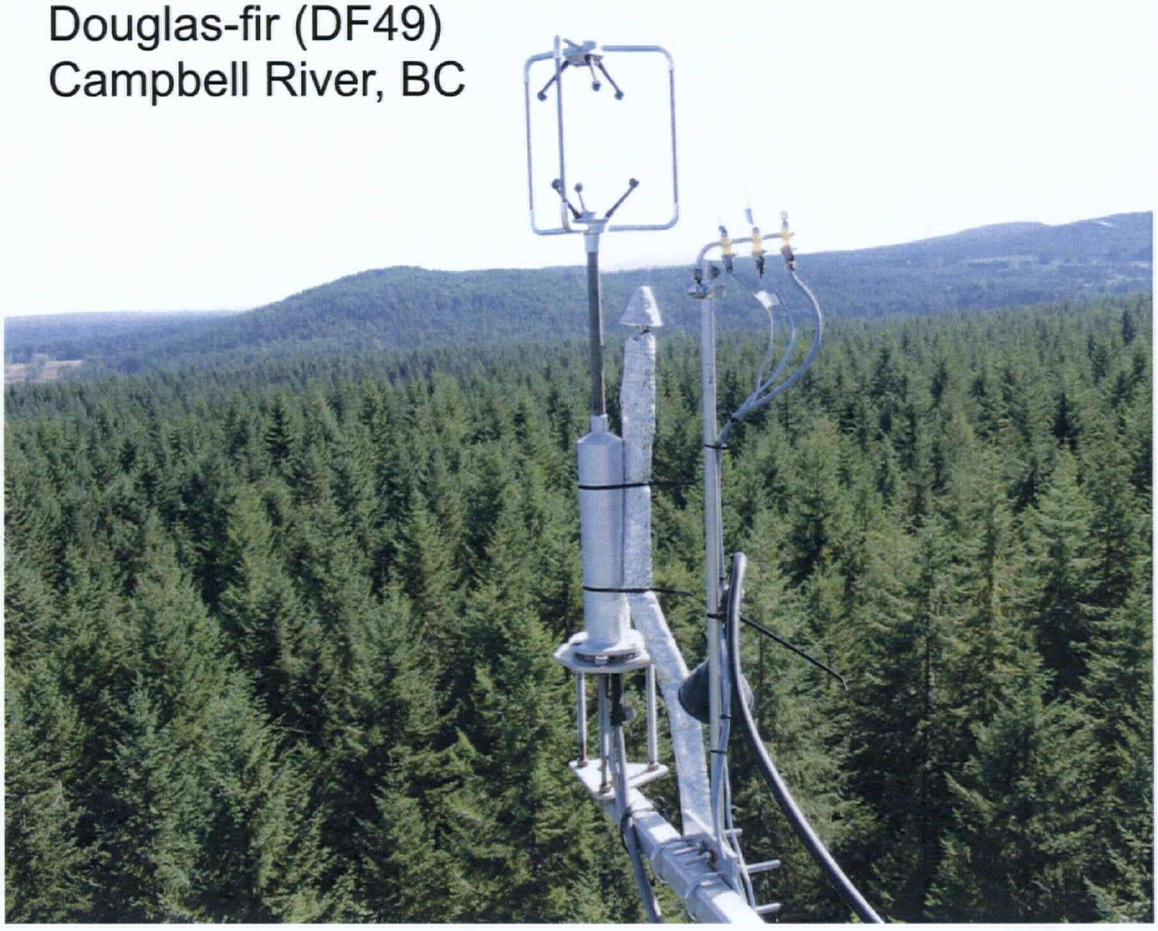

Figure A-2. View of the 56-year-old Douglas-fir stand on Vancouver Island. The (eddy covariance) system consists of a 3-*D* sonic anemometer and a closed-path infrared gas analyzer.

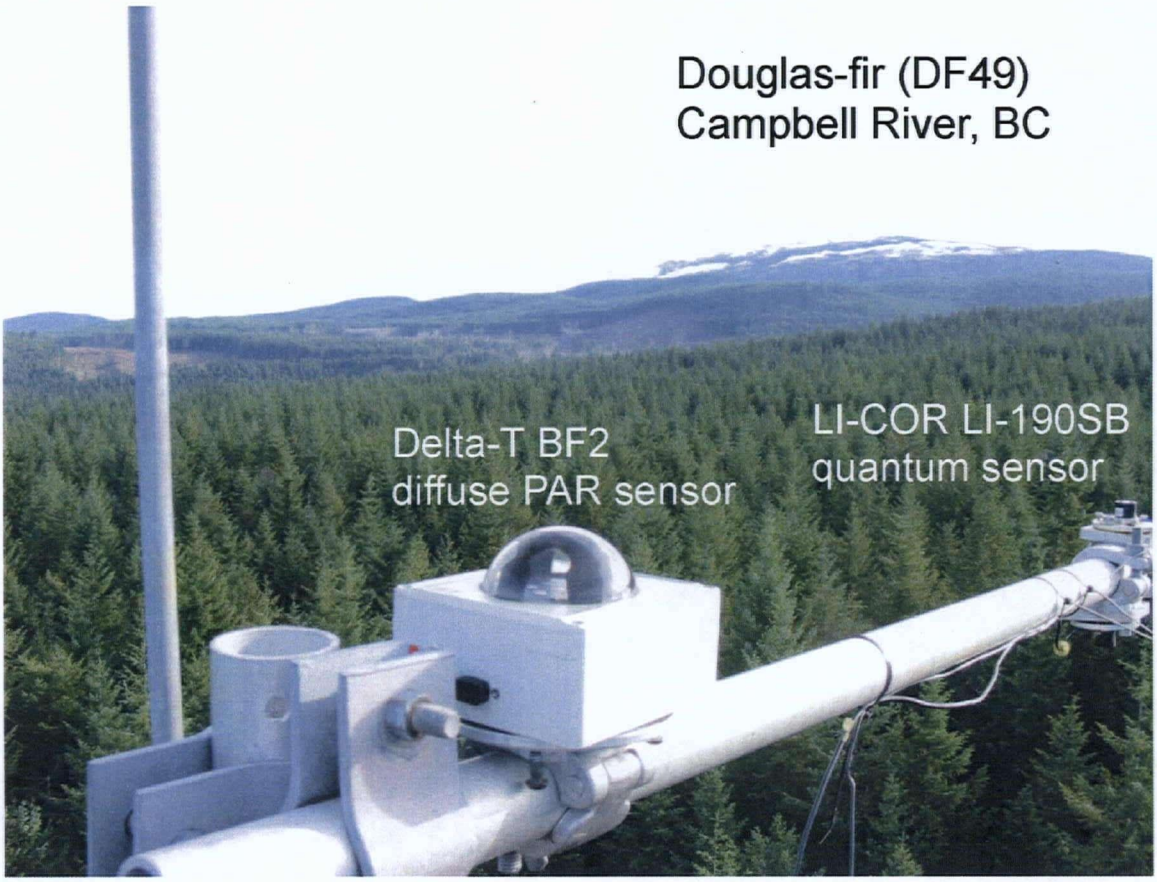

Figure A-3. Half-hourly values of total and diffuse PAR were measured using a LI-190SB quantum sensor and a Delta-T BF2 sensor, respectively.

Appendix B. Comparison of the PAR Measurements Made Using the BF2 and LI-190SB.

Since BF2 measures both Q_{t0} and Q_{d0} using the same algorithm (see Wood et al. 2003 for details), its half-hourly measurements of Q_{t0} were compared with those measured using LI-190SB in order to obtain an indirect quality check for its Q_{d0} measurements (Fig. A1). In addition, the quality of BF2 Q_{d0} measurements were directly checked by their comparison with LI-190SB Q_{t0} measurements made in overcast conditions (Fig. A2). The overcast conditions were determined as follows. First, we adopted a simple model from Campbell and Norman (1998) to predict Q_{t0} in a cloudless sky,

$$Q_{t0mdl} = a^{\tau} Q_0 \sin\beta \qquad \text{(B1)}$$

where Q_{t0mdl} is the modelled Q_{t0} in a cloudless sky, Q_0 is the extra-terrestrial PAR quantum flux (2413 μmol m^{-2} s^{-1}, converted from the solar constant of 1367 W m^{-2}), β is the solar elevation angle, a is an empirical coefficient (taken as 0.86 for this stand), and τ is the optical air mass. The value of τ was calculated as $1/\sin\beta$. Second, the overcast and sunny conditions were defined as Q_{t0} (LI-190SB)/Q_{t0mdl} < 0.5, and Q_{t0} (LI-190SB)/Q_{t0mdl} > 0.9, respectively. The rest of the half-hourly measurements were loosely classified as the partly cloudy conditions.

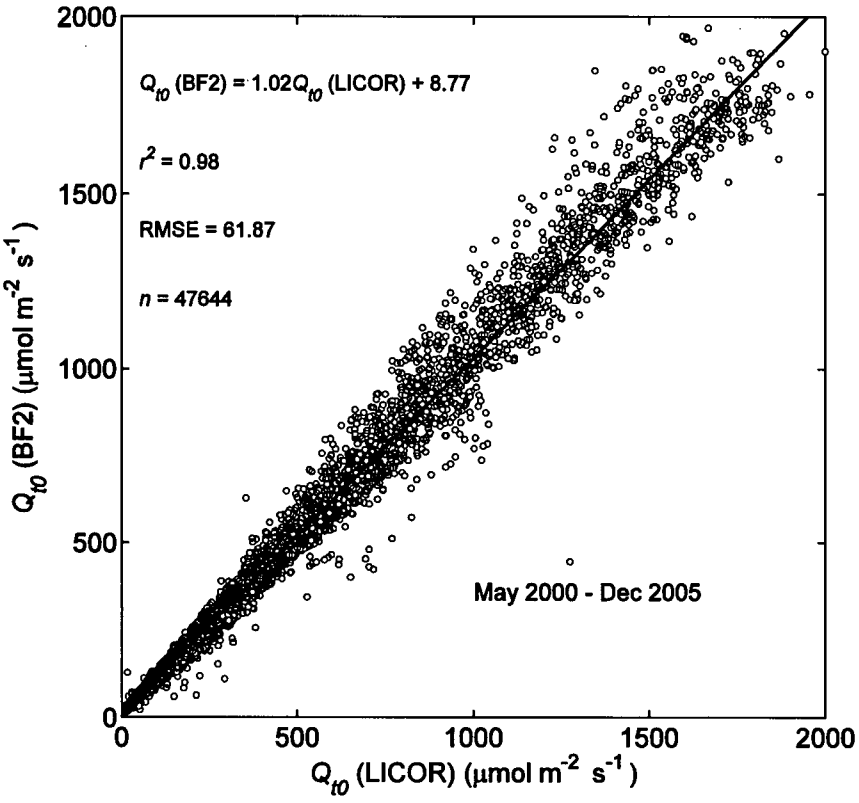

Figure B-1. Relationship between the half-hourly values of Q_{t0} from BF2 and those from LI-190SB for the 56-year-old Douglas–fir stand (DF49) in Campbell River. In order to reduce the figure size, only one tenth of the measurements were plotted (i.e., the half-hourly measurements were decimated for the plotting).

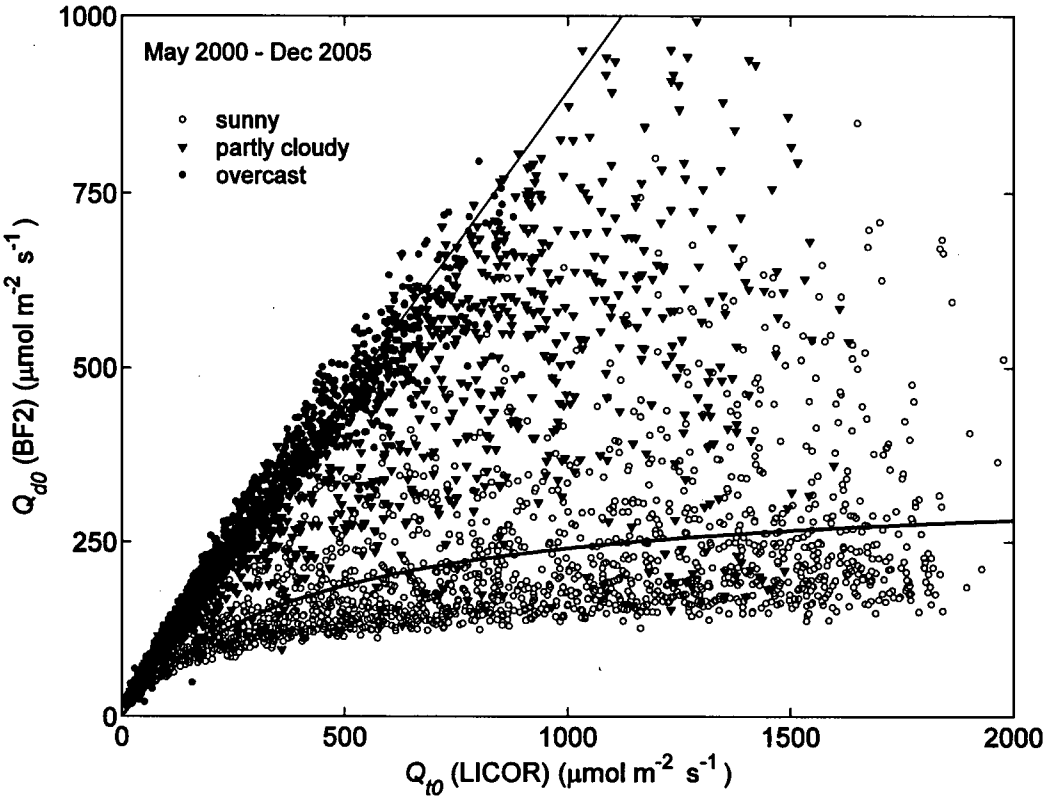

Figure B-2. Relationship between the half-hourly values of Q_{d0} measured using BF2 from May 2000 to December 2005 and the corresponding half-hourly values of Q_{t0} measured using LI-190SB (see also Fig. A1). In overcast conditions, Q_{d0} (BF2) = $0.87Q_{t0}$ (LI-190SB) + 22.72 (r^2 = 0.96, RMSE = 31.23 µmol m^{-2} s^{-1}, n = 16444) (the thin line). In sunny conditions, a hyperbolic equation was used to fit the relationship between Q_{d0} and Q_{t0}, i.e., $Q_{d0} = 0.85Q_{t0}337.11/(0.85Q_{t0} + 337.11)$ (r^2 = 0.49, RMSE = 84.89 µmol m^{-2} s^{-1}, n = 21021) (the thick curve). In order to reduce the figure size, the half-hourly Q_{d0} and Q_{t0} measurements in overcast, partly cloudy and sunny conditions were all decimated for the plotting.

Appendix C. Inadequacies in the Sun/Shade Model Developed by de Pury and Farquhar (1997)

1. Lack of consideration of the angle of incidence of Q_{b0} and the use of area-weighted APAR to calculate P of the big sunlit and shaded leaves, respectively.

The sun/shade model defines the sunlit leaves as those in the gaps, receiving both Q_{b0} (direct beam PAR) and Q_{d0} (diffuse PAR) regardless of their angles of orientation with respect to the solar beam. This is not correct, because as de Pury and Farquhar (1997) point out (their page 544) "(sunlit) leaves nearly perpendicular to the sun-beam direction have the highest absorbed irradiance (1830 - 2040 μmol m^{-2} s^{-1}), and are only a small proportion of the sunlit leaves, while (sunlit) leaves parallel to the beam direction absorbed only diffuse radiation (220 - 430 μmol m^{-2} s^{-1}) and are a high proportion of the sunlit leaves". This statement echoes the view of Norman (1980) (his page 60) "Although leaves oriented nearly perpendicular to the solar beam have the highest photosynthetic rate per unit leaf area, they have the lowest rate per unit soil area because relatively few leaves are so oriented in a canopy with a spherical leaf distribution." In fact, as pointed out by Norman (1979) (his page 254) "In a canopy with foliage spherically distributed, there is a continuous range of flux densities from the full beam flux density (perpendicular to the incident beam) to zero (parallel to the incident beam) because of the range of leaf angles." The continuous distribution of the incident beam flux density for sunlit leaves shown in the Figure 10 of Norman (1979) is reproduced here as Figure C-1.

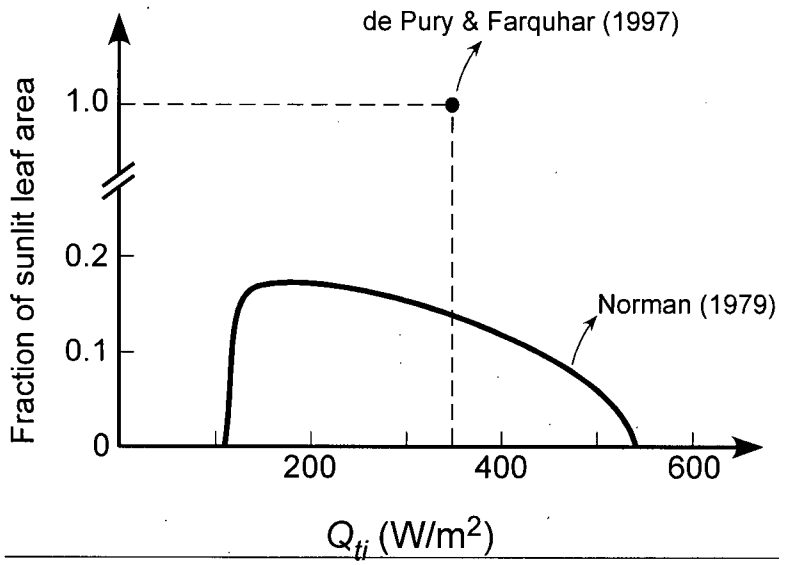

Figure C-1. Comparison of the distribution of the total incident PAR (Q_{ti}) on the sunlit leaves at L (total LAI) = 0.1 modelled by Norman (1979) (the solid line) (i.e., the continuous photon flux densities as a result of leaf-sun angles) with the value obtained using the sun/shade model of de Pury and Farquhar (1997) (the filled circle) (i.e., the average incident PAR for the big sunlit leaf formed by grouping all sunlit leaves together). The direct PAR incident on the big sunlit leaf was calculated as: $Q_{b0\_incident} = K_b Q_{b0} = 0.5 Q_{b0} / \sin\beta$, where Q_{b0} is the direct downwelling PAR above the canopy, K_b is the extinction coefficient for Q_{b0}, and β is the solar elevation angle. The incident sky diffuse PAR was calculated as $Q_d = Q_{d0} e^{-K_d L}$. Using Q_{b0} = 427 W m^{-2}, $\sin\beta$ = 0.95, Q_{d0} = 128 W m^{-2}, K_d = 0.7 and L = 0.1 from Table 2 of Norman (1979), $Q_{b0\_incident}$ = 225 W m^{-2}, and Q_d = 119 W m^{-2}. Q_{ti} for the big sunlit leaf is Q_d + $Q_{b0\_incident}$ = 119 + 225 = 344 W m^{-2}. The un-scattered Q_{b0} absorbed by the big sunlit leaf is $(1-\sigma)Q_{b0\_incident}$. The fraction of sunlit leaves at canopy depth ℓ (cumulative LAI) is given by $f_{Sun} = e^{-K_b \ell}$. Therefore, the total absorbed un-scattered Q_{b0} by the sunlit leaves (on the basis of ground area) is given by:

$$\int_0^L (1-\sigma) Q_{b0\_incident} f_{Sun} d\ell = \int_0^L (1-\sigma) K_b Q_{b0} e^{-K_b \ell} d\ell = Q_{b0}(1-\sigma)(1-e^{-K_b L}),$$

which is Eq. (20b) of de Pury and Farquhar (1997), where the term $f_{Sun} d\ell$ is used as a weighting factor. Disregarding the continuous distribution of direct PAR within the sunlit leaves and using only the averaged direct PAR (i.e., $Q_{b0\_incident}$) to calculate the P of the sunlit leaves (see the above integration) makes the same type of errors as using Q_{t0} to calculate P of the entire canopy. The latter is often implemented in the single big leaf models of canopy P.

This means that P_{sun} (photosynthesis of the big sunlit leaf) has to be further partitioned into a light-limited fraction (e.g., for the sunlit leaves receiving 220 μmol m^{-2} s^{-1}) and a light-saturated fraction (e.g., for the sunlit leaves receiving 1830 μmol m^{-2} s^{-1}). Similarly, on partly cloudy days (e.g., Q_{d0} = 900 μmol m^{-2} s^{-1}), the top shaded leaves are light-saturated while the bottom shaded leaves are light-limited, and we have to separate the top light-saturated shaded leaves from the bottom light-limited shaded leaves. Unfortunately, the sun/shade model aggregates all the sunlit leaves into one big sunlit leaf (group) and all the shaded leaves into one big shaded leaf (group), and treats each big leaf (group) as a homogenous photosynthetic entity. The APAR (absorbed PAR) for the big sunlit leaf is calculated using their Eq. 20 with the weighting of LAI_{sunlit} (the LAI for the sunlit leaves). The APAR for the big shaded leaf is calculated using their Eq. A26 or Eq. 21 with the weighting of LAI_{shaded} (the LAI for the shaded leaves).

Using the sunlit/shaded LAI-weighted APAR to calculate P_{sun} and P_{shaded} (photosynthesis of the big shaded leaf) while disregarding the distinctively different photosynthetic responses within each big leaf (group) (e.g., some parallel sunlit leaves are light-limited and some perpendicular sunlit leaves are light saturated) makes the same type of errors as using LAI-weighted APAR to calculate the P of the entire canopy. In this sense, the errors of the sun/shade model in modelling canopy P are likely worse than those of the single big leaf models, because it uses APAR twice (i.e., once for the big sunlit and once for the big shaded leaf).

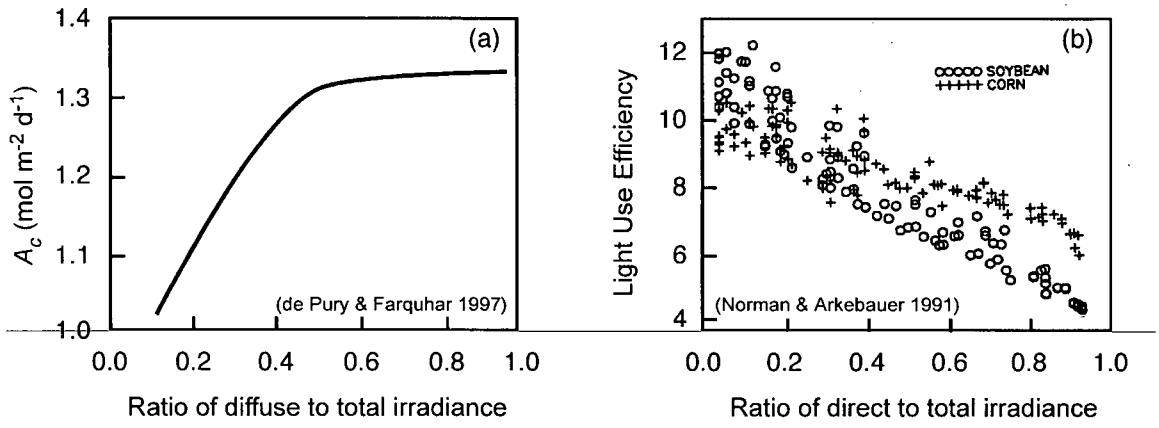

Figure C-2. The contrast in the relationship between LUE and fractions of diffuse/direct irradiance: the hyperbolic relationship predicted by the sun/shade model (a) and the linear relationship predicted by the CUPID model (b). The labels and units are preserved as in their original papers. In plot (a), A_c is the gross canopy photosynthetic assimilation modeled for a wheat crop. "The fraction of diffuse irradiance was varied by changing the atmospheric transmission coefficient but with constant total irradiance" (page 547 of de Pury and Farquhar 1997). In plot (b), the canopy light-use efficiency [g CO_2 (MJ IPAR)$^{-1}$] is based on IPAR (intercepted PAR) and results are for a C_3 (o) and C_4 (+) canopies.

Using APAR to calculate P_{sun} and P_{shaded} led to the mistake shown in their Figure 7b (reproduced here in Figure C-2a), the validity of which has long been questioned (Cohan et al. 2002). Their Figure 7b sharply contrasts with the findings in Norman and Arkebauer 1991 (reproduced here in Figure C-2b) and Choudhury (2000). The response of canopy P for a wheat crop predicted by the sun/shade model to Q_{d0}/Q_{t0} in Figure C-2a when $Q_{d0}/Q_{t0} < 0.5$ mainly reflects the response of the shaded leaves. Their sunlit leaves are not responsive to Q_{d0}/Q_{t0} at all (i.e., almost always Rubisco-limited as shown in their Figure 11 (reproduced here as Figure C-3), contradicting their statement that a high proportion of the sunlit leaves receive Q_{d0} and are light-limited. When $Q_{d0}/Q_{t0} > 0.5$ (e.g., on partly cloudy and overcast days), the sun/shade model is no longer responsive to the changes in the fraction of diffuse irradiance (Figure C-2a), because the big shaded leaf in the model also switches to being Rubisco-limited, and the P of the entire canopy is incorrectly predicted to be decoupled from the radiation it receives.

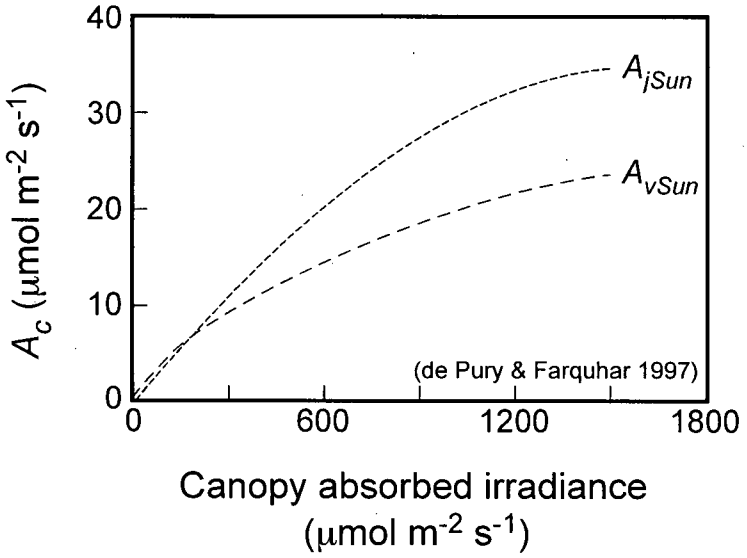

Figure C-3. Reproduction of Figure 11 of de Pury and Farquhar (1997) showing the response of the photosynthesis (A_c) of the big sunlit leaf to absorbed irradiance predicted using the sun/shade model. A_{jSun} and A_{vSun} are the modelled electron-transport-limited and Rubisco-limited rates of photosynthesis of the big sunlit leaf, respectively. A_c is taken as the minimum of A_{jSun} and A_{vSun}. Symbols and units are preserved as in the original paper. They say on their page 551 that "It is apparent that the sunlit leaves are usually Rubisco-limited ($A_{vSun} < A_{jSun}$), except when the absorbed irradiance is very low. The fraction of leaves in the sunlit fraction increased from 0% at low irradiance to 56% at the maximum solar elevation". In other words, photosynthesis of the big sunlit leaf (group) is always limited by its nitrogen content and has little to do with the irradiance it absorbed. For this wheat canopy, the fraction of sunlit leaves can go as high as 56% as they suggested, which means the photosynthesis of 56% of the leaves in this wheat canopy has nothing to do with the irradiance absorbed. This contradicts the fact that a high proportion of sunlit leaves are parallel to the solar beam and their photosynthesis is light-limited (i.e., electron-transport-limited rather than Rubisco-limited).

In addition, the photosynthetic Rubisco capacity for the big sunlit leaf (V_{cSun}) is calculated by the sun/shade model using (their Eq. (22)):

$$V_{cSun} = \int_0^L V_{c\max 0} e^{-K_n \ell} e^{-K_b \ell} d\ell = V_{c\max 0}(1 - e^{-(K_n + K_b)L})/(K_n + K_b)$$

where V_{cmax0} is the photosynthetic Rubisco capacity at the top of the canopy, ℓ is the cumulative LAI from canopy top, and K_n and K_b are the extinction coefficients for the nitrogen and direct solar beam, respectively. The formulation for V_{cSun} is problematic, because (1) the nitrogen gradient (i.e., K_n) in a canopy is more in a horizontal (i.e., related to leaf age) rather than in a vertical direction (Warren and Adams 2001, Rayment et al. 2002), and (2) it is difficult to scale V_{cmax0} from leaf-level to V_{cSun} at canopy level. For example, using V_{cmax0} = 40 μmol m^{-2} s^{-1} and K_n = 0.1 could give the same V_{cSun} as using V_{cmax0} = 80 μmol m^{-2} s^{-1} and K_n = 0.7, therefore V_{cmax0} can be parameterized in infinite number of ways as long as its combination with K_n gives the same V_{cSun}. In that sense, the leaf-level V_{cmax0} in the sun/shade model is not scalable.

It can be easily shown that the Q_e-MM model results from assuming that quantum efficiency in the MM model increases linearly with the diffuse PAR fraction. Replacing α in the MM model with $\alpha = \alpha_0(mQ_{d0}/Q_{t0} + n)$ (i.e., using a linear relationship between α and Q_{d0}/Q_{t0} suggested by Figure C-2b), gives:

$$P = \frac{\alpha_0(mQ_{d0}/Q_{t0} + n)Q_{t0}A_{\max}}{\alpha_0(mQ_{d0}/Q_{t0} + n)Q_{t0} + A_{\max}} \qquad (1)$$

where m and n are two empirical coefficients for the generalized linear relationship between α and Q_{d0}/Q_{t0}. Further expanding the terms in Eq. (1) gives:

$$P = \frac{\alpha_0(m+n)(Q_{d0} + \frac{n}{m+n}Q_{b0})A_{\max}}{\alpha_0(m+n)(Q_{d0} + \frac{n}{m+n}Q_{b0}) + A_{\max}} \quad (2)$$

Let $\alpha_1 = \alpha_0(m+n)$ and $k = \frac{n}{m+n}$, then Eq. (2) becomes the Q_e-MM model:

$$P = \frac{\alpha_1(Q_{d0} + kQ_{b0})A_{\max}}{\alpha_1(Q_{d0} + kQ_{b0}) + A_{\max}} = \frac{\alpha_1 Q_e A_{\max}}{\alpha_1 Q_e + A_{\max}} \quad (3)$$

where $Q_e = Q_{d0} + kQ_{b0}$. In fact, the Q_e-MM model supports the statement made by de Pury and Farquhar (1997) that a high proportion of the sunlit leaves are parallel to the solar beam and therefore receive mainly diffuse PAR.

Thus, it is not surprising that the sun/shade model performed as poorly as the regular MM model (Figure C-4). As we might have expected, the Q_e-MM model has virtually no systematic modeling errors in P with respect to Q_{d0}/Q_{t0}. The sun/shade and the MM models both systematically overestimate P in clear conditions and systematically underestimate P in cloudy conditions (Figure C-4).

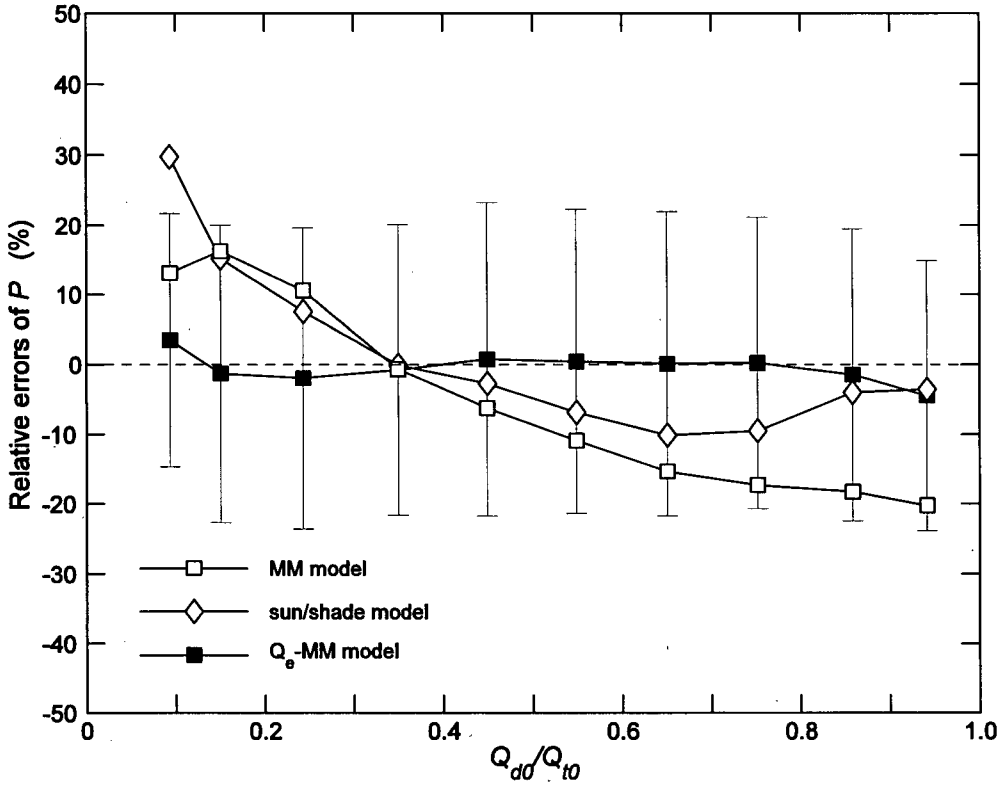

Figure C-4. The relative modelling errors of P for a 56-year-old Douglas-fir stand (DF49) obtained using the MM, sun/shade and Q_e-MM models. The relative errors of P are calculated as: $(P_{mdl} - P_{measurement})/P_{measurement}$, where P_{mdl} is the half-hourly values of P modeled using the aforementioned three models, and $P_{measurement}$ is the EC-derived half-hourly values of canopy P. Symbols represent bin averages and vertical lines indicate ±1 SD. n = 18,196. This figure is the same as Figure 4-8a in Chapter 4 except that (1) the x axis was changed from Q_{d0} to Q_{d0}/Q_{t0}, (2) the y axis was changed to the relative errors of P, and (3) only P_{mdl} and $P_{measurement}$ values greater than 10 μmol m^{-2} s^{-1} were bin averaged. Refer to Figure 4-8a for further details.

We can calculate the coefficient k for the soybean crop (Figure C-2b) by using its relationship between light use efficiency and the ratio of incident diffuse to incident total PAR. Let us rewrite $k = n/(m+n)$ (in Eq. (3)) as:

$$k = \frac{n(m+n)+n-n(m+n)}{m+n} = n + (1-n)\frac{n-mn/(1-n)}{m+n} \qquad (4)$$

Comparing Eq. (4) with the expression for k given by Eq. (22) of Chapter 4 (i.e., $k = \sigma + (1-\sigma)(2k_2)$, where σ is the leaf scattering coefficient) shows that

$$n = \sigma \qquad (5a)$$

and

$$\frac{n-mn/(1-n)}{m+n} = 2k_2 \qquad (5b)$$

where $k_2 = k_1\overline{\cos\gamma_1} + (1-k_1)\cos\gamma_{Threshold} + k_0(1-k_1)\overline{\Delta\cos\gamma_{Threshold}}$ given by Eq. (21) in Chapter 4. k_2 reflects the fraction of the photosynthetic contribution from the light-limited sunlit leaves ($k_1\overline{\cos\gamma_1}$) and that from the light-saturated sunlit leaves (mainly $(1-k_1)\cos\gamma_{Threshold}$). From Eq. (5a) and (5b), we can see that the intercept (i.e., $\alpha_0 n$) and slope (i.e., $\alpha_0 m$) in the linear relationship of $\alpha = \alpha_0(mQ_{d0}/Q_{t0} + n)$ (see Eq. (1)) reflect the magnitude of the scattered solar beam in the canopy (i.e., $n = \sigma$) and the photosynthetic contribution of the sunlit leaves by absorbing un-scattered solar beam, respectively.

Let us take the values of light use efficiency for the soybean (the C_3 plant) canopy of Figure C-2b as an example. When Q_{d0}/Q_{t0} = 0.1, light use efficiency (α)= 0.02 mol mol^{-1} by converting the 4 g CO_2/(MJ IPAR) (i.e., 4 g CO_2/(MJ IPAR) = 4 g CO_2/(MJ IPAR) × (1/44 mol CO_2 g^{-1} CO_2) × (1/4.6 MJ IPAR mol^{-1} photons IPAR) = 0.02 mol CO_2

mol^{-1} photons IPAR). When Q_{d0}/Q_{t0} = 0.9, α = 0.054 mol mol^{-1} by converting the 11 g CO_2/(MJ IPAR). Therefore, using $\alpha = \alpha_0(mQ_{d0}/Q_{t0} + n)$, we have:

$$\alpha_0(0.1m + n) = 0.020 \quad (6a)$$

$$\alpha_0(0.9m + n) = 0.054 \quad (6b)$$

Dividing Eq. (6b) by Eq. (6a) gives:

$$(0.9m + n)/(0.1m + n) = 2.7 \quad (7)$$

From Eq. (5a), $n = \sigma$ and the latter is given as 0.15 in the Table 2 of Norman (1980) (i.e., leaf transmittance = 0.05 and leaf reflectance = 0.10). Substituting n = 0.15 into Eq. (7) gives m = 0.41. Substituting m = 0.41 and n = 0.15 into Eq. (6a) or (6b) gives α_0 = 0.10. The k value for the soybean canopy can then be calculated as $k = n/(m + n)$ = 0.15/(0.41 + 0.15) = 0.27.

2. Inadequacies in its scaling algorithm

The sun/shade model assumes that the P of the big sunlit leaf or the big shaded leaf is either Rubisco-limited or RuBP-limited, ignoring the frequent crossing over of the two limitation curves (Figure C-5). The scaling algorithm used in the sun/shade model is shown in Figure C-5a. The defect of this scaling algorithm has been pointed out by Wang (2000) for the big sunlit leaf. It is difficult to correct this defect because of the uncertainty in determining L_1. Actually this scaling algorithm is problematic for the big shaded leaf as well (see Figure 4-16b in Chapter 4). For example, on partly cloudy days, the top shaded leaves are Rubisco-limited, while the bottom shaded leaves are RuBP-limited. The correct algorithm in the sun/shade model should have been (as shown in Figure C-5b): first integrate the Rubisco-limited curve from 0 to L_1, then integrate the RuBP-limited curve from L_1 to L, and finally sum the two integrations.

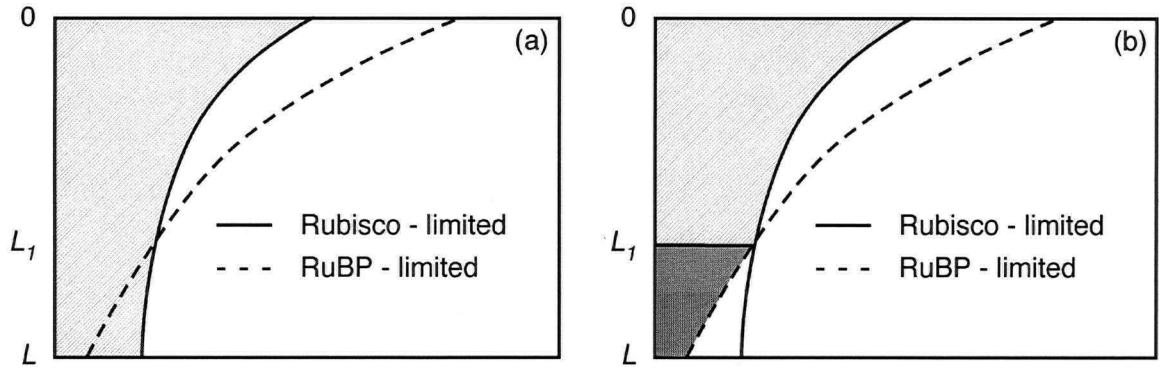

Figure C-5. (a) The scaling algorithm used in the sun/shade model. Integrations of the Rubisco-limited and RuBP-limited curves from 0 to L gives the photosynthetic rates associated with the two limiting processes, respectively. The minimum of the above two integrations is taken as the actual canopy P by the sun/shade model. (b) The correct algorithm for integrating the two limiting processes with the consideration of the crossover point (L_1).

It is worth noting that the big sun and the big shade leaves of the sun/shade model have little correspondence with the sun and shade leaves in the regular plant physiological context. The photosynthetic Rubisco capacity of the big sun (V_{cSun}) and shade (V_{cSh}) leaves were shown in Figure 10 of de Pury and Farquhar (1997) (reproduced here as Figure C-6a). The V_{cSh} at night was over 200 μmol m^{-2} s^{-1} while during the day was less than 100 μmol m^{-2} s^{-1}, and V_{cSh} was greater than V_{cSun} in the early morning (i.e., 6 – 9 am) and late afternoon (15 – 18 pm) periods (Figure C-6a). The perfect symmetry in the diurnal variation in V_{cSh} and V_{cSun} is an artifact of the model. It merely reflects that "the division of the leaves into sunlit or shaded fractions is changing", and has no real physiological meaning, defeating one of the purposes of doing bottom up models of canopy *P*. The photosynthetic light responses for the sun and shade leaves defined in regular physiological context (Björkman et al. 1972) are shown in Figure C-6b. As a result of the acclimation to (chronic) growth irradiance, the sun leaf (i.e., grown in high light) generally has higher photosynthetic capacity than the shade leaf (i.e., grown in low light).

As mentioned earlier, the sun/shade model failed to account for the crossing over of the Rubisco- and RuBP-limitation curves (Figure C-5). In fact, the scaling algorithm of the sun/shade model is also problematic within each limitation curve even if we disregard the crossing over. Let us assume that we have a canopy with only three leaves, marked by #1, #2 and #3 respectively in Figure C-6b. Their photosynthesis per unit leaf area can be calculated using Eq. (5) of de Pury and Farquhar as (the term $(C_i - \Gamma^*)/(4C_i + 8\Gamma^*)$ for P_i was ignored for simplicity):

$$\phi P_i - (\alpha Q_{tai} + J_{\max i})P_i + \alpha Q_{tai} J_{\max i} = 0 \qquad (8)$$

where P_i, Q_{tai} and J_{maxi} are the photosynthetic rate, total absorbed PAR and maximum electron transport rate for the i^{th} leaf (i = 1, 2, and 3) per unit leaf area, respectively. α is the quantum use efficiency which is assumed to be the same for all three leaves. ϕ is a curvature parameter. Therefore canopy P per unit ground area can be obtained as:

$$P = \sum_{i=1}^{3} P_i L_i \tag{9}$$

where L_i is the LAI for the i^{th} leaf which is used to convert P_i from leaf area basis to ground area basis and P_i is obtained from Eq. (8) as: $P_i = \frac{(\alpha Q_{tai} + J_{\max i}) - \sqrt{(\alpha Q_{tai} + J_{\max i})^2 - 4\phi\alpha Q_{tai} J_{\max i}}}{2\phi}$. Eq. (9) is used in the multi-layer models of canopy P (e.g., Eq. (13) of Norman 1980). However, the sun/shade model calculates canopy P of the three leaves as follows (see Eqs. (20) and (22) of de Pury and Farquhar 1997):

$$Q_{ta\_big} = \sum_{i=1}^{3} Q_{tai} L_i \tag{10a}$$

$$J_{\max\_big} = \sum_{i=1}^{3} J_{\max i} L_i \tag{10b}$$

Canopy P is then obtained by substituting Eqs. (10a) and (10b) into Eq. (8) by conceptually condensing the three leaves into one big leaf, i.e.,

$$P = \frac{(\alpha Q_{ta\_big} + J_{\max\_big}) - \sqrt{(\alpha Q_{ta\_big} + J_{\max\_big})^2 - 4\phi\alpha Q_{ta\_big} J_{\max\_big}}}{2\phi} \tag{11}$$

Comparison of the P obtained using Eq. (9) and Eq. (11) shows the difference in the scaling algorithms between Norman (1980) and de Pury and Farquhar (1997). Using Eq. (11) to calculate canopy P with J_{max_big} and Q_{ta_big} as bulk parameters for the aggregated

big leaf is invalid, because the photosynthetic light responses for the three leaves are different and nonlinear. In the example given in Figure C-6b, leaves #1, #2, and #3 are approximately at the photosynthetic saturating point, near the saturating point, and near the light-limited point, respectively. Even if all the three leaves are located on the linear portions of their respective photosynthetic curves, using Eq. (11) to calculate canopy P still doesn't have a sound mathematical basis, because the three leaves have three J_{max} values (i.e., J_{maxi}, i = 1, 2, 3) as opposed to having one common J_{max} value and have three different LAI values (i.e., L_i, i = 1, 2, 3). The sun/shade model assumes leaf level maximum electron transport rate (J_{max}) decreases with cumulative LAI (Figure 5 of de Pury and Farquhar is reproduced here as Figure C-6c). As a result, leaves at different canopy depths have different photosynthetic light responses curves (i.e, different J_{max} values) similar to the leaves #1, #2 and #3 shown in Figure C-6b. Using (10a) and (10b) to calculate canopy P involves averaging the irradiance and RuBP capacity profiles, respectively. Thus, it makes the same type of errors in calculating canopy P as the single models of canopy P. Furthermore, hypothesizing an exponential decrease of J_{max} with canopy depth is not completely valid, because J_{max} was found to be highly related to leaf age and its gradient is very significant in the horizontal direction.

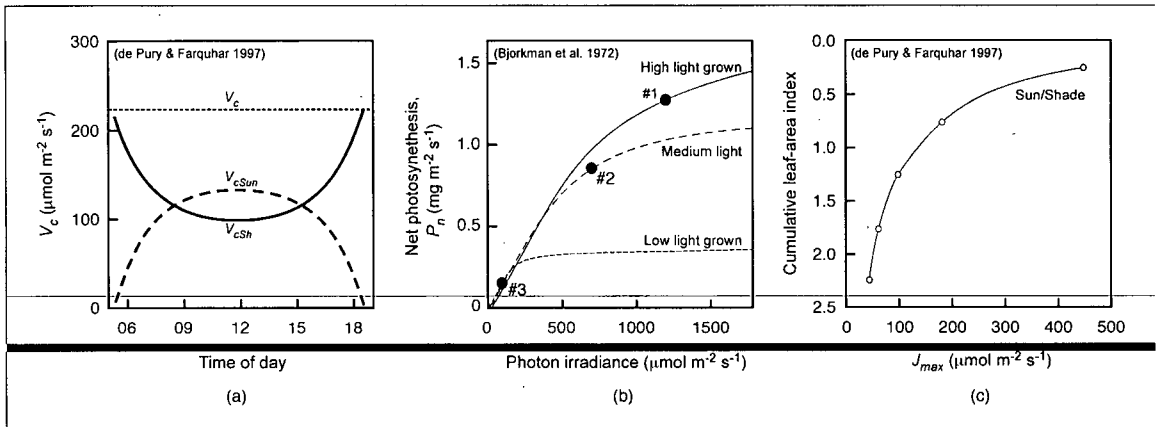

Figure C-6. Comparison of the sun and shade leaves defined by de Pury and Farquhar (1997) and those defined byBjörkman et al. (1972). The photosynthetic Rubisco capacity for the sun (V_{cSun}) and shade (V_{cSh}) leaves (V_c = V_{cSun} + V_{cSh}) in de Pury and Farquhar (1997) is simply driven by the LAI of the sunlit and shaded fractions of the canopy (a) and has no real physiological meaning. The sun and shade leaves defined in Björkman et al. (1972) are the leaves grown in high light and low light environment, respectively (b). As a result of the acclimation to the growth irradiance, the leaves grown in high light have higher photosynthetic capacity than the leaves grown in low light. The three filled circles in (b) represent three leaves in a canopy with different photosynthetic capacities and different LAI values (see the example in the main text). The sun/shade model assumes that leaf-level J_{max} decreases exponentially with canopy depth (c) and as a result, there is a J_{max} profile for the canopy. Therefore, even if the three leaves (i.e., #1, #2 and #3) in (b) are on the linear portions of their respective photosynthetic light response curves, their J_{max} values cannot be simply summed up with the multiplication of their respective LAI values to obtain the total photosynthesis of the three leaves (i.e., using Eq. 10b in the main text) because the photosynthetic responses for each of three leaves are very different and nonlinear.

3. Problems in its description of the geometry of light

The sun/shade model assumes that the solar beam is composed of parallel rays (Figure C-7a) and consequently divides the canopy foliage as either purely black (sunlit leaves) or purely white (shaded leaves). This representation of the solar beam will severely distort the predicted light environment in a canopy, particularly for a coniferous canopy with small needles. The algorithm should have taken into account the finite size of the solar disk and accounted for the significant effect of penumbrae. As shown in Figure C-7b, Δabc is similar to Δade, and from the similarity of the two triangles, the shadow length (umbra) can be calculated as: $d_{umbra} = 100 d_{leaf}$ since the ratio $d_{sun\text{-}earth}$ to d_{sun} is, to a good approximation, 100.

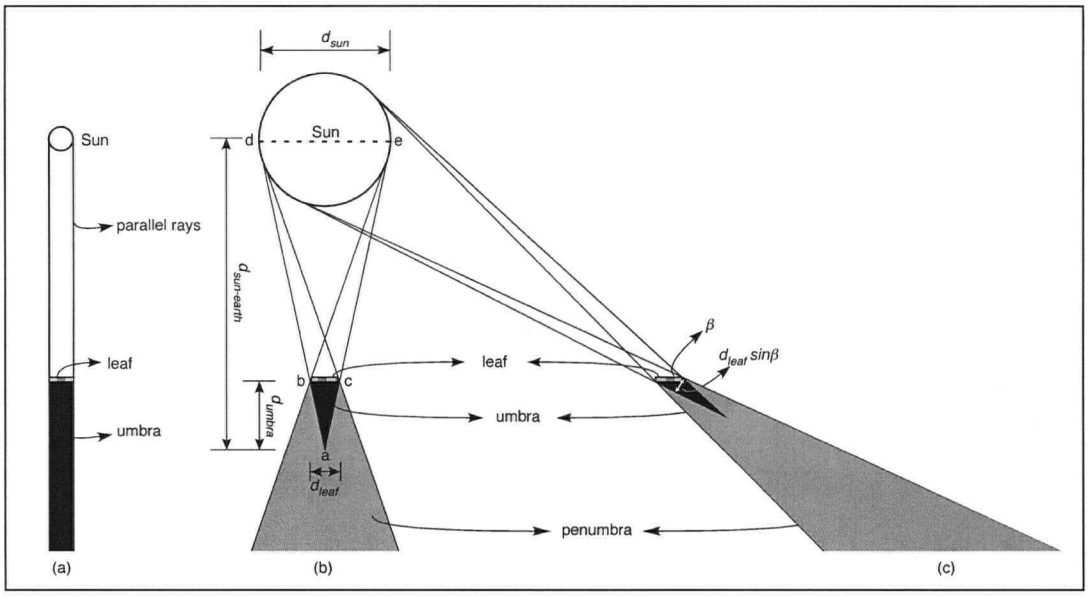

Figure C-7. The shadow of a leaf. In (a), the solar rays are assumed to be parallel in the sun/shade model. In (b) and (c), the shadow cast by a leaf is divided by geometry into the completely shaded umbra and partially shaded penumbra. A Douglas-fir needle is approximately 1 mm wide, so its umbra is no wider than 10 cm. In this schematic, only the shadow of one leaf is shown. In a deep coniferous stand, the umbra and penumbra cast by millions of needles overlap (i.e., multi-fold penumbra) and greatly reduce the heterogeneity in canopy radiation. Note that if the leaf were replaced by the moon, a total solar eclipse would be observed in the region of the umbra and a partial solar eclipse would be observed in the region of the penumbra.

4. Oversimplified representation of canopy structure.

The sun/shade model assumes that the leaves in a canopy are randomly distributed (Figure C-8a) in a manner similar to the randomly moving molecules in a solution, so the Beer's law of light attenuation can be strictly applied to the canopy. But in reality, leaves are clumped (grouped) at several levels: shoots (Figure C-8b), branches, whorls and tree crowns (Figure C-8c), and even groups of trees (Oker-Blom 1986, Chen et al. 1997). The effect of clumping on the measurement of canopy LAI is particularly significant for coniferous stands. For example, for a mature Southern Old Black Spruce (SOBS) stand (part of the BERMS project), the LAI obtained using the LAI-2000 plant canopy analyzer was approximately 2.3 (i.e., the effective LAI, L_e, is 2.3), while that obtained using allometic relationships was 6.3 (see Table 3 of Chen et al. 1997). After accounting for the woody components and clumping effect on L_e, the optical LAI was adjusted to 3.9, which is still 40% lower than the allometic LAI. Any uncertainties in the measurements of canopy LAI will translate into large errors in canopy P obtained using the sun/shade model, because the model is very sensitive to canopy LAI. Also, the clumping of foliage has a significant effect on the sunlit leaf area distribution and P of the foliage in the lower canopy. It remains a great challenge to properly incorporate the effect of clumping on P into the bottom up models of canopy P (e.g., the sun/shade model).

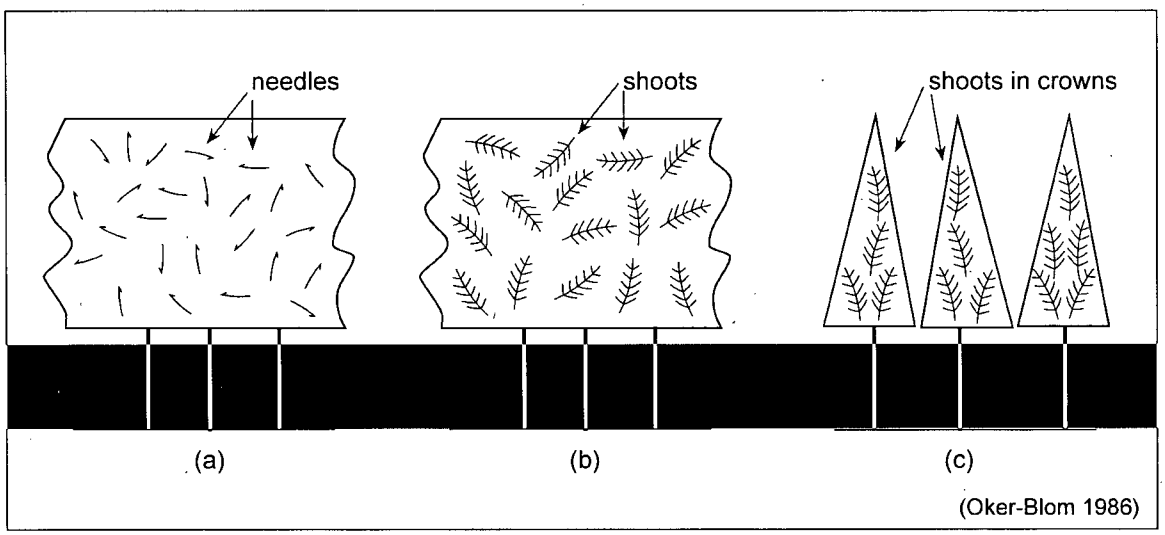

Figure C-8. Conceptual models of canopy structure (Oker-Blom 1986). (a) the needles are assumed to be randomly distributed in a canopy as described by the sun/shade model. In reality, the needles are clumped (grouped) into shoots (b) and the shoots are further clumped into tree crowns (c). The clumping of conifer needles at several levels (e.g., shoot- and crown-level) introduces large uncertainties in the canopy LAI obtained using optical methods (e.g., LAI-2000 plant canopy analyzer) and also changes the distribution of sunlit leaf area, both of which will cause great difficulty in parameterizing the sun/shade model and affect its accuracy. Although the Q_e-MM model was developed assuming that leaves are randomly distributed in the canopy, the canopy LAI is not a parameter for the Q_e-MM model. Thus the Q_e-MM model is not susceptible to the errors in the measurements of LAI, and can be used as a simple top down model to study whole canopy photosynthetic behaviour.

In conclusion, the sun/shade model fails to account for the additional non-linearity in P of the big sunlit and shaded leaves, thus making errors as large as those resulting from using single big leaf models. Interestingly, in order to solve the one non-linearity of P of the single big leaf model, the use of the sun/shade model introduces two non-linearities, one for the big sunlit leaf and the other for the big shaded leaf. In order to correct the additional non-linearity in P within the sunlit and shaded leaves, the sun/shade model will become a 4-leaf model, and if we consider the frequent crossovers in the Rubisco-limited and RuBP-limited rates (Figure C-5b), it will become a 8-leaf model. Furthermore, if we consider the penumbral effect of the solar beam (Figure C-7b) and the clumping of needles and leaves (Figure C-8c), plus the eventual coupling of the P model with a stomatal conductance model, the two-leaf model becomes very difficult to correct.

On the other hand, the extension of the findings of Norman and Arkebauer (1991) (Figure C-2b) leads to a simple modification of the MM model (i.e., the Q_e-MM model). Direct (e.g., Anderson et al. 2000) or indirect (e.g., Gu et al. 2002) applications of Norman and Arkebauer's findings have been made over a wide range of ecosystems, such as deciduous forests, coniferous forests, grasslands, and agricultural crops. The success of the Q_e-MM model (Figure C-4) in this analysis shows that the findings of Norman and Arkebauer (1991) are valid for a 56-year-old coastal Douglas-fir stand as well.

Appendix D. Derivation of Two Key Equations in Norman (1980)

The multilayer model of canopy photosynthesis developed by Norman (1980) remains the state of the art in canopy photosynthesis modeling. There are two key statements in his model. The first is (on his page 57) "For a canopy with a spherical leaf angle distribution, the fraction of sunlit leaf area exposed at various angles to the sun is independent of solar zenith angle and given by (his Eq. (7), which was rewritten as Eq. (10) in Chapter 4)":

$$f_\gamma = \sin\gamma d\gamma \qquad (1)$$

where γ is the angle between a sunlit leaf's normal and the solar beam. The second key statement is (on his page 57) "The distribution of leaf inclination angles to the horizontal is the same as the distribution of leaf-sun angles (for a canopy with a spherical leaf angle distribution)".

The objective of this appendix is to show the above two key statements graphically. Understanding the above two statements is the key to understand the theory presented in Chapter 4.

1. Derivation of $f_\gamma = \sin\gamma d\gamma$

First let us consider the distribution of the sunlit leaf surface area on a hemisphere. We do this because the leaves with a spherical inclination angle distribution can be arranged exactly to form a sphere (Figure D-1a) (see also Figure 4-2a).

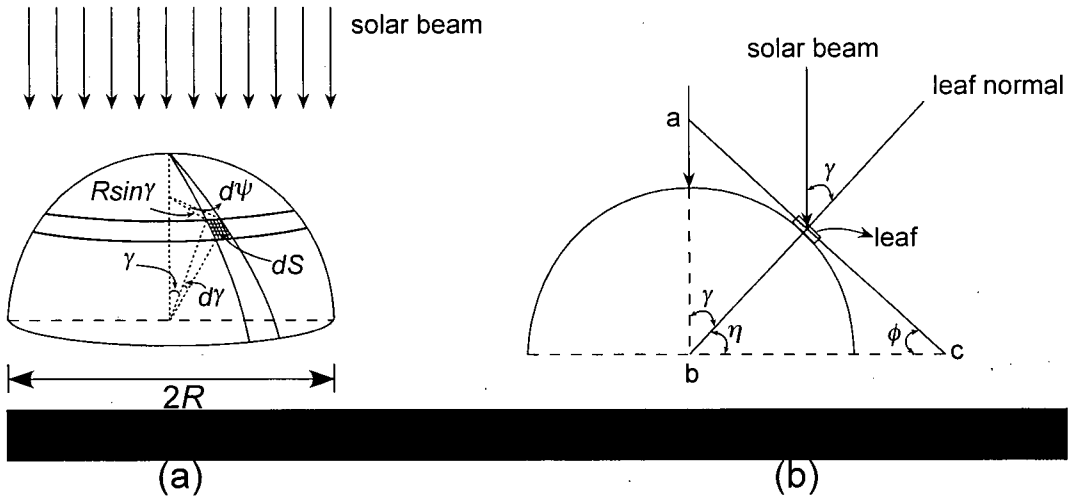

Figure D-1. In this schematic, the sun is positioned at the vertical for the sake of convenience. The absolute position of the sun is not a concern because here we are dealing with a sphere (formed by all the sunlit leaves). (a) The leaf area (dS) covered between angle γ and $\gamma + d\gamma$ and azimuth angle $d\psi$. dS is obtained as the product of its width ($R\sin\gamma d\psi$) and its length ($Rd\gamma$). (b) The leaf inclination angle to the horizontal (ϕ) equals the angle of incidence, i.e., the angle between the solar beam and leaf normal (γ), because $\gamma + \eta = 90^\circ$ and $\phi + \eta = 90^\circ$. The line ac, which is tangent to the hemisphere at the location of the leaf, is parallel to the leaf assuming the leaf is infinitesimally small compared to R.

We will consider only the upper hemisphere, because the relationships derived for the upper hemisphere hold for the lower hemisphere as well. Also, because the angle distribution of all the sunlit leaves is spherical, the absolute position of the sun doesn't matter any more. For the sake of convenience, let us assume the sun is at vertical as shown in Figure D-1a. The surface area (dS) of sunlit leaves covered between angle γ and $\gamma + d\gamma$ and azimuth angle $d\psi$ is given by:

$$dS = (R\sin\gamma d\psi)(Rd\gamma) \tag{2}$$

where R is the radius of the hemisphere. The first term (i.e., $R\sin\gamma d\psi$) and the second term (i.e., $Rd\gamma$) on the right hand side of Eq. (2) are the width and length of dS, respectively.

The total leaf area covered between γ and $\gamma + d\gamma$ over the hemisphere can be obtained by integrating Eq. (2) with respect to ψ from 0 to 2π, i.e.,

$$S = \int_0^{2\pi} (R\sin\gamma d\psi)(Rd\gamma)$$

$$= 2\pi R^2 \sin\gamma d\gamma \tag{3}$$

Thus, the fraction of sunlit leaves exposed at angle between γ and $\gamma + d\gamma$ is given by:

$$f_\gamma = \frac{2\pi R^2 \sin\gamma d\gamma}{2\pi R^2}$$

$$= \sin\gamma d\gamma \tag{4}$$

where the term $2\pi R^2$ in the denominator of Eq. (4) is the total surface area of the hemisphere, i.e., half the total area of sunlit leaves in the spherical leaf angle distribution.

2. Showing that "the distribution of leaf inclination angles to the horizontal is the same as the distribution of leaf-sun angles for a canopy with a spherical leaf angle distribution"

Let us assume that the leaf inclination angle to the horizontal is ϕ as shown in Figure D-1b, and the angle between the solar beam and the leaf's normal, i.e., the angle of incidence, is γ. It is reasonable to assume that the leaf is infinitesimally small in comparison with the radius (i.e., R) of the hemisphere, so the line passing through the leaf's surface (i.e., line ac) can be approximated as the tangent to the hemisphere at that point.

Therefore,

$$\begin{cases} \gamma + \eta = 90^\circ \\ \phi + \eta = 90^\circ \end{cases} \tag{5}$$

Then we have:

$$\gamma = \phi \tag{6}$$

As pointed out by Norman (1980) (on his page 57), "The sunlit leaves in the canopy must be divided into leaf classes that are distinguished by various angles between the leaf normal and the direction of the sun" because the solar beam is unidirectional. Eqs. (4) and (6) are very important, because Eq. (4) allows us to calculate how much the sunlit leaf area is exposed at angle γ and Eq. (6) allows us to calculate the beam flux density in that leaf angle class (i.e., γ) using Eq. (9) of Chapter 4 (i.e., $Q_b(\gamma) = (1-\sigma)Q_p \cos\gamma$, which is essentially the same as the Eq. (9) of Norman (1980)). Refer to Table 4 of Norman (1980) for a worked out example.

Using Eqs. (4) and (6), we also can calculate the mean leaf inclination angle of a canopy with spherical leaf angle distribution as:

$$\bar{\phi} = \bar{\gamma} = \int_0^{\pi/2} \gamma \sin\gamma d\gamma = (\sin\gamma - \gamma\cos\gamma)\Big|_0^{\pi/2}$$

$$= 1 \text{ (radian)} = 57.3^\circ \text{ (i.e., } 180/\pi) \qquad (7)$$

where $\bar{\phi}$ and $\bar{\gamma}$ are mean angles of ϕ and γ, respectively. In the integral of Eq. (7), the term $\sin\gamma d\gamma$ can be thought of as a weighting factor of γ. Therefore, the mean leaf inclination angle is 57.3° for a spherical leaf angle distribution.

Appendix E. Comparison of the Scaling Algorithms Used in the Complete Multilayer, 2-leaf Multilayer, 2-leaf Single-layer, MM and Q_e-MM Models of Canopy *P*

The objective of this appendix is to compare the scaling algorithms used in complete multilayer (e.g., Norman 1980, Norman and Arkebauer 1991), 2-leaf multilayer (e.g., Sinclair et al. 1976, Spitters 1986, Goudriaan and van Laar 1994, Leuning et al. 1995) and 2-leaf single-layer (e.g., de Pury and Farquhar 1997, Wang and Leuning 1998) models of canopy *P* with the two single leaf models discussed in this thesis: the MM and Q_e-MM models. Each type of the aforementioned models has the same scaling algorithms, although the details within each type models can differ greatly. For example, the 2-leaf single-layer model of Wang and Leuning (1998) has a stomatal conductance sub-model and uses a Michaelis-Menten equation to describe the rate of electron transport while that of de Pury and Farquhar (1997) doesn't have a stomatal conductance sub-model and uses a quadratic equation to describe the rate of electron transport, but the scaling algorithms for the two 2-leaf single-layer models are the same. In this analysis, the only difference between the complete multilayer, 2-leaf multilayer and 2-leaf single-layer models is their scaling algorithms. In other aspects of these models (e.g., leaf-level photosynthetic characteristics), they share the same initial parameters or equations. Also, the effects of stomatal conductance and temperature on canopy *P* have been ignored in this analysis.

Complete multilayer models divide the plant canopy into *N* layers, and in each layer, the foliage is further divided into sunlit and shaded leaves. In addition, the sunlit

leaves of each of the N layers are divided into M leaf inclination angle classes. The scaling algorithm of the complete multilayer model (see Eqs. (12) and (13) and Table 4 of Norman (1980)) can be described as:

$$P = \sum_{i=1}^{N}\sum_{j=1}^{M} P_{\gamma_j} f_{\gamma_j} L_{sun\_i} + \sum_{i=1}^{N} P_{shd\_i} L_{shd\_i} \qquad \text{complete multilayer model} \quad (1)$$

where N is the total number of canopy layers (e.g., N = 5), M is the total number of leaf inclination angle classes of the sunlit leaves, and γ_j is the midpoint angle of each leaf class (for M = 5, γ_1 = 9°, γ_2 = 27°, …, γ_5 = 81°), f_{γ_j} is the fraction of sunlit leaf area with leaf angle γ_j where $\sum_{j=1}^{M} f_{\gamma_j} = 1$. P_{γ_j} is the photosynthesis of sunlit leaves with leaf angle γ_j. L_{sun_i} and L_{shd_i} are the LAI of the sunlit and shaded leaves of the i^{th} layer, respectively. P_{shd_i} is the photosynthesis of the shaded leaves of the i^{th} layer. Shaded leaves of each layer only absorb diffuse PAR and scattered direct PAR. Sunlit leaves, in addition, absorb un-scattered direct PAR.

Two-leaf multilayer models of canopy P divide the canopy into N layers and in each layer the foliage is divided into sunlit and shaded leaves as in complete multilayer models. However, these models don't further divide the sunlit leaves of each layer into M leaf inclination angle classes. Instead, they reduce the M leaf angle classes of the sunlit leaves to a single mean leaf inclination angle class (i.e., $\bar{\gamma} = \sum_{0}^{\pi/2} f_{\gamma_j}\gamma_j$ = 57.3° ≈ 60°, see Appendix D for details). The scaling algorithm of 2-leaf multilayer models can be mathematically described as:

$$P = \sum_{i=1}^{N} P_{sun\_i} L_{sun\_i} + \sum_{i=1}^{N} P_{shd\_i} L_{shd\_i} \qquad \text{2-leaf multilayer model} \quad (2)$$

where P_{sun_i} is the photosynthesis of the sunlit leaves of the i^{th} layer.

Two-leaf single-layer models further simplify 2-leaf multilayer models of P. Let us assume that leaf-level photosynthesis (P_{leaf}) can be described using the Michaelis-Menten equation as: $P_{leaf} = \frac{\alpha Q_{ta} A_{\max}}{\alpha Q_{ta} + A_{\max}}$, where α, Q_{ta} and A_{max} are the quantum use efficiency, total absorbed PAR and maximum photosynthetic capacity, respectively. For the sake of simplicity, let us scale P_{leaf} to canopy P using fixed values of α and A_{max} as it was in Norman (1980) (his Eq. (11)), so different leaves of the canopy have different rates of photosynthesis simply as a result of the differences in their Q_{ta}. According to the scaling algorithm of 2-leaf single-layer models (see Eqs. (20) and (21), and Table 6 of de Pury and Farquhar (1997) for details), canopy P can be described as:

$$P = P_{sun} + P_{shd} \qquad \text{2-leaf single-layer} \qquad (3a)$$

$$P_{sun} = \frac{\int_0^L \alpha Q_{ta\_sun}(\ell) f_{sun}(\ell) d\ell \int_0^L A_{\max} f_{sun}(\ell) d\ell}{\int_0^L \alpha Q_{ta\_sun}(\ell) f_{sun}(\ell) d\ell + \int_0^L A_{\max} f_{sun}(\ell) d\ell} \qquad (3b)$$

$$P_{shd} = \frac{\int_0^L \alpha Q_{ta\_shd}(\ell) f_{shd}(\ell) d\ell \int_0^L A_{\max} f_{shd}(\ell) d\ell}{\int_0^L \alpha Q_{ta\_shd}(\ell) f_{shd}(\ell) d\ell + \int_0^L A_{\max} f_{shd}(\ell) d\ell} \qquad (3c)$$

where P_{sun} and P_{shd} are the photosynthesis of the big sunlit and shaded leaves (or groups), respectively. L is the total canopy LAI and ℓ is the cumulative LAI from canopy top. $Q_{ta\_sun}(\ell)$ and $Q_{ta\_shd}(\ell)$ are the total absorbed PAR by the sunlit and shaded leaves at canopy depth ℓ, respectively. $f_{sun}(\ell)$ and $f_{shd}(\ell)$ are the fractions of sunlit and shaded leaves at canopy depth ℓ, respectively. $f_{sun}(\ell) + f_{shd}(\ell) = 1$. If the plant canopy is

divided into infinitesimally small layers (i.e., N is infinitely large), we can write Eq. (2) in its integral form using Eqs. (4a)-(4d):

$$\lim_{N\to\infty} P_{sun\_i} L_{sun\_i} = P_{sun}(\ell) L_{sun}(\ell) = P_{sun}(\ell) f_{sun}(\ell) d\ell \tag{4a}$$

$$\lim_{N\to\infty} P_{shd\_i} L_{shd\_i} = P_{shd}(\ell) L_{shd}(\ell) = P_{shd}(\ell) f_{shd}(\ell) d\ell \tag{4b}$$

$$P_{sun}(\ell) = \alpha Q_{ta\_sun}(\ell) A_{\max} / (\alpha Q_{ta\_sun}(\ell) + A_{\max}) \tag{4c}$$

$$P_{shd}(\ell) = \alpha Q_{ta\_shd}(\ell) A_{\max} / (\alpha Q_{ta\_shd}(\ell) + A_{\max}) \tag{4d}$$

Substituting Eq. (4) into Eq. (2) yields:

$$P = \int_0^L \frac{\alpha Q_{ta\_sun}(\ell) A_{\max}}{\alpha Q_{ta\_sun}(\ell) + A_{\max}} f_{sun}(\ell) d\ell + \int_0^L \frac{\alpha Q_{ta\_shd}(\ell) A_{\max}}{\alpha Q_{ta\_shd}(\ell) + A_{\max}} f_{shd}(\ell) d\ell \tag{5}$$

Therefore, 2-leaf single-layer models of canopy P are not exactly the integral versions of the 2-leaf multilayer models (compare the Eqs. (3b) and (3c) with the first and second integrals of (5), respectively). Of course, if we substitute $Q_{ta\_sun}(\ell)$ and $Q_{ta\_shd}(\ell)$ with the corresponding light penetration equations from Spitters (1986) or Goudriaan and van Laar (1994), it is almost impossible to obtain an analytical solution for the integrals of Eq. (5).

The scaling algorithms of the complete multilayer, 2-leaf multilayer and 2-leaf single layer models of canopy P are compared in Figure E-1. In this example, the three models scaled $P_{leaf} = \dfrac{\alpha Q_{ta} A_{\max}}{\alpha Q_{ta} + A_{\max}}$ to canopy P using Eqs. (1), (2) and (3), respectively. The comparison of the complete multilayer and 2-leaf multilayer models was made in the same manner as it was with the comparison of Case 1 and Case 2 in Norman (1980). Eq. (3) is an extremely simplified version of the Sun/Shade model developed by de Pury and Farquhar (1997). Table 4 of Norman (1980) and Table 6 of de Pury and Farquhar (1997)

give detailed descriptions of the complete multilayer and 2-leaf multilayer models, and the 2-leaf single layer models, respectively. A hypothetical plant canopy is used here with the initial parameters for the complete multilayer, 2-leaf single layer and 2-leaf multilayer models given as: σ (leaf scattering coefficient for PAR) = 0.15, L (total canopy LAI) = 8, α = 0.06 mol mol^{-1} and A_{max} = 20 μmol m^{-2} s^{-1}. This hypothetical canopy has a perfect spherical leaf inclination angle distribution (also see Appendix D) with no clumping of its leaves, so the assumptions of the models can be fully met. The values of Q_{d0} and Q_{t0} are the half-hourly diffuse and total PAR measurements (n = 4219) taken from the data set for the 56-year-old Douglas-fir stand (DF49) for the period of April 1 – September 31, 2004. For the multilayer layer model, the hypothetical canopy was split into 80 layers with an LAI increment of 0.1, and the leaf inclination angles of the sunlit leaves were divided into 45 angle classes (i.e., γ_1 = 1°, γ_2 = 3°, … γ_{45} = 89°). The parameters of the MM and Q_e-MM models were obtained by fitting the MM and Q_e-MM models respectively to the total canopy P obtained using the complete multilayer model. The fitted MM model is: $P = \frac{\alpha Q_{t0} A_{\max}}{\alpha Q_{t0} + A_{\max}}$ with α = 0.054 mol mol^{-1} and A_{max} = 50.81 μmol m^{-2} s^{-1}. The term Q_{t0} of the MM model is the incident total PAR above the canopy, i.e., $Q_{t0} = Q_{d0} + Q_{b0}$. The fitted Q_e-MM model is: $P = \frac{\alpha Q_e A_{\max}}{\alpha Q_e + A_{\max}}$ with α = 0.052 mol mol^{-1}, A_{max} = 103.64 μmol m^{-2} s^{-1}, k = 0.46 and $Q_e = Q_{d0} + kQ_{b0}$.

Figure E-1a shows that P_{sun} obtained using the 2-leaf multilayer and 2-leaf single layer models has significant systematic errors with respect to Q_{d0}/Q_{t0} (the fraction of sky diffuse PAR). When Q_{d0}/Q_{t0} is close to 1, the relative errors of P_{sun} are close to zero for the 2-leaf multilayer models, because when the incoming irradiance has no direct PAR,

ignoring the leaf-sun angles (i.e., ignoring the incidence angles of solar beam) obviously has little consequence for estimating P_{sun}. But when it is in clear conditions (e.g., Q_{d0}/Q_{t0} = 0.15), the relative errors of P_{sun} for the 2-leaf multilayer models can be as high as 8% as a result of using a mean leaf inclination angle class to calculate P_{sun}. The relative errors of P_{sun} of the 2-leaf single layer models have a similar trend with respect to Q_{d0}/Q_{t0} as those of the 2-leaf multilayer models, but the errors of P_{sun} of the 2-leaf single layer models don't go to zero even when Q_{d0}/Q_{t0} approximates 1, i.e., when Q_{d0}/Q_{t0} = 1, the 2-leaf single layer models still make approximately 5% errors for P_{sun}.

P_{shd} calculated using the complete multilayer and 2-leaf multilayer models are the same (i.e., the term $\sum_{i=1}^{N} P_{shd\_i} L_{shd\_i}$ of Eqs. (1) and (2)). As a result of the scaling algorithms used in the 2-leaf single layer models (i.e., compare Eq. (3c) with the second integral of Eq. (5)), their relative errors of P_{shd} are strongly dependent on Q_{d0}/Q_{t0} and are as large as 18% (Figure E-1b). Interestingly, the relative errors of P_{sun} of the 2-leaf single layer models decrease with Q_{d0}/Q_{t0} (Figure E-1a) while their relative errors of P_{shd} increase with Q_{d0}/Q_{t0} (Figure E-1b), so the relative errors of total canopy P of the 2-leaf single layer models are almost independent of Q_{d0}/Q_{t0} (Figure E-1c). The maximum and minimum relative errors of the total canopy P for the MM, 2-leaf single layer, 2-leaf multilayer and Q_e-MM models are 12.17% (-11.46%), 11.42% (8.07%), 5.07% (0.04%) and 1.03% (-2.86%), respectively (Figure E-1c). Numbers in the brackets are the minimum relative errors. The 5% relative errors of P for the 2-leaf multilayer models are consistent with what was reported in Sinclair et al. (1976), but Sinclair et al. (1976) didn't mention these errors are systematic with respect to Q_{d0}/Q_{t0}.

Figure E-1d shows the direct comparison of canopy P modeled using the complete multilayer model and P obtained by fitting the Q_e-MM model to P values of the former. P (Q_e-MM model) = 1.00P (complete multilayer model) – 0.14, r^2 = 0.9956, RMSE = 0.5666 μmol m^{-2} s^{-1} and n = 4219. The magnitude of the relative errors of the 2-leaf multilayer and 2-leaf single-layer models may change with total canopy LAI and leaf-level photosynthetic characteristics (e.g., leaf-level A_{max}), but the trend of the relative errors for these two types of 2-leaf models shown in Figure E-1a, E-1b and E-1c remain the same (date not shown)..

In summary, if we take the complete multilayer models of canopy P as the reference, both the 2-leaf multilayer and 2-leaf single layer models have systematic errors in P with respect to Q_{d0}/Q_{t0} as a result of the averaging or simplifying schemes used in those models, although the errors of the latter type are much larger. Total PAR (i.e., Q_{t0}) has to be separated into its diffuse and direct components for serious modeling of canopy P. Diffuse PAR (including scattered direct PAR) can be reasonably assumed to be isotropic and thus is relatively straightforward to be modeled in a canopy. One of the most interesting parts of models of canopy P is to calculate the absorbed un-scattered direct PAR by the sunlit leaves as pointed out by de Wit (1965, his page 16) "To calculate canopy photosynthesis it has to be known what fraction of the light is intercepted at what angles". Ignoring the incidence angles between the sunlit leaves and the solar beam and using a mean incidence angle to calculate P_{sun} is over-simplistic. The excellent agreement between P of the complete multilayer model and P obtained by fitting the Q_e-MM model (Figure E-1d) demonstrates that the Q_e-MM model is a promising alternative to the 2-leaf models.

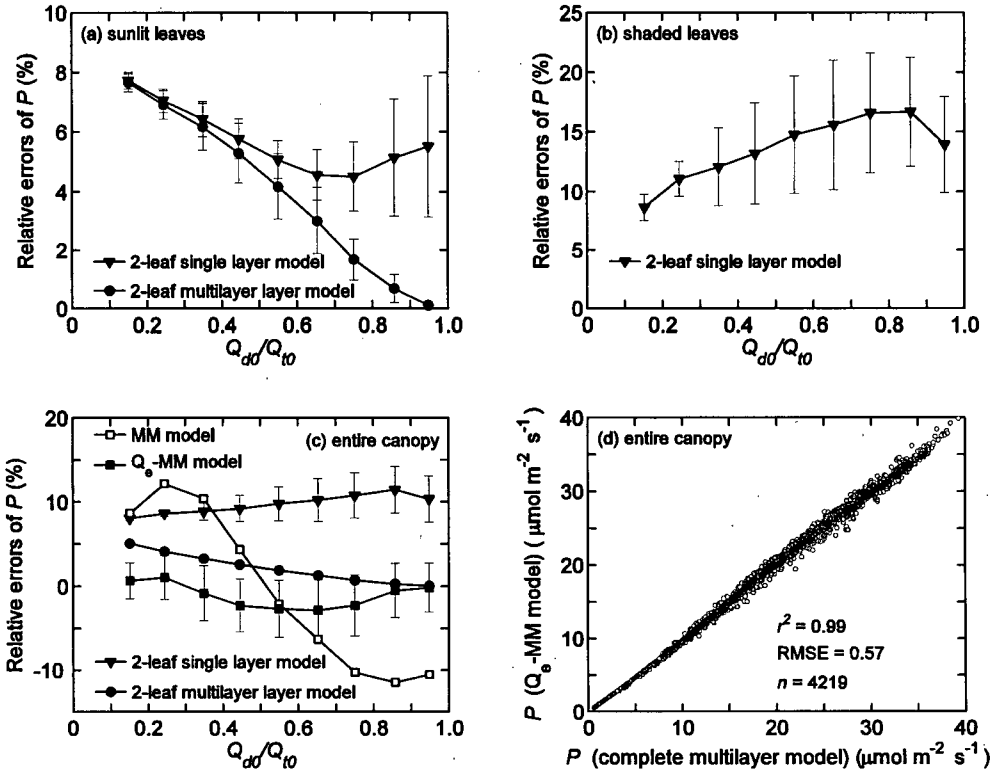

Figure E-1. The relative errors of P obtained using the 2-leaf single layer and 2-leaf multilayer, and MM and Q_e-MM models. The relative errors of P are calculated as: $(P_{mdl} - P_{complete}) / P_{complete}$, where P_{mdl} is P modeled using the aforementioned four canopy P models, and $P_{complete}$ is the corresponding P calculated using the complete multilayer model (see main text for details). In plots (a)-(c), symbols represent bin averages and vertical lines indicate ±1 SD. In plot (c), the SD for the 2-leaf multilayer model is too small to be discerned while the SD for the MM model is ignored for the clarity of the plot. The SD of the MM model is approximately 5 times larger than those of the Q_e-MM model. Q_{d0} and Q_{t0} are the sky diffuse PAR and total PAR incident above the plant canopy, respectively. In plot (d), the open circles represent modeled half hourly values of total canopy P.